TOMSK POLYTECHNIC UNIVERSITY

A. I. Pushkarev, Yu. I. Isakova, R. V. Sazonov, G. E. Kholodnaya

PHYSICS AND CHEMISTRY OF LOW-TEMPERATURE PLASMA FOR MATERIAL TREATMENT

It is recommended for publishing as a study aid by the Editorial Board of Tomsk Polytechnic University

Tomsk Polytechnic University Publishing House
2011

UDC 000000
BBC 00000
E00

A. I. Pushkarev

E00 Physics and Chemistry of Low-Temperature Plasma for Material Treatment/ A. I. Pushkarev, Yu. I. Isakova, R. V. Sazonov, G. E. Kholodnaya; Tomsk Polytechnic University. – Tomsk: TPU Publishing House, 2011. – 181 p.

The book describes some physical and technical aspects of plasma chemistry. The general concepts of plasma physics and chemical kinetics as well as the methods and sources for generation of nonequilibrium plasma are considered. The application of low-temperature plasmas in the chemical industry include: the synthesis and decomposition of inorganic compounds; synthesis of nanosized materials; conversion of hydrocarbon gases; synthesis of hydrogen and supramolecular carbon clusters (fullerenes); treatment of membranes and coatings, etc.

This book is recommended for students, studding on the specialty "Physics and technology of low temperature plasmas, plasma chemistry and plasma technology" course 140200 " Electroenergetics".

UDC 000000
BBC 00000

Reviewer professor of Tomsk State University
Kohanenko A.P.

TABLE OF CONTENTS

Preface

Plasma-chemical technologies are widely used in world practice, namely, in large-tonnage chemistry; synthesis of powder-like materials, deposition of coatings; semiconductor industry, microelectronics; in addressing the environmental issues and scientific research. This book mainly focuses on the plasma-chemical processes in which the non-equilibrium excitation of internal degrees of freedom of the reacting molecules makes a decisive influence on the kinetics of chemical reactions. It is shown that for the initiation of chemical reactions, the non-equilibrium excitation of vibrational degrees of freedom of the molecules is the most effective. Plasma-chemical processes occurring in these conditions have several advantages, which is important in traditional industry, allowing for a reduced energy costs and increased productivity. The conditions, occurring within the pulsed excitation of gas mixtures, are also favorable for the organization of chain chemical processes.

The book starts with a chapter devoted to the general concepts of plasma physics (describing a plasma Debye length, the ionization of plasma, etc.) and chemical kinetics (rate and reaction order, rate constant, Arrhenius equation, etc.). The types of the internal energy of molecules in the quantum electronic state as well as the basic laws of non-equilibrium excitation of the molecules are considered. The physical and chemical processes which are accompanied by high vibrational non-equilibrium reaction products, including the excitation of molecules by electron impact are studied. The results of experimental studies of gas-phase chain processes under external influence are also summarizes. Most of the studies of gas-phase chain processes under non-equilibrium conditions were conducted by Russian scientists, who continued a study of the Nobel laureate N.N. Semenov.

Introduction

The modern large-tonnage chemical industry, which uses a traditional approach of thermal activation of the chemical processes, is now faced with the problem of energy conservation. Further development of the industrial base leads to an unjustified cost of resources to build the equipment and the depletion of minerals, metals and fuels.

A natural way to help this situation, obviously, should be a transition to new technological solutions in metallurgy, chemistry, energy and other industries. The qualitative changes are noticed if the performance of equipment will be improved, namely, the productivity per unit volume of the reaction zone. This requires a significant increase in temperature in the reaction zone, since this chemical process, within the framework of classical kinetics, is accelerated exponentially in accordance with the Arrhenius law. The heating of the reactor and the reactants to high temperatures also requires increased energy consumption, and therefore needs the new ways to increase productivity while specific energy consumption is reduced.

The combination of the reaction zone with the discharge can locally heat the reactants to high temperatures without heating the reactor walls, which significantly decreases the energy consumption. These conditions are easily realized by excitation of the reagent gas mixture by a continuous electron beam or in arc discharge, etc. The reduction of the energy barrier of the reaction is also achieved through participation of free radicals and atoms, which are effectively produced in gas discharges due to a dissociative recombination and relaxation of excited molecules.

The next step is to reduce the energy costs for conducting a chemical process, which can be achieved by the following: using non-equilibrium plasma-chemical processes, characterizing by a significant excess energy of in the internal degrees of freedom of molecules (mainly vibrational) compared with the thermodynamic equilibrium state. In this case, the gas temperature may not exceed 300-400K, which reduces the energy loss in heating the reactor walls, as well as the original components of the gas mixture, which facilitates the hardening (stabilization) of the chemical products.

Over the last 30-40 years in Russia and abroad many studies have been devoted to the use of low-temperature plasma for gas-phase chemical processes. The formation of a low-temperature plasma by a pulsed electron beam, in contrast to many other methods, is showed to occur with a significant reduction in energy, consumed on the conversion of gaseous compounds. An analysis of experimental works devoted to the

decomposition of impurities of different compounds (NO, NO_2, SO_2, CO, CS_2, etc.) in the air by a pulsed electron beam showed that the energy used to decompose one molecule of the gas is lower than its dissociation energy. This is due to the fact that some favorable conditions for the occurrence of chain processes are formed when an electron beam is involved [1]. At low temperatures, when thermal initiation of the reaction does not occur, some active centers are formed due to the influence of plasma. These active centers are free radicals, ions or excited molecules, which can start a chain reaction. This chain reaction occur at a temperature of 150-200 degrees below the temperature of a normal thermal process, but with the same speed, since the plasma facilitates the most energy intensive stage - thermal initiation of the reaction. With a sufficient length of chain an electro physical set-up provides a small part of total energy consumption to the chemical process. The main source of energy in this case is the thermal energy of the original gas or exothermic energy of the chemical reactions of chain process (e.g. oxidation or polymerization). It is important to note that a chemical process, occurring at a temperature below the equilibrium, allows one to synthesize compounds which are unstable at higher temperatures and the selectivity of the synthesis of which at high temperatures is low. The increase in the temperature of chain chemical processes with the radioactive impact is analogues to a catalytic effect. But the chain process can entirely occur in the gas phase, which greatly increases the reaction rate in comparison with the heterophase catalytic process. A high speed of the reaction required for industrial technologies is achieved by the use of branched chain processes. However, their major drawback is associated with the occurrence of an explosive process, which significantly increases the risk of production. This disadvantage is eliminated by initiating of the chain process outside the scope of self-ignition under external influence. The above features gas-phase chemical processes with the electron beam involved indicate the prospects of their use in large-scale chemical production [2]. Most studies of chain gas-phase processes, including those under the external action, were performed by Russian scientists, who continued the works of the Nobel laureate N.N. Semenov. In his Nobel speech, he explained that the penetrating radiation will be used to initiate chain processes.

In plasma-chemical processes the energy transfer from an external source (a source of electrical energy) to the reacting molecules occur in several steps (see Fig. 1).

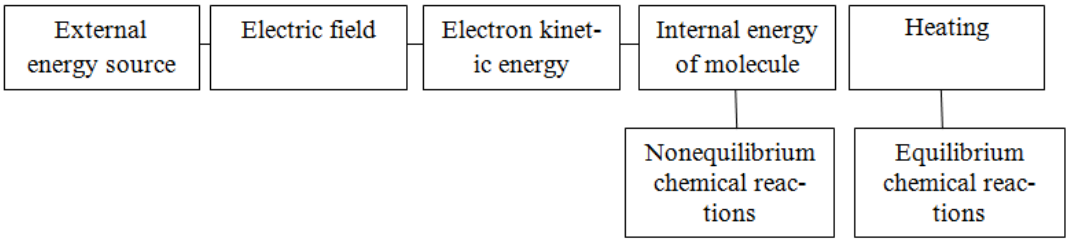

Fig. 1. Stages of energy transfer in a gas discharge

In quasi-equilibrium plasma chemical processes, chemical transformations occur only after the transfer of the energy from an external source to the kinetic energy of molecules of the reactive gas. In non-equilibrium processes the chemical transformations begin after the excitation of internal degrees and dissociation of these molecules.

Nowadays, plasma chemistry is one of the most promising directions in low-temperature plasma physics and high energy chemistry. The advantages of plasma chemistry as a new type of chemical technology are explained by a high level of energy introduced to a chemical system. This leads to a significant increase in the rates of chemical transformations, minimizing the size of a reactor, reduction of costs for the implementation of the processes and organization of chemical production. The processing of raw materials, which are poorly recyclable by conventional methods, as well as various waste facilities in order to protect the environment, became possible. In some cases the materials obtained by plasma-chemical methods have unique physical and chemical properties.

The transition to plasma chemical technology means a transition to higher levels of temperatures and higher velocities of chemical reactions. In many cases, the rates of chemical reactions are compared with the rates of transitions between the energy levels and even exceed it. In addition, the plasma-chemical systems, used in the laboratories and technological plants, are of an open type in the thermodynamic sense. An intense heat and mass exchange with the environment and the energy exchange with external fields (electric field, radiation field, etc.) are involved in plasma-chemical reactions. This leads to the creation of the following: physical non-equilibrium, temperature gradients, violation of the Maxwell- Boltzmann distribution of velocities and levels of the internal degrees of freedom. For example, in the plasmas of electrical discharge at low pressures or high values of electric field strength, and low degrees of ionization (in electric arcs, glow, high-frequency and microwave discharges at pressures below atmospheric, as well as in the corona, barrier and pulse discharges), the average electron energy exceeds the average energy of heavy particles and the electron distribution function in the velocities differ from the

equilibrium Maxwellian. A non-equilibrium concentration of charged particles and the particles which are excited by different degrees of freedom - rotational, vibrational and electronic levels is observed.

The object of plasma chemistry is a low-temperature plasma in molecular gases. Plasma chemistry studies the kinetics and mechanism of chemical reactions and physical-chemical processes in low-temperature plasmas. It should be emphasized that in plasma chemistry, the term "plasma" is understood as a substance containing not only the charged particles, but molecules in the ground electronic state with the excess (non -equilibrium) internal energy.

The object of plasma chemistry as a scientific discipline is a study of the relationship between physical and chemical phenomena in chemical reactions in the plasma, the possibility of plasma usage for various problems in applied chemistry. As a consequence, there is a conventional division into theoretical and applied plasma chemistry.

The terms "plasma chemistry", "plasma-chemical reactions" and "plasma-chemical processes" were introduced in Russian scientific literature since the publication of the book entitled "The kinetics and thermodynamics of chemical reactions in low-temperature plasmas", edited by L.S. Polak (Moscow: Nauka, 1965). They reflect the fact that the object of consideration is the specific chemical objects, which feature lies in the fact that chemical reactions are initiated or occur in plasma. It has been more than two hundred years since the existence of electrical discharge chemistry as a science. It has come a long way from a phenomenological description of phenomena to the creation of a new research area with its own apparatus, including theoretical and experimental techniques. The mechanisms of many plasma-chemical reactions have been studied and understood. Besides the theoretical aspects of plasma-chemistry, there are numerous applications of plasma-chemistry for the solution of practical problems that are grouped under the title "applied plasma chemistry.

Chapter 1 Introduction to plasma physics

1.1 What is a plasma?

First and foremost, a plasma is an ionized gas. When a solid is heated sufficiently that the thermal motion of the atoms break the crystal lattice structure apart, usually a liquid is formed. When a liquid is heated enough that atoms vaporize off the surface faster than they recondense, a gas is formed. When a gas is heated enough that the atoms collide with each other and knock their electrons off in the process, a plasma is formed: the so-called 'fourth state of matter'. Taking into consideration the energy of the particles constituting it, plasma is energetically the fourth state of the matter, apart from the solid, liquid, and gas states. Fig. 2 presents schematically the ranges of temperature, or particle energy, in which each of the four forms of matter occur in nature. For the plasma state, the temperature range reflects only the energy of the heavy particles (not of the electrons) for reasons to be explained later.

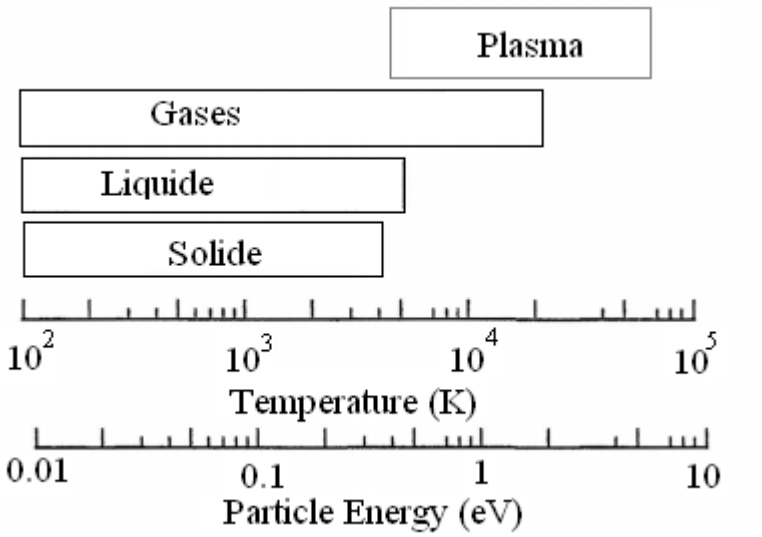

Fig. 2. State of matter versus temperature

The important point is that an ionized gas has unique properties. In most materials the dynamics of motion are determined by forces between near-neighbor regions of the material. In a plasma, charge separation between ions and electrons gives rise to electric fields, and charged particle flows give rise to currents and magnetic fields. These fields result in 'action at a distance', and a range of phenomena of startling complexity, of considerable practical utility and sometimes of great beauty.

Irving Langmuir, the Nobel laureate who pioneered the scientific study of ionized gases, gave this new state of matter the name ‘plasma’.

The reader who is more interested in plasma physics is referred to an excellent book written by Robert J. Goldston and Paul H. Rutherford [3] and the lectures of Professor Richard Fitzpatrick (The University of Texas at Austin) [4].

1.2 How are plasmas made?

A plasma is not usually made simply by heating up a container of gas. The problem is that for the most part a container cannot be as hot as a plasma needs to be in order to be ionized-or the container itself would vaporize and become plasma as well.

Typically, in the laboratory, a small amount of gas is heated and ionized by driving an electric current through it, or by shining radio waves into it. Either the thermal capacity of the container is used to keep it from getting hot enough to melt-let alone ionize during a short heating pulse, or the container is actively cooled (for example with water) for longer-pulse operation. Generally, these means of plasma formation give energy to free electrons in the plasma directly, and then electron-atom collisions liberate more electrons, and the process cascades until the desired degree of ionization is achieved. Sometimes the electrons end up quite a bit hotter than the ions, since the electrons carry the electrical current or absorb the radio waves.

1.3 Some applications of plasmas

There are all sorts of uses for plasmas. To give one example, if we want to make a short-wavelength laser we need to generate a population inversion in highly excited atomic states. Generally, gas lasers are ‘pumped’ into their lasing states by driving an electric current through the gas, and using electron-atom collisions to excite the atoms. X-ray lasers depend on collisional excitation of more energetic states of partially ionized atoms in a plasma. Sometimes a magnetic field is used to hold the plasma together long enough to create the highly ionized states. A whole field of ‘plasma chemistry’ exists where the chemical processes that can be accessed through highly excited atomic states are exploited. Plasma etching and deposition in semiconductor technology is a very important related enterprise. Plasmas used for these purposes are sometimes called ‘process plasmas’. Perhaps the most exciting application of plasmas such is the production of power from thermonuclear fusion.

1.4 Plasma parameters

A plasma, especially one sustained in a mixture of molecular gases, contains a multitude of different neutral and charged particles. A group of identical particles in a plasma is commonly referred to as a species.

The plasma is broadly characterized by the following basic parameters:

1 The density of the neutral particles, n_n.

2 The densities of the electrons and ions, n_e and n_i . In the quasi-neutral state of plasma the densities of the electrons and of the ions are usually equal, $n_i = n_e = n$ (n is called the plasma density.

3 The energy distributions of the neutral particles, $f_n(W)$ ions, $f_i(W)$; and electrons, $f_e(W)$.

The plasma density is an important parameter in plasma processing because the efficiency of the processes occurring in the plasma and their reaction rates are generally dependent directly on the density of the charged particles. The electrons are the main factor responsible for the transfer of the energy from the external electric field to the discharge gas. Being electrically charged, both electrons and ions interact with the applied external electric field and are accelerated by absorbing energy from it. Because the electrons are the lightest particles in the plasma, they are easiest accelerated and absorb the largest amount of energy from the external field. The electrons then transfer through collisions energy to the molecules of the gas and cause their ionization and dissociation. The effectiveness of these processes increases with increasing electron density. Ions, too, play a significant role in the chemical reactions taking place in the plasma. Many of the reactions occurring in a plasma are controlled, or affected, by ion chemistry. It is therefore important to achieve high ion densities to increase the rates of reactions involving the ions.

As in any gaseous system, particles in the plasma are in continuous motion, inducing collisions between them. The collisions which take place between the particles in the plasma are of two types, *elastic* or *inelastic*. Collisions between electrons and heavy targets (i.e., neutral or charged particles) that do not result in an excitation of the target are called *elastic collisions*, whereas those collisions that leave the target in an excited state are called *inelastic collisions*. Collisional processed in plasma will be discussed in more details in section 2.

The energy transfer W_{Tr} in an elastic collision between an electron and a heavy target is determined by the mass ratio of the particles

$$W_{Tr} = \frac{2m_e}{M} \cdot W \qquad (1)$$

where M–mass of the heavy particle;

W–energy of the electron;

m_e–mass of electron.

For an elastic collision of an electron with an argon atom, the fraction of transferred energy is therefore very small, about

$$\frac{W_{Tr}}{W} \approx \frac{1}{40000} \tag{2}$$

On the other hand, a significant amount of energy is transferred in a collision between two electrons.

The electrons gain energy through acceleration by the electric field, which sustains the plasma and transfers that energy by inelastic collisions with the neutral gas molecules. The inelastic collisions between energetic electrons and the heavy species of the plasma result in excitation, ionization, or dissociation of the target if it is multiatomic. Energy transfer in an inelastic collision is not controlled by the mass ratio of the colliding particles. In an inelastic collision between two particles, the fraction of transferred energy is given by

$$\frac{W_{Tr}}{W} = \frac{M}{m_{in} + M} \tag{3}$$

where m_{in} is the mass of particle losing energy.

According to Eq. (1.3), in an inelastic collision between an electron and a heavy particle ($m_{in} = m_e \ll M$), the electron can transfer almost all its energy to the heavy particle, creating an energetic plasma species. The inelastic collisions therefore sustain the plasma by producing the particles that form it and giving the plasma its special features. Inelastic collisions involve energy transfer in amounts that vary from less than 0.1 eV (for rotational excitation of molecules) to more than 10 eV (for ionization).

Electron-electron collisions can also play a significant role in the energy transfer processes in the plasma. Their importance depends on the degree of ionization prevalent in the plasma. For degrees of ionization below 10^{-10} the contribution of the electron-electron collisions to the energy transfer is negligible.

However, in electron cyclotron resonance (ECR) plasmas, where the degree of ionization can be above 10^{-3}, electron-electron collisions dominate[5].

The relative contribution of each type of collision to the processes taking place in the plasma depends on additional plasma parameters, which will be discussed next and which derive from the previously described parameters.

1.4.1 The Degree of Ionization

The parameter that defines the density of the charged particles in the plasma is the degree of ionization of the gas. It specifies the fraction of the particles in the gaseous phase which are ionized. The degree of ionization, α, is defined as

$$\alpha = \frac{n_i}{n} \qquad (4)$$

There are two basic processes of ionization, satisfying the conditions for conservation of momentum and energy: (a) impact ionization, where an electron strikes an atom, so that an ion and two electrons come off and (b) radiative ionization, where a photon with sufficient energy (often in the ultraviolet range) is absorbed by an atom, dissociating it into an ion and an electron. Ions can recombine into atoms by the reverse of these processes: (a) three - body recombination, where two electrons and an ion join to make a neutral atom plus a free electron; and (b) radiative recombination, where an electron and an ion combine into an atom, and a photon is emitted. These processes are illustrated in Fig. 3.

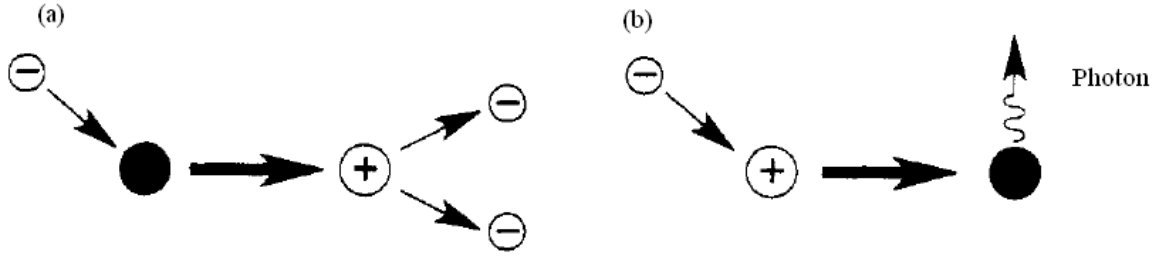

Fig. 3. Ionization and recombination processes: (a) electron-impact ionization, and (b) radiative recombination

The processes of three-body recombination and radiative ionization are the inverse of these processes and are obtained by reversing the direction of the arrows in (a) and (b), respectively. Neutral atoms are represented by black dots, while electrons and protons are represented by open circles labeled (-) and (+), respectively.

For plasmas sustained in low-pressure discharges, the degree of ionization is typically 10^{-6} to 10^{-3}. However, if the electrical discharge is assisted and confined by an additional magnetic field, the degree of ionization can reach values of 10^{-2} or higher, as for example, in an ECR plasma. Table 1 presents the range of values of the degree of ionization encountered in different low-pressure plasmas used for processing of solids.

Table 1. Ranges of Parameters for Various Low-Pressure Plasmas

Plasma Type	Pressure (torr)	Ion Density (cm^{-3})	Degree of Ionization
Deposition/etching	< 10	$< 10^{10}$	10^{-6}
Reactive ion Etching	$10^{-2} – 10^{-1}$	10^{10}	$10^{-6} – 10^{-4}$
Magnetron sputtering	10^{-3}	10^{11}	$10^{-4} – 10^{-2}$
Electron cyclotron resonance	$<10^{-4} – 10^{-2}$	10^{12}	$<10^{-1}$

The degree of ionization in a plasma is a function of the elements contained in the plasma. For example, in plasmas used in magnetron sputtering, the degree of ionization of the sputtered metal is higher than that of the process gas employed for the sputtering.

The value of the critical ionization is defined by [6]

$$\alpha \approx 1.73 \times 10^{12} \cdot \sigma_{ea} \cdot T_e^2 \qquad (5)$$

where σ_{ea} is the electron-atom collision cross section at the average electron velocity, expressed in cm^2; T_e is the electron temperature of the plasma, expressed in eV. The electron temperature will be defined later, in Sec. 1.4.2. If the degree of ionization is much bigger than the critical ionization value, the charged particles behave as in a fully ionized gas.

1.4.2 Plasma Temperature

One of the physical parameters defining the state of a neutral gas in thermodynamic quilibrium is its temperature, which represents the mean translational energy of the molecules in the system. A plasma contains a mixture of particles with different electric charges and masses. At a first approximation, the plasma may be considered, thermally, as consisting of two systems: the first containing only electrons and the second containing the heavy species, that is, neutral atoms or molecules, ions, and neutral molecular fragments.

The electrons gain energy from the electric field, which energizes the plasma, and lose part of it by transfer to the second system through elastic or inelastic collisions. The system of heavy particles loses energy to the surroundings, either by radiation or by heat transfer to the walls of the vessel containing the plasma.

The electrons and the heavy species in the plasma can be considered approximately as two subsystems, each in its own thermal quasi-equilibrium.

The ions and electrons in the plasma can therefore be characterized by their specific different average temperatures: the ion temperature, T_i and the electron temperature, T_e. Actually in some cases additional temperatures may characterize the particles in the plasma. For example, in the presence of a magnetic field, even a single plasma species, for example, the ions, is characterized by two different temperatures, one representing the translation of the ions parallel to the magnetic field, $T_{\|}$, and one representing the translation perpendicular to the magnetic field, $T_{\perp}$. This is caused by the fact that the forces acting on the species parallel to the magnetic field are different from those acting perpendicular to it [7].

The situation is even more complicated, as the heavy species in the plasma can be characterized by several temperatures at the same time, even in the absence of a magnetic field [8]: the temperature of the gas, T_g, which characterizes the translatory energy of the gas; the excitation temperature, T_{ex}, which characterizes the energy of the excited particles in the plasma; the ionization temperature, T_{ion}; the dissociation temperature, T_d, which characterize the energy of ionization and dissociation; and the radiation temperature, T_r which characterizes the radiation energy. Thermodynamic equilibrium will exist in the plasma only if the following equation is satisfied:

$$T_g = T_{вх} = T_{ion} = T_d = T_r = T_в \qquad (6)$$

Complete thermodynamic equilibrium cannot be achieved in the entir9e plasma because the radiation temperature, T_r at the envelope of the plasma cannot equal the temperature in the plasma bulk. However, under certain laboratory conditions, it is possible to achieve local thermodynamic equilibrium in plasma in volumes of order of the mean free path length (The reader who is unfamiliar with the term is referred to the Sect. 2.1). If this happens, the plasma is called a local thermodynamic equilibrium (LTE) plasma. In low pressure plasmas, produced by direct current glow discharge or radio frequency excitation, the LTE conditions are generally not achieved. These plasmas are therefore called non-LTE plasmas.

In non-LTE plasmas the temperatures of the heavy particles are normally too small to promote chemical reactions in thermodynamic equilibrium. The electron temperature is therefore the most important temperature in non-LTE plasmas, among all those different temperatures mentioned previously. The fraction of electrons that will cause the different reactions in the plasma, the overall efficiency of the plasma processes,

and the processing rates increase with increasing electron temperature. The electron temperature is discussed in further detail in the following section.

1.4.2.1 Electron Temperature

The velocity distribution $f(v)$ for a system of particles is defined as the density of particles in the velocity space that satisfies the equation

$$n(cm^{-3}) = 4\pi \cdot \int_0^\infty f(v)v^2 dv \qquad (7)$$

where *v* is the velocity; *f(v)* is the velocity distribution function (density in velocity space); *n* is the the density of the particles in the geometrical space.

If it is assumed that the velocity distribution of the electrons in the plasma is isotropic, that the effects of inelastic collisions act only as a perturbation to the isotropy, and that the effects of the electric fields are negligible, then the velocity distribution is Maxwellian. The Maxwellian distribution assumes that the temperature of the electrons equals the temperature of the gas, $T_e = T_g$.

If the distribution of the electron velocities can be considered Maxwellian, then it can be described by [3,9]

$$f(v) = n_e\left(\frac{m_e}{2\pi kT_e}\right)^{3/2} \exp\left(-\frac{m_e v^2}{2kT_e}\right) \qquad (8)$$

The electron energy distribution function $f(W)$ is related to the velocity distribution function *f(v)* through the relation [5]

$$f(W) = \frac{4\pi}{m_e} v \cdot f(v) \qquad (9)$$

Therefore, the Maxwellian energy distribution function for the electrons is given by

$$f(W) = 2.07 W_{av}^{-3/2} \cdot W^{1/2} \exp\left(\frac{-1.5W}{W_{av}}\right) \qquad (10)$$

where W_{av} is the average energy of electrons.

It can be shown that the average energy of the electrons is related to their temperature by

$$W_{av} = \frac{3}{2} kT_e \qquad (11)$$

Due to the simplifying assumptions, the Maxwellian distribution provides only a first approximation of the electron energy (or velocity) distribution in the plasma. The assumptions made for the Maxwellian dis-

tribution can be replaced in low-pressure plasmas by the following assumptions:

1 The electric field strength in the plasma is sufficiently low such that one can neglect the inelastic collisions, but large enough for the electron temperature to be much higher than the ion temperature, $T_в >> T_i$

2 The electric field is of sufficiently low frequency, that is, it is of a frequency ω much lower than the frequency of collisions v.

3 The collision frequency is independent of the electron energy.

1.4.3 Plasma Frequency

The plasma frequency,

$$\varpi_p^2 = \frac{nв^2}{\varepsilon_0 m} \tag{12}$$

is the most fundamental time-scale in plasma physics. Clearly, there is a different plasma frequency for each species. However, the relatively fast electron frequency is, by far, the most important, and references to "the plasma frequency" in text-books invariably mean the *electron* plasma frequency.

It is easily seen that ω_p corresponds to the typical electrostatic oscillation frequency of a given species in response to a small charge separation. For instance, consider a one-dimensional situation in which a slab consisting entirely of one charge species is displaced from its quasi-neutral position by an infinitesimal distance δ_x. The resulting charge density which develops on the leading face of the slab is $\sigma = en\delta_x$. An equal and opposite charge density develops on the opposite face. The x-directed electric field generated inside the slab is of magnitude $E_x = -\frac{\sigma}{\varepsilon_0} = -en\delta_x / \varepsilon_0$. Thus, Newton's law applied to an individual particle inside the slab yields

$$m\frac{d^2\delta x}{dt^2} = eE_x = -m\varpi_p^2\delta x \tag{13}$$

giving $\delta x = (\delta x)_0 \cos(\varpi_p t)$

Note that plasma oscillations will only be observed if the plasma system is studied over time periods τ longer than the plasma period $\tau \equiv 1/\omega_p$, and if external actions change the system at a rate no faster than ω_p. In the opposite case, one is clearly studying something other than plasma physics (*e.g.*, nuclear reactions), and the system cannot not usefully be considered to be a plasma. Likewise, observations over length-

scales L shorter than the distance $v_t \tau_p$ traveled by a typical plasma particle during a plasma period will also not detect plasma behaviour. In this case, particles will exit the system before completing a plasma oscillation. This distance, which is the spatial equivalent to τ_p, is called the *Debye length*, and takes the form

$$\lambda_D \equiv \sqrt{T \Big/ m \varpi_p^{-1}} \tag{14}$$

Note that

$$\lambda_D \equiv \sqrt{\frac{\varepsilon_0 T}{n e^2}} \tag{15}$$

is independent of mass, and therefore generally comparable for different species. Clearly, our idealized system can only usefully be considered to be a plasma provided that

$$\frac{\lambda_D}{L} << 1 \tag{16}$$

$$\frac{\tau_p}{\tau} << 1 \tag{17}$$

Here, τ and L represent the typical time-scale and length-scale of the process under investigation.

It should be noted that, despite the conventional requirement (16), plasma physics *is* capable of considering structures on the Debye scale. The most important example of this is the *Debye sheath*: *i.e.*, the boundary layer which surrounds a plasma confined by a material surface.

1.4.4 Debye Shielding

Plasmas generally do not contain strong electric fields in their rest frames. The shielding of an external electric field from the interior of a plasma can be viewed as a result of high plasma conductivity: *i.e.*, plasma current generally flows freely enough to short out interior electric fields. However, it is more useful to consider the shielding as a *dielectric* phenomena: *i.e.*, it is the *polarization* of the plasma medium, and the associated redistribution of space charge, which prevents penetration by an external electric field. Not surprisingly, the length-scale associated with such shielding is the Debye length.

Let us consider the simplest possible example. Suppose that a quasi-neutral plasma is sufficiently close to thermal equilibrium that its particle densities are distributed according to the Maxwell-Boltzmann law,

$$n_s = n_0 e^{-e_s \phi / T} \tag{18}$$

where $\Phi(\mathbf{r})$ is the electrostatic potential, and n_0 and T are constant. From $e_i = {}^{-}e_e = e$, it is clear that quasi-neutrality requires the equilibrium potential to be a constant. Suppose that this equilibrium potential is perturbed, by an amount $\delta\Phi$, by a small, localized charge density δp_{ext}. The total perturbed charge density is written

$$\delta_p = \delta p_{\exp} + e(\delta n_i - \delta n_e) = \delta p_{\exp} - 2e^2 n_0 \delta\Phi / T \tag{19}$$

Thus, Poisson's equation yields

$$\nabla^2 \delta\Phi = -\frac{\delta p}{\varepsilon_0} = -\left(\frac{\delta p_{\exp} - 2e^2 n_0 \delta\Phi / T}{\varepsilon_0} \right) \tag{20}$$

which reduces to

$$\left(\nabla^2 - \frac{2}{\lambda_D^2} \right) \delta\Phi = -\frac{\delta p_{\exp}}{\varepsilon_0} \tag{21}$$

If the perturbing charge density actually consists of a point charge q, located at the origin, so that , $\delta p_{ext} = q\delta(r)$ then the solution to the above equation is written

$$\delta\Phi(r) = \frac{q}{4\pi\varepsilon_0 r} e^{-\sqrt{2r/\lambda_D}} \tag{22}$$

Clearly, the Coulomb potential of the perturbing point charge q is shielded on distance scales longer than the Debye length by a *shielding cloud* of approximate radius λ_D consisting of charge of the opposite sign.

Note that the above argument, by treating n as a continuous function, implicitly assumes that there are many particles in the shielding cloud. Actually, Debye shielding remains statistically significant, and physical, in the opposite limit in which the cloud is barely populated. In the latter case, it is the *probability* of observing charged particles within a Debye length of the perturbing charge which is modified.

1.5 The plasma parameter: strongly and weakly coupled plasmas

Let us define the average distance between particles,

$$r_d \equiv n^{-1/3} \tag{23}$$

and the distance of closest approach,

$$r_d \equiv \frac{e^2}{4\pi\varepsilon_0 T} \tag{24}$$

Recall that r_c is the distance at which the Coulomb energy

$$U(r,v) = \frac{1}{2} m v^2 - \frac{e^2}{4\pi\varepsilon_0 r} \tag{25}$$

of one charged particle in the electrostatic field of another vanishes. Thus, $U(r_c,v_t)= 0$.

The significance of the ratio r_d/r_c is readily understood. When this ratio is small, charged particles are dominated by one another's electrostatic influence more or less continuously, and their kinetic energies are small compared to the interaction potential energies. Such plasmas are termed *strongly coupled*. On the other hand, when the ratio is large, strong electrostatic interactions between individual particles are occasional and relatively rare events. A typical particle is electrostatically influenced by all of the other particles within its Debye sphere, but this interaction very rarely causes any sudden change in its motion. Such plasmas are termed *weakly coupled*. It is possible to describe a weakly coupled plasma using a standard Fokker-Planck equation (*i.e.*, the same type of equation as is conventionally used to describe a neutral gas). Understanding the strongly coupled limit is far more difficult, and will not be attempted in this course. Actually, a strongly coupled plasma has more in common with a liquid than a conventional weakly coupled plasma.

Let us define the *plasma parameter*

$$\Lambda = 4\pi n \lambda_D^3 \tag{26}$$

This dimensionless parameter is obviously equal to the typical number of particles contained in a Debye sphere. However, Eqs. (8), (16), (17), and (19) can be combined to give

$$\lambda = \frac{\lambda_D}{r_C} = \frac{1}{\sqrt{4\pi}} \left(\frac{r_d}{r_C}\right)^{3/2} = \frac{4\pi\varepsilon_0^{3/2}}{e^3} \cdot \frac{T^{3/2}}{n^{1/2}} \tag{27}$$

It can be seen that the case λ «1, in which the Debye sphere is sparsely populated, corresponds to a strongly coupled plasma. Likewise, the case λ » 1, in which the Debye sphere is densely populated, corresponds to a weakly coupled plasma. It can also be appreciated, from Eq. (1.28), that strongly coupled plasmas tend to be cold and dense, whereas weakly coupled plasmas are diffuse and hot. Examples of strongly coupled plasmas include soliddensity laser ablation plasmas, the very "cold" (*i.e.*, with kinetic temperatures similar to the ionization energy) plasmas found in "high pressure" arc discharges, and the plasmas which constitute the atmospheres of collapsed objects such as white dwarfs and neutron stars. On the other hand, the hot diffuse plasmas typically encountered in ionospheric physics, astrophysics, nuclear fusion, and space plasma physics are invariably weakly coupled.

Table 2. Lists the key parameters for some typical weakly coupled plasmas

	$n(m^{-3})$	T(eV)	$\omega_{p\,(sec^{-1})}$	$\lambda_{D(m)}$	λ
Interstellar	10^{6}	10^{-2}	6×10^{4}	0.7	4×10^{6}
Solar Chromosphere	10^{18}	2	6×10^{4}	5×10^{-6}	2×10^{3}
Solar Wind (1AU)	10^{7}	10	2×10^{5}	7	5×10^{10}
Ionosphere	10^{12}	0.1	6×10^{7}	2×10^{-3}	1×10^{5}
Arc Discharge	10^{20}	1	6×10^{11}	7×10^{-7}	5×10^{2}
Tokamak	10^{20}	10^{4}	6×10^{11}	7×10^{-5}	4×10^{8}
Inertial Confinement	10^{28}	10^{4}	6×10^{15}	7×10^{-9}	5×10^{4}

In conclusion, characteristic *collective* plasma behaviour is only observed on time-scales longer than the plasma period, and on length-scales larger than the Debye length. The statistical character of this behaviour is controlled by the plasma parameter. Although ω_p, λ_D, and λ are the three most fundamental plasma parameters, there are a number of other parameters which are worth mentioning.

1.6 Plasma types

The plasma state exists in natural form in the cosmos or is created under unique conditions for specific purposes. The plasmas found in nature cover a very large range of electron densities and temperatures. As shown in Fig. 4, the plasma density, n_e, spans the range between 1 and 10^{-20} cm^{-3} , while the electron temperature, T_e can vary between 10^{-2} and 10^{5} eV.

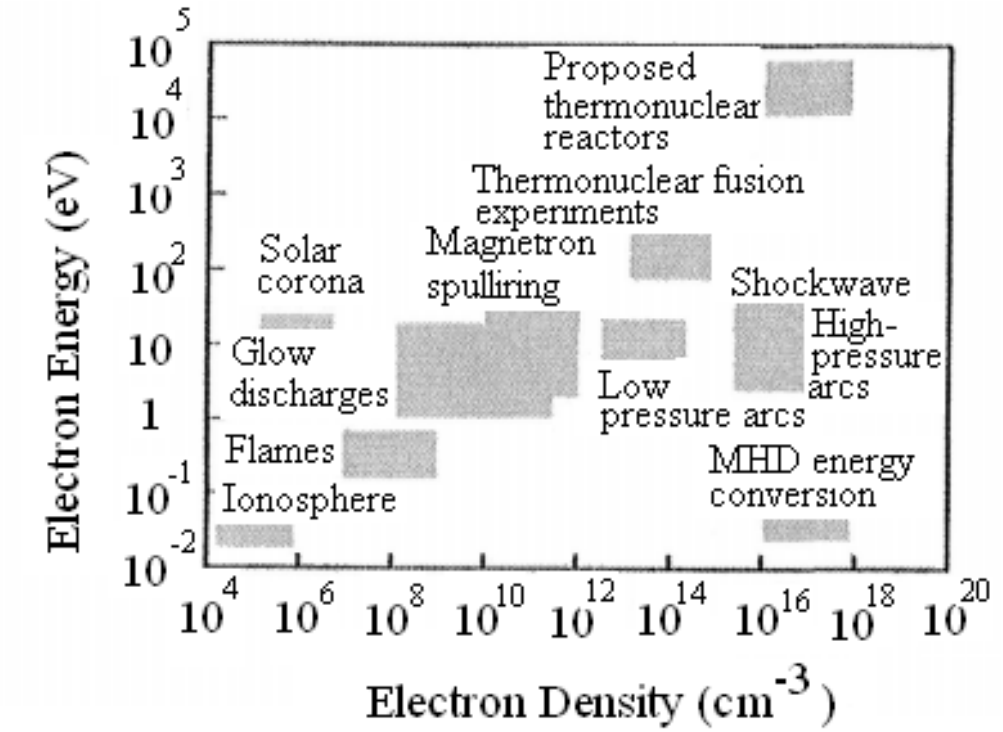

Fig. 4. Plasma types by electron density and temperature

Solar winds are a continuous stream of charged particles with n_e = 5 cm^{-3} and T_e = 50 eV. The interstellar material contains a hydrogen plasma with a density of 1 cm^{-3}. The ionosphere, which extends approximately from 50 km upward from the earth's surface, is populated by a weak plasma with a density varying up to 10^6 cm^{-3} and an electron temperature of 0.1 eV, while the sun and stars have surface temperatures ranging from 5000 to more than 70,000 °K (0.5 to 7 eV). They consist entirely of plasma, the outer layer being partially ionized and the interior hot enough to be completely ionized. The temperature at the center of the sun is at about 2 keV.

In the quest for controlled thermonuclear fusion, it is necessary to create plasmas with electron temperatures above 10 keV and with ion densities of (1–2) x 10^{14} cm^{-3}. These values are required in order to obtain the nuclear fusion reaction between deuterium and tritium atoms, because reasonable crosssections for the fusion reactions are obtained only for energies above 5 KeV. Central ions temperature of T_i « 35 KeV and electron temperature of Te = 15 KeV have been reached in Tokomak fusion reactors [10].

Taking into account the wide ranges of parameters, the plasmas are classified into several categories:

– Plasmas in complete thermodynamic equilibrium (CTE plasmas). CTE plasmas exist only in stars or during the short interval of a strong

explosion. They have no practical importance because they do not exist in controlled laboratory conditions.

– Plasmas in local thermodynamic equilibrium (LTE plasmas). These are plasmas in which all temperatures, except the radiation temperature, T_r, are equal in each small volume of the plasma.

– Plasmas that are not in any local thermodynamic equilibrium – non – LTE plasmas. These plasmas, also named cold plasmas.

The plasmas produced for research or manufacturing purposes are either LTE or non – LTE type plasmas, designated in daily use, respectively, as thermal and cold plasmas.

1.7 Coalitional processes in plasma

Collisions between charged particles in a plasma differ fundamentally from those between molecules in a neutral gas because of the long range of the Coulomb force. In fact, it is clear from the discussion in Sect. 1.7 that *binary* collision processes can only be defined for weakly coupled plasmas. Note, however, that binary collisions in weakly coupled plasmas are still modified by collective effects – the many-particle process of Debye shielding enters in a crucial manner. Nevertheless, for large Λ we can speak of binary collisions, and therefore of a *collision frequency*, denoted by $\nu_{ss'}$.

$$V_s \approx \sum_{s'} \nu_{ss'} \tag{28}$$

Here, $\nu_{ss'}$ measures the rate at which particles of species s are scattered by those of species s′. When specifying only a single subscript, one is generally referring to the *total* collision rate for that species, including impacts with all other species. Very roughly,

1.7.1 Collision cross sections, mean-free paths and collision frequencies

Before proceeding with quantitative treatments of these effects, we must introduce the idea of a collision ‘cross section’. A cross section can be defined for any kind of collision, but for present purposes it is sufficient to consider the case of an electron colliding with a neutral atom. Even in this restricted case there can be two types of collisions: (1) ‘elastic collisions’ in which the electron essentially ‘bounces’ off the atom, with the two particles retaining their identities as electron and atom, and the atom remaining in the same energy state; and (2) ‘inelastic collisions’, such as ionization or excitation, in which one or more of the particles

changes its identity or internal energy state. In the first case, the electron may lose any fraction of its initial momentum, depending on the angle at which it rebounds. The probability of momentum loss can be expressed in terms of the equivalent cross section σ that the atoms would have if they were perfect absorbers of momentum. In the second case, the probability of ionization, for example, can be expressed in terms of the equivalent cross section σ that an atom would have if it were ionized by all electrons striking within this cross sectional area.

In Fig. 5, electrons are incident upon a thin slab of thickness *dx* containing *n*, neutral atoms per unit volume. The atoms are imagined to be opaque spheres of cross sectional area a: i.e. every time an electron strikes the area blocked by the atom, either it loses all of its momentum (elastic collision) or it ionizes the atom (inelastic collision).

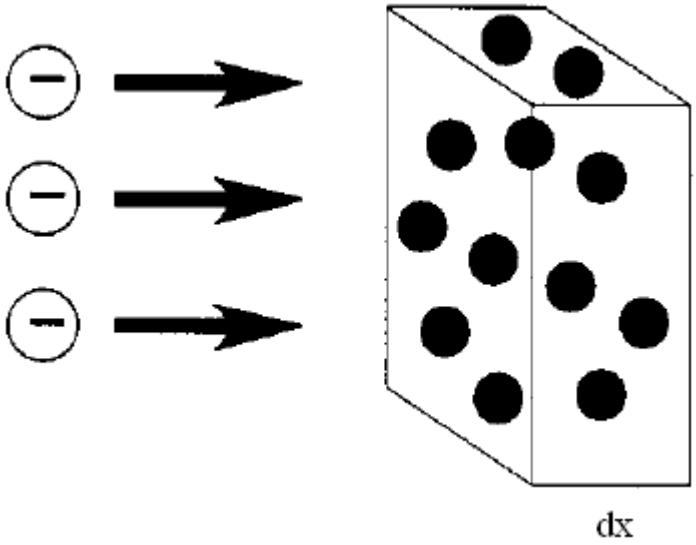

Fig. 5. Electrons incident on a thin slab of thickness ***dx*** *containing neutral atoms of density* ***n***

The number of atoms per unit area of the slab is $n_n dx$ and the fraction of the slab blocked by atoms is $n_n \sigma dx$. If a flux *r* of electrons is incident on the slab, the flux emerging on the other side is $\Gamma+d\Gamma = \Gamma(1-n\sigma dx)$, so that the change of flux r with distance x is given by

$$\frac{d\Gamma}{dx} = -n_n \sigma \Gamma \qquad (29)$$

which has the solution

$$\Gamma = \Gamma_0 \exp(-n_n \sigma x) = \Gamma_0 \exp(-x/\lambda_{mfp}) \qquad (30)$$

where

$$\lambda_{mfp} = (n_n \sigma)^{-1} \tag{31}$$

The quantity A_{mfp} is called the mean-free path for collisions. In a distance A_{mfp}, the flux would be decreased to 1/e of its initial value. In other words, an electron travels a distance λ_{mfp} before it has a reasonable probability of colliding with an atom. For electrons of velocity v, the mean time between collisions is given by

$$\tau = \lambda_{mfp} / v \tag{32}$$

The 'collision frequency', namely the inverse of τ, is usually defined in terms of an average over all velocities in the Maxwellian distribution (which may have different individual collision frequencies), namely

$$v = \left\langle \tau^{-1} \right\rangle = n_n \left\langle \sigma v \right\rangle = (n_n / n_e) \int f_e(v) \sigma(v) v d^2 v \tag{33}$$

As is implied by this formula, for more complex collisional processes than that illustrated in Fig. 4, the cross section σ is often itself a function of the velocity v of the incident particle.

1.8 Coronal equilibrium

In the case where the collision of the electron with the atom results in ionization of the atom, we may calculate the rate of production of new electrons per unit volume simply by multiplying the ionization collision frequency of the electrons, equation (34), by the electron density, n_e. This 'source rate' S_e of electrons is given by

$$S_в = n_в n_n \left\langle \sigma_{ion} v_в \right\rangle \tag{34}$$

where σ_{ion} is the cross section for electron-impact ionization and where we assume that the electron velocities υ_e greatly exceed the neutral velocities υ_n so that the velocity of impact comes mainly from the electron's motion. This cross section is definitely a strong function of electron velocity, at least below energies of about 30 eV, so the averaging over the Maxwellian distribution of electrons is necessary. There is, of course, an equal and opposite 'sink rate' for neutral atoms, i.e. neutral atoms are lost by ionization at the same rate per unit volume, S_e.

The dependence of the ionization cross section σ_{ion} for hydrogen atoms on the energy of the bombarding electron is shown in Fig. 6, and the ionization rate (σ_{ion} v_e) averaged over a Maxwellian distribution of electrons is shown in Fig. 7. The maximum cross section σ_{ion} reached for electrons with energies somewhat above E_i (the Rydberg ionization energy,

which is about 13.6eV for hydrogen) and is in the neighborhood 10^{20} m^2, the 'size' of the hydrogen atom. However, the ionization rate is significant even for electron temperatures well below E_i, because a Maxwellian distribution still contains a few energetic electrons that are efficient ionizers. A good approximation to the data is given by the simple formula

$$\langle \sigma_{ion} v_e \rangle = \frac{2.0\times10^{-13}}{6.0+\frac{T_e(eV)}{13.6}} \left(\frac{T_e(eV)}{13.6}\right)^{1/2} \exp\left(-\frac{13.6}{T_e(eV)}\right) m^3 s^{-1} \qquad (35)$$

The source rate for neutrals (corresponding to a sink term for electrons) in a plasma in coronal equilibrium is given by

$$S_n = n_e n_i \langle \sigma_{rec} v_e \rangle \qquad (36)$$

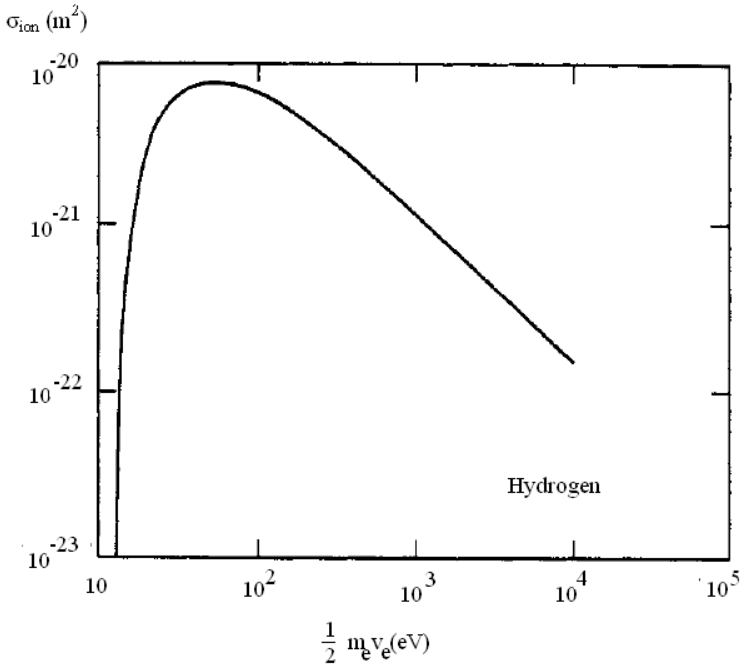

Fig. 6. Ionization cross section σ for hydrogen atoms as a function of the energy of the bombarding electron

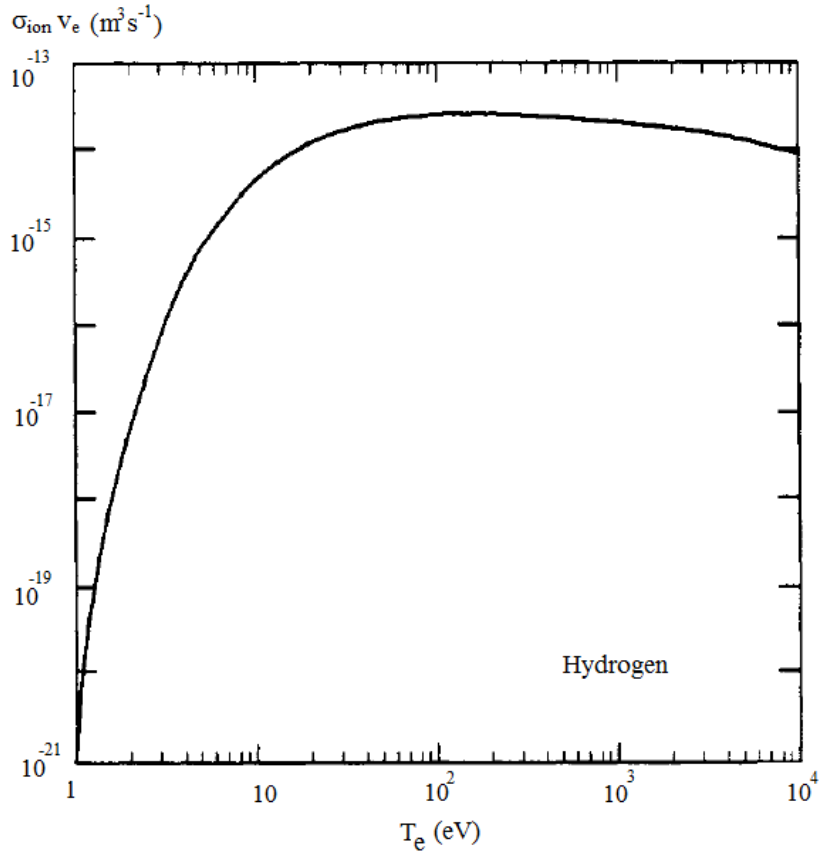

Fig. 7. Ionization rate ($\sigma_{ion}\, v_e$) of electron-impact ionization of hydrogen atoms averaged over a Maxwellian distribution of electrons, temperature T_e

where $\sigma_{\mathbf{rec}}$ is the cross section for radiative recombination. For a neutral hydrogen plasma, $n_i=n_e$. A good approximation to the data on radiative recombination in the relevant temperature regime is given by the simple formula

$$\langle \sigma_{ion} v_e \rangle = 0.7\times 10^{-19} \left(\frac{13.6}{T_e(eV)}\right)^{1/2} m^3 s^{-1} \qquad (37)$$

The degree of ionization of a homogeneous hydrogen plasma in coronal equilibrium is given by balancing the source of electrons by collisional ionization against the sink of electrons by radiative recombination. We find that, at an electron temperature of approximately the ionization potential, i.e. 13.6 eV, the plasma is almost fully ionized so that the neutrals constitute only about one part in10^5. Only at electron temperatures below about 1.5 eV is the plasma less than 50 % ionized. Fig. 8 shows the degree of ionization, i.e. n_e/n_n, against electron temperature for the coronal equilibrium model, and also for higher-density plasmas where three-body recombination has been included.

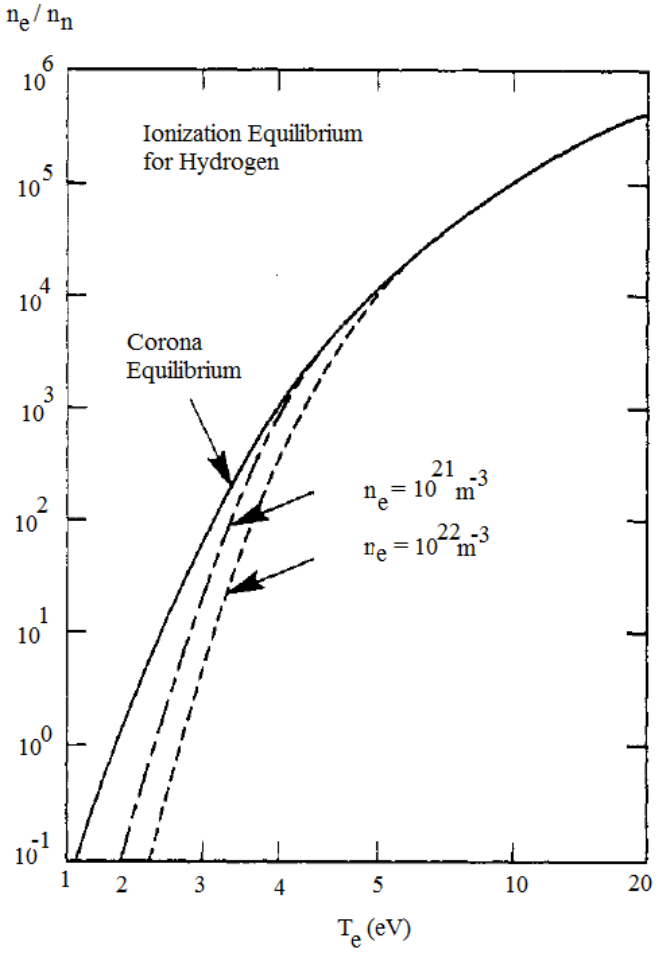

Fig. 8. Ionization equilibrium for hydrogen in the coronal equilibrium model, and at higher electron densities with three-body recombination included

The concept of coronal equilibrium can be generalized to the case of a plasma composed of, or containing an admixture of, high-Z ions. In such cases, depending mainly on the electron temperature, the ions will be stripped of their outer-shell electrons but will retain some bound inner-shell electrons. An equilibrium distribution among the various ionization states arises which, in the solar corona for example, is determined by balancing the processes of impact ionization and radiative recombination for each ionization state. A particular case is illustrated in Fig. 9, which shows the fractional abundances in the various ionization levels of oxygen as a function of electron temperature in coronal equilibrium. We see that oxygen ions are stripped of all six outer-shell electrons (giving an ion with charge – number $Z = 6$) at electron temperatures of about 30eV, but to remove the final two inner-shell electrons to produce fully stripped oxygen with Z = 8 requires temperatures in excess of about *200* eV. The va-

lidity of any coronal equilibrium model depends on the time-scale for reaching ionizationhecombination balance (for the *slowest* such process, generally at the highest relevant ionization state, in the case of high-Z ions) being much shorter than the timescale on which particles are introduced into, or lost from, the plasma. If this 'confinement' time begins to be comparable to the slowest atomic processes, the ionization balance shifts towards lower charge states. If hydrogen neutrals are present, there is also the possibility of a 'charge-exchange' event, in which the electron of a neutral hydrogen atom is captured by a high-Z ion; this process also lowers the charge-state balance of the high-Z ions. Both electrons then decay to the ground state, emitting photons. Dielectronic recombination has not been included in calculating the charge-state distribution shown in Fig. 9.

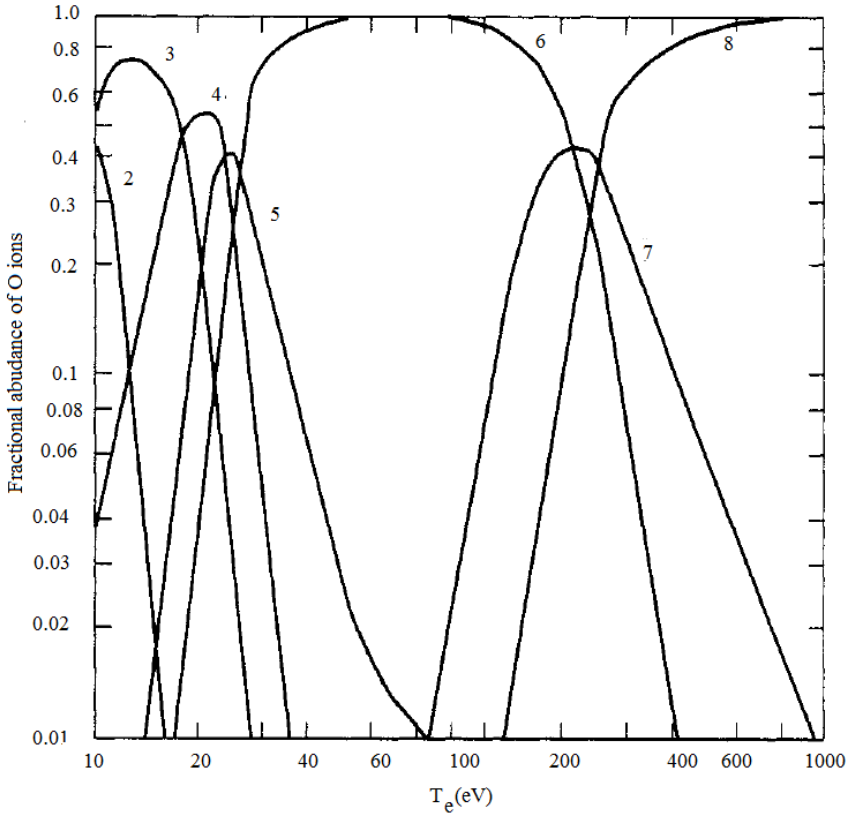

Fig. 9. Fractional abundances in the various ionization levels for oxygen ions as a function of electron temperature in coronal equilibrium. Fully ionized oxygen has Z = 8

For high-Z ions, another process known as 'dielectric recombination' can play a significant role in the charge – state balance. In this recombination process, a free electron is captured into an excited state and the excess energy that is available is invested in excitation of a different bound electron to a higher state.

1.9 Penetration of neutrals into plasmas

To complete our discussion of neutrals in plasmas, we should consider what happens at the edge of a hot dense plasma that is enveloped by neutral gas. This situation arises in many laboratory plasmas-magnetically confined fusion plasmas or low-pressure arc discharges, for example. In such cases, the plasma is often hot and dense enough to be fully ionized, but the electrons and ions that diffuse out of the plasma recombine into neutral atoms when they strike the containing vessel. The neutral atoms thus formed are often reflected back into the plasma (or other neutrals are desorbed from 'saturated' vessel walls), where they are ionized again. Depending on the surface material of the containing vessel (and whether its surface is already saturated with a layer of hydrogen molecules), this process of recycling can be almost 'perfect', i.e. the plasma density is maintained almost indefinitely despite diffusive losses of charged particles, because the lost particles reappear one – for – one as neutrals which are readily ionized again by the plasma. For hot dense laboratory plasmas, this recycling process occurs entirely at the plasma edge, because the main body of the plasma is 'opaque' to neutrals, i.e. a neutral atom has almost no chance of reaching the center of the plasma before being ionized. Recombination in the plasma (as distinct from at the vessel surface itself) is usually unimportant in this situation: the neutral density in the edge region of the plasma is set by a balance between the influx from outside and the ionization within the plasma.

Neutral atoms entering the plasma with velocity v_n, will penetrate a distance given by the neutral 'mean-free path' for ionization, i.e.

$$\lambda_n = \frac{v_n}{n_в(\sigma_{ion} v_в)} \tag{38}$$

This can be derived by noting that the volumetric ionization rate is given by $n_в n_n$ (σ_{ion} v_e) for $v_e >> v_n$, implying that the effective 'collision frequency' of the neutrals must be $n_в$ (σ_{ion} v_e). The thermal velocity of neutral hydrogen `atoms at 'room temperature' is about 2×10^3 m s^{-1}. If the electron temperature in the edge – region of the plasma reaches (10 – 20) eV, the ionization rate **(**σ_{ion} υ_e**)** is about 10^{-14} m^3 s^{-1}. Thus, we have $\lambda_n(m) = 2 \times 10^{17} / n_e(m^{-3})$. For example, if the density of the edge-region plasma is about 10^{19} m^{-3}, typical of many magnetically confined fusion plasmas, the neutrals will only penetrate about 2 cm into the plasma. In many practical cases, such as neutrals re-emerging from a saturated surface, the hydrogen appears initially in molecular, rather than atomic, form. In such cases, the first effect of electron impact is molecular disso-

ciation, which produces two atoms with equal and opposite momenta and each with energy of about 3eV; the atom with momentum directed toward the plasma can penetrate somewhat further into the plasma.

A second atomic process-known as 'charge exchange'-allows much deeper penetration of hot dense plasmas by neutrals. In hydrogen charge exchange, an energetic plasma proton captures the electron from a lower-energy neutral. As a result, it can escape from the plasma, or move further into the plasma, as an energetic neutral, as illustrated in Fig. 10.

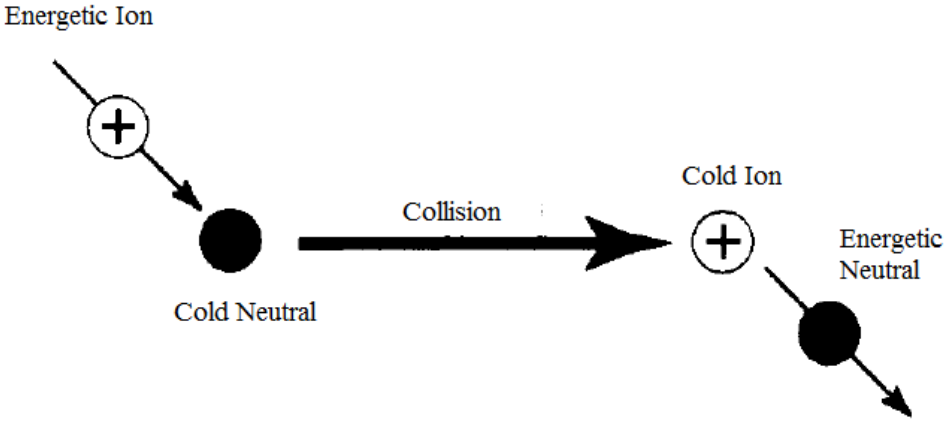

Fig. 10. Charge-exchange process in which an energetic ion takes an electron from a cold neutral, thereby becoming an energetic neutral

In Fig. 10 time just before the charge-exchange collision is shown to the left of the thick black arrow; a time just after the collision is shown to the right.

Not much energy is exchanged by the charge – exchange collision itself the emerging neutral has about the same energy as the incident plasma ion.

The cross section for charge-exchange of hydrogen atoms bombarded by protons of various energies is shown in Fig. 11. In the energy range of most interest for laboratory plasmas and the edge-region of fusion plasmas ((10 – 100) eV), the cross section is seen to be quite large ($\sim$4 x 10^{-19} m^2), almost a hundred times larger than the ionization cross section. (The cross section is large because charge exchange is a *resonant* process, where the initial and final quantum mechanical states have no difference in energy.) For a plasma with $T_e \approx T_i$ the charge-exchange rate (ν_i) is usually two-to-three times larger than the ionization rate ($\sigma_{ion}\, v_e$). The process of charge exchange essentially prevents a *hot-ion* plasma from ever being formed with an appreciable neutral-gas density in the hot region. The cross section for charge exchange is so large that, if this were to occur, each energetic ion would readily turn into an energetic neutral, which

would escape, so that the hot plasma would quickly be converted into cold plasma.

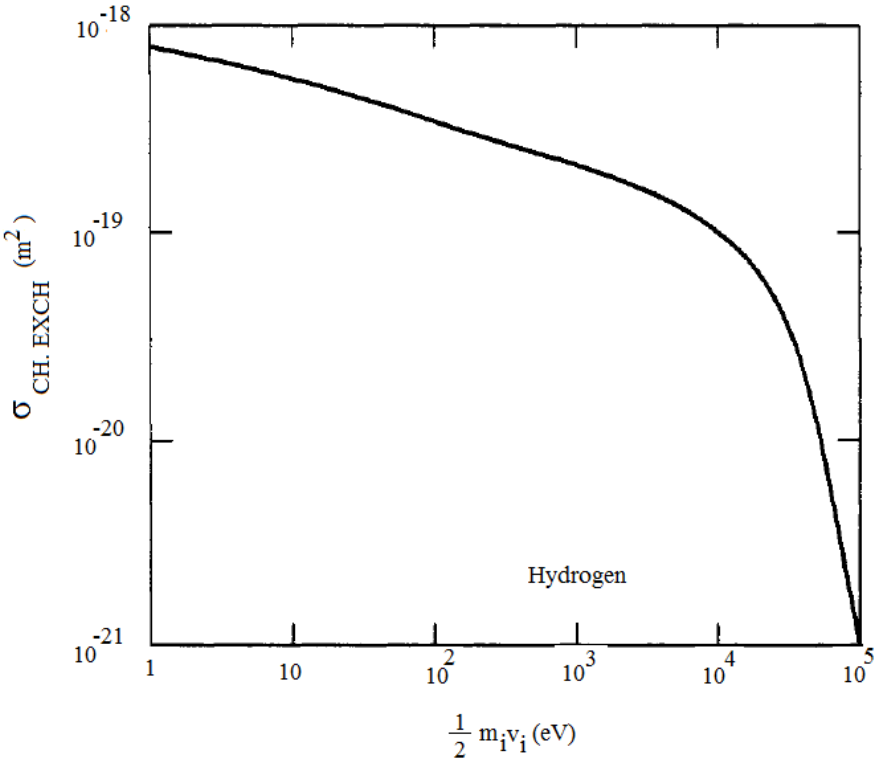

Fig. 11. Cross section for charge exchange in hydrogen against the energy of the bombarding ion

A low-energy neutral atom injected into the edge-region of a plasma has a somewhat higher probability of undergoing a charge-exchange event than of being ionized. Thus, it might appear that charge exchange would *reduce* the penetration of neutrals into hot dense plasmas. In fact the opposite is true, because charge exchange produces a second generation of more energetic neutrals, with energies comparable to the ion energies in the region of the plasma where charge exchange occurs. While some of these more energetic second-generation charge-exchange neutrals will escape from the plasma, others will penetrate much more deeply into the plasma interior than did the first generation neutrals, until these neutrals themselves are ionized or produce a third generation of charge-exchange neutrals with even higher energies. Two neutral trajectories-one ionized and one charge-exchanged – are illustrated in Fig. 12. The production of multiple generations of increasingly penetrating neutral atoms by charge exchange is primarily responsible for the presence of any neutrals at all in the center of a hot dense plasma. In the core of the plasma, these neutrals have ‘thermalized’ with the plasma ions-i.e. they have

about the same average energy. However, charge-exchange transport still provides an avenue for ion energy loss from the plasma.

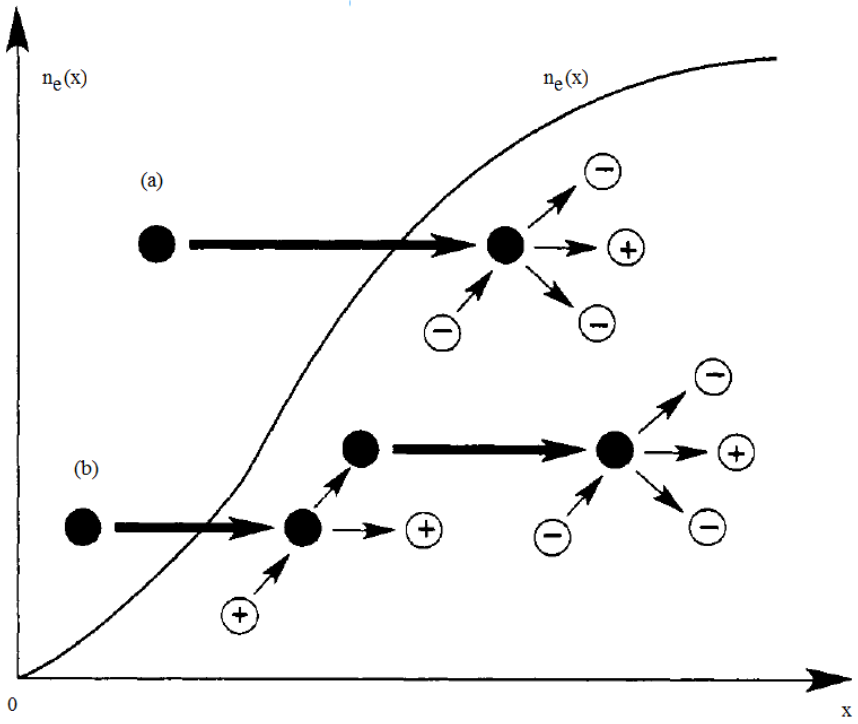

Fig. 12. Trajectories of two neutrals incident (thick arrows on the left) upon a plasma of increasing density

Neutral (a) is ionized. Neutral (b) undergoes charge exchange, producing a more energetic neutral that penetrates (thick arrows on the left) further into the plasma before being ionized.

1.10 Collisions with neutrals and with charged particles: relative importance

Finally, we return to the question raised of the beginning of this Chapter: what is the relative importance of collisions of charged particles in a plasma with other charged particles versus collisions with neutral particles?

The cross section for elastic scattering of an electron by a neutral atom may be estimated very roughly as

$$\sigma_n \approx \pi a_0^2 \approx 10^{-20}\, m^2 \tag{39}$$

At the distance a_0, an incoming electron has a substantial chance of undergoing a large-angle collision. On the other hand, when an electron

comes within a distance r of a singly charged (e.g. hydrogen) ion, it experiences an attractive Coulomb force:

$$F_r = -e^2 / 4\pi\varepsilon_0 r^2 \qquad (40)$$

which tends to deflect the electron orbit toward the ion. When the angle of deflection is as much as 90^0, the electron's initial momentum is mostly lost.

Thus, from the viewpoint of momentum exchange, a 'close encounter' with the Coulomb force of another charged particle is essentially the same as a 'collision'. The angle of deflection will be large when the potential energy of the Coulomb interaction equals the kinetic energy of the colliding electron, i.e.

$$e^2 / 4\pi\varepsilon_0 b \approx mv^2 / 2 \approx T_e \qquad (41)$$

where m and $\boldsymbol{U}$ are the mass and velocity of the electron, and where b is the distance of closest approach of the electron to the ion. This serves to define an effective 'Coulomb cross section' of the ion, namely

$$\sigma_i \approx \pi b^2 \approx \frac{\pi e^4}{(4\pi\varepsilon_0)^2 T_e^2} \approx 10^{-17} / T_e(eV)^2 m^2 \qquad (42)$$

where $T_e(eV)$ denotes the electron temperature measured in *eV*.

Comparing σ_n with σ_i, simply using equation (40) for the latter, and consulting Fig. 12 to relate the degree of ionization to T_e, we see that Coulomb collisions will dominate over collisions with neutrals in any plasma that is even just a few per cent ionized. Only if the ionization level is very low ($<10^{-3}$) can neutral collisions dominate. Moreover, a plasma becomes almost fully ionized at electron temperatures above about 1 eV. Thus, the case of collisions with neutrals is not of much concern to the physicist interested in high-temperature plasmas. Not only are high-temperature plasmas almost fully ionized, but the dynamical behavior of charged particles even in partially ionized plasmas with more than very small ionization levels tends to be dominated by Coulomb collisions with other charged particles, rather than by collisions with neutrals. Of course, the various inelastic scattering processes involving high – Z ions discussed in the previous Section, i.e. ionization, recombination and excitation, are still more important than Coulomb collisions in determining the radiation from high – temperature plasmas, provided only that there remains a sufficient fraction of these ions in partially stripped ionization levels.

Chapter 2. Introduction to gas discharge physics

2.1 What Is the Subject of Gas Discharge Physics?

The term "gas discharge" originates with the process of discharge of a capacitor into a circuit incorporating a gap between electrodes. If the voltage is sufficiently high, electric break down occurs in the gas and an ionized state is formed. The circuit is closed and the capacitor discharges. Later the term "discharge" was applied to any flow of electric current through ionized gas, and to any process of ionization of the gas by the applied electric field. As gases ionized to a sufficient degree emit light, it has become customary to say that a discharge "lights up", or is "burning".

As a rule, the flow of electric current is associated with the notion of a circuit composed of conductors. Actually, a closed circuit or electrodes are not needed for a directed motion of charges (electric current) in rapidly oscillating electric fields, and even less so in the field of electromagentic radiation. However, quite a few effects observed in gases subjected to oscillating electric fields and electromagnetic waves (breakdown, maintaining the state of ionization, dissipation of energy of the field) are not different, in principle, from dc phenomena. Nowadays all such processes are referred to as discharges and included within gas discharge physics. The fact that electric current flow in open circuits in the field of electromagnetic waves is of no general significance. In such cases, the dissipation of the energy of the field is described not as the release of the Joule heat by electric current, but as the absorption of radiation.

The modern field of gas discharge physics is thus occupied with processes connected with electric currents in gases and with generating and maintaining the ability of a gas to conduct electricity and absorb electromagnetic radiation. Gas discharge physics covers a great variety of complex, multi-faceted phenomena; it is full of an enormous amount of experimental facts and theoretical models.

The reader who is interested in this field of gas discharges is referred to an excellent book written by Yuri Raizer [11].

Before we begin their analysis, it is expedient to single out the main types of discharge processes and clarify them.

2.2 Typical Discharges in a Constant Electric Field

A relatively simple experiment introduces us to several fundamental types of discharge. Two metal electrodes connected to a dc power supply are inserted into a glass tube (Fig. 13). The tube can be evacuated and

filled with various gases at different pressures. The quantities measured in the experiment are the voltage between the electrodes and the current in the circuit. This classical device served the study of discharge processes for nearly 150 years, and still remains useful.

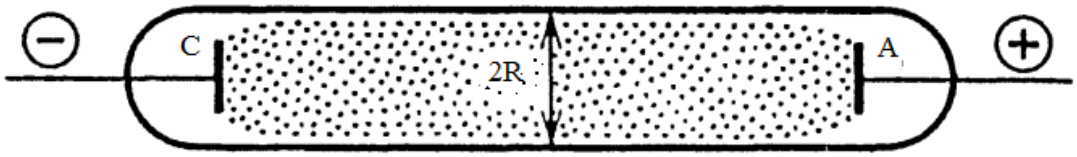

Fig. 13. Typical gas discharge tube

If a low voltage is applied to the electrodes, say several tens of volts, no visible effects are produced, although a supersensitive instrument would record an extremely low current, on the order of 10 ~15 A. Charges are generated in the gas by cosmic rays and natural radioactivity. The field pulls them to the opposite - sign electrodes, producing a current. If the gas is intentionally irradiated by a radioactive or X-ray source, a current of up to 10 ~6 A can be produced. The resultant ionization is nevertheless too small to make the gas emit light. A discharge and an electric current that survive only while an external ionizing agent or the emission of electrons or ions from electrodes is deliberately maintained (e.g. by heating the cathode) are said to be non-self-sustaining. As the voltage is raised, the *non-self-sustaining current* first increases because most of the charges produced by ionization are pulled away to electrodes before recombination occurs. However, if the field manages to remove all new charges, the current ceases to grow and reaches saturation, being limited by the rate of ionization.

As the voltage is raised further, the current sharply increases at a certain value of V and light emission is observed. These are the manifestations of breakdown, one of the most important discharge processes. At pressure $P \sim 1$ Torr and interelectrode gap $L \sim 1$ cm, the breakdown voltage is several hundred volts. Breakdown starts with a small number of spurious electrons or electrons injected intentionally to stimulate the process: The discharge immediately becomes *self- sustaining*. The energy of electrons increases while they move in the field. Having reached the atomic ionization potential, the electron spends this energy on knocking out another electron. Two slow electrons are thus produced, which go on to repeat the cycle described above. The result is an electron avalanche, and electrons proliferate. The gas is appreciably ionized in 10^{-7} to 10^{-3} s, which is sufficient for the current to grow by several orders of magnitude.

Several conditions determine how the process develops at higher voltage. At low pressure, say 1 to 10 Torr, and high resistance of the external circuit (it prevents the current from reaching a large value), *a glow discharge* develops. This is one of the most frequently used and important types of discharge. It is characterized by low current, $i \sim 10^{-6}$-10^{-1} A in tubes of radius $R \sim 1$ cm, and fairly high voltage: hundreds to thousands of volts. A beautiful radiant column, uniform along its length, is formed in sufficiently long tubes of, say, $L \sim 30$ cm at $P \sim 1$ Torr. (This is how glowing tubes for street advertisements are made.) The ionized gas in the column is electrically neutral practically everywhere except in the regions close to the electrodes; hence, this is a plasma. The glow discharge plasma is very weakly ionized, to $x = 10^{-8}$-10^{-6} (where x denotes the fraction of ionized atoms), and is non-equilibrium in two respects. Electrons that get energy directly from the field have a mean energy $\bar{\varepsilon} \approx 1eV$ and a temperature $T_e \approx 10^4 K$. The temperature T of the gas, including the ions, is not much higher than the ambient temperature of 300 K. This state, with widely separated electron and gas temperatures, is sustained by a low rate of Joule heat release under conditions of relatively high specific heat of the gas and high rate of its natural cooling. Also as a result of the high rate of charge neutralization in a cold gas, its degree of ionization is many orders of magnitude lower than the thermodynamic equilibrium value corresponding to the electron temperature.

If the pressure in the gas is high (about the atmospheric level) and the resistance of the external circuit is low (the circuit allows the passage of a high current), *an arc discharge* usually develops soon after breakdown. Arcs typically burn at a high current ($i > 1$ A) at a low voltage of several tens of volts; they form a bright column. The arc releases large thermal power that can destroy the glass tube: Arcs are often started in open air! Atmospheric-pressure arcs usually form thermodynamic equilibrium plasmas (the so-called low-temperature plasma), with $T_e \approx T \approx 10^4 K$ and the ionization of $x = 10^{-3} \div 10^{-1}$ corresponding to such temperatures. The arc discharge differs essentially from the glow discharge in the mechanism of electron emission from the cathode, which is vital for the flow of dc current of the arc. In the glow discharge, electrons are knocked from the surface of the cold metal by impacts of positive ions. In the arc discharge, the high current heats up the cathode, and thermionic emission develops.

If $P \sim 1$ atm, the interelectrode gap $L > 10$ cm, and the voltage is sufficiently high, sparking occurs. The *breakdown* in the gap develops by rapid growth of the plasma channel from one electrode to another. Then

the electrodes are as if short - circuited by the strongly ionized spark channel. Lightning, whose "electrodes" are a charged cloud and the ground, is a giant variety of the *spark discharge*.

Finally, *a corona discharge* may develop in strongly nonuniform fields that are insufficient for the breakdown of the entire gap: A radiant corona appears at sharp ends of wires at sufficiently high voltage and also around power transmission line conductors.

2.3 Brief History of Electric Discharge Research

Leaving lightning aside, man's first acquaintance with electric discharges was the observation, dating back to 1600, that friction-charged insulated conductors lose their charge. Coulomb proved experimentally in 1785 that charge leaks through air, not through imperfect insulation. We understand now that the cause of leakage is the non-self-sustaining discharge.

Occasional experiments were conducted in the 18th century with sparks produced by charging a body by an electrostatic generator, and with atmospheric electricity, experiments with lightning sometimes having tragic consequences.

Sufficiently powerful electric batteries were developed at the beginning of the 19th century to allow the discovery of the arc discharge. V.V. Petrov, who worked in the Saint Petersburg Medical Surgery Academy in Russia, reported the discovery in 1803. The arc was obtained by bringing two carbon electrodes connected to battery terminals into contact and then separating them. Several years later Humphrey Davy in Britain produced and studied the arc in air. This type of discharge became known as "arc" because its bright horizontal column between two electrodes bends up and arches the middle owing to the Archimedes' force. In 1831-1835, Faraday discovered and studied the glow discharge. Faraday worked with tubes evacuated to a pressure $P \sim 1$ Torr and applied voltages up to 1000 V. The history of physics of gas discharges in the late 19th and early 20th centuries is inseparable from that of atomic physics. After William Crookes's cathode ray experiments and J.J. Thomson's measurements of the *e/m* ratio, it became clear that the current in gases is mostly carried by electrons. A great deal of information on elementary processes involving electrons, ions, atoms, and light fields was obtained by studying phenomena in discharge tubes.

Beginning in 1900, J.S.E. Townsend, a student of J.J. Thomson and the creator of a school in the physics of gas discharges discovered the laws governing ionization and the gaseous discharge (known as the

Townsend discharge) in a uniform electric field. Numerous experimental results were gradually accumulated on cross sections of various electron-atom collisions, drift velocities of electrons and ions, their recombination coefficients, etc. This work built the foundations of the current reference sources, without which no research in discharge physics would be possible. The concept of a plasma was introduced by I. Langmuir and L. Tonks in 1928. Langmuir made many important contributions to the physics of gas discharge, including probe techniques of plasma diagnostics.

As regards different frequency ranges, the development of field generators and the research into the discharges they produce followed the order of increasing frequencies. Radio frequency (*rf*) discharges were observed by N. Tesla in 1891. This kind of discharge is easily produced if an evacuated vessel is placed inside a solenoid coil to which high-frequency voltage is applied. The electric field induced by the oscillating magnetic field produces breakdown in the residual gas, and discharge is initiated. The understanding of the mechanism of discharge initiation came much latter, in fact, after the work of J.J. Thomson in 1926-1927. Inductively coupled *rf* discharges up to tens of kW in power were obtained by G.I. Babat in Leningrad around 1940.

The progress in radar technology drew attention to phenomena in microwave fields. S.S. Brown in the USA began systematic studies of microwave discharges in the late 1940s. Discharges in the optical frequency range were realized after the advent of the laser: A spark flashed in air when the beam of a ruby laser producing so-called giant pulses (of more than 10 MW in power) was focused by a lens, this success being achieved in 1963. Continuously burning optical discharges, in which dense steady-state plasma is sustained by the energy of light radiation, were first initiated in 1970 by a cw CO_2 laser. Optical discharges (this term reflects a large degree of similarity with conventional discharges) immediately attracted considerable attention. Both microwave and optical discharges have by now been studied with at least the same thoroughness that the discharges in constant electric fields has been during nearly 100 years of research.

The physics of the glow discharge, one of the oldest and, presumably, best- studied fields, has lived through an unparallel revival in the past 15-20 years, and numerous new aspects of this phenomenon have been revealed. This surge of attention was stimulated by the use of glow discharges in electric-discharge CO_2 lasers developed for the needs of laser technologies. Likewise, the application of plasmatrons (generators of dense low-temperature plasma) to metallurgy, plasma chemistry, plasma welding and cutting, etc. provided a stimulus for new extensive, detailed

studies of arc plasma at **P** ~ 1 atm, T ~ 104 K, and of similar discharges in all frequency ranges. These, and many other practical applications of gas discharge physics place it within the range of sciences that lie at the foundation of modern engineering.

2.4 Mechanism of electrical discharges

2.4.1 Cathode processes

In general, laboratory discharges are created between electrodes and these electrodes can supply the discharge with electrons through various physical processes. Under normal conditions electrons in a metal are prevented from leaving that metal by electrostatic forces between the electrons and the ions in the metal lattice. As shown in Fig. 14 a the electrons in the metal are trapped in a potential well. The energy necessary to remove an electron from the top of the Fermi energy levels is known as the work function of the metal. This is denoted by φ in Fig. 14 a [12].

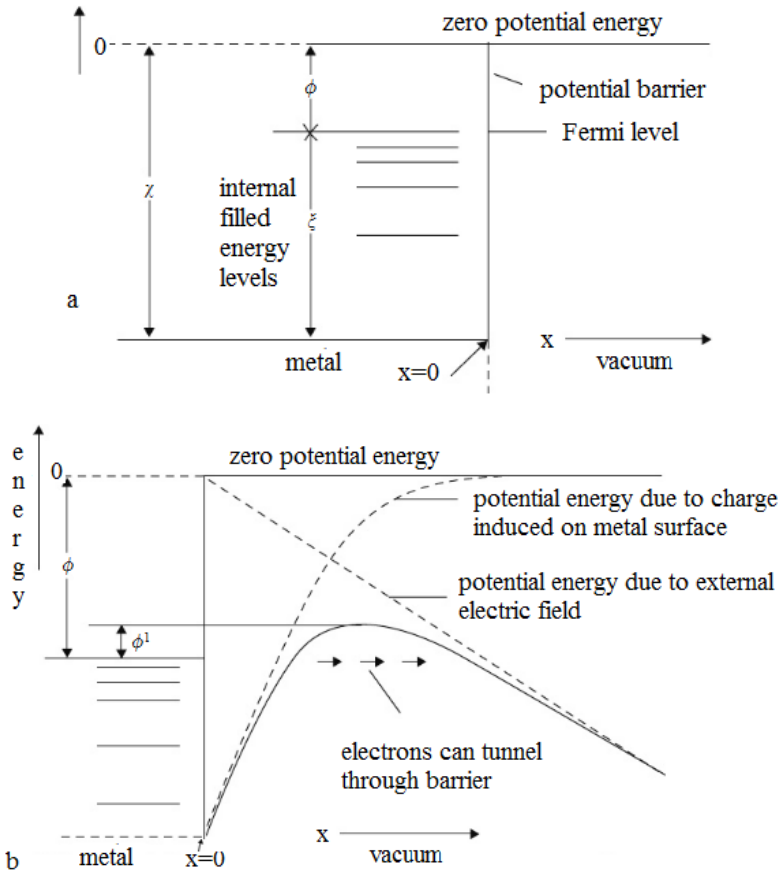

Fig. 14. Energy diagram: a) electrons in a metal; b) when an electric field is applied

Note that the electric field not only reduces the height of the barrier but it also reduces the thickness of the barrier. This makes it easier for the energetic electrons to jump over the barrier (Schottky effect) and a certain percentage of the electrons to tunnel through the barrier

The work functions of typical metals are tabulated in Table 3 [13].

Table 3. Work function for typical elements

Element	Ag	Al	Cu	Fe	W
W_α(eV)	4.74	2.98-4.43	4.07-4.7	3.91-4.6	4.35-4.6

Electrons can be removed from the metal either by giving the electrons sufficient kinetic energy to surmount the potential barrier, or the work function, at the surface, by reducing the height of the barrier so that the electrons can overcome it or by reducing the thickness of the barrier so that the electrons can tunnel through it. The first can be achieved by the application of heat to the electrode, through impact of photons on the surface of the electrode or by the incidence of particles such as other electrons, positive ions, neutral molecules, metastable atoms onthe electrode. The reduction in the potential barrier height or its thickness can beachieved by the application of an electric field in the correct direction so that the electrons will experience a force directed out of the metal surface (see figure 14 b).Let us consider different physical processes that can cause emission of electrons from metals.

2.4.2 Photoelectric emission

When a photon is incident on a metal it can transfer all its energy to an electron in the metal so that the latter can surmount the potential barrier at the surface. Thus, an electron at the Fermi level after absorbing the energy of the quanta can escape with energy E_e given by:

$$E_e = h\nu - \phi \tag{43}$$

Where $h\nu$ is the energy of the photon. For a clean Ag surface φ=4.74eV (Table 3) and the threshold frequency corresponds to a wavelength of 2616 Å.

2.4.3 Thermionic emission

In metals at room temperature the energy of the conduction electrons is not sufficient for them to surmount the potential barrier at the surface of metals. However, heating a metal will increase the kinetic energy of its electrons. With increasing temperature one may expect the number of electrons surmounting the barrier to increase. Since this process is caused by the heating of the electrode it is called thermionic emission. The thermionic current density, J_t , is given by the following equation [14]:

$$J_t = AT^2 \exp(-\phi / kT) \tag{44}$$

Where k is the Boltzman constant, φ is the work function of the metal, T is the absolute temperature and A is a constant equal to 120 A cm^{-2} deg^{-2}.

Actually, the experimentally obtained current densities are smaller than those predicted by his equation because this equation does not take into account the wave nature of electrons and the possibility that some of the electrons will be reflected at the barrier even if they have enough energy to overcome it.

2.4.4 Schottky effect

As one can see from the equation given in the previous section, the thermionic current depends on the height of the barrier that the electrons have to surmount in order to come out of the metal. The height of this barrier can be decreased by the application of an electric field in such a way that the electrons in the metal experience a force out of the metal. This is illustrated in Fig. 14 b.

In the presence of such an electric field the work function is effectively reduced to [15]:

$$\phi_1 = \phi - \sqrt{\frac{e^3 E}{4\pi\varepsilon_0}} \tag{45}$$

This reduction in the barrier height will lead to a change in the thermionic emission current. Thus, if J_0 is the thermionic emission current density for zero electric field at temperature T then the current density at the same temperature in the presence of an electric field E is given by:

$$J_s = J_0 \exp(4.4\sqrt{E/T}) \tag{46}$$

where the electric field E is given in *V/cm* and T in Kelvins. This was shown to be valid for electric fields up to about 10^6 V/cm. This process of enhancement of the thermionic emission current due to the reduction in the barrier height is called *Schottky emission*.

2.4.5 Field emission

Calculations done with the Schottky equation show that the thermionic emission current at T = 293K for values of φ about 4.5eV is negligible even when the electric field reaches values as high as10^6 V/cm. However, experiments show that electrodes in vacuum do emit appreciable currents, in the range of μA, at such electric fields. The reason for this is the quantum nature of the elementary particles. The illustration in Fig. 14 b shows that the application of the electric field not only reduces the height of the barrier but will also decrease its thickness. In the absence of the electric field the barrier is infinitely thick but its thickness decreases with increasing electric field.

Electrons incident on the barrier can be represented by a wave; during the inter-action part of the wave will be reflected and the other part of the wave will be transmitted. The transmitted wave attenuates rapidly when moving into the barrier, but if the thickness of the barrier is not large a small fraction of the wave may be able to penetrate it. Of course, in the case of electrons, the reflection and transmission coefficients have to be regarded as probability functions, so there is a certain probability that an electron incident on the barrier will penetrate it. If the number of electrons incident on the barrier per unit time is known, quantum mechanical calculations can be performed to evaluate the number of electrons coming out of the barrier. Fowler and Norheim [16] analysed this process in detail and obtained the following expression for the field emission current density, J_f , for pure metallic surfaces in vacuum.

$$J_f = 61.6\times10^{-7}\frac{\xi^{1/2}E^2}{(\xi+\phi)\phi^{1/2}}\exp(-6.8\times10^7\phi^{3/2}/3E) \qquad (47)$$

Where ξ =5eV (typical value for metals),φ is the work function in eV, E is the electric field in *V/cm* and the current density is given in A/cm^2.

This equation indicates that measurable currents should be obtained for electric fields of the order of 10^7 V/cm. This has been found to be valid for very clean surfaces. Experiments show, however, that an appreciable electric field dependent emission current can be obtained for electric fields one to two orders of magnitude smaller than this in the presence of

surface contamination. The reason for this is that surface contamination causes a reduction in the width of the barrier thus enhancing the field emission process. Moreover, if there are protrusions on the surface the electric field at the tip of these protrusions can reach very high values leading to field emission from them. The field emission process is very important in providing initiatory electrons in the creation of electrical discharges.

2.5 Electrical breakdown

The physical processes that take place during the formation of an electric discharge can be summarised as follows. The electrical breakdown in a gas starts with a single electron which will lead to an avalanche of electrons created through the electron collision ionisation. As the avalanche grows the electric field created by charges concentrated at the avalanche head starts to modify the electric field in the vicinity of the head of the avalanche. When this space charge electric field reaches a critical value the avalanche will convert itself to a streamer discharge. If the gap is short then the streamer discharge may bridge the gap and, after streamer to spark transition, the complete breakdown of the gap may take place. If the gap is long many streamers may start from the electrode having their origin at a common streamer stem. The heat generated by the streamer currents will increase the temperature of the streamer stem and when the temperature reaches a critical value the thermal ionisation sets in the stem, the conductivity of the stem increases and it will convert itself to a leader discharge. Since the leader channel is a good conductor the potential of the electrode is now transferred to the head of the leader channel and the resulting high electric field will cause streamers to grow from the head of the leader channel. The leader elongates in the gap through the action of streamers that forge further and further into the gap. When the leader discharge reaches the grounded electrode the current in the channel increases, and the applied voltage collapses, leading to the formation of a spark. In the following sections the processes mentioned above are described.

2.5.1 Electron avalanche

Consider a free electron originated at x=0 in space and moving under the influence of a background electric field directed in the *x* direction. If the background electric field is larger than the critical value necessary for cumulative ionisation the electron may produce another electron through

ionisation collisions and these two electrons in turn will give rise to two more electrons. In this way the number of electrons increases with increasing *x*.

Assume that the number of electrons at a distance *x* from the origin is n_x. Let α be the number of ionising collisions per unit length made by an electron travelling in the direction of the electric field and η be the number of attachments over the same length. Here α is *Townsend's ionization coefficient* and η is the *attachment coefficient*. Consider an elementary length of width *dx* located at a distance x from the origin. In travelling across the length *dx*, n_x number of electrons will give rise to dn additional electrons:

$$dn = n_x(\alpha - \eta)dx \tag{48}$$

The solution of this equation is:

$$n_x = e^{(\alpha-\eta)x} \tag{49}$$

This equation shows that the number of electrons increases exponentially with dis-tance. This exponential growth of electrons with distance is called an *electron avalanche*. Fig. 15 shows a photograph of an electron avalanche obtained in a cloud chamber [17].

The equation also shows that cumulative ionisation is possible only if $(\alpha-\eta) > 0$. The quantity $(\alpha-\eta)$ is known as the *effective ionisation coefficient* and denoted by $\bar{\alpha}$.

Fig. 15. Cloud chamber photograph of a single electron avalanche (from [18])

It is important to note, however, that the value of n_x given in eqn. 49 is a mean value and it is subject to considerable variations due to the sta-

tistical nature of the collision process. The probability that one electron at the origin results in an avalanche of total number n at a distance x is given by

$$P(n,x) = \frac{1}{n_{\text{mean}}}\left[1-\frac{1}{n_{\text{mean}}}\right]^{n-1} \tag{50}$$

with a standard deviation given by:

$$\sigma = n_{\text{mean}}\left[1-\frac{1}{n_{\text{mean}}}\right]^{1/2} \tag{51}$$

Where

$$n_{\text{mean}} = e^{(\alpha-\eta)x} \tag{52}$$

For large values of n this becomes:

$$P(n,x) = \frac{1}{n_{\text{mean}}} e^{-n/n_{\text{mean}}} \tag{53}$$

With $\sigma = n_{\text{mean}}$. That is, the size of an electron avalanche originating from a single electron follows an exponential distribution. It is important to note that this result is based on the assumptions that the space charge of the avalanche does not have significant influence on the background electric field and the probability of an electron ionising a gas molecule is constant and is independent of the distance it has travelled in the electric field direction since the last ionising collision.

2.5.2 Formation of a streamer

A schematic description of the formation of a positive streamer is shown in Fig. 16 [19]. As the electron avalanche propagates towards the anode low mobile positive space charge accumulates at the avalanche head. When the avalanche reaches the anode, the electrons will be absorbed into it leaving behind the net positive space charge. Due to the recombination of positive ions and electrons, the avalanche head is a strong source of high energetic photons. These photons will create other avalanches in the vicinity of the positive space charge. If the number of positive ions in the avalanche head is larger than a critical value the electric field created by the space charge becomes comparable to the background electric field and the secondary avalanches created by the photons will be attracted towards the positive space charge. The electrons in the secondary avalanches will be neutralised by the positive space charge of the primary avalanche leaving behind a new positive space charge, a little bit

closer to the cathode. The process repeats itself and the positive space charge head travels towards the cathode as a consequence. This discharge is called *a cathode directed streamer* or *a positive streamer*.

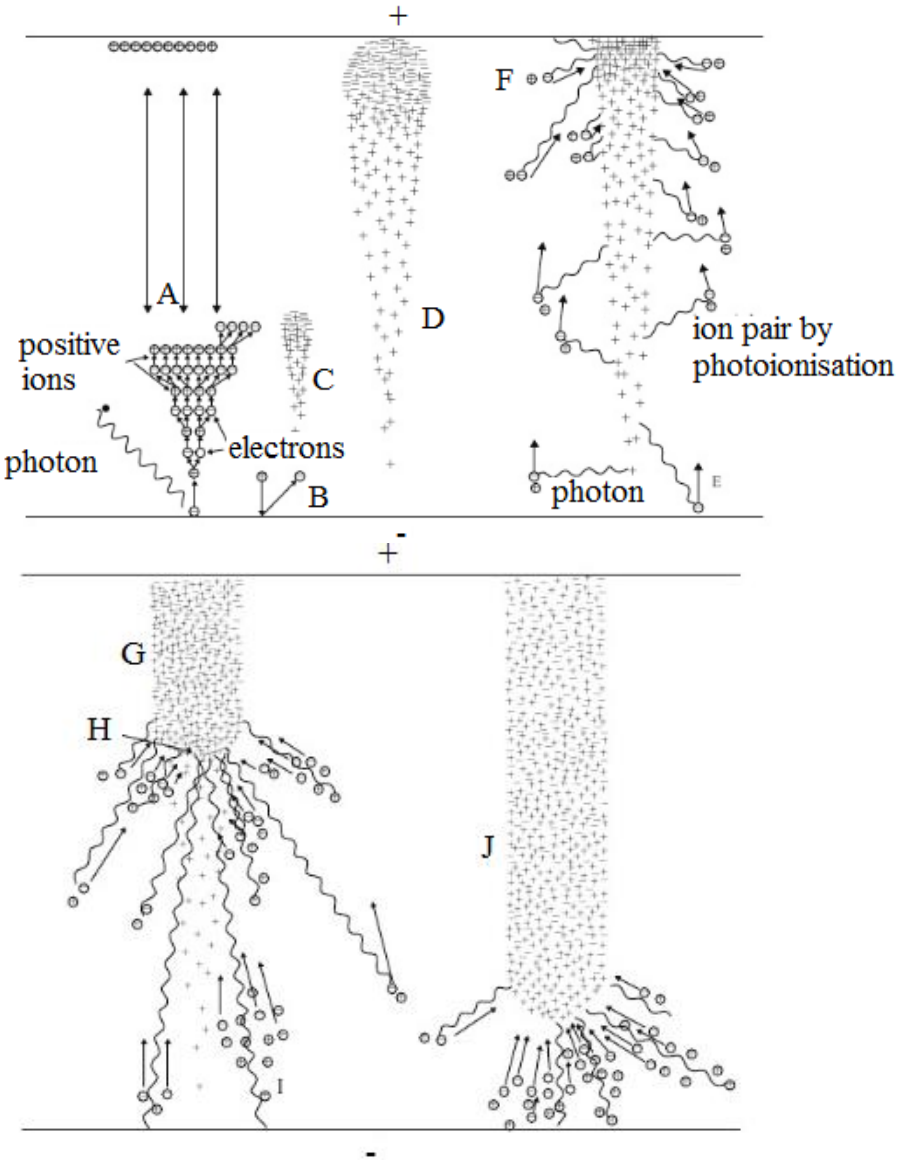

Fig. 16. Schematic diagrams showing the formation a positive streamer

A: an external photon triggers an avalanche. B: a positive ion strikes the cathode and starts an avalanche C,D: the avalanche tip reaches the anode. E: photons originating from the avalanche produce free electrons both from the cathode and in the gas. F: the positive space charge close to the anode increases the electric field and a streamer is just about to be formed. G: plasma of positive ions and electrons forms the streamer channel. H: streamer tip. I: production of free electrons by photons. J: streamer close to the cathode (from [7]).

The formation of *a negative streamer* or *an anode directed* streamer is shown in Fig. 17. The electrons of the avalanche move into the gap leaving behind positive charge close to the cathode. When the avalanche reaches the critical size the secondary avalanches extend the positive space charge towards the cathode (as in a cathode directed streamer). When the positive channel reaches the cathode both the field enhancement associated with the proximity of positive space charge to the cathode and the collision of positive ions on the cathode lead to the emission of electrons from the latter. These electrons will neutralize the positive space charge creating a weakly conducting channel that connects the negative head of the electron avalanche to the cathode. The high electric field at the head of the avalanche pushes the negative space charge further into the gap while the positive space charge left behind is neutralized by the electrons supplied by the cathode and travelling along the weakly conducting channel connecting the streamer head and the cathode.

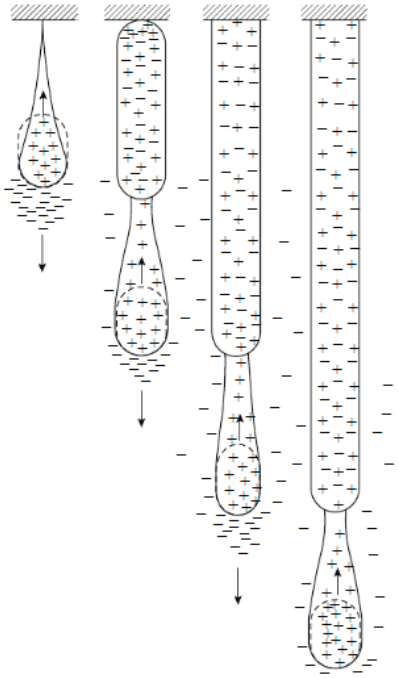

Fig. 17. Schematic representation of the formation of a negative streamer and the physical processes taking place at the streamer head (adapted from [20])

As the streamer propagates it may lead to the formation of branches. The avalanche to streamer transition takes place when the number of charged particles at the avalanche head exceeds a critical value, *Nc*. From cloud chamber photographs of the avalanches and streamers, Raether [21] estimated that an avalanche will convert to a streamer when the number

of positive ions in the avalanche head reaches a critical value of about 10^8. A similar conclusion is also reached independently by Meek [22]. Thus the critical avalanche length for transition to a streamer is given by

$$e^{\bar{\alpha}x_c} = 10^8 \tag{54}$$

or

$$\bar{a}x_c \approx 18 \tag{55}$$

Note that the critical avalanche length decreases with increasing electric field.

2.5.3 Propagation of the streamer discharges

A schematic representation of the propagation of a positive streamer is shown in Fig. 18. The local but strong electric field resulting from the concentration of positive charge at the streamer head attracts the secondary avalanches towards it. These avalanches neutralise the positive space charge of the original streamer head leaving behind an equal amount of positive space charge at a location slightly ahead of the previous head. The repetition of the process leads to an effective forward propagation of the streamer head connected to the anode by a weakly conducting channel. Since the electron multiplication in the active region is supported by the space charge electric field of the streamer head, the streamer can propagate in electric fields which are much smaller than the critical electric field necessary for cumulative electron ionisation. Indeed, Dawson and Winn have shown that a spherical space charge containing 10^8 electrons confined within a radius of 30 μm can propagate in zero electric field for a short time [23].

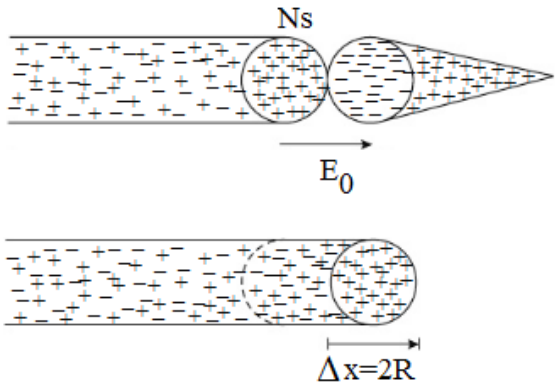

Fig.18. Schematic presentation of the propagation of positive streamers (from [11])

The mechanism of propagation of negative streamers is a little bit more complicated than that for positive streamers. This is shown in Fig. 19.

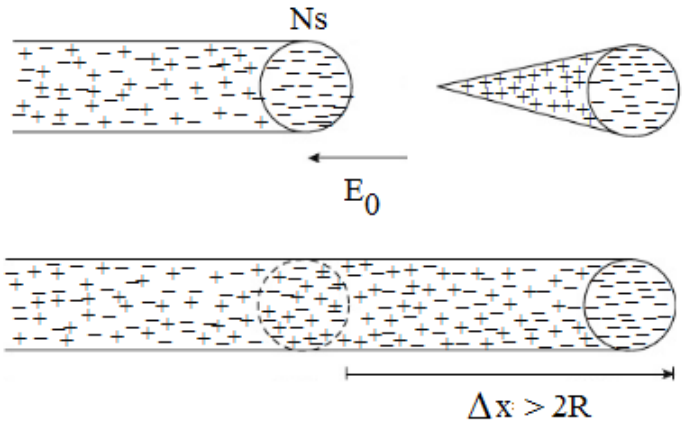

Fig. 19. Schematic presentation of the propagation of negative streamers (from [24])

Note that there are two main differences between the negative and positive streamers. In the negative streamer, the electrode has to supply the electrons necessary for the neutralisation of the positive space charge left behind by the avalanches whereas in the positive streamers the anode absorbs the extra electrons generated by the secondary streamers. The latter is a much easier process than the former. Second, in the positive streamers the electrons propagate towards the positive charge head of the streamer and therefore into an increasing electric field. In the case of negative streamers the electrons move into the low electric field region and some of them will be captured by electronegative atoms which create an immobile negative space charge region that will impede the streamer propagation. Both these features make the propagation of positive streamers easier than that of negative streamers.

We have seen before that for the inception of a streamer the number of charged particles at the avalanche head should reach a critical value. Similarly, for the continuous propagation of a streamer the number of charged particles in the streamer head has to be larger than a critical number, N_{stab}. The value of N_{stab} partly depends on the background electric field, E_b, and can be calculated from the following equation [25]:

$$N_{stab} = 0.558 \times 10^8 - 0.231 \times 10^3 E_b \quad for E_b \le 2 \times 10^5 V/cm \tag{56}$$

$$N_{stab} = 3.34 \times 10^8 e^{-1.614 \times 10^{-5} E_b} \quad for E_b \ge 2 \times 10^5 V/cm \tag{57}$$

2.6 Electrical breakdown in very small gaps – Townsend's breakdown mechanism

As described previously, avalanche to streamer transition requires that the avalanche grows to about 10^8 electrons and the space charge in the avalanche tip creates an electric field that significantly adds to the background electric field in the vicinity of the avalanche tip. This avalanche to streamer transition has been observed when the product of the pressure and the electrode spacing in plane uniform gaps exceeds about 0.5 bar.cm. Below this limit the space charge of the avalanche is not large enough to change the background field significantly. This will inhibit the avalanche to streamer transition. Under such conditions the breakdown takes place according to the Townsend mechanism.

2.6.1 Townsend's experiment

In Townsend's experiment (Fig. 20) a plane parallel electrode gap was located in a cell, the gas pressure of which was of the order of a few torr [26]. The cathode was illuminated with a steady beam of ultraviolet radiation which led to a steady stream of electrons from it. The current flowing across the gap was measured as a function of the voltage. Townsend found that the voltage and the current vary in a manner shown in Fig. 21.

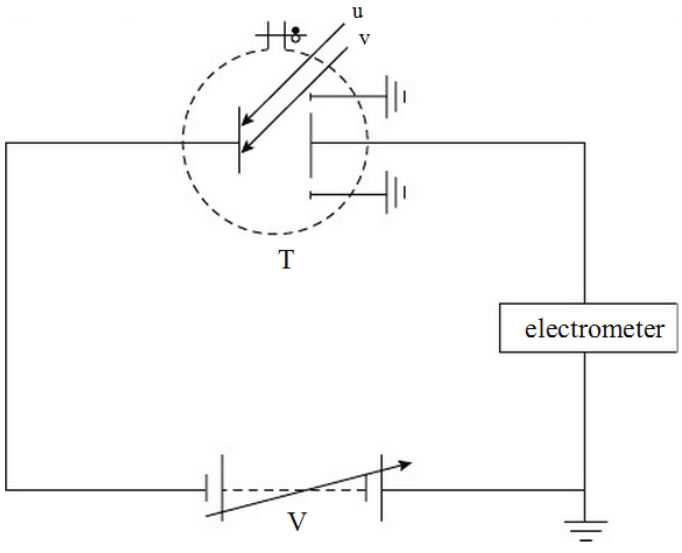

Fig. 20. Schematic representation of the apparatus used by Townsend in his experiment. V is the voltage source and T is the vacuum tube

The discharge gap is located in the vacuum tube and the cathode is illuminated by ultraviolet radiation.

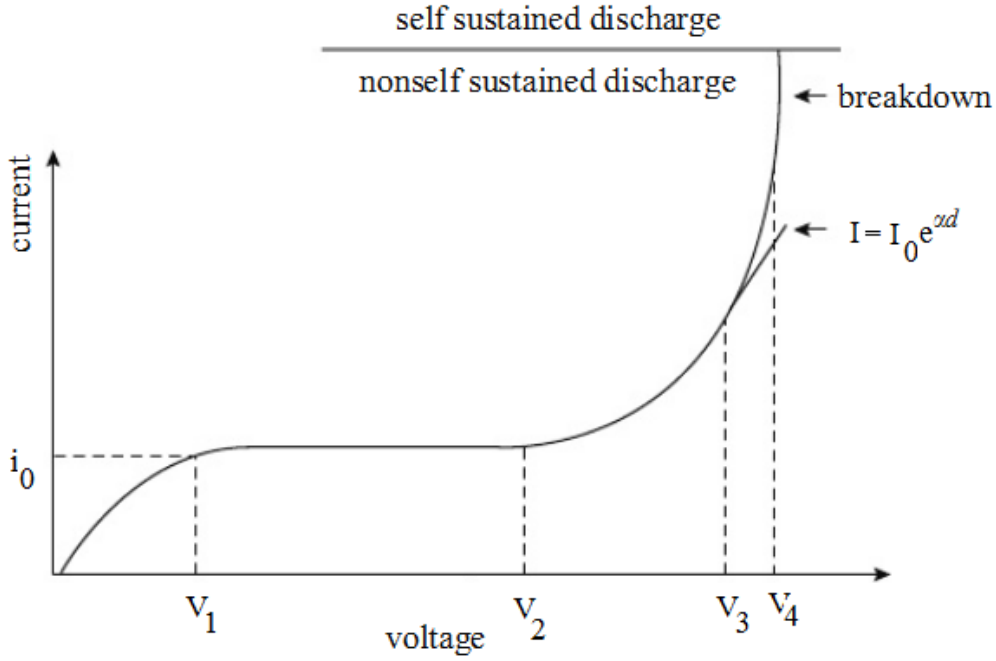

Fig. 21. Variation of the current flowing across the discharge tube of Townsend's experiment as a function of the applied voltage

Let us investigate the features of this curve in detail. Initially, the current in the gap increases with increasing voltage. The reason for this is that some of the electrons emitted by the cathode diffuse back into it and some of the electrons are lost to the walls. This diffusion and the losses to the walls of the tube decrease with increasing voltage. When the voltage increases to a certain level almost all the electrons emitted by the cathode are collected by the anode, thus producing the saturation in current. In reality, however, the current will only approach but not sustain a saturation level. The reason for this is that even though the back diffusion decreases with increasing voltage not all the emitted electrons will reach the anode even when the voltage is close to the sparking potential. As the voltage increases further, Townsend found that the current starts to increase exponentially with the applied voltage. This exponential growth of the current was sustained over a certain range of applied voltage but with further increase in voltage the current started to increase faster than the exponential growth. Further increase in voltage resulted in the electrical breakdown of the gap.

2.6.2 Townsend's theory of electrical breakdown

Townsend assumed that the initial exponential growth of the current in the discharge tube is caused by the production of secondary electrons through the collision of primary electrons, generated from the cathode, with gas atoms. The second phase of the discharge in which the current grows faster than exponential is assumed to be caused by the ionization of the atoms through the collision of ions. However, today we know that the correct explanation is the additional production of electrons by the collision of positive ions with the cathode. Let us consider the mathematical treatment of the discharge process taking place in Townsend's experiment and come up with an equation which matches the experimental data.

2.6.2.1 Primary ionization stage

$$n_d = n_0 e^{\alpha d} \tag{58}$$

Consequently, the current inside the tube is given by:

$$I_d = I_0 e^{\alpha d} \tag{59}$$

Where d is the gap length, $I_d = n_d e$, $I_0 = n_0 e$, α is Townsend's first ionization coefficient and e is the electronic charge. This equation explains the exponential growth of current with increasing voltage. Note that even though the voltage does not appear explicitly in this equation it indirectly appears in α which increases with increasing electric field (and hence with increasing voltage when d is constant). Note that I_0 is the current generated by the ultraviolet radiation at the cathode. Consequently, if the source of ultraviolet radiation is removed (i.e. I_0 = 0) then the current in the discharge tube will go to zero. Thus, the discharge is not self-sustained, that is, it needs the support of the external agency for its continuation.

2.6.2.2 Secondary ionization stage

Townsend observed that with increasing voltage the current in the discharge tube begins to increase with voltage at a rate faster than that predicted by eqn. 59. This departure from eqn.59 is shown in Fig. 22 where log(I) is plotted as a function of the gap spacing, d. The upcurving occurs when the current departs from this equation. Townsend assumed that the cause of this departure of the experimental data from that predicted by eqn.59 is the ionization of the gas atoms due to the collision of

positive ions. But, in reality, the energy gained by the positive ions at electric fields encountered in Townsend's experiment is not sufficient to create significant ionization. However, one process that may cause this departure from eqn. 59 is the generation of electrons from the cathode by positive ion bombardment. As the voltage increases the positive ions gain more and more energy and this energy is released at the cathode. With increasing energy a stage will be reached in which these positive ions will start liberating electrons from the electrode. In order to explain the variation of current with voltage one has to take this effect into account. Let us now derive a mathematical expression for the current in the discharge tube taking into account the electron current created by the bombardment of positive ions on the cathode.

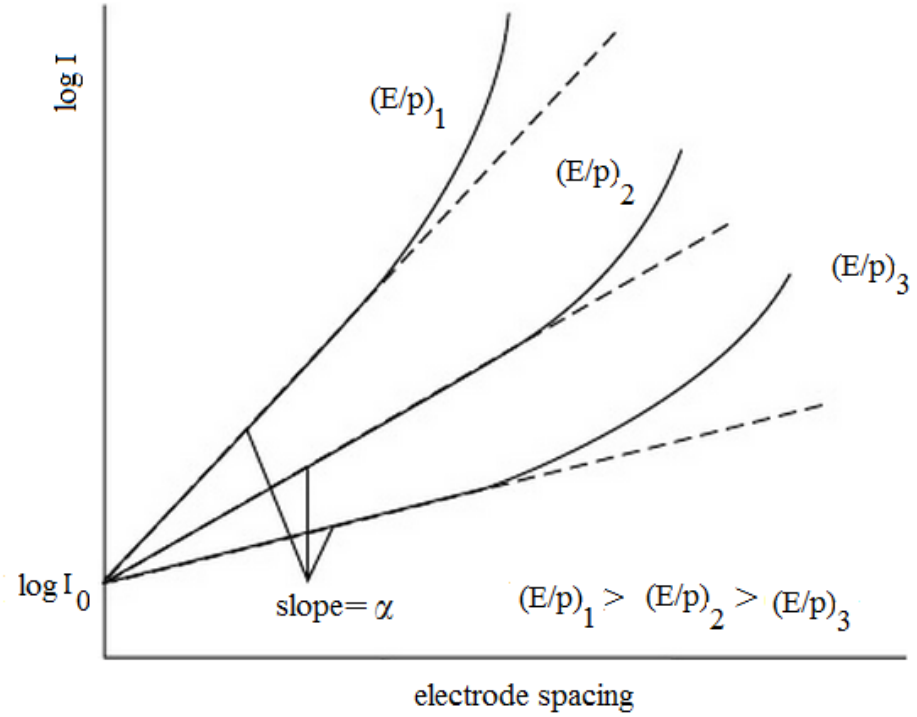

Fig. 22. Variation of the logarithm of the current flowing across the discharge tube in Townsend's experiment as a function of the logarithm of the electrode spacing for different values of (E/p)

Here E is the electric field in the gap and p is the pressure.

Let n_0 be the number of electrons emitted by the cathode per second due to ultra-violet illumination and n_+ be the number of electrons released from the cathode per second due to bombardment of positive ions. Then the number of electrons reaching the anode at steady state per second, n, is equal to:

$$n = (n_0 + n_+)e^{\alpha d} \qquad (60)$$

The number of positive ions created by the electrons reaching the anode per second is equal to $n-(n_0-n_+)$ and at steady state the number of positive ions reaching the cathode per second is equal to this number. Consequently, the number of electrons released by the positive ion bombardment at the cathode per second is given by:

$$n_+ = \{n-(n_0-n_+)\}\gamma \tag{61}$$

Where γ is the average number of electrons released by each positive ion striking the cathode. This parameter is called Townsend's secondary ionisation coefficient. Substituting this expression in eqn. 60 one obtains:

$$n = \frac{n_0 e^{\alpha d}}{1-\gamma(e^{\alpha d}-1)} \tag{62}$$

The current in the discharge tube is given by:

$$I = \frac{I_0 e^{\alpha d}}{1-\gamma(e^{\alpha d}-1)} \tag{63}$$

This equation predicts a faster current growth than eqn. 60 with increasing electric field (or voltage) providing an explanation for Townsend's experimental results.

In deriving the above equation we have considered the bombardment of positive ions on the cathode as the only secondary ionization process. Let us now consider the other secondary ionization processes.

(I) Ionization of gas by positive ions: Townsend in his original derivation assumed that the secondary ionization mechanism is due to the ionization in the gas by positive ions. However, as mentioned above, positive ions cannot produce significant ionisation in electric fields at which electrical breakdown is observed in Townsend's experiment. Nevertheless, if we assume that the ions will contribute to the ionization the resulting equation for the current will take the form [12]:

$$i = i_0 \frac{e^{(\alpha-\beta)d}}{(\alpha/(\alpha-\beta))-(\beta/(\alpha-\beta))e^{(\alpha-\beta)d}} \tag{64}$$

Where β is the ionisation coefficient of positive ions. Since electrons ionize more readily than positive ions one can replace $(\alpha-\beta)$ by α and the equation will reduce to:

$$i = i_0 \frac{e^{(\alpha)d}}{(1-(\beta/\alpha)e^{(\alpha)d}} \tag{65}$$

This equation has the same form as that of the expression obtained for positive ion bombardment at the cathode (i.e. eqn. 63).

(II) Photo emission from the electrode: Another secondary emission process that one may take into account is the interaction of photons in the

discharge with the electrodes. If the incident photon has an energy larger than the work function of the electrode then the interaction may lead to the liberation of an electron. If this process is taken in to account as a secondary mechanism then the expression for the current will take the form [6]:

$$i = i_0 \frac{e^{(\alpha)d}}{(1-(\Delta g\theta/\alpha - \mu))[e^{(\alpha-\mu)d} - 1]} \tag{66}$$

Where g is the fraction of photons emitted in the gas that are headed towards the cathode, μ is the coefficient of absorption of photons in the gas and Δ is the probability of photoelectric emission from the photons incident on the electrode (note that only a fraction of the incident photons will have sufficient energy to cause photo ionization).

In general $\alpha >> \mu$ and the equation will reduce to:

$$i = i_0 \frac{e^{(\alpha)d}}{(1-(\Delta g\theta/\alpha)[e^{(\alpha)d} - 1]} \tag{67}$$

This again has the same form as that of the eqn. (68).

(III) Collision of meta-stable ions on the cathode: Collision of meta-stable atoms on the cathode can also liberate electrons from the cathode. If the meta-stable level has a higher energy than the work function of the metal, such an interaction can lead to the emission of electrons. If this is taken into account [27]:

$$i = i_0 \frac{e^{(\alpha)d}}{1-\gamma_m\left[e^{(\alpha)d} - 1\right]} \tag{68}$$

where γ_m is the number of electrons liberated by the incidence of a meta-stable atom on the cathode.

(IV) Ionisation of the gas by photons: Another process that may contribute to electron production in the gas is the ionisation of the gas by photons. If this is taken into account, one can show that the resulting equation will have the form [13]:

$$i = i_0 \frac{e^{(\alpha)d}}{(1-(\zeta g f\mu/\alpha - \mu))[e^{(\alpha-\mu)d} - 1]} \tag{69}$$

where μ is the coefficient of absorption of photons, ζ is the fraction of absorbed photons that will cause ionisation, $f = \theta/\alpha$ where θ is the number of excited states or photons created per unit path in the electric field direction per electron and g is a geometrical factor that will describe the fraction of photons directed in a given direction.

(V) Final expression for the current in the presence of secondary processes: The results presented above show that irrespective of the sec-

ondary ionisation process under consideration the final expression for the current has the same form. Indeed one can include all of them in a single formula as follows:

$$i = i_0 \frac{e^{(\alpha)d}}{(1-(\gamma_i)[e^{(\alpha)d}-1]} \tag{70}$$

Where

$$\gamma_i = \gamma + (\alpha/\beta) + \Delta g\theta/\alpha + \gamma_m + (\frac{\zeta g f \mu}{\alpha - \mu}) \tag{71}$$

2.6.3 Townsend's electrical breakdown criterion

The final expression for the current given in eqn. 69 shows that the discharge is still non self-sustained. That is, the discharge current goes to zero if the UV illumination on the cathode is removed (i.e. as $I_0 \rightarrow 0$). However, as the voltage continues to increase a stage will be reached at which the discharge will transform itself from a non self-sustained discharge to a self-sustained discharge. At this stage the discharge will continue to burn between electrodes even after removing the background ultraviolet radiation (i.e. when $I_0 = 0$). This change of state of the discharge is accompanied by a several orders of magnitude increase in the current (provided that the voltage supply can sustain such an increase in the current) in the discharge gap. This is the stage of electrical breakdown in the gap. Townsend defined the electrical breakdown condition as the condition which makes the current in the discharge gap go to infinity.

From eqn. 69 one can see that $I_0 \rightarrow \infty$ when the denominator of the expression for the current goes to zero. That is when:

$$1-\gamma_i[(e^{(\alpha)d}-1)] = 0 \tag{72}$$

This condition is known as Townsend's breakdown criterion.

One can indeed show that this criterion has a physical significance. Assume that γ is the dominant secondary process. Assume that n_0 primary electrons leave the cathode per second. These electrons will give rise to $n_0\,(e^{(\alpha)d}-1)$ positive ions in the gap, and these positive ions on incidence on the cathode produce $\gamma_i n_0(e^{(\alpha)d}-1)$ secondary electrons. When Townsend's breakdown criterion is satisfied the number of secondary electrons is equal to the original number of electrons which has been drawn away from the cathode and later passed into the anode. Consequently, each avalanche will give rise to another avalanche through secondary processes

and so cause a repetition of the avalanche process. That is, the discharge process becomes self-sustained.

An alternative expression for Townsend's breakdown criterion can be obtained by rewriting the above equation as:

$$\alpha d = \ln(1+\frac{1}{\gamma_i}) \tag{73}$$

The value of γ_i is greatly affected by the cathode surface and gas pressure. However, γ_i is a very small number ($<10^{-2}$–10^{-3}) so $1/\gamma_i$ is very large. Therefore, $\ln(1+(1/\gamma_i))$ does not change too much and is of the order of eight to ten in a Townsend's discharge.

2.6.4 Townsend's mechanism in the presence of electron attachment

In the experiments conducted by Townsend the gases under investigation were noble gases. In this case electron attachment to atoms can be neglected. However, in air, one cannot neglect the electron attachment. Let us consider the effect of electron attachment in Townsend's equation. In the presence of attachment, the number of electrons reaching the cathode per second is given by:

$$n_0 = n_0 e^{(\alpha-\eta)d} \tag{74}$$

Consider an elementary length dx located at distance x from the cathode. Let n_x be the number of electrons reaching x in a unit time. In travelling across dx these electrons will generate dn_- number of negative ions per second. Then:

$$dn_- = n_x \eta dx \tag{75}$$

substituting for n_x one obtains:

$$dn_- = \eta n_0 e^{(\alpha-\eta)x} dx \tag{76}$$

Since the number of negative ions at the cathode is equal to zero the solution of this equation is given by:

$$n_- = \frac{\eta n_0}{\alpha-\eta}\left[e^{(\alpha-\eta)x} - 1\right] \tag{77}$$

Where n_- is the number of negative ions crossing a plane at a distance x from the cathode per second. Thus the number of negative ions reaching the anode per second, n_{-d}, is given by:

$$n_{-d} = \frac{\eta n_0}{\alpha-\eta}\left[e^{(\alpha-\eta)d} - 1\right] \tag{78}$$

The total current reaching the anode, both due to the electrons and to negative ions, is given by:

$$i = \frac{i_0}{\alpha - \eta}\left[\alpha e^{(\alpha-\eta)d} - \eta\right] \tag{79}$$

In the presence of secondary ionisation due to bombardment of positive ions on the cathode one can show using the procedure outlined in the section 2.6.2.2

$$i = i_0 \frac{\alpha e^{(\alpha-\eta)d} - \eta}{\alpha - \eta - \alpha\gamma\left\{e^{(\alpha-\eta)d} - 1\right\}} \tag{80}$$

This reduces to eqn.80 in the absence of attachment (i.e. η=0). From this equation the breakdown condition in the presence of electron attachment is given by:

$$1 - \left\{\frac{\alpha\gamma}{(\alpha - \eta)}\right\}[(e^{(\alpha-\eta)d} - 1)] = 0 \tag{81}$$

This criterion shows that if $\alpha \succ \eta$ then electrical breakdown is possible irrespective of the values of α, η and γ provided that d is large enough. That is, for a given electric field there is a particular value of d at which the gap breaks down. For $\alpha \prec \eta$, with increasing d, the above equation approaches an asymptotic form:

$$\frac{\gamma\alpha}{(\alpha - \eta)} = -1 \quad \text{or} \quad \alpha = \frac{\eta}{(1 + \gamma)} \tag{82}$$

This defines the limiting condition at which electrical breakdown is possible in an electronegative gas. This condition depends only on E/p. Noting that the value of γ<<1,the limiting value of E/p which can cause electrical breakdown in electronegative gases can be obtained from the relationship $\alpha = \eta$ (see section 2.5). This point is illustrated in the plot given in Fig. 23.

2.7 Paschen's law

If a slowly increasing voltage is applied across two plane parallel electrodes the electrical breakdown of the gap occurs at a certain critical voltage. The experimental data shows that the breakdown voltage, V_s, is only a function of the gas pressure, P (or gas density), multiplied by the gap length, d . That is:

$$V_s = f(Pd) \tag{83}$$

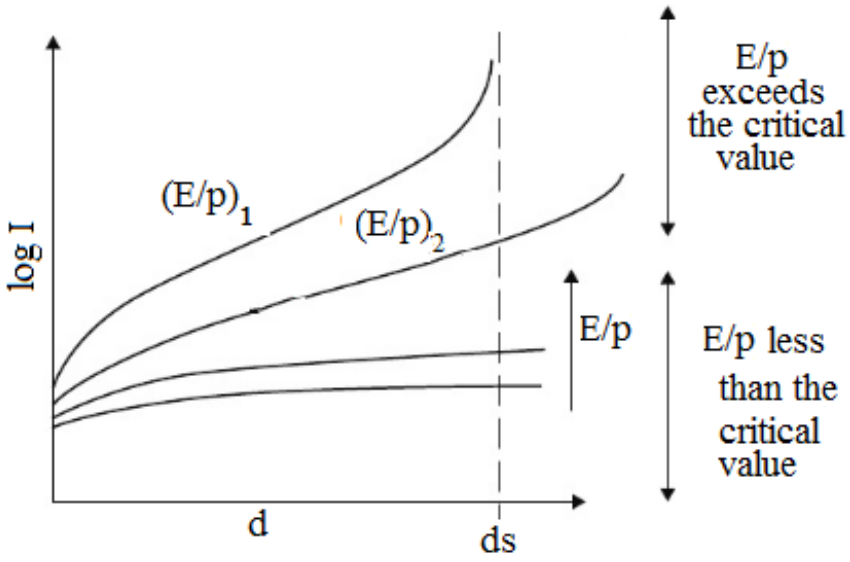

Fig. 23. Variation of the logarithm of the current flowing across the dischargetube in Townsend's experiment as a function of the logarithm of the electrode spacing for different values of (E/p) for electronegative gases

This is known as Paschen's law. The Paschen curve for air is shown in Fig. 24; the data points correspond to measurements by several authors and the solid black dots are generated from the equation $V_s = 6.72\sqrt{Pd} + 24.4(Pd))$ (P in bar and d in mm).

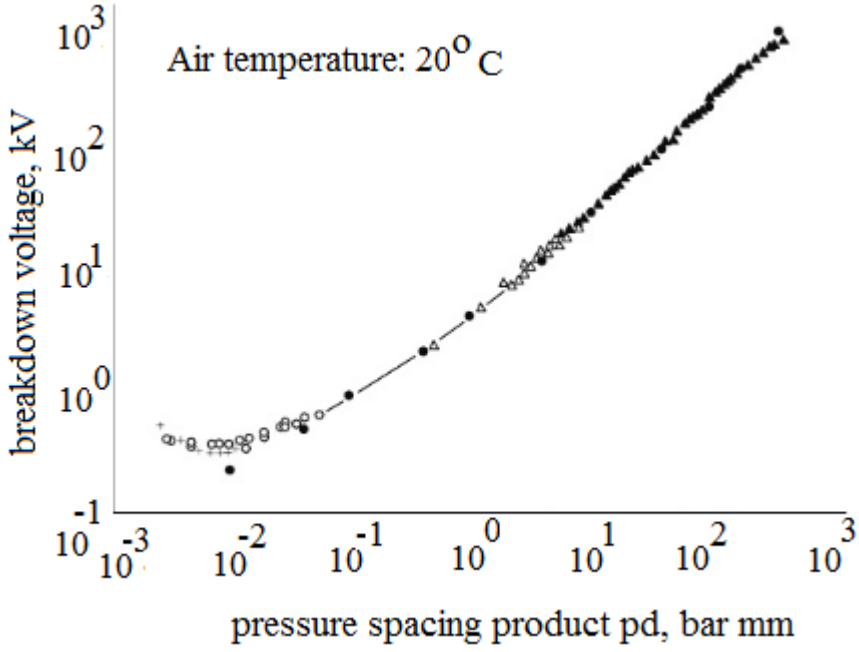

Fig. 24. Paschen curve for air in log–log scale at temperature 20°C [28]

In this Fig. the results are given in terms of Pd corresponding to a temperature of 293 K. Note that the sparking potential is high both in the

case of low and high values of Pd but there is a minimum at a certain value of pd. This minimum is called the Paschen minimum. The Paschen minimum in air is about Pd=10^{-2} bar.mm. One can show that the breakdown voltage estimated using either Townsend's or Raether and Meek's criterion adheres to Paschen's law. The electrical breakdown criterion of a uniform gap of length d is given by

$$\alpha d = K \tag{84}$$

Where K is a constant. Depending on the value of K this equation represents both Townsend's breakdown criterion and the streamer breakdown criterion. Substituting the expression for α given in eqn. 80 we obtain:

$$K = Apde^{-Bpd/V_s} \tag{85}$$

Where V_s is the voltage at which electrical breakdown is observed. Note that in deriving this equation we have used $E=V_s/d$. Rearranging the above equation we find that

$$V_s = \frac{Bdp}{\ln\{Apd/K\}} \tag{86}$$

This equation shows that V_s is a function of pd. The general shape of this equation is in agreement with the Paschen curve.

2.7.1 Physical interpretation of the shape of the Paschen curve

In order to give a physical interpretation for the shape of the Paschen curve let us rewrite eqn. 86 as follows

$$E_s = \frac{B_1(d/\lambda)}{\ln\{A_1(d/\lambda)/K\}} \tag{87}$$

Where A_1 and B_1 are constants, λ is the mean free path of the electrons $E_s=V_s/d$,and we have used the relationship that the mean free path is inversely proportional to the pressure. This equation has the same form as eqn. 87 except that Pd is now replaced by d/λ. It thus predicts that the breakdown electric field has a minimum corresponding to a certain value of d/λ, say $(d/\lambda)_{min}$, and it increases when the value of d/λ moves away from this minimum. The reason for the existence of this minimum can be explained qualitatively as follows. Let E_m be the electric field in the gap corresponding to $(d/\lambda)_{min}$. At $(d/\lambda)_{min}$ an electron crossing the gap will make a certain number of ionisation collisions. Consider the case $d/\lambda > (d/\lambda)_{min}$. Now, the number of collisions made by an electron in crossing the gap, and hence the energy lost in collisions in crossing the gap, is higher than at $(d/\lambda)_{min}$. If the background electric field remained at E_m the

total number of ionisation collisions made by an electron crossing the gap would be less than the corresponding value at $(d/\lambda)_{min}$. Consequently, the electric field should be increased in order to compensate for the losses and to increase the probability of ionisation. For $d/\lambda < (d/\lambda)_{min}$ the number of collisions, and hence the number of ionisation collisions, made by an electron in crossing the gap is less than the corresponding value at $(d/\lambda)_{min}$. In this case the only way to increase the number of ionisation collisions is to increase the probability of ionisation in each collision. This can be achieved only by increasing the energy gained by electrons within a mean free path. This requires a higher electric field than the one which corresponds to $(d/\lambda)_{min.}$

2.7.2 Validity of Paschen's law

In section 2.7 it was shown that Paschen's law follows directly if the dominant collision processes, as is often the case, are such that the coefficients representing them, for example α, are directly proportional to p at a given value of E/p. When this is the case the processes are said to obey similarity. In general, the experimental data obeys Paschen's law and any deviations are relatively small and arise from the existence of collision processes in the gas which do not conform to similarity. The deviations from Paschen's law can occur at high pressures and at temperatures above about 3000–4000 K. At high pressures exceeding a few atmospheres the processes such as field emission may play a significant role in the breakdown process. The role of field emission at high pressures and its influence on Paschen's law is clearly demonstrated by the observation that when very clean molybdenem electrodes are used Paschen's law holds up to very high pressures. The clean electrodes do not have oxide layers that generate field emission at low electric fields. At high temperatures experimental data departs from Paschen's law partly due to the dominant role of thermal ionisation and partly due to the gradual change of chemical composition of the gas, for example, by dissociation. Paschen's law may also break down at low pressures because the breakdown process is governed by preionisation processes caused by electrodes such as thermionic emission and the break down phenomena has to be described by vacuum breakdown processes.

2.8 Classification of Discharges

Discharges in a dc electric field can be classified into (a) non-self-sustaining and (b) self-sustaining types. The latter are more widespread,

more diversified, and richer in physical effects. Steady and quasi-steady self-sustaining discharges contain A) glow and B) arc discharges. We have already mentioned in Sect. 2.2 that the cathode processes of two types differ in principle. A close relation of the glow discharge is C) Townsend's dark discharge. It proceeds with a cold cathode and at very weak current. The D) corona discharge, also self-sustaining and also at a low current, is a special case.

Typical conditions under which each of the combinations can be observed are summarized in Table 4.

Table 4. Classification of discharge processes

	Breakdown	Nonequilibrium plasma	Equilibrium plasma
Constant electric field	Initiation of glow discharge in tubes	Positive column of glow discharge	Positive column of high- pressure arc
Radio frequencies	Initiation of rf discharge in vessels filled with rarefied gases	Capacitivcly coupled rf discharges in rarefied gases	Inductively coupled plasma torch
Microwave range	Breakdown in waveguides and resonators	Microwave discharges in rarefied gases	Microwave plasmatron
Optical range	Gas breakdown by laser radiation	Final stages of optical breakdown	Continuous optical discharge

Corona has common features with glow and dark discharges. Among transient discharges, the E) spark discharge stands out sharply, among others. Many features of purely plasma processes, characterizing breakdown in a dc electric field, as well as the glow and arc discharges, are typical for discharges in rapidly oscillating fields, where electrodes are not necessary at all. It is therefore expedient to construct a classification avoiding the attributes related to electrode effects, and the following two properties will be basic for the classification: the state of the ionized gas and the frequency range of the field. The former serves to distinguish between A) breakdown in the gas, B) sustaining non-equilibrium plasma by the field, and C) sustaining equilibrium plasma. Frequency serves to classify fields into A) dc, low-frequency, and pulsed fields (excluding very

short pulses), B) radio-frequency fields (f ~ 10^5 - 10^8Hz), C) microwave fields (f ~ 10^9 - 10^{11} Hz, $\lambda \sim 10^2 - 10^{-1}$ cm), and D) optical fields (far from infrared to ultraviolet light). The field of any subrange can interact with each type of discharge plasma. In total, we have 12 combinations. All of them are experimentally realizable, and quite a few are widely employed in physics and technology.

Chapter 3 Basic principles of plasma chemical processes

Plasma chemistry has developed naturally from the low temperature plasma physics of molecular gases, and especially of their multicomponent mixtures. Plasma chemical reactions (particularly in electrical discharges) usually occur under non-equilibrium conditions and themselves create non-equilibrium. Reactions of charged particles and excited molecules play a very important if not principal role; chemical reactions under plasma conditions result in excited particles which have non-equilibrium distributions. From this the need arose for new developments of certain theoretical ideas and experimental methods of plasma chemistry.

Chemically active plasma is a multi-component system highly reactive due to large concentrations of charged particles (electrons, negative and positive ions), excited atoms and molecules (electronic and vibrational excitation make a major contribution), active atoms and radicals, and UV photons. Each component of the chemically active plasma plays its own specific role in plasma-chemical kinetics. Electrons, for example, are usually first to receive the energy from an electric field and then distribute it between other plasma components and specific degrees of freedom of the system. Changing parameters of the electron gas (density, temperature, electron energy distribution function) often permit control and optimization of plasma-chemical processes. Ions are charged heavy particles, that are able to make a significant contribution to plasma-chemical kinetics either due to their high energy (as in the case of sputtering and reactive ion etching) or due to their ability to suppress activation barriers of chemical reactions. This second feature of plasma ions results in the so-called ion or plasma catalysis, which is particularly essential in plasma-assisted ignition and flame stabilization, fuel conversion, hydrogen production, exhaust gas cleaning, and even in the direct plasma treatment of living tissue.

The vibrational excitation of molecules often makes a major contribution to plasma-chemical kinetics because the plasma electrons with energies around 1 eV primarily transfer most of the energy in such gases as N_2, CO, CO_2, H_2, and so forth into vibrational excitation. Stimulation of plasma-chemical processes through vibrational excitation permits the highest values of energy efficiency to be reached. Electronic excitation of atoms and molecules can also play a significant role, especially when the lifetime of the excited particles is quite long (as in the case of metastable electronically excited atoms and molecules). As an example, we can mention plasma-generated metastable electronically excited oxygen molecules O_2 ($^1\Delta_g$) (singlet oxygen), which effectively participate in the plasma-

stimulated oxidation process in polymer processing, and biological and medical applications.

The contribution of atoms and radicals is obviously significant. As an example, we can point out that O atoms and OH radicals effectively generated in atmospheric air discharges which play a key role in numerous plasma-stimulated oxidation processes. Plasma-generated photons play a key role in a wide range of applications, from plasma light sources to UV sterilization of water.

Plasma is not only a multi-component system, but often a very non-equilibrium one. Concentrations of the active species described earlier can exceed those of quasi-equilibrium systems by many orders of magnitude at the same gas temperature.

The successful control of plasma permits chemical processes to be directed in a desired direction, selectively, and through an optimal mechanism. Control of a plasma-chemical system requires detailed understanding of elementary processes and the kinetics of the chemically active plasma. The major fundamentals of plasma physics, elementary processes in plasma was discussed in Chapters 1 and 2, and plasma kinetics are to be discussed in Chapters 3.

3.1 Chemical kinetics

Kinetics is the study of the rates of chemical processes in an effort to understand what it is that influences these rates and to develop theories which can be used to predict them. A knowledge of reaction rates has many practical applications, for example in designing an industrial process, in understanding the complex dynamics of the atmosphere and in understanding the intricate interplay of the chemical reactions that are the basis of life.

At a more fundamental level we want to understand what happens to the molecules in a chemical reaction – that is what happens in a single reactive encounter between two reagent molecules. By understanding this we may be able to develop theories that can be used to predict the outcome and rate of reactions.

For more detail on this section Principles of Chemical Kinetics by J. E. House (Elsevier 2007) [29] is a good source.

3.1.1 Rates of reactions

The rate of a chemical reaction is expressed as a change in concentration of some species with time. Therefore, the dimensions of the rate

must be those of concentration divided by time (moles=liter/sec, moles=liter/min, etc.). A reaction that can be written as

$$A \rightarrow B \tag{88}$$

has a rate that can be expressed either in terms of the disappearance of A or the appearance of B. Because the concentration of A is *decreasing* as A is consumed, the rate is expressed as -*d*[A]/dt. Because the concentration of B is *increasing* with time, the rate is expressed as +d[B]/dt. The mathematical equation relating concentrations and time is called the rate equation or the rate law. The relationships between the concentrations of A and B with time are represented graphically in Fig. 25 for a first-order reaction in which $[A]_o$ is 1.00 **M** and k =0:050 min^{-1}.

If we consider a reaction that can be shown as

$$aA + bB \rightarrow cC + dD \tag{89}$$

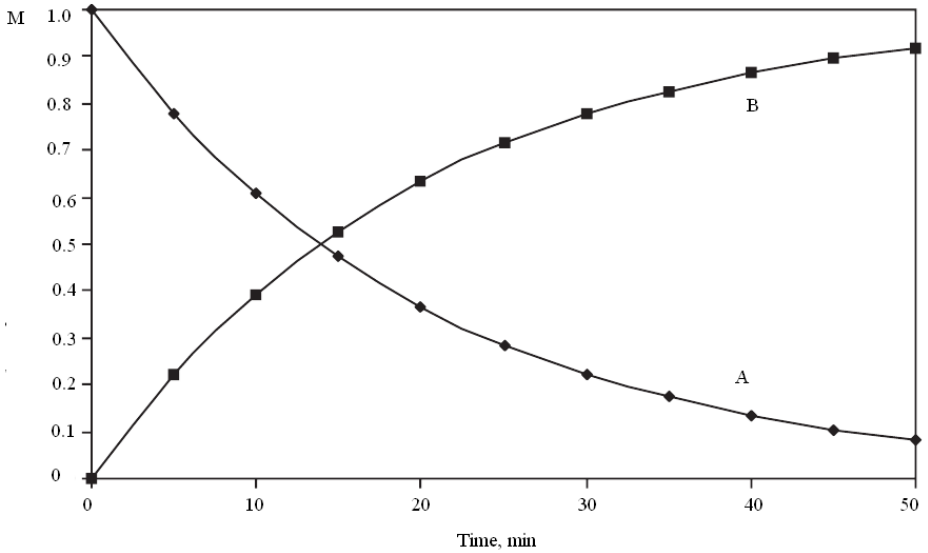

Fig. 25. Change in concentration of A and B for the reaction A → B

The rate law will usually be represented in terms of a constant times some function of the concentrations of A and B, and it can usually be written in the form

$$Rate = k[A]^x[B]^y \tag{90}$$

where x and y are the exponents on the concentrations of A and B, respectively. In this rate law, k is called the *rate constant* and the exponents x and y are called the *order of the reaction* with respect to A and B, respectively. As will be described later, the exponents x and y may or may not be the same as the balancing coefficients a and b in Eq. (89). The overall order of the reaction is the sum of the exponents x and y. Thus, we speak of a second-order reaction, a third-order reaction, etc., when the

sum of the exponents in the rate law is 2, 3, etc., respectively. These exponents can usually be established by studying the reaction using different initial concentrations of A and B. When this is done, it is possible to determine if doubling the concentration of A doubles the rate of the reaction. If it does, then the reaction must be first-order in A, and the value of *x* is 1. However, if doubling the concentration of A quadruples the rate, it is clear that [A] must have an exponent of 2, and the reaction is second-order in A. One very important point to remember is that there is no necessary correlation between the balancing coefficients in the chemical equation and the exponents in the rate law. They may be the same, but one can not assume that they will be without studying the rate of the reaction.

If a reaction takes place in a series of steps, a study of the rate of the reaction gives information about the slowest step of the reaction. We can see an analogy to this in the following illustration that involves the flow of water,

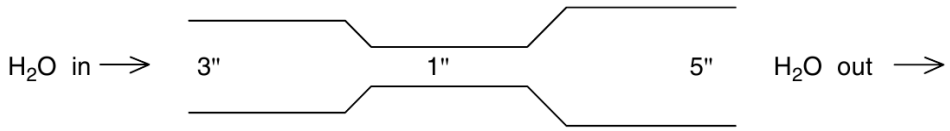

If we study the rate of flow of water through this system of short pipes, information will be obtained about the flow of water through a 1cm pipe since the 3 cm and 5 cm pipes do not normally offer as much resistance to flow as does the 1cm pipe. Therefore, in the language of chemical kinetics, the 1cm pipe represents the *rate-determining step*.

Suppose we have a chemical reaction that can be written as

$$2A + B \rightarrow Products \qquad (91)$$

and let us also suppose that the reaction takes place in steps that can be written as

$$A + B \rightarrow C\ (slow) \qquad (92)$$

$$C + A \rightarrow Products\ (fast) \qquad (93)$$

The amount of C (known as an *intermediate*) that is present at any time limits the rate of the overall reaction. Note that the sum of Eqs. (92) and (93) gives the overall reaction that was shown in Eq. (91). Note also that the formation of C depends on the reaction of one molecule of A and one of B. That process will likely have a rate that depends on $[A]^1$ and $[B]^1$. Therefore, even though the balanced overall equation involves two molecules of A, the *slow step* involves only one molecule of A. As a result, formation of products follows a rate law that is of the form *Rate* =

k[A][B], and the reaction is second-order (first-order in A and first-order in B). It should be apparent that we can write the rate law directly from the balanced equation only if the reaction takes place in a *single step*. If the reaction takes place in a series of steps, a rate study will give information about steps up to and including the slowest step, and the rate law will be determined by that step.

3.1.2 Dependence of rates on concentration

In this section, we will examine the details of some rate laws that depend on the concentration of reactants in some simple way. Although many complicated cases are well known, there are also a great many reactions for which the dependence on concentration is first-order, second-order, or zero-order.

3.1.2.1 First-Order

Suppose a reaction can be written as

$$A \rightarrow B \tag{94}$$

and that the reaction follows a rate law of the form

$$Rate = k[A]^1 = -\frac{d[A]}{dt} \tag{95}$$

This equation can be rearranged to give

$$-\frac{d[A]}{[A]} = kdt \tag{96}$$

Equation (96) can be integrated but it should be integrated between the limits of time =0 and time equal to *t* while the concentration varies from the initial concentration $[A]_o$ at time zero to [A] at the later time. This can be shown as

$$-\int_{[A]_0}^{[A]} \frac{d[A]}{[A]} = k\int_o^t dt \tag{97}$$

When the integration is performed, we obtain

$$\ln\frac{[A]_0}{[A]} = kt \quad \text{or} \quad \log\frac{[A]_0}{[A]} = \frac{kt}{2.303}t \tag{98}$$

If the equation involving natural logarithms is considered, it can be written in the form

$$\ln[A]_0 - \ln[A] = kt \tag{99}$$

or

$$\ln[A] = \ln[A]_0 - kt \quad (100)$$

$$y = b + mx \quad (101)$$

It must be remembered that $[A]_o$, the initial concentration of A, has some fixed value so it is a constant. Therefore, Eq. (100) can be put in the form of a linear equation where y=ln[A], m=-k, and b=ln $[A]_o$. A graph of ln[A] versus *t* will be linear with a slope of -k. In order to test this rate law, it is necessary to have data for the reaction which consists of the concentration of A determined as a function of time. This suggests that in order to determine the concentration of some species, in this case A, simple, reliable, and rapid analytical methods are usually sought. Additionally, one must measure time, which is not usually a problem unless the reaction is a very rapid one.

It may be possible for the concentration of a reactant or product to be determined directly within the reaction mixture, but in other cases a sample must be removed for the analysis to be completed. The time necessary to remove a sample from the reaction mixture is usually negligibly short compared to the reaction time being measured. What is usually done for a reaction carried out in solution is to set up the reaction in a vessel that is held in a constant temperature bath so that fluctuations in temperature will not cause changes in the rate of the reaction. Then the reaction is started, and the concentration of the reactant (A in this case) is determined at selected times so that a graph of ln[A] versus time can be made or the data analyzed numerically. If a linear relationship provides the best fit to the data, it is concluded that the reaction obeys a first-order rate law. Graphical representation of this rate law is shown in Fig. 26 for an initial concentration of A of 1.00 **M** and *k*=0:020 min^{-1}. In this case, the slope of the line is - *k*, so the kinetic data can be used to determine *k* graphically or by means of linear regression using numerical methods to determine the slope of the line.

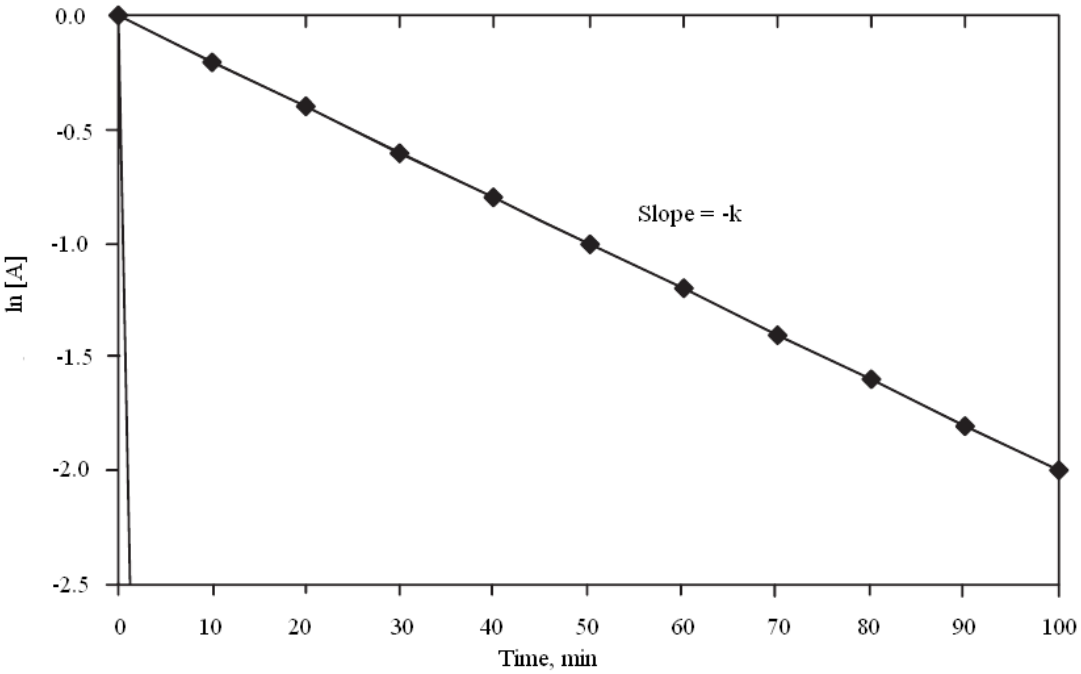

*Fig. 26. First-order plot for A → B with $[A]_o$ = 1:00 **M** and k = 0:020 min $^{-1}$*

The units on *k* in the first-order rate law are in terms of time^{-1}. The left-hand side of Eq. (98) has [concentration]/[concentration], which causes the units to cancel. However, the right-hand side of the equation will be dimensionally correct only if *k* has the units of time^{-1}, because only then will kt have no units

The equation

$$\ln[A] = \ln[A]_0 - kt \qquad (102)$$

can also be written in the form

$$[A] = [A]_0 e^{-kt} \qquad (103)$$

From this equation, it can be seen that the concentration of A decreases with time in an exponential way. Such a relationship is sometimes referred to as an *exponential decay*.

Radioactive decay processes follow a first-order rate law. The rate of decay is proportional to the amount of material present, so doubling the amount of radioactive material doubles the measured counting rate of decay products. When the amount of material remaining is one-half of the original amount, the time expired is called the *half-life*. We can calculate the half-life easily using Eq. (98). At the point where the time elapsed is equal to one half-life, $t=t_{1/2}$, the concentration of A is one-half the initial concentration or $[A]_o=2$. Therefore, we can write

$$\ln \frac{[A]_0}{[A]} = \ln \frac{[A]_0}{\frac{[A]_0}{2}} = kt_{1/2} = \ln 2 = 0.693 \qquad (104)$$

The half-life is then given as

$$t_{1/2} = \frac{0.693}{k} \qquad (105)$$

and it will have units that depend on the units on *k*. For example, if *k* is in hr^{-1}, then the half-life will be given in hours, etc. Note that for a process that follows a first-order rate law, the half-life is independent of the initial concentration of the reactant. For example, in radioactive decay the half-life is independent of the amount of starting nuclide. This means that if a sample initially contains 1000 atoms of radioactive material, the half-life is exactly the same as when there are 5000 atoms initially present. It is easy to see that after one half-life the amount of material remaining is one-half of the original; after two half-lives, the amount remaining is one-fourth of the original; after three half-lives, the amount remaining is one-eighth of the original, etc. This is illustrated graphically as shown in Fig. 27.

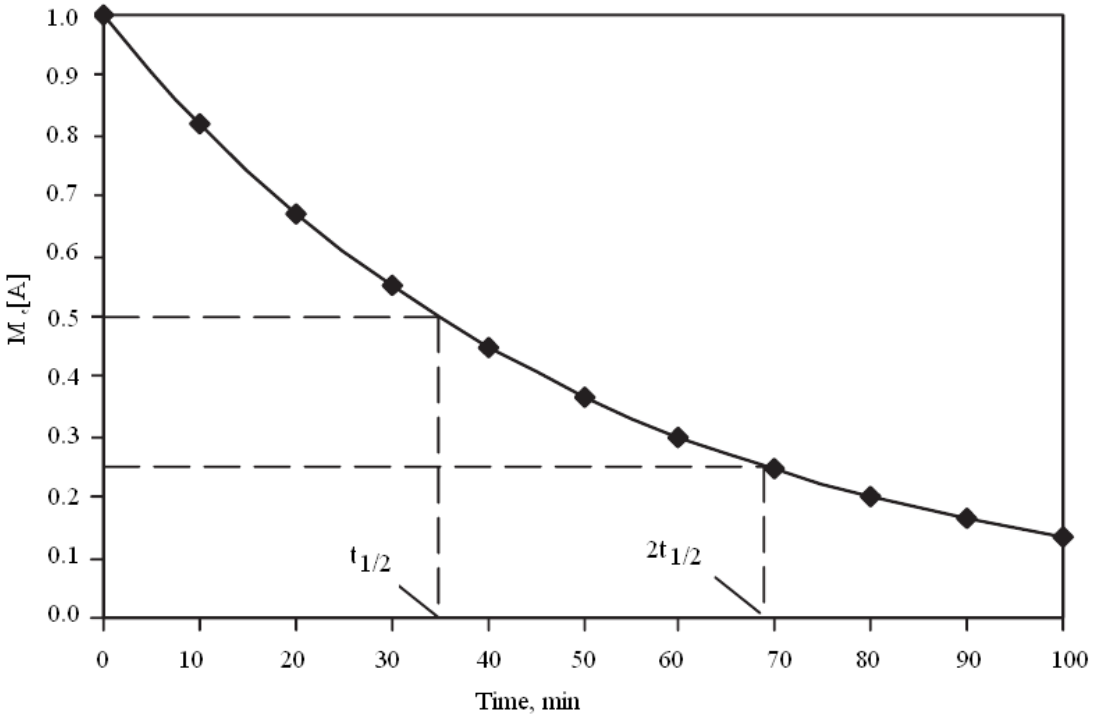

Fig. 27. Half-life determination for a first-order process with $[A]_o$ *= 1:00* ***M*** *and k = 0:020* min^{-1}

While the term half-life might more commonly be applied to processes involving radioactivity, it is just as appropriate to speak of the half-

life of a chemical reaction as the time necessary for the concentration of some reactant to fall to one-half of its initial value.

3.1.2.2 Second-Order

A reaction that is second-order in one reactant or component obeys the rate law

$$Rate = k[A]^2 = -\frac{d[A]}{dt} \tag{106}$$

Such a rate law might result from a reaction that can be written as

$$2A \rightarrow \mathrm{Pr}oducts \tag{107}$$

However, as we have seen, the rate law cannot always be written from the balanced equation for the reaction. If we rearrange Eq. (106), we have

$$\frac{-d[A]}{[A]^2} = kdt \tag{108}$$

If the equation is integrated between limits on concentration of $[A]_o$ at t =0 and [A] at time *t*, we have

$$\int_{[A]_0}^{[A]} \frac{d[A]}{[A]^2} = k\int_0^t dt \tag{109}$$

Performing the integration gives the integrated rate law

$$\frac{1}{[A]} - \frac{1}{[A]_0} = kt \tag{110}$$

Since the initial concentration of A is a constant, the equation can be put in the form of a linear equation,

$$\frac{1}{[A]} = kt + \frac{1}{[A]_0} \tag{111}$$

As shown in Fig. 28, a plot of 1/[A] versus time should be a straight line with a slope of *k* and an intercept of $1/[A]_o$ if the reaction follows the second-order rate law. The units on each side of Eq. (111) must be

1/concentration. If concentration is expressed in mole/liter, then 1/concentration will have units of liter/mole. From this we find that the units on *k* must be liter/mole time or M^{-1} $time^{-1}$ so that *kt* will have units M^{-1}.

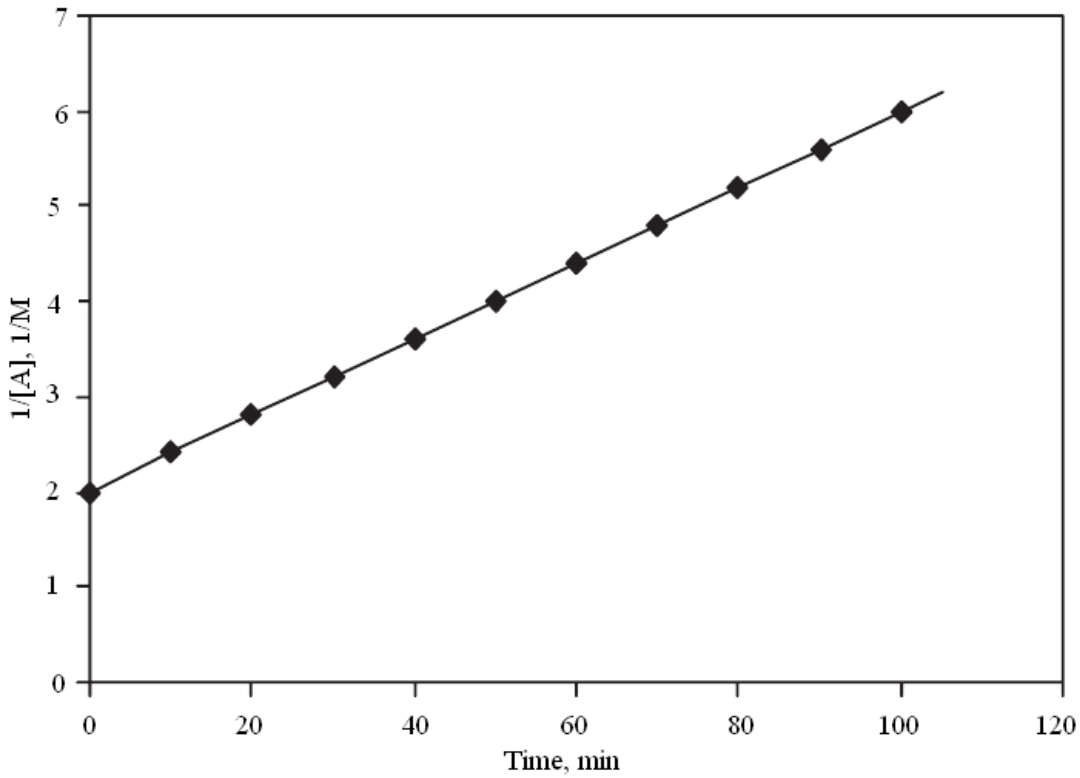

Fig. 28. A second-order rate plot for A → B with $[A]_o$ = 0:50 M and k = 0.040 liter/mol min

The half-life for a reaction that follows a second-order rate law can be easily calculated. After a reaction time equal to one half-life, the concentration of A will have decreased to one-half its original value. That is, $[A] = [A]_o/2$, so this value can be substituted for [A] in Eq. (110) to give

$$\frac{1}{\frac{[A]_0}{2}} - \frac{1}{[A]_0} = kt_{1/2} \qquad (112)$$

Removing the complex fraction gives

$$\frac{2}{[A]_0} - \frac{1}{[A]_0} = kt_{1/2} = \frac{1}{[A]_0} \qquad (113)$$

Therefore, solving for $t_{1/2}$ gives

$$t_{1/2} = \frac{1}{k[A]_o}$$

Here we see a major difference between a reaction that follows a second-order rate law and one that follows a first-order rate law. For a first-order reaction, the half-life is independent of the initial concentration of the reactant, but in the case of a second-order reaction, the half-life is inversely proportional to the initial concentration of the reactant.

3.1.3 Dependence of Rate on Temperature

In order for molecules to be transformed from reactants to products, it is necessary that they pass through some energy state that is higher than that corresponding to either the reactants or products. For example, it might be necessary to bend or stretch some bonds in the reactant molecule before it is transformed into a product molecule.

The essential idea is that a state of higher energy must be populated as a reaction occurs. This is illustrated by the energy diagram shown in Fig. 29. Such a situation should immediately suggest that the Boltzmann Distribution Law may provide a basis for the explanation because that law governs the population of states of unequal energy. In the case illustrated in the figure, denotes the high-energy state, which is called the transition state or the activated complex. The height of the energy barrier over which the reactants must pass on the way to becoming products is known as the activation energy.

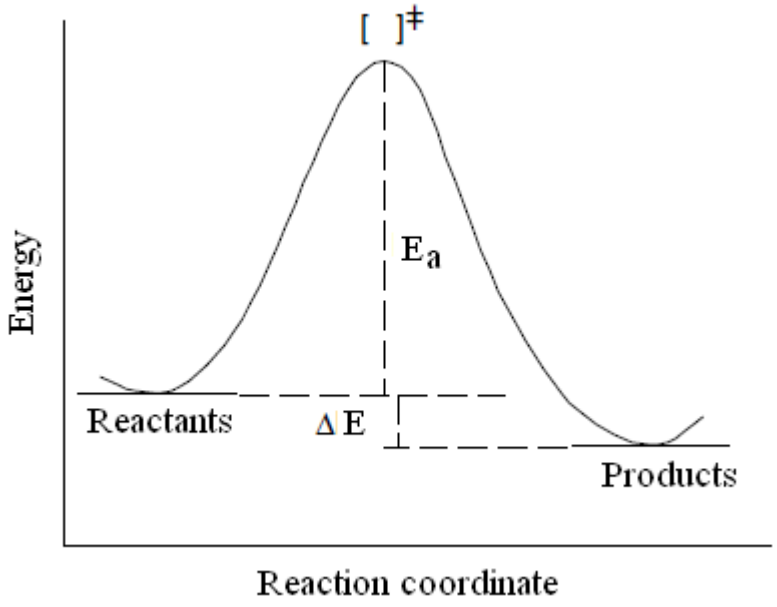

Fig. 29. The energy profile for a chemical reaction

The example illustrated in the figure represents an exothermic reaction because the overall energy change is negative since the products have a lower energy than the reactants. When the various rate laws are inspected, we see that only k can be a function of temperature because the concentrations remain constant or very nearly so as the temperature changes only a small amount. Therefore, it is the rate constant that incorporates information about the effect of temperature on the rate of a reaction.

There are several types of behavior exhibited when the rates of reactions are studied as a function of temperature. Three of the most common variations in rate with temperature are shown in Fig. 30.

The first case shows the variation followed by most reactions, that of an exponentially increasing rate as temperature increases. The second shows the behavior of some material that becomes explosive at a certain temperature. At temperatures below the explosive limit, the rate is essentially unaffected by the temperature. Then, as the temperature is reached at which the material becomes explosive, the rate increases enormously as the temperature is increased only very slightly. In the third case, we see the variation in rate of reaction that is characteristic of many biological processes. For example, reactions involving enzymes (biological catalysts) frequently increase in rate up to a certain temperature and then decrease in rate at higher temperatures. Enzymes are protein materials that can change conformation or become denatured at high temperatures.

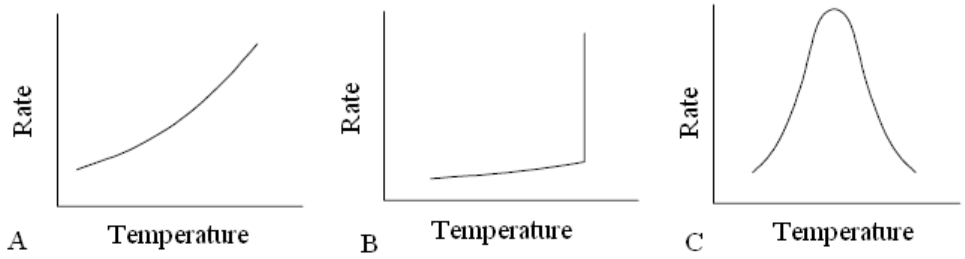

Fig. 30. Some of the ways in which reaction rates vary with temperature

Svante August Arrhenius suggested in the late 1800s that the rates of most reactions vary with temperature (as shown in Fig. 30 a) in such a way that

$$k = Ae^{-E_a/RT} \qquad (114)$$

where k is the rate constant, A is the frequency factor (or pre-exponential factor), R is the molar gas constant, E_a is the activation energy, and T is the temperature (K). This equation is generally referred to as the *Arrhenius equation*. If we take the natural logarithm of both sides of Eq. (114), we obtain

$$\ln k = -\frac{E_a}{RT} + \ln A \qquad (115)$$

By rearrangement, this equation can be put in the form of a straight line,

$$\ln k = -\frac{E_a}{R} \cdot \frac{1}{T} + \ln A \qquad (116)$$

$$y = m \cdot x + b$$

Therefore, a plot of ln *k* versus 1/T can be made or linear regression performed after the rate constants have been determined for a reaction carried out at several temperatures. The slope of the line is - E_a/R and the intercept is ln *A*. Such a graph, like that shown in Fig. 31, is often called an *Arrhenius plot*. It is from the slope, determined either numerically or graphically, that the activation energy is determined.

For a particular reaction, the following rate constants were obtained when the reaction was studied at a series of temperatures which yielded the data shown on the next page.

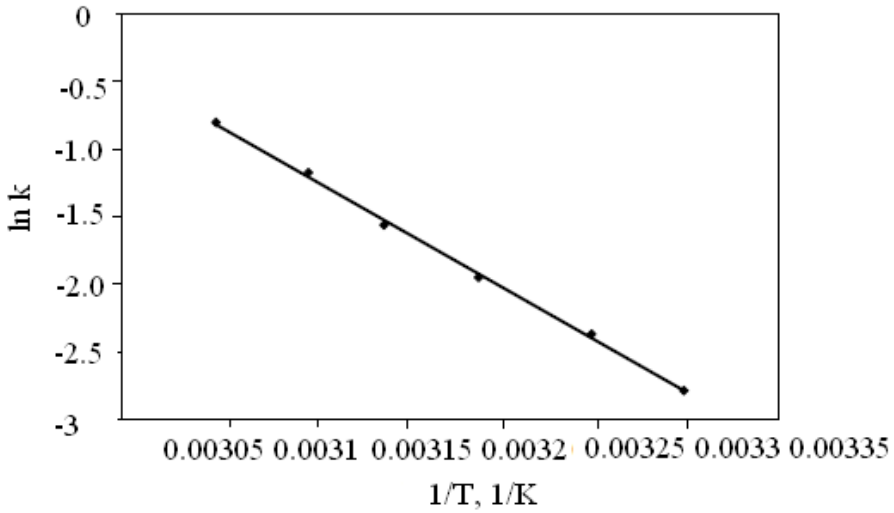

Fig. 31. An Arrhenius plot constructed using the data in the text

In determining the activation energy from an Arrhenius plot, it is important to observe several precautions. For example, if the reaction is being studied at 300 K, the value of 1/T will be 0:00333 K^{-1}. If the reaction is then studied at 305 K, the value of 1/T will be 0:00328K^{-1}.

Such small differences in 1/T make it very difficult to determine the slope of the line accurately, especially if the temperature has not been controlled very accurately. Consequently, it is desirable to study a reaction over as large a range of temperature as possible and to use several temperatures within that range in order to minimize errors. For most reac-

tions, the temperature range in which the reaction can be studied is rather limited because at low temperatures the reaction will be very slow and at high temperatures the reaction will be very fast. Therefore, it is generally desired to study a reaction over a range of at least 20–25^{0}C.

If the rate constant for a reaction is determined at only two temperatures, it is still possible to evaluate the activation energy, but such a case is not nearly as desirable as the procedure described earlier. Small errors in the rate constants will cause inaccuracy in the activation energy determined, because all of the errors in placing the line are present in only two points. More data would be needed to ‘‘average out’’ the error in the value of any one rate constant. If k_1 is the rate constant at T_1 and k_2 is the rate constant at T_2, we can write the Arrhenius equation as

$$\ln k_1 = \ln A - \frac{E_a}{RT_1} \qquad (117)$$

$$\ln k_2 = \ln A - \frac{E_a}{RT_2} \qquad (118)$$

Subtracting the equation for $\ln k_2$ from that giving $\ln k_1$ gives

$$\ln k_1 - \ln k_2 = (\ln A - \frac{E_a}{RT_1}) - (\ln A - \frac{E_a}{RT_2}) \qquad (119)$$

We can simplify this equation to obtain

$$\ln \frac{k_2}{k_1} = \frac{E_a(T_2 - T_1)}{RT_1T_2} \qquad (120)$$

3.2 The object and the main features of the plasma chemistry

Plasma chemistry studies the kinetics and mechanisms of chemical reactions and physicochemical processes in low-temperature plasmas. It should be emphasized that in the plasma chemistry, the term "plasma" is understood as a substance containing not only the charged particles, but molecules in the ground electronic state with an excess (non-equilibrium) internal energy.

In plasma chemistry it is particularly important to discriminate low-temperature plasma on the quasi-equilibrium that exists at pressures above atmospheric, and characterized by a common temperature for all particles, and the non-equilibrium in which the temperature of free electrons is much higher than the temperature of heavy particles (molecules, ions). This division is due to the fact that the kinetics of the quasi-

equilibrium plasma chemical processes is determined only by a high temperature of the interacting particles, whereas the specific of the non-equilibrium plasma-chemical processes is due to a large contribution of the internal energy of the molecules into their chemical activity.

A low-temperature plasma is plasma with a temperature of 10^3-10^5 K and the degree of ionization of 10^{-6}-0.1, obtained from electric, high-frequency and microwave gas discharges, in shock tubes, adiabatic compression machines and by other methods.

Plasma chemistry today is a rapidly expanding area of science and engineering, with applications widely spread from micro-fabrication in electronics to making protective coatings for aircrafts, from treatment of polymer fibers and films before painting to medical cauterization for stopping blood and wound treatment, and from production of ozone to plasma TVs.

Applications of plasma technologies today are numerous and involve many industries. High-energy efficiency (energy cost with respect to the minimum determined by thermodynamics), high specific productivity (productivity per unit volume of reactor), and high selectivity may be achieved in plasmas for a wide range of chemical processes. As an example, for CO_2 dissociation in non-equilibrium plasma under supersonic flow conditions, it is possible to selectively introduce up to 90 % of the total discharge power in CO production when the vibrational temperature is about 4000 K and the translational temperature is only about 100 K. The specific productivity of such a supersonic reactor achieves 1,000,000 L/h, with power levels up to 1 MW. This plasma process has been examined for fuel production on Mars, where the atmosphere mostly consists of CO_2. On the Earth, it was applied as a plasma stage in a two-step process for hydrogen production from water.

3.2.1 Quasi-equilibrium plasma-chemical processes

A plasma in which the particle states (the velocity distribution and internal states) can be well described by the Maxwell-Boltzmann distribution with a single temperature is called a quasi-equilibrium plasma. In equilibrium plasmas this is fulfilled very strictly. This distribution is often called an equilibrium distribution. In this case, the plasma composition (concentrations of ions, electrons, atoms, radicals, etc.) is equilibrium and determined, except for the initial conditions, by a single parameter - the temperature T, which is the same for all particles. Usually, quasi-equilibrium plasmas are formed at pressures close to atmospheric. Since in the gas-discharge plasmas the energy from an external source is deliv-

ered to a heavy component by the electrons, the full balance in such a system cannot be achieved. To transfer energy to the gas the electron energy (temperature) is always greater than the temperature of heavy particles (unlikely to the plasma which is produced in adiabatic compression). Plasma-chemical processes carried out in such conditions, are considered as quasi-equilibrium processes.

Despite the equilibrium character of the physical and chemical processes in plasmas formed in the temperature range of 3000-5000 K the chemical reactions occur with a very high speed, so that their characteristic times are of the same order that the times of heat and mass transfer. As a result, the processes can be transformed from the kinetic region of percolation to the diffusion. The reaction mechanisms are undergoing significant changes, in particular, can enter the reaction with the walls of a reactor. The plasma in this case is considered only as an effective energy carrier.

3.2.2 Non-equilibrium plasma-chemical processes

As it was shown above in case of thermodynamic equilibrium the energy supplied, used to initiate chemical reactions, is very inefficient. There is a wide distribution of the total energy of molecules and a broad distribution of the internal energy of molecule.

A fundamentally different situation takes place when the initiation of chemical reactions occurs in plasma. The energy of the electric field of the gas discharge is transferred to the electrons, which give it to other plasma particles while colliding with them. In elastic collisions due a low mass of electrons the efficiency of electron energy transfer into kinetic energy of heavy particles is small and proportional to the ratio of the electron mass to molecule mass, i.e., does not exceed 0.05 % for hydrogen atom.

Therefore, most of the electron energy is transferred to internal degrees of freedom of the molecules, creating an unbalanced distribution of the energy input. In turn, the ions and excited particles (especially in the metastable electronic states) may have a decisive influence on the mechanism and kinetics of plasma chemical reactions. The rates of reactions with participation of excited particles, ions and radicals is much higher than the rate of formation of these particles, so the overall rate of chemical reactions is limited by the stage of formation.

Low-temperature plasma is bounded by solid walls of the vessel in which it is generated, and at reduced pressures, the characteristic time of

particle diffusion to the walls of the vessel approaches the characteristic times of chemical reactions. As a result, the role of heterogeneous (on the walls), physic-chemical processes is increasing to such an extent that they should be considered when analyzing the mechanisms and kinetics of plasma chemical reactions.

In non-equilibrium plasma the distribution of velocity and the internal states are different, in general, from that in Maxwell-Boltzmann distribution. In this situation we should use a set of Boltzmann equilibrium distributions with different temperatures for different particle states. The internal state of the particles are divided into rotational, vibrational, and electronic, the populations of which are described by the equilibrium Boltzmann distribution with temperatures T_r, T_v, T_e, respectively. If the electron velocity distribution is Maxwellian with the temperature T_e, and the distribution of atoms and molecules by velocities (a translational degree of freedom) is also Maxwellian with the temperature T_g (gas temperature), then, for a non-equilibrium plasma

$$T_g \neq T_r \neq T_v \neq T_e$$

Typically, this situation is observed in the plasma at low pressures (less than 100 Torr). It often happens that $T_g \approx T_r < T_v < T_e$, and if T_g and T_r are close to room temperature (300K), the electron temperature corresponds to the average energy of several electron volts (1 eV = 11600K). Non-equilibrium thermodynamics is a consequence of "openness" of the system. Plasma-chemical processes carried out in such conditions, are defined as non-equilibrium processes.

3.3 Elementary Plasma-Chemical Reactions

The yield of a total plasma-chemical process is due to synergistic contributions of numerous different elementary reactions taking place simultaneously in a discharge system. The sequence of transformations of initial chemical substances and electric energy into products and thermal energy is usually referred to as the *mechanism of the plasma-chemical process*. Elementary reaction rates are determined by the micro-kinetic characteristics of individual reactive collisions (like, for example, reaction cross sections or elementary reaction probabilities) as well as by relevant kinetic distribution functions (like the electron energy distribution function [EEDF], or population function of excited molecular states).

The elementary reaction rate is actually a result of integration of the reaction cross section or probability over the relevant distribution function and characterizes the energy or excitation state of reactants. We will focus

in this chapter mostly on the micro-kinetics of the elementary reactions – on their cross sections and probabilities.

3.3.1 Ionization processes

Plasma is an ionized gas. The key process in plasma is ionization, which means conversion of neutral atoms or molecules into *electrons* and *positive ions*. Thus, ionization is the first elementary plasma-chemical processes to be considered.

Usually the number densities of electrons and positive ions are equal or close in quasineutral plasmas, but in "electronegative" gases (like O_2, Cl_2, SF_6, UF_6, $TiCl_4$, etc.) with high electron affinity, negative ions are also effectively formed. Because ionization is the first plasma-chemical reaction to consider, let us first briefly discuss the main features of elementary charged particles in plasma and their elastic and inelastic collisions. Electrons are first in getting energy from electric fields, because of their low mass and high mobility. Electrons then transmit the energy to all other plasma components, providing energy for ionization, excitation, dissociation, and other plasma-chemical processes. The rates of such processes depend on how many electrons have enough energy to do the job. It can be described by means of the *electron energy distribution function (EEDF) f* (ε), which is the probability density for an electron to have energy ε.

The EEDF strongly depends on electric field and gas composition in plasma (especially in non-thermal discharges) and often can be very far from the equilibrium distribution.

Sometimes, however (even in non-equilibrium plasmas), the EEDF is determined mostly by the electron temperature T_e and, therefore, can be described by the quasi-equilibrium Maxwell-Boltzmann distribution function:

$$f(\varepsilon) = 2\sqrt{\varepsilon / \pi (kT_e)}^{3} \exp(-\varepsilon / kT_e) \qquad (121)$$

where k is a Boltzmann constant (when temperature is given in energy units, then $k = 1$ and can be omitted). The *mean electron energy*, which is the first moment of the distribution function, in this case is proportional to temperature in the conventional way:

$$\langle \varepsilon \rangle = \int_0^\infty \varepsilon f(\varepsilon) d\varepsilon = \frac{3}{2} T_e \qquad (122)$$

Numerically, in most plasmas under consideration, the mean electron energy is from 1 to 5 eV.

Atoms or molecules lose their electrons in the ionization process and form positive ions. In hot thermonuclear plasmas, the ions are multi-charged, but in relatively cold plasmas of technological interest their charge is usually equal to +1e ($1.6 \cdot 10^{-19}$ C). Ions are heavy particles, so usually they cannot receive high energy directly from electric fields because of intensive collisional energy exchange with other plasma components. The collisional nature of the energy transfer results in the fact that the ion energy distribution function at lower pressures is often not far from the Maxwellian one (120), with an ion temperature Ti close to neutral gas temperature T0.

Electron attachment leads to formation of negative ions with charge−1e (1.6 10^{-19} C). Attachment of another electron and formation of multi-charged negative ions is actually impossible in the gas phase because of electric repulsion. Negative ions are also heavy particles, so usually their energy balance is due not to electric fields but to collisional processes. The energy distribution functions for negative ions, similar to that for the positive ones, are not far from the Maxwellian distributions (121) at pressures that are not too low. Their temperatures in this case are also close to those of a neutral gas.

3.3.2 Classification of Ionization Processes

Mechanisms of ionization can be very different in different plasma-chemical systems and may be subdivided generally into the following five groups.

1 *Direct ionization by electron impact* is ionization of neutral and previously unexcited atoms, radicals, or molecules by an electron whose energy is high enough to provide the ionization act in one collision. These processes are the most important in cold or non-thermal discharges, where electric fields and therefore electron energies are quite high, but where the excitation level of neutral species is relatively moderate.

2 *Stepwise ionization by electron impact* is ionization of preliminary excited neutral species. These processes are important mostly in thermal or energy-intense discharges, when the ionization degree n_e/n_0 as well as the concentration of highly excited neutral species is quite high.

3 *Ionization by collision of heavy particles* takes place during ion–moleculeor ion–atom collisions, as well as in collisions of electronically or vibrationally excited species, when the total energyof the collision partners exceeds the ionization potential. The chemical energy of colliding neutral species can also contribute to ionization in the so-called associative ionization processes.

4 *Photo-ionization* takes place in collisions of neutrals with photons, which result in the formation of an electron–ion pair. Photo-ionization is mostly important in thermal plasmas and in some mechanisms of propagation of non-thermal discharges.

5 *Surface ionization (electron emission***)** is provided by electron, ion, and photon collisions with different surfaces or simply by surface heating. This ionization mechanism is quite different from the first four.

3.3.3 Direct Ionization by Electron Impact

Direct ionization is a result of the interaction of an incident electron, having a high energy ε, with a valence electron of a preliminary neutral atom or molecule. Ionization occurs when the energy $\Delta\varepsilon$ transferred to the valence electron exceeds the ionization potential *I*. Analysis of the elementary process obviously requires a quantum mechanical consideration, but a clear physical understanding can be obtained from the classical Thomson model (1912). The valence electron is assumed to be at rest in this model, and interaction of the two colliding electrons with the rest of the atom is neglected. The differential cross section of the incident electron scattering with energy transfer $\Delta\varepsilon$ to the valence electron can be defined by the Rutherford formula:

$$d\sigma_i = \frac{1}{(4\pi\varepsilon_0)^2}\frac{\pi e^4}{\varepsilon(\Delta\varepsilon)^2}d(\Delta\varepsilon) \qquad (123)$$

When the transferred energy exceeds the ionization potential, $\Delta\varepsilon \geq$ I, direct ionization takes place. Thus, integration of (120) over $\Delta\varepsilon \geq 1$ gives an expression for the ionization cross section by direct electron impact, known as the *Thomson formula:*

$$\sigma_i = \frac{1}{(4\pi\varepsilon_0)^2}\frac{\pi e^4}{\varepsilon}\left(\frac{1}{I}-\frac{1}{\varepsilon}\right) \qquad (124)$$

Expression (121) should be multiplied, in general, by the number of valence electrons, Z_v. At high electron energies, ε » I, the Thomson cross section (121) is falling as $\sigma_i \sim 1/\varepsilon$. Quantum-mechanical treatment gives a more accurate but close asymptotic approximation: $\sigma_i \sim \ln \varepsilon/\varepsilon$. When ε=2I, the Thomson cross section reaches the maximum value:

$$\sigma^{\max}{}_i = \frac{1}{(4\pi\varepsilon_0)^2}\frac{\pi e^4}{4I^2} \qquad (125)$$

The Thomson formula can be rewritten taking into account the kinetic energy ε_v of the valence electron:

$$\sigma_i = \frac{1}{(4\pi\varepsilon_0)^2}\frac{\pi e^4}{\varepsilon}\left(\frac{1}{\varepsilon} - \frac{1}{I} + \frac{2\varepsilon_v}{3}\left(\frac{1}{I^2} - \frac{1}{\varepsilon^2}\right)\right) \qquad (126)$$

The Thomson formula (124) agrees with (123), assuming the valence electron is at rest and $\varepsilon_v = 0$. An interesting variation of the Thomson formula (124) can be obtained assuming a Coulomb interaction of the valence electron with the rest of the atom and taking $\varepsilon_v = I$:

$$\sigma_i = \frac{1}{(4\pi\varepsilon_0)^2}\frac{\pi e^4}{\varepsilon}\left(\frac{5}{3I} - \frac{1}{\varepsilon} - \frac{2I}{3\varepsilon^2}\right) \qquad (127)$$

All the modifications of the Thomson formula can be combined using the generalized function f (ε/I) common for all atoms:

$$\sigma_i = \frac{1}{(4\pi\varepsilon_0)^2}\frac{\pi e^2}{I^2} Z_v f\left(\frac{\varepsilon}{I}\right) \qquad (128)$$

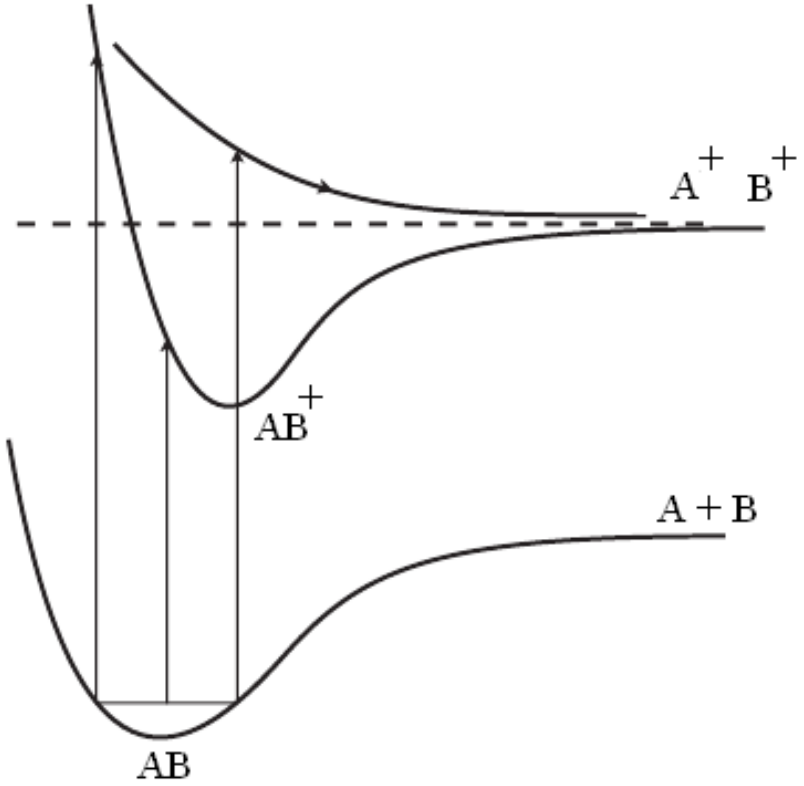

Fig. 32. Molecular and ionic terms illustrating dissociative ionization of molecules AB

3.3.4 Stepwise ionization by electron impact

When the plasma density and, therefore, the concentration of excited neutrals are high enough, the energy *(I)* necessary for ionization can be provided in two different ways. First, like in the case of direct ionization, it could be provided by the energy of plasma electrons. Second, the high

energy of preliminary electronic excitation of neutrals can be converted in the ionization act, which is called stepwise ionization. If the level of electronic excitation is high enough, stepwise ionization is much faster than direct ionization, because the statistical weight of electronically excited neutrals is greater than that of free plasma electrons. In other words, when $T_e \ll I$, the probability of obtaining high ionization energy I is much lower for free plasma electrons (direct ionization) than for excited atoms and molecules (stepwise ionization).

In contrast to direct ionization, the stepwise process includes several steps to provide the ionization event. At first, electron–neutral collisions prepare highly excited species, and then a final collision with a relatively low-energy electron provides the actual ionization event.

In thermodynamic equilibrium, the ionization process $e+A \rightarrow A^+ + e + e$ is inverse to the three-body recombination $A^+ + e + e \rightarrow A^* + e \rightarrow A + e$, which proceeds through a set of excited states. According to the principle of detailed equilibrium, the ionization process $e+A \rightarrow A^+ + e +$e should go through the set of electronically excited states as well, which means the ionization should be a stepwise process. However, this conclusion can only hold true for quasi-equilibrium or thermal plasmas.

A description of the stepwise ionization and the calculation of rate coefficient can be found in Fridman (2008) [1]

3.3.5 Ionization in collisions of heavy particles: adiabatic principle and Massey parameter

An electron with a kinetic energy only slightly exceeding the ionization potential is often quite effective in producing the ionization event; however, this is not true for ionization by collisions of heavy particles – ions and neutrals. Even when they have enough kinetic energy, they actually cannot provide ionization, because their velocities are much less than those of electrons in atoms. Even if it has enough energy, a heavy particle is very often unable to transfer this energy to an electron inside an atom because the process is far from resonant. Such slow motion may be termed “adiabatic” and is unable to transfer energy to a fast-moving particle. The adiabatic principle can be explained in terms of the relationship between low interaction frequency $\omega_{int} = \alpha \upsilon$ and high frequency of electron transfers in atoms, $\omega_{tr} = \Delta E / \hbar$. Here $1/\alpha$ is a characteristic size of the interacting neutral particles, υ is their velocity, and ΔE is a change of electron energy in the atom during the interaction. Only fast Fourier components of the slow interaction potential between particles with frequen-

cies about $\omega_{tr} = \Delta E/\hbar$ provide the energy transfer between the interacting particles. The relative weigh to probability of these fast Fourier components is very low if $\omega_{tr} \gg \omega_{int}$; numerically it is about $\exp(-\omega_{tr}/\omega_{int})$. As a result, the probability P_{EnTr} of energy transfer processes (including the ionization process under consideration) are usually proportional to the so-called Massey parameter:

$$P_{EnTr} \propto \exp(-\frac{\omega_{tr}}{\omega_{\text{int}}}) \propto \exp(-\frac{\Delta E}{\hbar \alpha \upsilon}) = \exp(-P_{Ma}) \qquad (129)$$

where $P_{Ma} = \Delta E/\hbar\alpha\upsilon$ is the adiabatic Massey parameter. If $P_{Ma} \gg 1$, the process of energy transfer is adiabatic and its probability is exponentially low. It takes place in collisions of heavy neutrals and ions.

3.3.6 Penning ionization effect and associative ionization

If the electronic excitation energy of a metastable atom A^* exceeds the ionization potential of another atom B, their collision can lead to an act of ionization, the so-called Penning ionization.

The Penning ionization usually proceeds through the intermediate formation of an unstable excited quasi molecule in the state of autoionization; cross sections of the process can be very high. Cross sections for the Penning ionization of N_2, CO_2, Xe, and Ar by metastable helium atoms *He(2^3S)*with an excitation energy of 19.8eV reach gas-kinetic valuesof about 10^{-15} cm^2. Similar cross sections can be attained in collisions of metastable neon atoms (excitation energy 16.6 eV) with argon atoms (ionization potential 15.8 eV).

An exceptionally high cross section of 1.4 10^{-14} cm^2 (Smirnov, 1974) can be achieved in Penning ionization of mercury atoms (ionization potential 10.4 eV) by collisions with the metastable helium atoms *He(2^3S, 19.8 eV).* If the total electronic excitation energy of colliding particles is not sufficient, ionization is still possible when heavy species stick to each other, forming a molecular ion. Such a process is called the *associative ionization*; for example,

$$Hg(6^3P_1, E = 4.9eV) + Hg(6^3P_{0,} E = 4.7eV) \rightarrow Hg_2^+ + e \qquad (130)$$

The total electronic excitation energy here (9.6 eV) is less than the ionization potential of mercury atoms (10.4 eV) but higher than ionization potential for a Hg^{-2} molecule. This is actually the main "trick" of the associative ionization. Cross sections of the associative ionization (similar to the Penning ionization) can be quite high and close to the gas-kinetic value (about 10^{-15} cm^2). Associative ionization $A^*+B \rightarrow AB^+ + e$ takes place effectively when there is a crossing of the electronic energy term of the

colliding particles with an electronic energy term of the molecular ion AB^+ and, as a result, the process is non-adiabatic. Such a situation takes place only for a limited number of excited species.

3.4 Elementary plasma-chemical reactions of positive ions

Positive ions are obviously major players in plasma-chemical processes. Their exothermic reactions with neutrals usually have no activation energy, which makes their contribution significant in many specific plasma-chemical processes, particularly in plasma catalysis.

In addition to high chemical activity, the ions can have significant kinetic energy, which determines their contribution, for example, in reactive ion etching.

3.4.1 Different Mechanisms of Electron–Ion Recombination in Plasma

Electron–ion recombination is a highly exothermic process. Therefore, the process should have a specific channel of accumulation of the energy released during the neutralization of a positive ion and anelectron. Most of these channels of recombination energy consumption are related, either to dissociation of molecules or to three-body collisions or to radiation, which determines the following three major groups of mechanisms of *electron–ion recombination.*

1 The fastest electron neutralization mechanism in molecular gases, or in the presence of molecular ions, is *dissociative electron–ion recombination*:

$$e + AB^+ \rightarrow (AB)^* \rightarrow A + B^* \qquad (131)$$

Recombination energy in these processes goes into dissociation of the intermediately formed molecule ion and to excitation of the dissociation products. These processes are common for molecular gases, but they can also be important in atomic gases because of the formation of molecular ions in the ion conversion processes:

$$A^+ + A + A \rightarrow A_2^+ + A \qquad (132)$$

2 *Electron–ion neutralization* is due to a three-body electron–ion recombination in atomic gases in the absence of molecular ions:

$$e + e^+ A^+ \rightarrow A^* + e \qquad (133)$$

Energy excess in this case is going into the kinetic energy of a free electron, which participates in the recombination act as “a third-body partner”. We must remark that heavy particles (ion and neutrals) are una-

ble to accumulate electron recombination energy fast enough in their kinetic energy and, therefore, are ineffective as the third- body partner.

3 Finally, the recombination energy can be converted into radiation in the process of *radiative electron–ion recombination*:

$$e + A^+ \rightarrow A^* \rightarrow A + \hbar\varpi \qquad (134)$$

The cross sectionof this process is relatively low and can competewith the three-body recombination only when the plasma density is not high.

3.5 Elementary plasma-chemical reactions involving negative ions

3.5.1 Dissociative electron attachment to molecules as a major mechanism of negative ion formation in electronegative molecular gases

The dissociative attachment is effective when the products have positive electron affinities

$$e + AB \rightarrow (AB^-)^* \rightarrow A + B^- \qquad (135)$$

The mechanism of the process is similar to the dissociative recombination (Section 2.2.2) and proceeds by intermediate formation of an autoionization state $(AB^-)^*$. This excited state is unstable and decays, leading either to the reverse reaction of auto-detachment (AB+e) or to the dissociation ($A+B^-$). An electron is captured during the attachment and is not able to provide the energybalance of the elementary process. Therefore, the dissociative attachment is a resonant reaction requiring a quite definite electron energy.Typical potential energy curves are presented in Fig. 33. The process starts with a vertical transition from the AB ground state to a repulsive state of AB− following the Frank-Condon principle [30]. During the repulsion, before $(AB^-)^*$ reaches the inter section point of AB and AB^- electronic terms, the reverse auto-detachment reaction (AB+e) is very possible. But after passing the intersection, the AB potential energy exceeds that of $AB^-$and further repulsion results in dissociation ($A+B^-$).

Some halogen compounds have an electron affinity of a product exceeding the dissociation energy; corresponding potential energy curves are presented in Fig. 34.

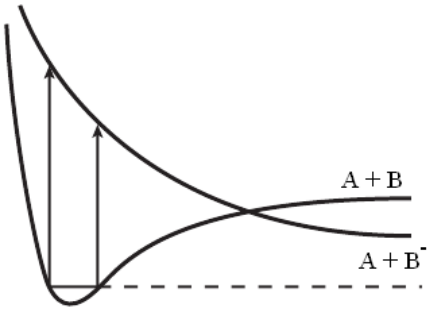

Fig. 33. Elementary process of dissociative attachment in the case of low electron affinity

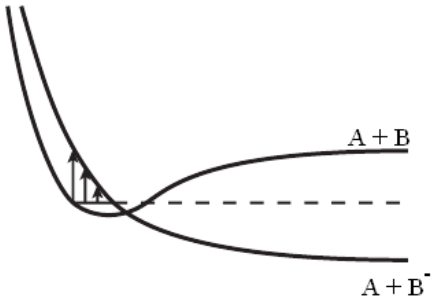

Fig. 34. Elementary process of dissociative attachment in the case of high electron affinity

In this case, in contrast to Fig. 33, even very-low-energy electrons provide dissociation. The intersection point of AB and AB^- electronic terms (Fig. 34) is actually located in this case inside of the so-called geometric size of the dissociating molecule. As a result, during the repulsion of $(AB^-)^*$, the probability of the reverse auto-detachment reaction (AB+e)is very low and the cross section of the dissociative attachment reaches the gas-kinetic value σ_0 of about 10^{-16} cm^2.

3.5.2 Three-body electron attachment and other mechanisms of formation of negative ions

Electron collisions with two heavy particles also can result in the formation of negative ions:

$$e + A + B \rightarrow A^- + B \qquad (136)$$

The three-body electron attachment can be a principal channel for electron losses when electron energies are not high enough for the dissociative attachment, and when pressure is elevated (usually more than 0.1 atm) and the third-order kinetic processes are preferable.

In contrast to the dissociative attachment, the three-body process is exothermic and its rate coefficient does not depend strongly on electron temperature. Electrons are usually kinetically less effective as a third body B because of a low degree of ionization. Atmospheric-pressure non-thermal discharges in air are probably the most important systems, where the three-body attachment plays a key role in the balance of charged particles:

$$e + O_2 + M \rightarrow O_2^- + M \qquad (137)$$

This process proceeds by the two-stage Bloch-Bradbury mechanism (Bloch&Bradbury, 1935; Alexandrov, 1981) starting with the formation

of a negative ion (rate coefficient k_{att}) in an unstable auto-ionization state (τ is the time of collisionless detachment):

$$e + O_2 \xleftrightarrow{k_{att},\tau} (O_2^-)^* \qquad (138)$$

The second stage of the Bloch-Bradbury mechanism includes collision with the third-body particle M (density n_0), leading to relaxation and stabilization of O^-_2 or collisional decay of the unstable ion:

$$(O_2^-)^* + M \xrightarrow{k_{st}} O_2^- + M \qquad (139)$$

$$(O_2^-)^* + M \xrightarrow{k_{dec}} O_2 + e + M \qquad (140)$$

Taking into account the steady-state conditions for number density of the intermediate excited ions $(O^-_2)^*$, the rate coefficient for the total attachment process (138) can be expressed as

$$k_{3M} = \frac{k_{att} k_{st}}{\frac{1}{\tau} + (k_{st} + k_{dec}) n_0} \qquad (141)$$

Usually, when the pressure is not too high, $(k_{st} + k_{dec}) n_0 \ll \tau^{-1}$, and (141) can be simplified

$$k_{3M} \approx k_{att} k_{st} \tau \qquad (142)$$

Thus, the three-body attachment (137) has a third kinetic order and depends equally on the rate coefficients of formation and stabilization of negative ions. The latter strongly depends on the type of the third particle: the more complicated molecule a third body (M) is, the easier it stabilizes the $(O^-_2)^*$ and the higher the rate coefficient k_{3M}. Numerical values of the total rate coefficients k_{3M} are presented in Table 5; dependence of the total rate coefficients on electron temperature is shown in Fig.35. For simple estimations, when T_e =1eV and T0 =300K, one can take $k_{3M} \approx 10-30$ cm^6/s.

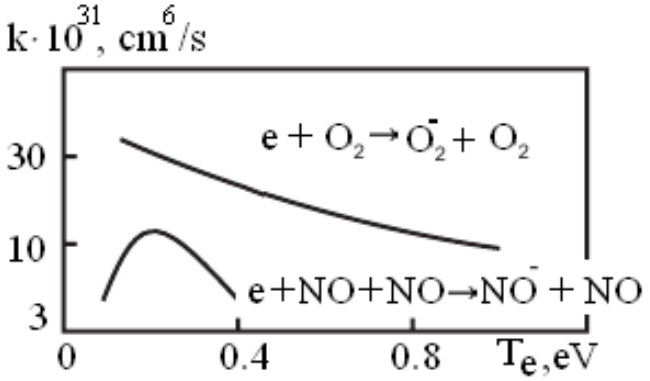

Fig. 35. Rate coefficients of electron attachment to different molecules in three-body collisions as a function of electron temperature; molecular gas is assumed to be at room temperature

The rate of the three-body process is greater than for dissociative attachment (k_a) when the gas number density exceeds a critical value $n_0 > k_a(T_e)/k_{3M}$. Numerically in oxygen, with T_e =1eV,T_0 =300K, the rate requires $n_0 > 10^{18}$ cm^{-3}, or in pressure units p>30 torr. Three other mechanisms of formation of negative ions are usually less significant. The first process is polar dissociation

$$e + AB \rightarrow A^+ + B^- + e \qquad (143)$$

This process includes both ionization and dissociation; therefore, the threshold energy is quite high. On the other hand, an electron is not captured here, and the process is non-resonant and is effective over a wide range of high electron energies. For example, in molecular oxygen, the maximum value of the cross section for polar dissociation is about $3 \cdot 10^{-19}$ cm^2 and corresponds to an electron energy of 35 eV.

To stabilize the formation of a negative ion during electron attachment, the excessive energy can be in principal emitted. As a result, the negative ion can be formed in the process of radiative attachment:

$$e + M \rightarrow (M^-)^* \rightarrow M^- + \hbar\varpi \qquad (144)$$

Such an electron capture can take place at low electron energies, but the probability of the process is very low: 10^{-5}–10^{-7}.Corresponding values of attachment cross sections are about 10^{-21}–10^{-23} cm^2.

Finally, some electronegative polyatomic molecules like SF_6 have a negative ion state very close to a ground state (only 0.1 eV in the case of SF_6). As a result, the lifetime of such metastable negative ions is fairly long. Such a direct one-stage attachment process is resonant and for very low electron energies has maximum cross sections of about 10^{-15} cm^2.

3.6 Special features of plasma-chemical reactions, their dynamics and kinetics

Chemical reaction dynamics are described both by the frequency of reacting particle collisions and by the fields affecting them. The total result of the study in the field of reaction dynamics can be presented as the function, $\sigma(kl/ij;\varepsilon)$ [31].

The *'elementary act'* (i.e. collision dynamics) of a chemical process in 'classical' Arrhenius chemistry occurs under the following conditions: the mean energy of the relative motion of colliding particles (molecules)

is not above 0.1 eV; the population of the first vibrational level of the ground electronic state predominates over the others; reactions of the following type: $e+M, M^{\mp}+M, e+M^{-}$ etc. are practically absent; reaction products are not usually excited; elastic collisions predominate over non-elastic ones. In general molecules may be represented as hard elastic spheres.

In the field of interest (plasma chemistry, radiation chemistry, etc.) the situation is quite different: mean molecule energies are ≥ 0.1 eV; excited molecules are frequently in collision, and chemical reaction products produced by collisions appear often to be in excited states; collisions of molecules with electrons and ions (as well as collisions between molecules) are essential, and there is usually wide difference between translational rates and energy (in the laboratory coordinate system) of the charged particles of small mass (~1-50 eV) and those of heavy particles (~ 0.03-2.3 eV), as well as in the vibrational energy of the latter (~0.2-0.8 eV). The model of elastic spheres is therefore inapplicable [32].

The kinetics of chemical reactions describes the particular type of molecule ensemble behaviour, and this description has a statistical character. Because of this, the kinetic description of ensemble behaviour of various particles is defined, assuming the dynamics of collisions (for instance binary ones) to be known, by molecule quantum level populations and the function for particle distributions by translational energy as well as by ratios of flux probabilities over various channels, for instance

$$M(i)-M(j), \quad M(i)-M'(k),$$

where *i, j, k* is the totality of molecule quantum state parameters.

In classical chemistry this is not so obvious, as it produces a distribution of a Maxwell type occurring at the initial stage, which at later stages is not (or is only slightly) disturbed by a chemical reaction; the population is considered to be of a Boltzmann type with ground level populations predominating.

The transitions of $M(i)-M(j),$ type are therefore disregarded; all the reacting particles have the same mean energy (temperature) giving uniform Maxwell distribution. In plasma chemistry the situation is different; the initial distribution may not be of Maxwell type, and the population may not be Boltzmannian.

Even when the initial distribution is a Maxwell type it is disturbed by a chemical reaction, and the new distribution produced affects the reaction rate; various reaction components may have distribution functions differing in form and mean energy, which can change in the course of

time with various relaxation times. The transitions of $M(i)-M(j)$, type can no longer be neglected in chemical reaction descriptions; non-elastic collision frequencies are not small by comparison with elastic collision frequencies.

Naturally, the chemical reactions possible in a molecule, and their rates, depend on the structure of the molecule (and for non-monomolecular reactions also on other reaction component structures). This, in particular, prevents the introduction of the term 'reactivity', with respect to molecules. The concept of molecular structure can be formulated differently. For our purpose the following definition is believed to be the best: the structure of a molecule, comprising several atoms, is a system of its quantum levels and space distribution of the component particles.

The problem of connecting reactivity with molecular structure is often considered of paramount importance in 'classical' chemical kinetics. However, it cannot be solved within the limits of the molecular model used. Automatically, according to the character of the reactions described using generalized chemical kinetics, the problem is being solved within the latter. This, however, takes place when the vague term 'reactivity' is substituted for k_i.

2. Plasma-chemical reactions may be of the non-equilibrium or quasi-equilibrium types. Various types of plasma-chemical reactions are enumerated in Table 5.

Table 5. Types of plasma-chemical reactions

	Processes occurring in the system	Characteristics of the system	Process Characteristics
Non-equilibrium	Chemical reactions in non-equilibrium systems	Difference between vibrational and translational temperatures	Stationary or relaxing
		Two subsystems, one Maxwellian and the other non-Maxwellian	
Qua-si-	Non-equilibrium in the system due to the occurrence	Two subsystems with different temperatures	Stationary or relaxing

	of chemical reactions	Both subsystems are non-Maxwellian (and non-Boltzmannian)	

The kinetics of plasma-chemical reactions, as seen from Table 5, can be considered as a particular case of non-equilibrium chemical kinetics.

Plasma-chemical reactions in the gas phase (only these reactions will be discussed further) are characterized by the following:

1. Non-elastic collisions[1] are more important in 'hot' gases than in 'ordinary' (monatomic) gases, the properties of which are described well by the kinetic theory based upon the consideration of only elastic collisions. The kinetic theory also explains some properties of polyatomic and reacting gases, assuming the non-elastic collision frequency to be small; such a treatment fails when the gas temperature is increased sufficiently.

2. The difference between the characteristic times of various physical and chemical processes decreases and it becomes impossible to distinguish between the various processes as is possible in classical chemical kinetics.

3. Chemical kinetics cannot be considered independently of physical kinetics in the field of interest. If the reaction rate exceeds the collision frequency for the momentum-transfer collisions, deviations from equilibrium conditions occur. These can lead to violations of the equilibrium Maxwell-Boltzmann energy distribution and to a relative decrease in density of the highly energetic molecules, owing to the occurrence of chemical reactions.

The highly energetic 'tail' of the distribution cannot be maintained at the expense of momentum-transfer collisions since the frequency of such collisions is too small. Hence, the basic principles of the simple kinetic theory of chemical reactions and of absolute reaction rate theory are violated.

A general solution for the distribution function disturbed by chemical reactions has not yet been found. However, this problem has been studied in some particular cases. The effect of a fast chemical reaction upon the Maxwell-Boltzmann distribution and the effect of the distribution thus produced upon the reaction rate were studied in Ref. [33] using the Monte Carlo method. There are well known conditions in which trans-

[1] Non-elastic electron collision cross sections for many molecular gases may be considered to have maxima both at energies of 1-2 eV and above 4--b eV due to excitation of vibrational and rotational, and electronic levels, respectively.

lational, vibrational, and rotational temperatures differ and/or various components of a system (electrons, ions, and neutral molecules, for instance) have different temperatures, and/or a system cannot be described at all using the concept of temperature * (non-equilibrium, stationary, and relaxing systems).

Strictly speaking, Arrhenius-type kinetics cannot be used in these cases and the ordinary expression for the rate of a chemical reaction is inapplicable.

4. Multichannel processes should be considered in plasma-chemical kinetics. From the quantum mechanical point of view (we shall consider only two channels for simplicity), in a certain energy range two pairs of particles (A1, B1) and (A2, B2) can exist, so that there are two independent wave functions which satisfy boundary conditions for a given system. It is known that in a one-channel problem the S-matrix contains all the information about interaction properties of the system, while in a multichannel case a similar theorem has not yet been proved6. Moreover, in order to compose the Hamiltonian using the results of scattering all components of the S-matrix should be known for all energies.

5. The barrier-type nature of the reactions (the existence of an energy barrier opposing the reaction), being peculiar to the Arrhenius classical kinetics, can be completely changed in reactions under plasma conditions. It is necessary to allow for the occurrence of chemical reactions from different quantum levels of the system, and for one of the subsystems as a whole to have above-barrier energy.

6. These five special features of plasma-chemical reactions are peculiar to non-equilibrium chemical processes, and chemical reactions under low-temperature plasma conditions are particular (but still important) cases of such processes. In this section some special features of reactions under plasma conditions are discussed briefly. The degree of ionization is the most important characteristic of a plasma under equilibrium conditions; given the temperature and pressure the degree of plasma ionization may be found using the Saha equation.

Ionization processes result from such factors as mutual collisions of heavy particles at high temperatures (energies), their collisions with electrons, photo-ionization, and ion-molecular reactions. A detailed description of all these processes under non-equilibrium conditions necessitates a generalization of the kinetic gas theory for the plasma state. Such a generalization is still under development. In low-temperature plasmas long range collisions occur, due to electromagnetic interaction between charged particles, in addition to ordinary short-range collisions, such as take place in gases. Thus, very small scattering angles and consequently

many interactions resulting in small momentum transfer must be considered. Moreover, interaction of charged particles with external electromagnetic fields should also be taken into account [34,35,36]

When electron, ion, and molecular gases are not in thermal equilibrium there is energy exchange between electrons and neutral particles and between electrons and ions. The latter occurs through Coulomb-type collisions. Both processes may lead, either directly or through successive steps of excitation, to chemical reactions. The mechanisms and probabilities of these reactions may be studied by plasma-chemical kinetics on the basis of a detailed analysis of all interactions occurring in a system, and using the basic principles of non-equilibrium chemical kinetics. At present the limited usefulness of Arrhenius kinetics, which are valid only close to equilibrium (for example under small perturbations when a system can still be considered in quasi-equilibrium), is evident. In other words, this type of kinetics can be used when a single value of temperature (being the parameter of the Maxwell-Boltzmann distribution) can be defined for the system.

Non-equilibrium distribution of reactants takes place, for instance, when the energy is injected pulsewise into the equilibrium system, provided that the condition $\tau_i \prec \tau_{Ch.r}$ is satisfied, where τ_i is the duration of the pulse and $\tau_{Ch.r}$ is the chemical relaxation time (pulse electrical discharges, shock tubes, flash photolysis). The treatment of kinetic problems which depend more upon the molecular interaction mechanism and molecular quantum level populations* requires far more information about the system [37,38,39]. The importance of the effect of vibrational excitation upon the rate of chemical reaction has been confirmed by the results of experiments[40]. As the vibrational temperature of N_2 molecules is increased from 1000 K to 6000 K (under T_{trans} = 300K) the rate constant for the reaction $O^+ + N_2 \rightarrow N_2^+ + O$ increases by forty times (see Fig. 36). The same change in the translational temperature (under T_{vibr} = const) would lead, in accordance with the Arrhenius equation, to a rate constant increase of sixty times. The effects are comparable.

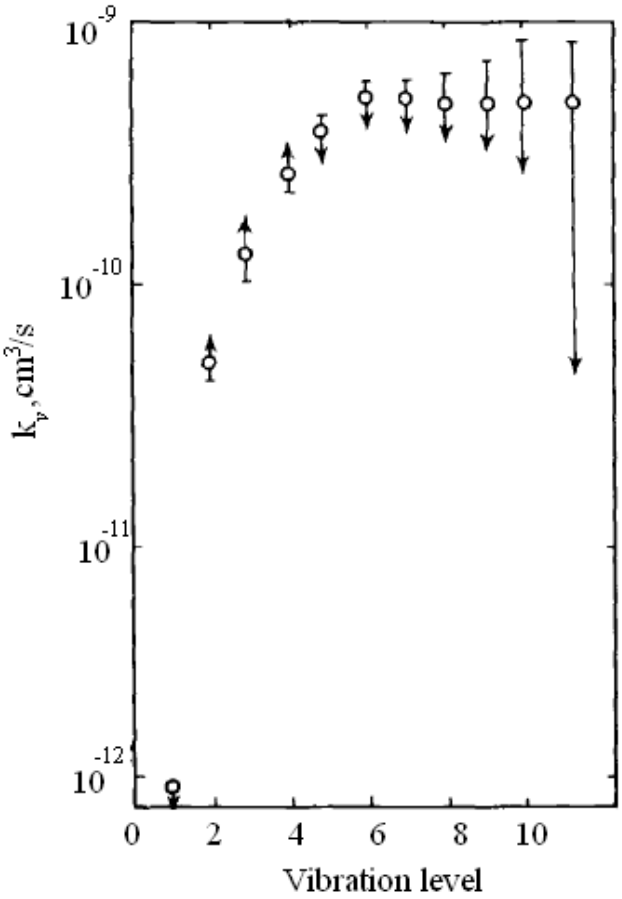

Fig.36. Experimental rate constant dependence on vibrational level numbers up to 10

Non-equilibrium effects may be observed in a system initially in equilibrium if any processes are occurring at finite rates within the system. Such processes inevitably result in a violation of the Maxwell distribution. In particular, such a violation may be due to non-elastic collisions resulting in mass exchange and internal energy redistribution of colliding particles. Hence, the occurrence of chemical reactions always produces non-equilibrium in a system. This non-equilibrium can be neglected (although with a rather vague degree of accuracy) in the classical Arrhenius kinetics when reaction rates are comparatively small. However, at high temperatures in plasma-chemical processes, in radiation chemistry, shock tubes and other conditions, the effects of these reactions must be taken into account. For instance, thermal dissociation of diatomic molecules is known not only to violate the Boltzmann distribution but also to decrease the vibrational temperature in relation to the translational temperature. These changes affect both dissociation rates and vibrational relaxation processes. Non-equilibrium due to a chemical reaction and further occurrence of the reaction under non-equilibrium conditions is the problem to

be studied for non-equilibrium, generalized chemical kinetics. The Arrhenius kinetics appears to be an extreme case and thus are believed to be rigorously founded, their applicability limits being clearly defined. The solution of this problem must be based upon a consideration of the Pauli equation or the Boltzmann equation (or any equation of the Liouville type). Using one of these equations and taking into account chemical reactions and relaxation processes of the internal degrees of freedom of reacting molecules, specific solutions under various conditions can be obtained, including ordinary chemical kinetic equations and expressions for the rate factors (constants) for chemical reactions.

Three solutions to the problems under discussion may be suggested, allowing for the possibility that a set is found of cross sections $\sigma(\varepsilon)$ for the processes involved; all the required information about the system can be obtained through averaging.

3.7 Initiation of plasma-chemical processes by electron-beams

A significant advance in the development of pulsed electron beams sources in recent years [41] encouraged scientists to study plasma formation initiated by high-energy electrons and their energy dissipation channels. In contrast to the space discharge, the use of pulsed electron beams can easily solve the problem of excitation of large volumes of reactive gas at high pressure, which is important for creating high-performance processing facilities.

However, as it was shown by in many articles, the pulsed electron beam is inefficient for direct plasma chemical processes in which the energy of electron impact is the only source for the initiation of chemical reactions. In case with a plasma produced by electron beams, the low-energy electrons (as compared with the energy carried by the electrons in a beam) is only to play a role in plasma chemistry. These low-energy electrons are formed due to relaxation of an electron beam during the formation of ionization cascade of secondary emitted electrons. The excitation of vibrational levels of molecules consumes a small fraction of the energy of a pulsed electron beam, as the electron energy must exceed 20-30 keV in order to overcome the anode foil between the beam generation region and the reactor (see Fig. 37). Calculations performed by the authors [42] showed that with the electron kinetic energy of more than 30 eV, the energy of degradation cascade in nitrogen is spent mostly on the ionization and excitation of electronic levels of the molecule. The energy balance of the electrons cascade with energies above 30 eV is shown in Fig. 38. An electron may loose energy through the excitation of rotation-

al, vibrational and translational degrees of freedom about the ground state of the molecule. At low energy these losses do not exceed 17% and are reduced to 10% with increasing electron energy (curve 5). As a result, the energy of the electron beam consumed on the decomposition of one molecule of the original gas mixture is significantly (10-100 times) higher than its dissociation energy.

In case of high-current beams a significant role is played by the electromagnetic fields and collective electrodynamics processes which have an affect both on the interaction of an electron beam with gases, and on the kinetics of plasma chemical processes taking place.

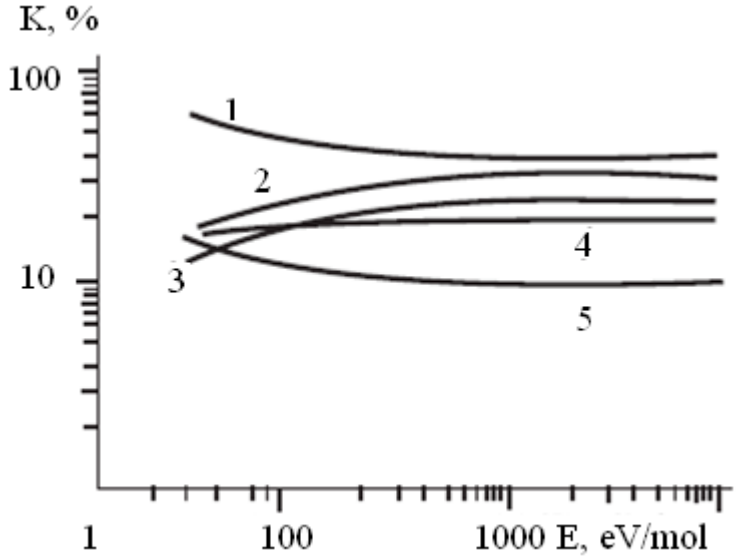

Fig. 37. The energy distribution of the electron with energy T_e on ionization levels and excitation in nitrogen: 1 – total loss on excitation, 2-total loss on ionization, 3 - loss pn excitation of electronic levels, 4 - loss on dissociative ionization, 5 - other losses

The change in the energy distribution of a pulse electron beam on different dissipation channels, taking into account the collective effects is shown in Fig. 38 [43].

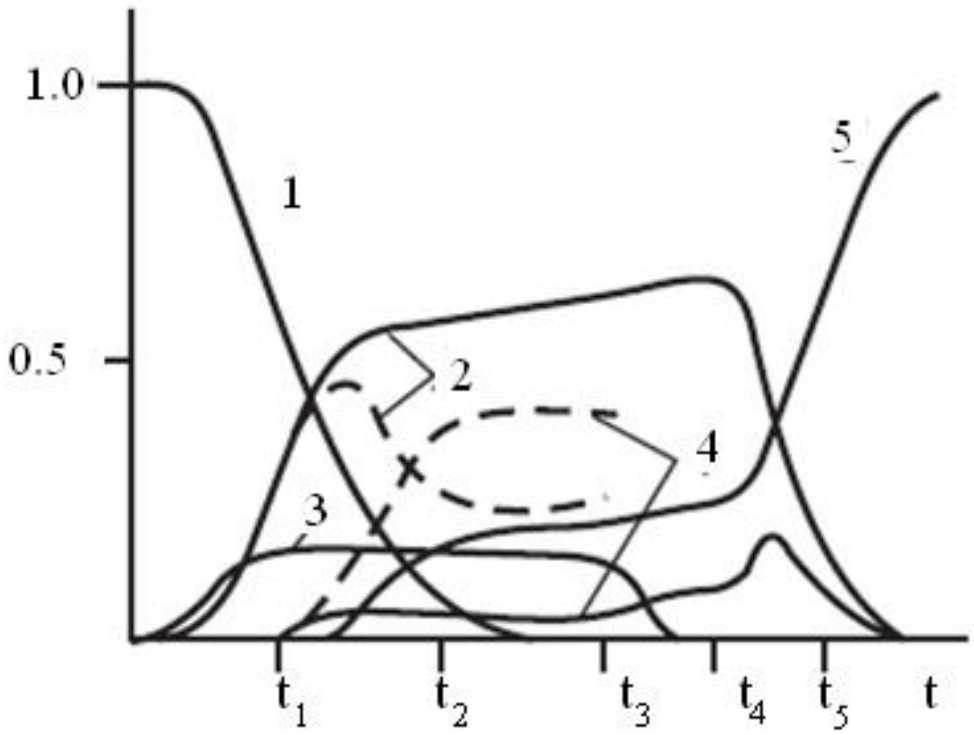

Fig. 38. Redistribution of the energy spent on ionization and ohmic losses of the electron beam at different degrees of freedom of molecular gas plasma: ionization (1), dissociation (2), electron (3) and vibrational (4) excitation and heating of the gas (5). Solid lines - without electric fields, dotted line - in the presence of electric fields

In assessing the effectiveness of plasma-chemical processes in the case of excitation of the reaction gas mixture by a pulsed electron beam one must also take into account that the efficiency of the accelerator (the ratio of the electron beam energy to the total energy consumed by the accelerator) does not usually exceed 50%.

Chapter 4 Chain gas-phase processes in the external action

Over the past 30-40 years in Russia and abroad extensive studies on gas-phase chemical processes initiated by the gas discharge have been carried out. It was found that some favorable conditions for the occurrence of chain processes are formed when the gas discharge has an effect on gas-phase medium. With a sufficient length of the chain an electrophysical installation makes it possible to reduce the total energy consumption required for the chemical process. The primary source of energy in this case is the thermal energy of the initial reactionary gas or the energy of the exothermic elementary reactions of chain process (e.g., reactions of oxidation or polymerization). This can greatly reduce the power inputs of the electrophysical installation. The reduction of the temperature of chain chemical processes at radiation exposure is similar to the catalytic effect. But the chain process can occur entirely in the gas phase, which greatly increases the reaction rate compared to the hetaeraphase catalytic process. Carrying out a chemical process at a temperature below the equilibrium allows one to synthesize compounds which are unstable at higher temperatures or the selectivity of their synthesis at higher temperatures is low. These peculiarities of the behavior of chemical processes under plasma action have shown to be a quite promising in the use of large-scale chemical production. A high speed of the reaction which is required for industrial technologies is achieved by using of branched chain processes. But their major drawback is associated with the occurrence of an explosive process, which significantly increases the risk of production. This disadvantage is eliminated by initiating the chain process under external action out of the self-ignition region.

4.1 Classification of chain processes

Chain processes are the chemical and nuclear transformation, where a large number of elementary reactions (chain) occur due to an active particle (free radical, an atom with an unpaired electron, an excited particle - an ion, a molecule - in chemical reactions, a neutron - in nuclear transformations). The active particle is regenerated as a result of the elementary process.

A chain process consists of three stages: the initiation, the continuation and the termination of the chain. The initiation involves the formation of radicals through the decay of a molecule of the intial product. It requires a high activation energy (~ 3.5 eV/molecule for hydrocarbons), i.e. the reaction can occur in the equilibrium with an appreciable rate only

at temperatures above 1200 K. The continuation of chain consists of the interaction of free radicals with the initial molecules resulting in the formation of a stable molecule of the reaction product and a new radical. The new radical, in turn, interacts with the initial molecules. This stage of the chain process requires much lower activation energy (0.87 eV/molecule for CH_4), therefore, its implementation requires a lower temperature. It is important to note that the major part of chemical reactions occur at the stage of the continuation. An active radical that is formed at the initiation stage can initiate 10^3 - 10^5 of the reactions at the stage of the chain process.

Fig. 39 shows the change in energy consumption for conducting the chemical transformation at different stages of the chain process of radiation-thermal cracking of methane.

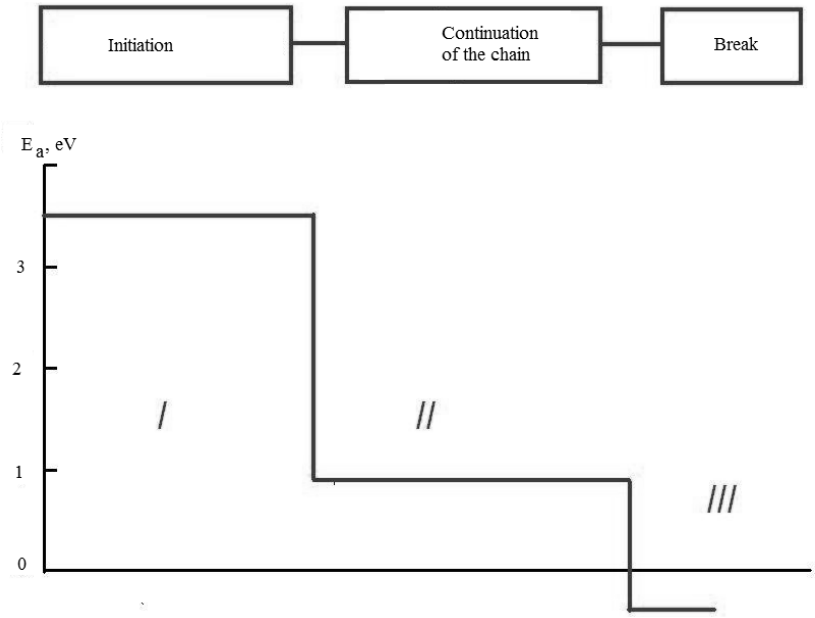

Fig.39. The chart illustrating the power inputs at stages of chain process of methane conversion

At temperatures below 700 K, when the thermal initiation of reaction does not occur, under the influence of the electron beam the active centers - free radicals, ions or excited molecules are formed, which can start a new chain reaction. Such a reaction will take place at a temperature of 150-200 degrees below than the temperature of a normal thermal process, but with the same speed because the impact of plasma facilitates the most energy-intensive phase –the phase of the reaction initiation.

Since 1913 when M. Bodenstein first discovered chain reactions many other different types of chain reactions have been found. There are unbranched chain reactions, chain reactions with quadratic branching,

chain reactions with degenerate branching, chain reactions with energy branching and others.

4.1.1 Unbranched chain reactions

An example of unbranched chain reaction is a reaction of synthesis of hydrogen chloride from a mixture of chlorine and hydrogen molecules. In 1916, W. Nernst (Nobel Prize in 1920) proposed a mechanism of chain reactions which involves Cl atoms.

Initiation of chain process by electron impact

In the plasma formed though electric discharge in the gas mixture of $Cl_2 + H_2$, the following processes may occur:

1 Dissociative ionization: $Cl_2 + e + 11.6\ эВ \rightarrow (Cl_2)^+ + 2e \rightarrow 2e + Cl + Cl^+$

2 Dissociative electron attachment $Cl_2 + e + 2.4\ эВ \rightarrow (Cl_2)^- \rightarrow Cl + Cl^-$

3 Dissociation though inelastic collision $Cl_2 + e + 2.4\ эВ \rightarrow Cl + Cl + e$

Development of chain process

At the stage of chain development the following reactions take place:

$Cl + H_2 \rightarrow HCl + H + 0.05\ eV$ at 100 °C $k_1 = 5 \cdot 10^7$ l/ mole ·c (145)
(slow reaction)

$H + Cl_2 \rightarrow HCl + Cl + 1.97\ eV$ at 100 °C $k_2 = 3 \cdot 10^{10}$ l/ mole ·c (146)
(fast reaction)

Cl atom, formed in the reaction (146) is identical to the Cl atom, reacted in the reaction (145) therefore, the sequence of reactions could be repeated many times (basicly 10^5-10^6 times), the same as the chain links are repeated.

4 Chain termination

At formation of hydrogen chloride from a mixture of $H_2 + Cl_2$, the active particles, which continue the chain, are the atoms of H and Cl. The rate of reaction (2) is much higher than the rate of reaction (1), so the concentration of hydrogen atoms is low and the reaction of chain termination is most likely to occur

$$Cl + Cl + M = Cl_2 + M$$

4.1.2 Chain reactions with quadratic branching

The experimental studies have shown that there exists a class of chain reactions, which are characterized by the fact that at the interaction of the active particles with the initial product along with the reaction product a new active particle is formed. In the course of the reaction the number of active particles increases continuously which leads to a sharp increase in its velocity. This reaction can end up by the explosion. Thus, in the case of the reactions of H_2 with O_2 the cycle of chain consists from the following reactions [44]:

$$H^* + O_2 \rightarrow OH^* + O^*,$$
$$OH^* + H_2 \rightarrow H_2O + H^*,$$
$$O^* + H_2 \rightarrow OH^* + H^*,$$

This cycle of reactions is called the cycle of chain with quadratic branching. Each of the H* and OH* particles formed begins a new cycle of the chain. As a result, their concentration and thus the reaction rate avalanche-like increases, and the entire reaction is completed in a fraction of a second at the initiation of combustion. It is important to note that the heat of the reaction of $2H_2 + O_2 = 2H_2O$, which is equal to 483 kJ/mole, is not immediately converted into kinetic energy of the reaction products, and partially transformed into chemical energy of the active chemical particles of H* and OH*.

It is obvious that branching reactions can occur only as exothermic reactions such as the following: the oxidation of hydrogen, phosphorus and sulfur vapors as well as methane, other hydrocarbons, CS_2 carbon disulfide, carbon monoxide, SiH_4 silane and the decomposition of NCl_3. All of these reactions are characterized by the existence of the so-called ignition peninsula – a region with a pressure and temperature at which the reaction proceeds.

4.1.3 Chain reactions with degenerate branching

This name was given to the numerous radical-chain reactions, which are characterized by the formation of intermediate metastable products. After reaching a maximum speed the reaction is slowed down. The characteristic time of their occurrence is not a fraction of a second, but tens of minutes or hours. The most studied chain reaction with degenerate branching is the oxidation of hydrocarbons. These reactions will be discussed in the more details in Section 4.4.

4.1.4 Electron-induced chain reactions

When an external electric field is applied to a chemically reactive plasma the free electrons may act as active particles of chain process. In this case, during the time between the release of an electron (ionization of the molecule) and its collision with a neutral molecule the electron gains an additional kinetic energy in the external electric field. The scheme of this process was first proposed by Yu. N. Novoselov. It is shown that in the case of non-self-sustained discharge initiated by an electron beam, the energy consumption for the formation of a molecule of methanol can be 4-5 times less than at the self-sustained discharge, which is several electron volts. Much attention was given to the ion-molecular processes that may lead to the emergence of the radicals. In particular, the chain of reaction of

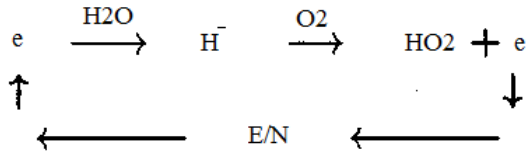

yields OH radicals, HO_2 and the electron, which can repeatedly participate in their formation, obtaining the necessary energy from the electric field.

4.2 Chain chemical processes under external action

The initiation and development of chain processes in external action have been only researched for the last 10-15 years. The development of chain processes such as oxidation of hydrogen, cracking of hydrocarbon gases, partial oxidation of methane, and others under equilibrium conditions has been well studied. Changing the conditions of the chain process is interesting from the standpoint of the synthesis of new products or elimination of defects such as explosibility.

4.2.1 Investigation of the induction period of ignition of the oxygen - hydrogen mixture

A significant drawback of the chain reaction of hydrogen oxidation from the standpoint of technological application is a significant delay (induction period) in ignition. Fig.40 shows the change in pressure in the reactor during the development of the chain process of oxidation of hydrogen in equilibrium, reflecting the presence of the induction period [44].

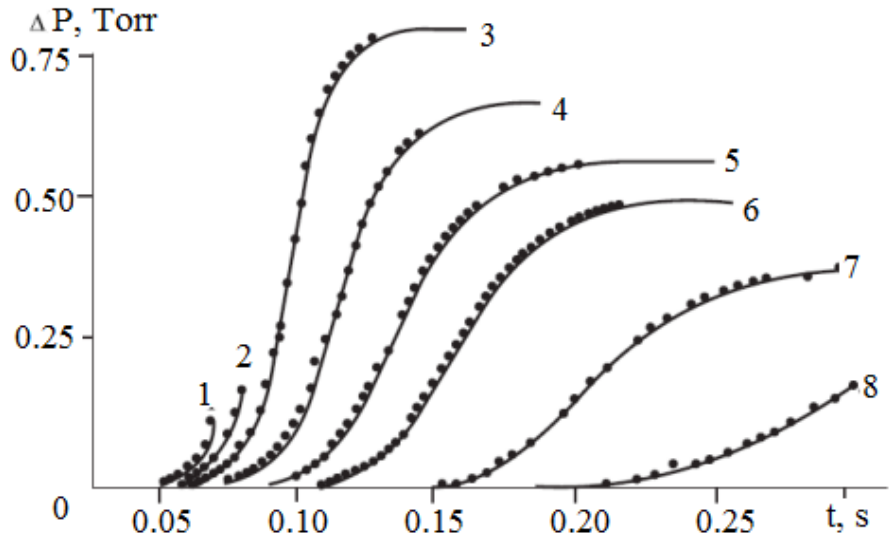

Fig. 40. The curves of the oxidation kinetics of the mixture of $2H_2 + O_2$ at 485°C and at various initial pressures of: 1 - 8.2 Torr; 2 - 7.8 Torr; 3 - 7.4 Torr; 4 - 7.1 Torr; 5 - 6.8 Torr; 6 - 6.4 Torr; 7 - 6.1 Torr; and 8 - 5.8 Torr

The dependence of the initial induction period on the pressure of a stoichiometric mixture of hydrogen and oxygen for the equilibrium conditions is shown in Fig. 41.

To reduce the induction period of ignition of the mixture of $2H_2 + O_2$ in [45] were proposed using a pulsed laser excitation of the gas mixture. It is shown that the excitation of O_2 molecules by resonance laser radiation with $\lambda = 762$ nm leads to the formation of new channels of O, H and OH, and acceleration of the ignition.

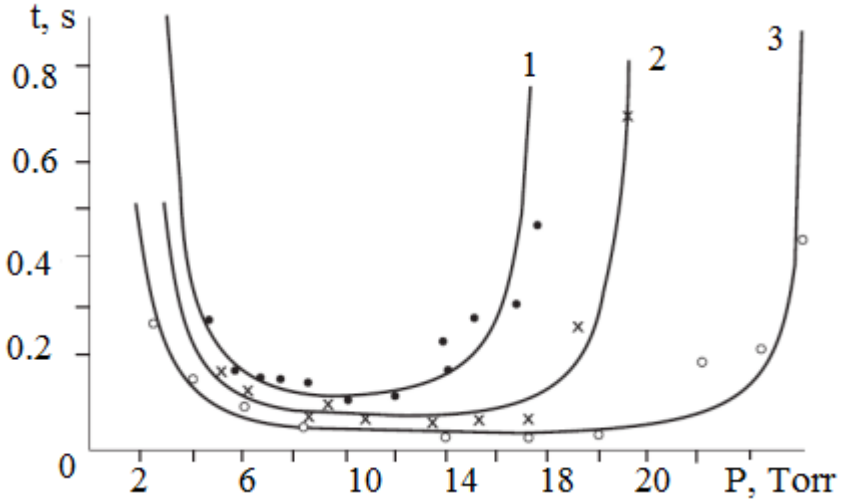

Fig. 41. Relationship between the induction period and the pressure of mixture of $2H_2 + O_2$ at different temperatures: 1 - 435 °C; 2 - 445 °C; 3 - 458 °C. Curves are calculation

Fig. 42 shows the calculated dependences of the induction on the initial temperature of the stoichiometric oxygen-hydrogen mixture at a pressure of 1 kPa in the case of a 1 ms laser irradiation and different values of radiation density.

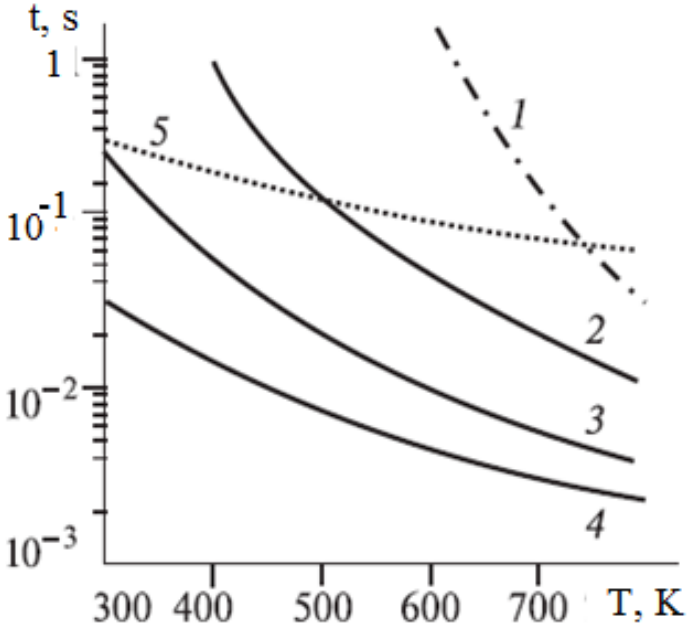

Fig. 42. The induction period versus temperature with the laser radiation energy of 0 (1), 0.017 (2), 0.082 (3) and 0.15 (4) eV /molecule. Curve 5 - The diffusion time of hydrogen from the excitation region versus temperature

At laser energy of 0.082 eV/molecule and a temperature of 300 K, the estimated induction period was 0.2 sec. At a temperature of 735K and pressure of 1 kPa the duration of the induction period of ignition of the oxygen-hydrogen mixture reduced from 0.15 to 0.005 sec, trough the laser radiation with energy of 0.082 eV/molecule. Under the equilibrium conditions for the ignition of the oxygen-hydrogen mixture to occur at the given pressure it is necessary to heat the gas mixture to a temperature above 758K (see Fig. 42), which corresponds to the energy input of over 0.13 eV/molecule for oxygen or hydrogen. Fig. 43 shows the scheme of formation of chain processes.

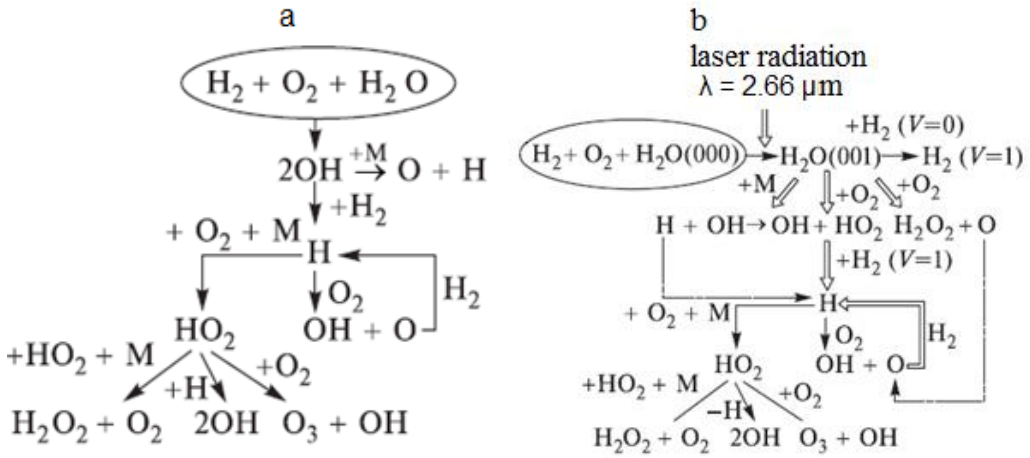

Fig. 43. Formation of the chain mechanism by ignition of $H_2 + O_2 + H_2O$ mixture without the excitation of H_2O molecules (a) and with the excitation of asymmetric vibrations of H_2O caused by the radiation with $\lambda = 2.66$ μm (b)

In [46, 47,] the experimental studies on the dynamics of the induction period of ignition of hydrogen and oxygen stoichiometric mixture by a pulsed electron beam were presented. The studies were performed on a TEU-500 high-current electron accelerator [48]. The parameters of the electron beam were as follows: the kinetic energy was 450-500 keV, the half-height pulse duration was 60 ns, the pulse energy was up to 200 J, the beam diameter of 5 cm. The electron beam was injected into a closed reactor which is a stainless steel cylinder with an inner diameter of 9 cm and a volume of 1.6 liters. The reactor pressure was controlled by a fast-response pressure sensor [49, 50]. The initial temperature of the gas mixture was 300K.

When the pressure in the reactor is 110 Torr (curve 1) the electron beam initiates a chain reaction of oxidation, which is accompanied with the energy release and the gas heating, which causes an increase in pressure in the reactor. The pulse radiolysis leads to a significant reduction in the induction period. Fig. 44 shows the waveform of pressure in the closed reactor which is filled with the stoichiometric mixture of oxygen and hydrogen, in the initial period after the injection of an electron beam. The time (t = 0) when the electron beam was injected corresponds to a spike in the waveform. This spike is due to an electrical signal from the recording equipment when the accelerator launches. Fig. 44 shows that the time delay between the electron beam injection and the beginning of the raise in pressure in the reactor (induction period) is a few milliseconds. This is significantly lower than the calculated values of the induction period in similar conditions. For example, for laser energy of 0.082

eV/molecule (absorbed dose is 260 kGy) at a temperature of 300 K the induction period was estimated to be 0.2 according to the data in [2].

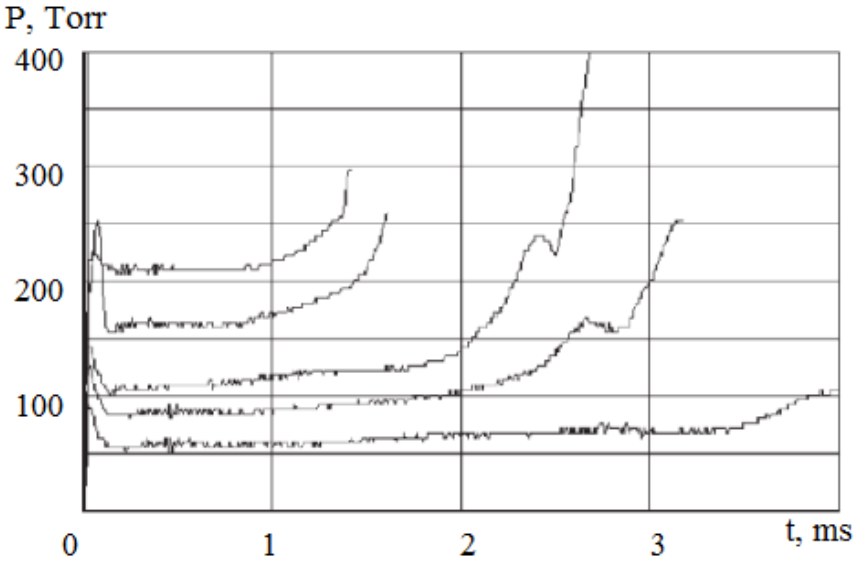

Fig. 44. The change in pressure (initial part) in the reactor filled with a mixture of $2H_2 + O_2$ at different initial pressures of the mixture. The initial temperature is 300 K

Similarly to the processes of self-ignition of a stoichiometric mixture of oxygen and hydrogen under equilibrium conditions [1], it was revealed that the induction period changes when the initial pressure of the gas mixture is changed though the impact of a pulsed electron beam. Fig. 45 shows the dependence of the induction period of ignition of $2H_2 + O_2$ mixture on the initial pressure of the reagent mixture.

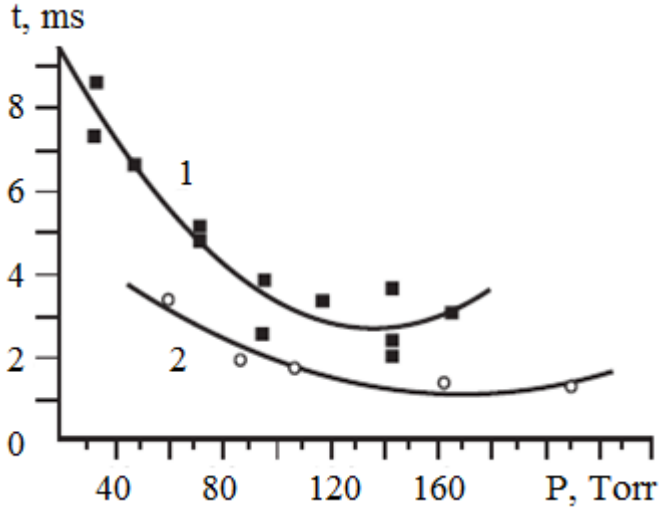

Fig. 45. The dependence of the induction period on the initial pressure of the gas mixture for different volumes of the reactors: 1.6 liters (1) and 3.2 liters (2)

The dependence of the induction period on the pressure has a shape which is peculiar to chain processes – an increase in the induction period near the combustion region (see Figure 40.). Increasing the reactor volume reduces an inhibitory effect of the reactor walls on the development of the chain process, which increases the speed of the chain process and thus causes a decrease in the induction period (curve 2 in Fig. 45). This confirms that under the influence of a pulsed electron beam on the stoichiometric oxygen-hydrogen mixture the hydrogen oxidation occurs as a chain process.

To compare the effectiveness of different types of impact on the initiation of ignition of oxygen-hydrogen mixture the values of the induction period for similar conditions are shown in Table 6. At high temperatures, when the ignition of oxygen-hydrogen mixture is possible even without an external action, a laser, or ionizing radiation causes a sharp acceleration of the ignition and reduction in the induction period. The initiation of the ignition occurs at low temperatures, under the external action, with a low-energy input, which does not exceed a few percent of the dissociation energy of the original molecules.

Table 6. The values of the induction period under different external effects

Type of external effect	Mixture of gases	Pressure	Temperature	Energy input, eV/molucule	Induction period
No effect	$2H_2 + O_2$	7.6 Torr	730K	0	0.15 s
No effect	$2H_2 + O_2$	25 Torr	730K	0	0.2 s
Laser, λ = 762 nm	$2H_2 + O_2$	7.6 Torr	300 K	0.082	0.2 s
Laser, λ = 762 nm	$2H_2 + O_2$	7.6 Torr	600K	0.082	0.01 s
Laser, λ = 762 nm	$2H_2 + O_2$	100 Torr	400K	0.082	0.2 s
Laser, λ = 2.66 μm	$2H_2+O_2$ + 5% H_2O	7.6 Torr	300K		
Pulsed discharge	5%H_2+air	76 Torr	770K	0	10^3 s
Pulsed discharge	5%H_2+ air	76 Torr	770K	0.23	$5\cdot10^{-4}$ s
Pulsed	5%H_2+ air	7.6 Torr	400K	2.3	0.1 s

discharge					
Continuous ionizing radiation	Hydrogen-aerial mixture	380 Torr 0.05 Mpa	400K	0.003 (20 kGy)	2 s
Pulsed electron beam	$2H_2 + O_2$	100 Torr	300K	0.013 (114 kGy)	0.003 s

The analysis of theoretical and experimental data shows that, under the comparable conditions, ionizing radiation is more effective for the initiation of ignition than the laser radiation. At a temperature of 400K with the laser radiation (λ = 762 nm), the energy input of more than 0.08 eV/molecule is needed to initiate the ignition. With a continuous or pulsed radiolysis the ignition occurs when the energy input is below 0.01 eV/molecule. At the same time the pulse radiolysis by the electron beam leads to a significant reduction in the induction period compared to the continuous ionizing radiation. At a lower temperature and lower initial pressure the induction period, in the case of the electron beam impact, was 3 ms, which is nearly 1,000 times smaller than for the continuous radiation.

4.2.2 Investigation of the displacement of the ignition limits of a stoichiometric oxygen-hydrogen mixture under external action

A significant drawback (for technological applications) of chain reactions of the oxidation of hydrogen is also a high ignition temperature, which exceeds 700K. Fig. 46 shows the limits of self-ignition of oxygen-hydrogen mixture under equilibrium conditions [1].

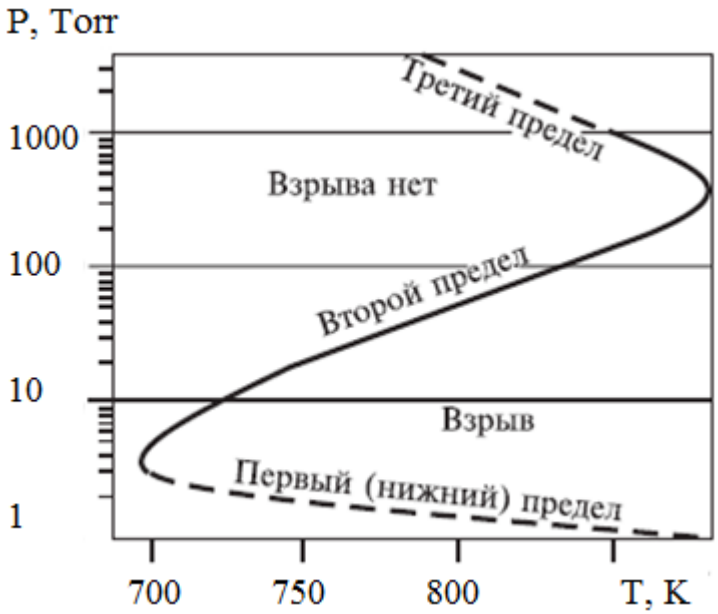

Fig. 46. The limits of ignition of a stoichiometric of hydrogen-oxygen mixture in a spherical vessel with a diameter of 7.4 cm, covered with KCl. The first and third limits are extrapolated (dashed line)

In [2] it is shown that the excitation of O_2 molecules though the resonant laser radiation leads to the formation of new channels of O, H and OH, which also leads to the reduction in self-ignition temperature. The theoretical analysis has shown that with the laser excitation (λ = 762 nm, τ = 1 ms) of oxygen molecules with an absorbed dose of 260 kGy (0.082 eV/molecule) at a pressure of 100 Torr, the temperature of self-ignition of the mixture should decrease to 300K. The ignition temperature in the first approximation was determined by the authors from the equation of the induction period and the diffusion time of hydrogen atoms.

In [51] the authors studied the influence of the initial concentration of free radicals and the rate of radiolysis of the molecular hydrogen and oxygen on the displacement of ignition limits of the stoichiometric hydrogen-oxygen gas mixture. The values of the minimum initial concentration (pulse radiolysis) and minimum rate of generation (continuous radiolysis) of hydrogen and oxygen, at which the reduction of the ignition temperature of the gas mixture begins with, were obtained. It was shown that the ignition temperature of the first and second limits is the most sensitive to the rate of radiolysis of molecular hydrogen and oxygen. The results of numerical simulations [13] showed that a significant shift of the limits of ignition for the pulse radiolysis begins with the magnitude of the initial mole fraction of hydrogen atoms of $[H]_0 > 10^{-4}$. The results of the calculations of ignition limits at a value of $[H]_0$ = 0.002 showed that the

temperature of ignition at the first limit should reduce to 100-140 degrees (see Figure 47).

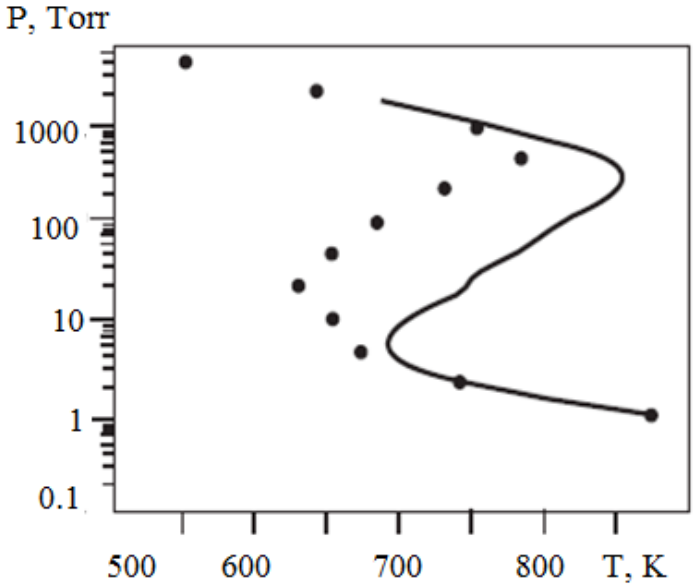

Fig. 47. The displacement of the ignition limits at the initial mole fraction of hydrogen atoms: solid curve is $[H]_0 = 0$, points is $[H]_0 = 2\ 10^{-3}$

With the radiation output of hydrogen atoms equal to 2.14 per 100 eV, for the production of $1.2 \cdot 10^{21}$ of hydrogen atoms in 1 mole, the energy of electron beam of 1350 J is required. For the mass of gas of 2.12 g in one mole, the absorbed dose is 110 kGy. This value of the absorbed dose of electron beam energy is consumed only for the decomposition of hydrogen molecules. In a mixture of oxygen and hydrogen the injected electron beam is scattered not only by the hydrogen molecules but also the oxygen.

To estimate the total absorbed dose let us take into account that the energy loss of an electron with a kinetic energy of 0.5 MeV in hydrogen is 4.2 4.2 MeV·cm^2/g, and in oxygen is MeV·cm^2/g [52]. Then, for a stoichiometric mixture of oxygen and hydrogen the electron with an energy of 0.5 MeV 3.4 more loses energy on 1 cm path due to the scattering by oxygen molecules than due to the scattering by hydrogen molecules. Therefore, the electron beam absorbed dose required for the production the molar fraction of hydrogen atoms of $2 \cdot 10^{-3}$ in the stoichiometric mixture of hydrogen and oxygen is 480 kGy. In [3, 4], the experimental studies on the initiation of ignition of the stoichiometric oxygen-hydrogen mixtures by a pulsed electron beam were presented. For this investigation a TEU-500 high-current electron accelerator was used. The studies of the ignition of $2H_2 + O_2$ mixture thought the pulsed electron beam irradiation showed that with the injection of electrons (the absorbed dose is not more

than 114 kGy) the ignition of the gas mixture occurs in a room temperature. The temperature bias, as a result of the pulse radiolysis, for the first limit of ignition is much greater than the calculated values given in [13] where it was estimated by a numerical simulation method. When the initial mole fraction of hydrogen atoms equals to 0.002 (absorbed dose of electrons is 480 kGy), the lower temperature limit of ignition should decrease to 100-140 degrees and be equal to 600K.

To compare the effectiveness of different types of impact on the displacement of the ignition limits both the experimental and theoretical data for similar conditions are shown in Table 7.

Table 7. The effect of different types of external action on the displacement of the ignition limits

Type of external effect	Mixture of gases	Pressure	Temperature	Energy input, eV/molucule
No effect	$2H_2 + O_2$	7.6	0	710
No effect	$2H_2 + O_2$	25	0	755
Laser, λ = 762 nm	$2H_2 + O_2$	7.6	0.017	500
Laser, λ = 762 nm	$2H_2 + O_2$	7.6	0.082	300
Laser, λ = 762 nm	$2H_2 + O_2$	100	0.082	400
Laser, λ = 2.66 μm	$2H_2+O_2+5\%$ H_2O	7.6	2.5 J/cm^2	300
Pulsed discharge	$5\%H_2$+air	76	0.23	770
Pulsed discharge	$5\%H_2$+ air	7.6	2.3	400
Continuous ionizing radiation	Stoichiometric hydrogen-aerial mixture	380	0.003 (20 kGy)	400
Pulse radiolysis	$2H_2 + O_2$	100	0.05 (460 kGy)	680
Pulsed electron beam	$2H_2 + O_2$	100	0.013 (114 kGy)	300

The ionizing radiation helps reducing the limits of ignition more effectively than the laser radiation. With an initial pressure 100 Torr in the mixture of $2H_2 + O_2$ under the influence of resonant laser radiation (λ = 762 nm) with an energy of 0.08 eV/molecule the ignition temperature limit is shifted to 400K. With the same initial pressure, in the case of the pulsed electron beam radiation with an energy of 0.013 eV/molecule the ignition of $2H_2 + O_2$ mixture at temperatures below 300K occur.

The use of the electron beam to initiate the ignition of oxygen - hydrogen mixture creates a unique environment for a study of the originality, development and termination of t combustion processes. This is because the duration of the electron beam effect is much smaller than the induction period. The change in pressure in the mixture does not affect the absorbed dose (at a low-pressure) provided that the density of electron beam is constant. Furthermore, the change in the conditions of chain is possible by introducing the atomic hydrogen into the reactor volume. The initiation of ignition of oxygen - hydrogen mixture in gas discharge provides a high uniformity of the initial concentration of the atoms and radicals in the reactor volume (ideal mixing).

4.3 Radiation-thermal cracking of methane

A great number of studies on the decomposition of hydrocarbons during heating show that the process is implemented as a chain (thermal cracking). The reactions of thermal cracking of normal alkanes occur at high temperatures, for example it is about 800-900K for heptane –vapor [53]. According to the chain theory of cracking, this process consists of three stages:

1 The initiation of the reaction though radicals, due to the thermal decomposition of molecules of the original product;

2 The continuation of the chain, which is due to the interaction of the free radicals with the molecules. This leads to the formation a stable molecule of the reaction product and a new radical;

3 The chain termination.

The stage of initiation requires the activation energy of 3.5 eV/molecule (80 kcal/mol), i.e., the reaction can proceed at a noticeable rate, but only after the temperature exceeds 900K. The stage of the chain continuation requires activation energy of about 0.87 eV/molecule (20 kcal/mol), and therefore for its implementation a lower temperature is required.

At low temperatures, the thermal initiation of the reaction does not occur due to the absence of the radiation. In this case, with the radiation

exposure the active centers which are free radicals, may occur, which can start a chain reaction of hydrocarbon cracking. The interaction of the radicals, which contain a small number of carbon atoms, with the initial hydrocarbon is a distinct chain process, which is initiated by the radicals formed due to the radiation.

In a nook of V.V.Sarajeva [54] there are four temperature regions of the radiation-thermal cracking, they are shown in Fig. 48.

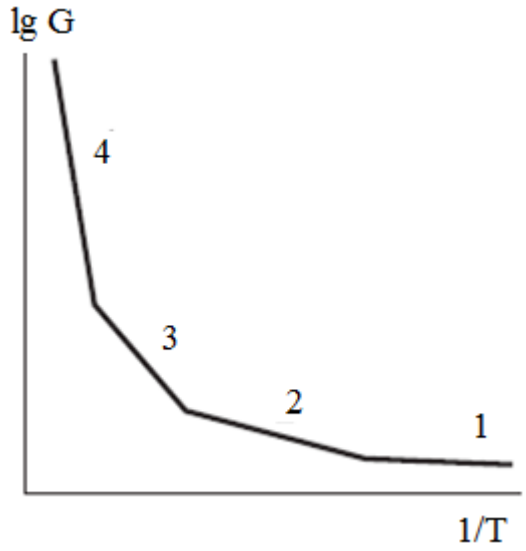

Fig. 48. The influence of the temperature on the radiation decomposition of hydrocarbons. The temperature ranges are: 1 – radiation, 2 - radiation-thermal, 3 – Thermal – radiation 4 – Thermal [39]

The first region is radiation, at which the radicals are generated only by the radiation. In this region, the process is not a chain, and the activation energy is only 0.04 eV/molecule, which characterizes the radiolysis process.

The second region is the thermal radiation. Within this temperature range the process becomes a chain with activation energy of 0.87 eV/molecule.

$$RH + e\ (3.5\ эВ) \rightarrow R^* + H^*$$

$$R^* + RH + 0.87\ эВ \rightarrow \text{stable product} + R_1^*$$

The third region is the thermal radiation. It occurs when the R1 radical is thermally unstable and can decompose into two active radical due to the reaction of

$$R_1^* \rightarrow R_2^* + R_3^*$$

In this temperature range it is branched chain process (the activation energy is of the order of hundreds of kilojoules per mole).

The fourth region is thermal. Here the generation rate for the active radicals is determined by the reaction

$$RH + t^{o}\ (3.5\ e) \rightarrow R^{*} + H^{*}$$

The generation rate increases due to the radiation. The activation energy in this temperature range is determined only by the thermal process and is equal to 3.5 eV. The speed of the chain process depends on the rate of radical generation, which also depends on the dose. The influence of the temperature and dose on the development of the chain process in described in more details in [16] as an example of radiation oxidation of hydrocarbons.

Based on the analysis of experimental data on the radiolysis of liquid hydrocarbons of the paraffin series it was obtained that:

1 The reaction yield of radical formation in γ-radiolysis, and a temperature of 300 K is 7-10 radicals. Assuming that the average energy is 3.5 eV, it is easy to see that the chemical reaction consumes no more than 30% of the absorbed energy of ionizing radiation, and the rest of the energy is spent on heating (by collisions or energy transfer).

2 The yield of the radiolysis products at 300K contains about 80% of the products of C - H bond breaking. It results in formation of molecular hydrogen and hydrocarbon, and about 20% are the products of C - C bond breaking.

3 With an increase of the temperature above 600 K the radiation-chemical yields rise dramatically, reaching 1.5 10^4 molecules per 100 eV at 600 K, and the product composition approaches the composition of the products peculiar to the thermal cracking.

Chain process of the decomposition of methane (radiation-thermal cracking) can be described by the following basic equations [55]:

Chain initiation due to the thermal influence	$CH_4 + 3.5\ эВ = (CH_3)^{*} + H^{*}$
Chain initiation due to the radiation influence	$CH_4 + e = (CH_3)^{*} + H^{*}$
Continuation of the chain	$CH_4 + H^{*} = (CH_3)^{*} + H_2$ $(CH_3)^{*} + CH_4 = C_2H_6 + H^{*}$
Termination of the chain	$(CH_3)^{*} + H^{*} = CH_4$ $(CH_3)^{*} + (CH_3)^{*} = C_2H_6$ $H^{*} + H^{*} = H_2$

In [56, 57] the experimental data on plasma catalysis in the conversion of methane into carbon and hydrogen were presented. Preheated to a temperature of 700 - 1100K methane was treated for a short time pulse microwave discharge (frequency 9 GHz, pulse power up to 100 kW, pulse length 1 ms, repetition rate 1 kHz), which caused a sharp increase in its degree of conversion. It was shown that this effect can not be explained

by the thermal influence of discharge and the role of plasma is to generate the active particles, which accelerates the conversion process. Fig. 49 shows the experimental dependence of the degree of conversion of methane in the microwave discharge plasma on the temperature.

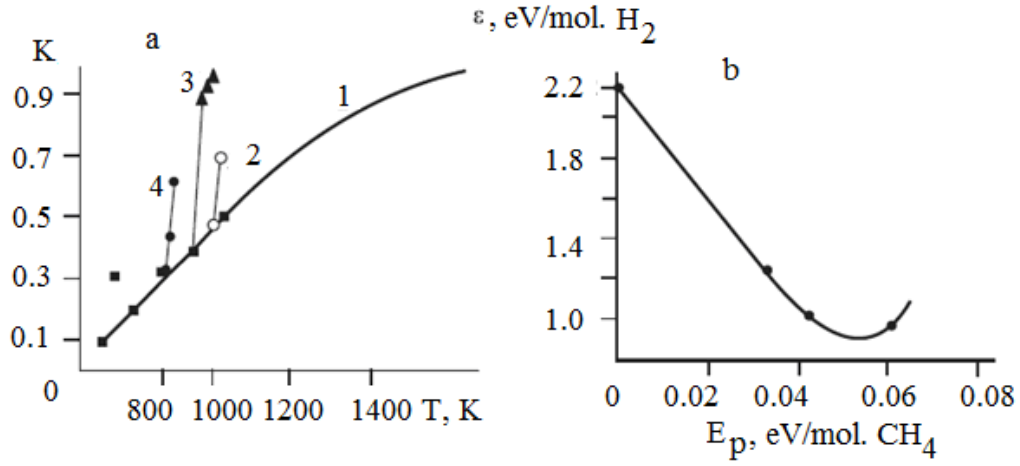

Fig. 49. The dependence of the degree of methane conversion on the temperature (a): 1 - decomposition of methane without the influence of plasma, 2, 3, 4 - influence of plasma on gas, preheated to 950, 850 and 750K, respectively. (b)The dependence of energy consumption for the formation of hydrogen molecule on the plasma energy

It is important to note that the products of the plasma pyrolysis (H_2 and nanosized graphite) were significantly different from the products of the pyrolysis of CH_4 in equilibrium conditions (acetylene, ethylene and ethane).

4.4 Chain oxidation of methane under external action

It is known that the oxidation of the hydrocarbon is a branched degenerate chain process [58, 59]. The most energy-consuming element is the formation of primary radicals, i.e., the initiation of the chain. Under the equilibrium conditions, the initiation of the chain process is a result of thermal decomposition of the valence-saturated molecules or the interaction of two valence-saturated molecules. The remaining links are initiated by the free radicals, which significantly reduces their activation energy compared with the molecular reactions. Thus, the low-temperature boundary of the oxidation region should be considered as a boundary with the minimum temperature, which, in the given conditions of pressure, mixture composition, surface of the reactor, could still initiate chain oxidation. Further reduction in temperature will lead to their elimination of

the initiation reaction and, for this reason, the disappearance of the rest of the chain. Thus, if it were possible to carry out the initiation of free radicals at a lower temperature than the temperature of the low boundary of a slow oxidation region, then the oxidation and further conversion of hydrocarbons could be continued even in these conditions.

With this oxidative conversion of hydrocarbons at low temperatures, the synthesis of new compounds may occur. In a complex chain process the radicals can enter not into one reaction but also in two or more reactions. The temperature influences on the outcome of the radical reactions. The lower the temperature of the process is, the smaller activation energies is required for radical to determine the preferred direction of the reaction. For example, at 400K the difference between the activation energies of two reactions of 0.04 eV/molecule leads to the fact that 93% of the response will take the path with a lower activation energy (provided that cross the sections for interaction are equal).

The oxidation at the temperatures lower than the normal temperatures in oxidation, should result in a significant decrease in the quantities of hydrocarbons which decompose and oxidize. This follows from the fact that out of two possible reactions of alkyl radicals - the decomposition and the oxidation

1 The decomposition of R → products of decomposition, the activation energy of 1.1-1.7 eV/molecule.

2 The oxidation of R + O2 → RO_2 the activation energy of 0.02-0.09 eV/molecule at temperature of the oxidation of hydrocarbons of 450 K. We can assume that the cracking does not occur.

The second consequence of lowering the temperature of the reaction is the formation a significant amount of peroxides as a result of conversion of peroxide radicals RO_2 .Here there are two ways: the disintegration of RO_2 radicals with the formation of aldehydes and alcohols, and its interaction the initial hydrocarbon with the formation of the alkylhydroperoxides. The activation energy of decomposition is about 0.8 - 0.9 eV/molecule. The energy of activation of the bimolecular interaction of RO_2 with hydrocarbon does not exceed 0.2-0.3 eV/molecule. For a mixture of 150 Torr RH + 150 Torr O_2 at 450 K the ratio of the rate of the decomposition reaction of RO_2 to the reaction of alkylhydroperoxides formation is 0.53. In the case of the oxidation at 400K, this ratio is equal to 0.043. Thus, the reduction in the oxidation temperature should facilitate the formation of the alkylhydroperoxides and cause a decrease in the yield of aldehydes and alcohols, which are, according to the mechanism, the decomposition products of the RO_2 radicals.

One can also assume that at a low temperature of oxidation the alkylhydroperoxides will have an isometric structure rather than the normal structure. The difference in the energy of a bond breakage of the primary and the secondary C-H bonds is about 0.17 eV/molecule. This difference will lead to the fact that at low temperatures the separation of the hydrogen atom from CH_2group (rather than CH_3) will occur in hydrocarbon and the peroxide formed will have an isomeric structure.

In general, it is expected that a significant reduction in the reaction temperature causes a change in the direction of oxidative conversion. The alkylhydroperoxides will be mainly formed. The reduction in the temperature of oxidation can be achieved by facilitating the generation by primary free radicals. This can be done either by supplying the active radicals from the outside, or addition of certain substances that are able to decompose to radicals at low temperatures (i.e. below the boundary of the normal region slow oxidation of hydrocarbons).

4.4.1 Oxidation of methane in the equilibrium conditions at a low pressure

The oxidation of methane under equilibrium conditions is well studied and described in the books written by V.J. Stern [20], and V.S. Arutyunov [21]. Experimental studies have shown that at a low pressure (below 10 atm.) in the initial mixture $CH_4 + O_2$ the oxidation process is very slow. Fig. 50 shows the dependence of the oxidation of methane on the pressure and area of ignition of the methane-air mixture under equilibrium conditions. You can see that the chain process of methane oxidation of occurs at temperatures above 800 K.

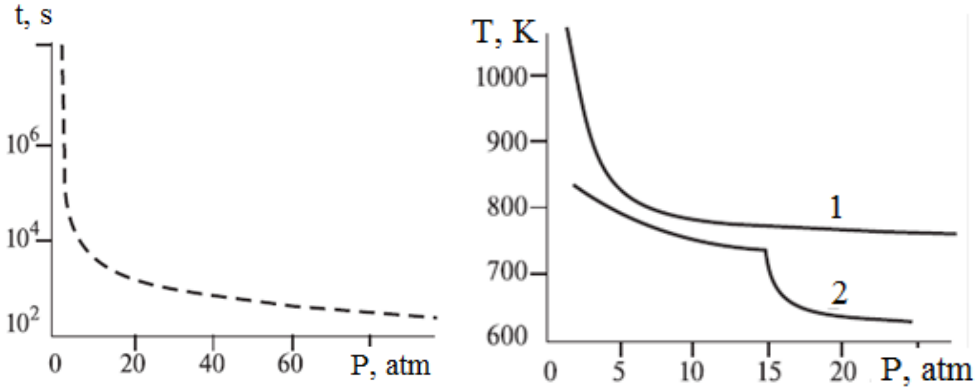

Fig. 50. The dependence of the oxidation time of methane on the mixture pressure at temperature of 650 K and the region of ignition of hydrocarbon-air mixtures. 1 – 13% CH_4, 2 – 10 % C_2H_6

Fig. 51 and Fig. 52 show the kinetic curves of the accumulation of the products of methane oxidation.

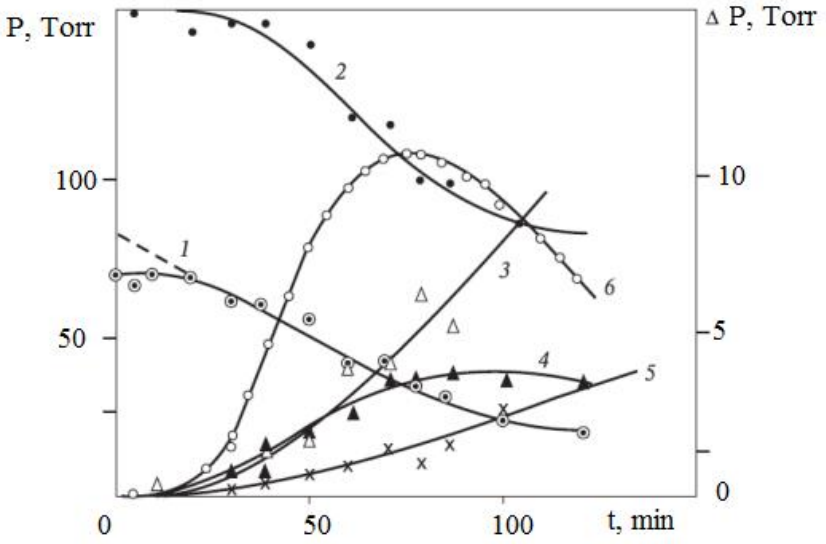

Fig. 51. The kinetics of methane oxidation obtained by: changing the total pressure, consumption of the initial products and the accumulation of the end products of the reaction.

A mixture of $CH_4 + 2O_2$; $R_{initial}$ = 235 Torr, T = 723 K. 1 – CH_4; 2 – O_2; 3 – H_2O; 4 – CO; 5 – CO_2; 6 – ΔP

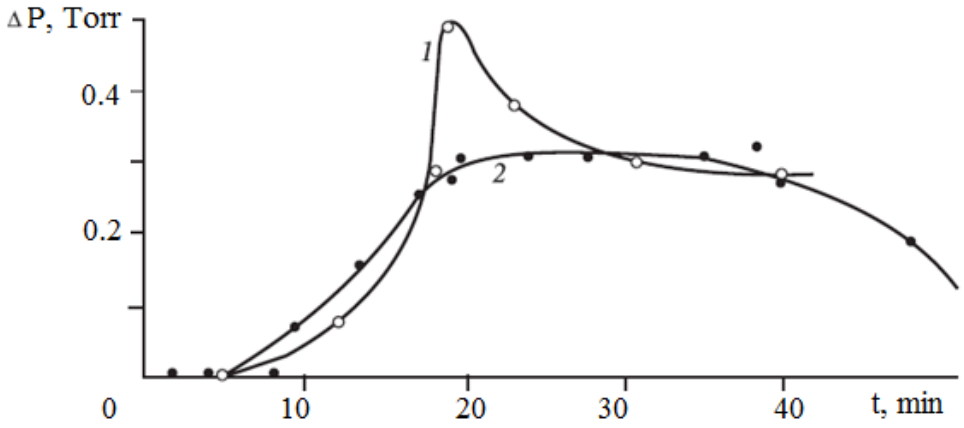

Fig. 52. The accumulation kinetics of formaldehyde and hydrogen peroxide at the oxidation of methane. A mixture of CH_4+$2O_2$; P_{init} = 235 Torr; T = 723 K. 1 – peroxide, 2 – formaldehyde

The experiments were conducted under static conditions in a quartz vessel within the temperature interval of 723-813 K with a mixture of $CH_4 + 2O_2$. The main products of oxidation of methane under equilibrium conditions were CO_2, CO and H_2O. The formaldehyde was oxidized at high temperatures to carbon monoxide and water, so in the reaction products the content of it is negligible. The slow oxidation of methane under

equilibrium at low temperature is characterized by a low degree of conversion. The oxidation process is terminated long before the formation of the original products (see Fig. 51, lines 1 and 2).

4.4.2 The initiation of methane oxidation by an external influence

The mercury and bromine sensitized photochemical oxidation of hydrocarbons is reviewed in a book of V.J. Stern [20]. The photochemical oxidation of propane at room temperature was the most studied. The main product of the oxidation was hydroperoxide of isopropyl (see Fig.53).

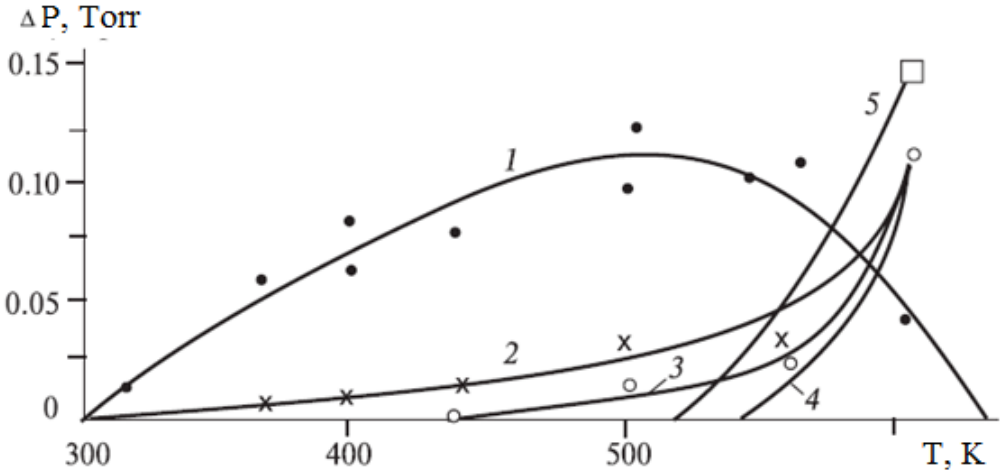

*Fig. 53. The dependence of the yield of photochemical propane oxidation on the temperature [*60*].Contact time 30 sec. 1 – peroxide, 2 – acetaldehyde, 3 – formaldehyde, 4 – acetone, 5 – CO*

The quantum yield of the reaction was determined. It was calculated as the ratio of an amount of the molecules of isopropyl hydroperoxide which are formed per unit time to the number of photons absorbed by the system. It turned out that the lower limit of the quantum yield equals two, i.e. the length of the chain oxidation of propane in the studied conditions is very small. In the all experiments carried out at room temperature no more than 0.5 % of propane entered into the oxidation reaction.

The photochemical oxidation of methane and ethane was studied by A.B. Nalbandian and N.V. Fok, both at room and elevated temperatures. It was found that at the room temperature the main products are the hydroperoxides. As a temperature increases, together with the peroxides, the aldehydes start formimg. Starting from 500K, the yield of peroxides decreases, while the yield of aldehydes continues growing and at 600 K the main products are the aldehydes CO and CO_2. The kinetic curves of the

peroxides and aldehydes formation are similar to the curves obtained by the oxidation of propane.

The study of photochemical oxidation of hydrocarbons at low pressures showed that:

1 The facilitation of the initiation enables the oxidation at low temperatures

2 The main product of the low-temperature oxidation is the corresponding alkylhydroperoxides

3 If the conversion is very low, the oxidation process is slow as well.

A small chain length in these conditions makes, however, the low-temperature oxidation of hydrocarbons ineffective with respect to the yields of products and the degree of conversion.

In 1958, the oxidation of methane (a mixture of $4SN_4 + O_2$ and $CH_4 + O_2$) under the action of a fast electron beam at room temperature was studied by B.M. Mikhailov and others [61]. The dose rate (at P_{init} = 760 Torr) was $2{,}7 \cdot 10^{16}$ eV/cm^3·s (for the mixture of $CH_4 + O_2$ the dose was 4 kGy/s). The source of fast electrons was an electron tube with an accelerating voltage of 120 kV and an output current of 100 μA. The experiments were conducted with a steel vessel, the irradiation time was 30 min. The reaction yield for the mixture $CH_4 + O_2$ was equal to 7 molecules of O_2 and 6.2 molecules of CH_4 at 100 eV. Fig. 54 shows the change in pressure in the irradiated methane-oxygen mixture during the reaction.

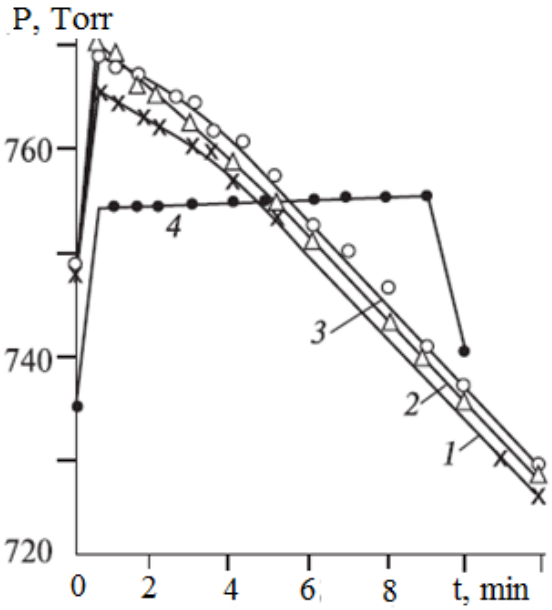

Fig. 54. The change in pressure of nitrogen and methane-oxygen mixtures in the initial period of the irradiation by the fast electrons at room temperature[31]. 1 – CH_4:O_2 = 4:1, 2 – CH_4:O2 =1:2, 3 – CH_4:O2 = 1:1, 4 – N_2

A sharp increase in pressure for 20-30 seconds in the beginning of the curve in Fig. 16 is associated with heating. Later the pressure curve dpops during 3-4 min, then straight-line section can be obsereved, which lasts until one of the initial components of the mixture is used up. After that, the pressure drop slows down. It was found that the reaction rate increases with an increase of the partial pressure of methane and the total pressure. The consumption of methane and oxygen is proportional to the time of irradiation. It is important to note that the rate of oxidation of methane in the case of the irradiation by the electron beam is much higher than under equilibrium conditions, although the temperature of the gas mixture was significantly lower (300 K at the irradiation, 723K under equilibrium conditions).

At room temperature, and initial pressure of 760 Torr the methane mixture was subjected to transformation by 32 % (a mixture of CH_4 + O_2). This greatly exceeds the degree of conversion in the mercury sensitized photochemical initiation (0.5 % for propane). The products of oxidation found are CO and CO_2, H_2O, H_2, HCOOH and a small amount of CH_3OH and peroxides. The formaldehyde was found only in trace amounts (see Fig. 55).

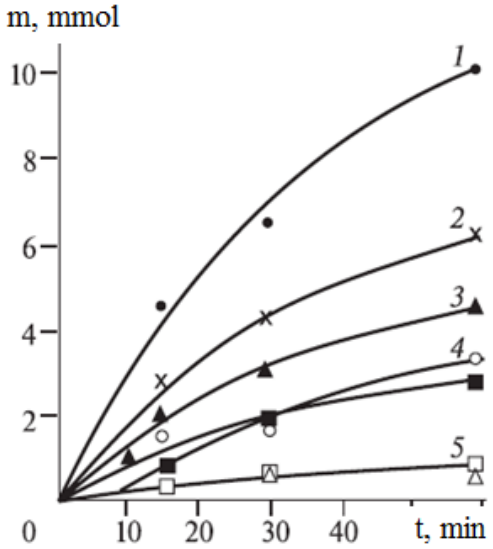

Fig. 55. The dependence of the oxidation products of methane on the duration of electron beam irradiation. CH_4 + O_2 mixture: P_{init} = 760 Torr., T = 300 K. 1 – H_2O, 2 – H_2, and 3 – HCOOH, 4 – CO and CO_2, 5 – peroxides and alcohols

About 50 % of methane consumed goes into the liquid phase, the main product of which is HCOOH.

These data suggest that during the methane oxidation initiated by radiation at room temperature, in contrast to the thermal and photochemical

oxidation, the degree of conversion is higher (32% with the irradiation and 0.5 % under equilibrium). The authors believe that when bombarded with the fast electrons 50% of the exposed methane is converted to the excited molecules, and 50 % to the ions.

In [62, 63]] the partial oxidation of methane by the two types of microwave discharge was studied. These discharges are: the pulse-periodic discharge (streamer pseudo-corona discharge, the wavelength of 3 cm, pulse power of 300 kW, average power of 300 W, pulse duration of 1 ms, repetition rate of 1 kHz) and the continuous discharge (coaxial jet discharge, the frequency of 2.45 GHz, the power of 1-5 kW). The initial reactants were heated up to 800-1200 K and supplied into the discharge chamber, which were combined with the methane combustion zone. The authors note that the use of the microwave discharge acts on the system in two ways. Firstly, it effectively introduces an additional thermal energy even in strongly heated reagents due to the high temperature of plasma. Secondly, the plasma generates the active particles which contribute to the oxidation of methane in the chain reactions, and play a role of the initiator of the combustion. For the reaction of partial oxidation of methane the energy consumption of the microwave discharge were 0.25 eV/molecule when the degree of conversion methane was 70 %, and increased to 0.5 eV/ molecule with the degree of conversion about 100 %. In this case the energy input due to thermal heating (according to the degree of conversion) was 2.6 -2.8 eV/molecule. The heating of the mixture of gases has greatly increased the length of the chain reaction of oxidation and with the inexternal initiation of the chain process significantly increased the degree of methane conversion at the given temperature.

4.5 The conversion of carbon disulfide CS_2 in the atmospheric air

Chain mechanism of the reaction was discovered by a group headed by N. Novoselov while they studied the decomposition of carbon disulfide under the electron beam and in the semi-self-maintained discharge initiated by an electron beam. In [64, 65] the results of experimental and theoretical studies of the action of the pulsed processes of nano - and microsecond duration on the nitrogen-oxygen mixture at atmospheric pressure with an addition of carbon disulfide CS_2 were presented. The two regimes of the conversion of impurities were found. These regimes depend on the type of beam and are characterized by the mechanism and the end products. The effect an external electric field on the conversion of impurities was investigated.

For the experiments the model gas mixtures of nitrogen and oxygen were used. The content of nitrogen N_2 was ranged from 89 to 99 % and oxygen from 0.1 to 10 %. The content of the investigated impurities CS_2 varied from 0.005 to 1 %. For the irradiation of the gas mixtures two electron accelerators with different parameters were used. A compact "Radan"accelerator was used in a nanosecond time scale. It generated the electron beam with the following parameters: the electron energy was 180 kV, the half-hight pulse duration of 3 ns, the current density of 800 A/cm^2, the pulse repetition rate of 10 Hz. In some experiments the nonself-sustained discharge, initiated by a nanosecond electron beam was observed. The discharge was ignited in a gap with a length of 1 cm when a 12 nF capacitor, charged to 1-25 kV was connected to the gap. In the microsecond time scale an accelerator with a plasma-cathode was used. This accelerator formes a radially divergent electron beam with the following parameters: the area of ~ 1.5 m^2, the electron energy of 280-300 keV, the current density raged from 0.1 to 10 mA/cm^2, the pulse duration of 48 ms. The volume of 170 liters was subjected to the irradiated. In the same volume the nonself-sustained discharge maintained by an electron beam was ignited in the gap of 10 cm in length. The maximum field strength in the volume discharge plasma was 5 kV/ cm.

In a mixture irradiated by a nanosecond electron beam the initial concentration of CS_2 has a little effect on the angle of the dependence of concentration of the carbon disulfide molecules on the number of irradiation pulses. The minimum value of energy consumption was equal to 0.8 eV/molecule, which is ignificantly less than the energy of dissociation of carbon disulfide, equal to 7.6 eV. The conversion process of CS_2 in the nonself-sustained discharge initiated by a nanosecond beam was also investigated. Fig. 56 shows the dependence of the energy consumption on the electric field strength in the volume discharge. It was found that in a range of the electric field strength from 0 to 1.5 kV/cm, the value of energy varies slightly and is ranged from 0.6 to 0.9 eV/molecule. This is much lower than the dissociation energy of carbon disulfide and oxygen.

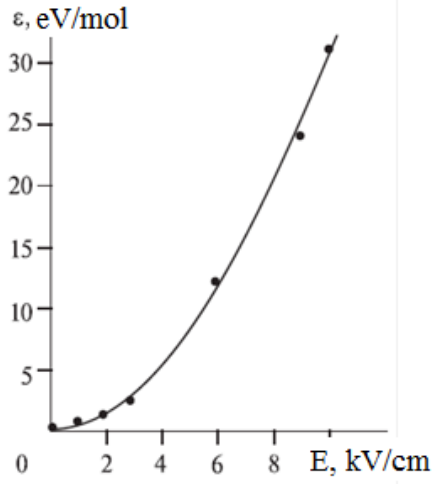

Fig. 56. The dependence of the energy required for the removal of one molecule of the impurity on the field strength in the column of the nonself-sustained discharge initiated by a nanosecond electron beam

The experiments showed that with the comparable values of energy introduced to a gas by the electron beam the irradiation regimes are different and characterized by the end-products of CS_2 conversion. As a result of the gas irradiation by high-current electron beam of nanosecond duration the main products of the reaction are the sulfur and carbon oxides. After irradiation of the initial mixture by an electron beam of low current density and microsecond duration in a plasma-chemical reactor a solid phase as well as viscous liquid were found. The analysis showed that these substances are composed of $(-CS-)_n$, the presence of SO_2 with trace amounts was detected.

According to the analysis the ionization by a high-current electron beam of nanosecond duration leads to a chain mechanism of oxidation of CS_2, in which a triggering agent is atomic oxygen:

$$CS_2 + O_2 \rightarrow CS + SO \quad (147)$$

$$SO + CS \rightarrow CO + S_2 \quad (148)$$

$$O + S_2 \rightarrow SO + S \quad (149)$$

$$SO + O_2 \rightarrow SO_2 + O \quad (150)$$

$$S + O_2 \rightarrow SO + O \quad (151)$$

The recovery of atomic oxygen occurs under the influence of the beam through the electronic states of O_2, and in the reactions with electronically excited nitrogen molecules N_2*:

$$e + O_2 \rightarrow 2O \quad (152)$$

$$N_2^* + O_2 \rightarrow N_2 + 2O \quad (153)$$

With an electron beam of a sufficient intensity in the reactions (153) the quantity of O radicals is enough to trigger a chain mechanism (147) -

(152). By reducing the concentration of CS_2 below a certain critical value the chain mechanism is interrupted, the atomic oxygen ceases to turn out in the reactions (152), (153) and the oxidation of carbon disulfide is terminated. According to the calculations, the main products of decomposition of CS_2 are sulfur oxides SO_2 and carbon oxides CO. In small quantities NO, SO and S_2 were produced, which was observed in the experiments. The presence of nitrogen in a mixture leads to the loss of radicals O in the reactions of nitrogen oxide synthesis:

$$N_2(\nu) + O \rightarrow NO + N \qquad (154)$$
$$N + O_2 \rightarrow NO + O$$

Here $N_2(\nu)$ is the vibrationally excited nitrogen molecules.

Another mechanism for the conversion of carbon disulfide is implemented with the excitation of N2-O2 -CS_2 mixture by a low-current electron beam of microsecond duration. In this case, the beam does not have enough intensity and the density of plasma electrons is two orders of magnitude lower. The concentration of charged particles generated by a low-current beam is low and comparable with the concentration of free radicals O. In this case the chain mechanism does not occur, although the oxidation takes place: the estimated concentration of SO_2 is three orders of magnitude smaller than in the high-current irradiation regime. In the case of the low-current electron beam the ion losses due to electron-ion recombination are sharply reduced and the plasma conditions are more favorable for the conversion of CS_2 via the formation of the cluster ions. The concentration of these ions is $[A^{\pm}] \sim 10^3$ cm^{-3}. The reduction in the concentration of CS_2 occurs in the fast reactions of clusters formation of $A \pm (CS_2)$, followed by the polymerization of carbon disulfide and the formation of $(-CS-)_n$ molecules. The rate of these processes is much higher than the rate of the reactions involving free radicals O. It was found that the cluster ions in these experiments are the negative ions O_2^-, the rate of which is almost entirely controlled by the process of three-body attachment of the electrons to molecular oxygen.

When the ignition of a volume discharge is initiated by an electron-beam of nanosecond duration, the influence of the electric field is manifested in a monotonic decrease in the number of converted molecules of $\Delta [CS_2]$, which leads to an increased energy consumption. The main reason for the decrease in $\Delta [CS_2]$ is the loss of atomic oxygen in the reaction (12), becausee with an increase in electric field strenth in the discharge the rate of vibrational excitation of nitrogen increases as well

$$e + N_2 \rightarrow e + N_2(\nu)$$

A more complex nature of the influence of an electric field is obsereved in the discharge, maintained by a weak electron beam. [66]. Since

the loss of molecules of carbon disulfide in this regime is associated with the formation of clusters which are the ions of O_2-, the behavior of Δ [CS_2] should be determined by the rate of the cluster ions formation in the reaction of the three-body attachment

$$e + M + O_2 \rightarrow M + O_2^-$$

Fig. 57 shows the scheme of basic processes of the decomposition of CS_2 caused by a pulsed electron beam

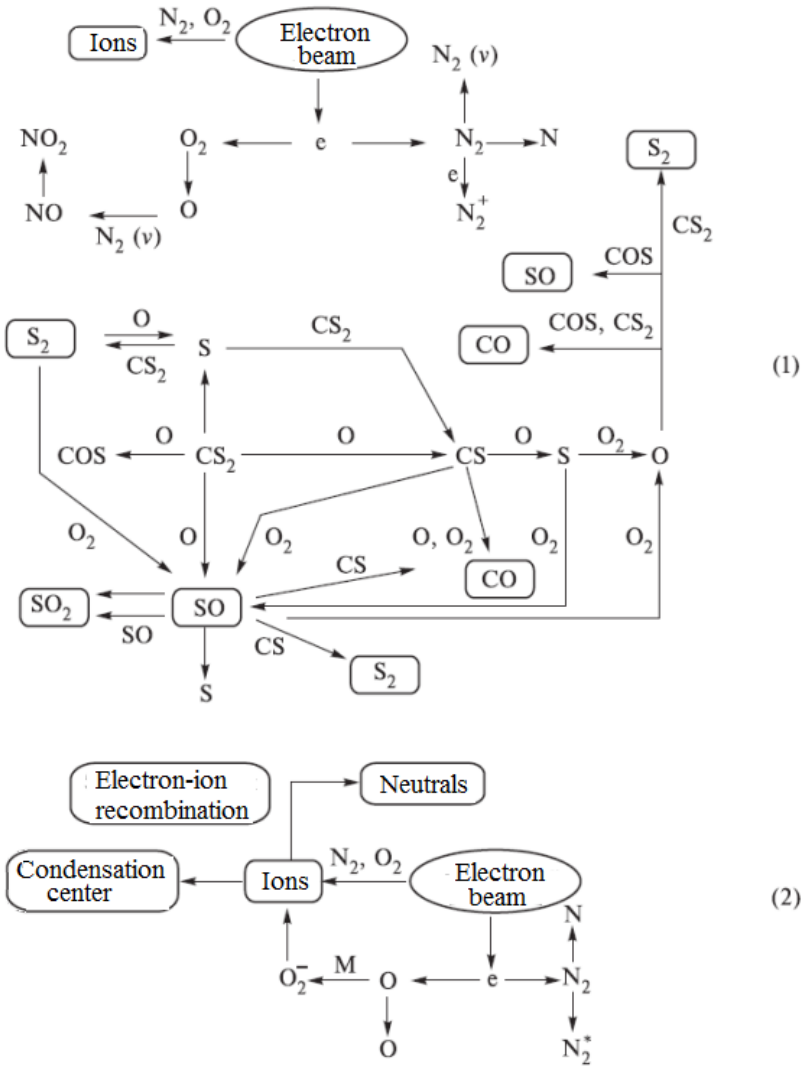

Fig. 57. The scheme of processes occurring in mixture of N_2 + O_2 + CS_2 initiated by a pulsed electron beam of 3 ns (1) and 48 ms (2) in duration

To analyze the mechanisms of conversion of CS_2 a model of plasma-chemical processes initiated by a pulsed electron beam in nitrogen-oxygen mixture with an addition of carbon disulfide, has been designed. [30].

Chapter 5. Applied plasma-chemistry

Gas discharges and other sources of low-temperature plasmas are widely used in chemical manufacture, namely in the following: synthesis and decomposition of inorganic compounds, plasma-chemical synthesis of nanosized materials, catalytic plasma-chemical processes and others. Low-temperature plasma is applied in organic chemistry as well: conversion of hydrocarbon gases (methane, propane, landfill gas) into high molecular weight compounds, synthesis of hydrogen and carbon clusters (fullerenes), processing of polymer coatings, leather, fur, etc.

5.1 Nonequilibrium synthesis of nanosized oxide powders

Titanium dioxide (TiO_2) is one of the most important inorganic materials. It is used as a white pigment, a photocatalyst, a semiconductor in solar cells, etc. The world consumption of TiO_2 in 2001 exceeded 4 million tons. Titanium dioxide nanoparticles have been studied well and are prepared by various processes; therefore, the basic features of different manufacturing processes can be compared by considering the characteristics of synthetic TiO_2. The use of nonequilibrium plasma-assisted processes is a promising way of oxide synthesis. The nonequilibrium character of the synthesis process makes it possible to considerably lower power consumption for the reaction and to alter its conditions.

The use of nonequilibrium plasma-assisted processes is a promising way of oxide synthesis. The non-equilibrium character of the synthesis process makes it possible to considerably lower power consumption for the reaction and to alter its conditions. Nanosized silicon dioxide (SiO_2) was prepared in a nonequilibrium plasma-chemical process induced by a pulsed electron beam [67, 68]. The energy consumption in an electrophysical unit for the conversion of silicon tetrachloride ($SiCl_4$) did not exceed 0.02 eV/molecule.

5.1.1 Comparison of the available processes for production of nanosized TiO_2 particles

1 The chlorine process is the most widespread vapor phase procedure for the preparation of TiO_2 from titanium tetrachloride ($TiCl_4$). This process makes it possible to synthesize crystalline TiO_2 with a given ratio between the rutile and anatase crystalline phases. In this process, titanium tetrachloride is oxidized by oxygen

$$TiCl_4\,(gas) + O_2\,(gas) = TiO_2\,(solid) + 2Cl_2\,(gas)$$

However, the high synthesis temperature (1400–1700°C) complicates the manufacturing process [69, 70] and requires a considerable power input. To reduce the temperature and to decrease the powder particle size, Bin *et al.*[69] investigated the gas phase hydrolysis of $TiCl_4$:

$$TiCl_4\,(gas) + 2H_2O\,(gas) = TiO_2\,(solid) + 4HCl\,(gas)$$

They showed that amorphous TiO_2 was produced at a synthesis temperature of 260-400°C and a crystalline material (anatase) was formed at 400-600°C. The average particle size decreased with an increase in the synthesis temperature from 120 nm (at 260°C) to 18 nm (at 525°C). The results of investigation of the preparation of TiO_2 nanoparticles by thermal vapor-phase decomposition of tetrabutoxytitanium $(C_4H_9O)_4Ti$ are reported in [71, 72, 73]. The degradation temperature (T_d) of $(C_4H_9O)_4Ti$ is below 500°C, but the onset of formation of particles with the crystalline phase (anatase) was detected only at T_d > 500°C and all particles possessed this structure at T_d > 600°C. The formation of the rutile crystal structure began at T_d > 1200°C [71]. Ayllón et al. [72] carried out the decomposition of $(C_4H_9O)_4Ti$ in a mixture with oxygen in an RF discharge plasma. Despite of a high temperature in the discharge zone, the degradation of$(C_4H_9O)_4Ti$ yielded amorphous TiO_2 particles with an average size of 25 nm and the crystal structure was formed during subsequent annealing at 600–800°C. The rutile lattice in noticeable amounts was formed only at T > 800°C. Li et al. [73] also detected the formation of TiO_2 nanoparticles with the anatase lattice at T_d of tetrabutoxytitanium of 600°C. During the annealing of these particles (>800°C), rearrangement into the rutile lattice took place.

The investigation of the synthesis of TiO_2 nanoparticles from ablation plasma produced by a pulse laser showed that it is the formation conditions, not the initial temperature of particles, that are important for the formation of the crystal lattice. Upon laser ablation of titanium or titania (rutile or anatase) rods in an He + O_2 atmosphere, the formation of TiO_2 (anatase) particles of 10–50 nm in size was revealed [74]. The laser ablation of a TiO_2 rod in an inert atmosphere generated amorphous TiO_2 nanoparticles. Seto et al. [75] reported the results of study of nanoparticles prepared by pulsed laser ablation of a TiO_2 (rutile) substrate in a helium atmosphere. It was shown that the particles had a metallic titanium core and a shell composed of crystalline TiO_2 (rutile and anatase).

In the synthesis of TiO_2 nanoparticles, the appearance of the initial titanium-containing material has no determining effect on the crystal structure of the particles produced. Oh et al. [76], reported the results of investigation of TiO_2 preparation by oxidation of titanium nitride (TiN) particles in a microwave plasma. A TiN powder was carried to the dis-

charge zone by a stream of oxygen mixed with an inert carrier gas. At a low oxygen concentration, the particles had a TiN core and a TiO_2 (rutile) shell. When oxygen was in excess, the particles were composed completely of TiO2 but had the anatase structure.

Unlike vapor-phase processes for the manufacture of TiO_2 nanoparticles, liquid-phase synthesis occurs at a lower temperature; for example, at T < 100°C in the sulfate process [69]. However, the particles produced are amorphous and the formation of a crystal structure requires subsequent annealing at T > 600°C. In addition, thermogravimetric studies [69, 70] have shown that the removal of hydroxyl groups and residual organic components take place at T > 500°C. Heating amorphous or anatase TiO_2 to this temperature leads to the formation of the rutile lattice, thus complicating the synthesis of anatase TiO_2 by the liquid-phase procedure.

The explosion of conducting wires, providing a non-equilibrium nature of the formation of nanoparticles [77, 78], allows one to synthesize particles with new properties, in particular with a high excess energy. In this method, a mixture micrometer-sized and nanosized particles is formed. Be means of special filters it is posiible to collect the synthesized nanoparticles with a specific area of up to 40-80 m^2/g, which make up 30 % of the total mass of the particles. The capacity of the plant is 100-200 g/h. The explosion of metal wires in oxygen or air leads to the formation of nanosized metal oxides. It was found that with the oxygen concentration in the mixture of an inert gas over 20 % (volume persent) the degree of oxidation of metal particles synthesized by the wire explosion is up to 100 %. Synthesized nanooxides have a spherical shape and relatively smooth surface.

The data from the comparison of parameters of titanium dioxide synthesized via different processes are summarized in Table 8.

Table 8. Comparison of parameters of TiO_2 particles synthesized by different technologies

Preparation methods	Reactants	Grain size	Temperature of synthesis	Lattice structure
Chlorine process	$TiCl_4 + O_2$	100-400 nm	1400-1500 ºC	rutile +anatase
Oxidation in diffuse flame	$TiCl_4 + O_2$	15–30 nm	1700 ºC	anatase + rutile
Gas-phase hydrolysis	$TiCl_4 + H_2O$	18-120 nm	lower than 600 ºC	amorphous+

				anatase
Droplet-to-particle method	TTIP. + propanol	20 – 40 nm	500–1200 ºC	anatase
Decomposition in RF-discharge plasma	TTIP. + O_2	Average size 25 nm		amorphous
Laser ablation	Ti (or TiO_2) + O_2	10 - 50 nm		anatase
Ablation by pulsed ion-beam	Ti + O_2	4 - 45 nm 0.3-2 μm		rutile +anatase
Oxidation in thermal microwave-discharge plasma	TiN + O_2	average 50 nm		anatase
Sulfate process (wet method)	$TiOSO_4$ + H_2O	100-400 nm	hydrolysis up to 80ºC, annealing - above 700ºC	rutile +anatase
Non-equilibrium plasmochemical synthesis	$TiCl_4$ + H_2 + O_2	30 - 200 nm	lower 600 ºC	rutile +anatase

The review of different processes for the synthesis of nanosized titanium dioxide has shown that crystalline particles are formed at the temperatures above 500 ºC (anatase) and 800 ºC (rutile) only.

5.1.2 An overview of the techniques to synthesize nanosized $(TiO_2)_x(SiO_2)_{1-x}$

Along with pure TiO_2 nanoparticles, a composite material containing TiO_2 and SiO_2 is of great interest. Many useful properties of TiO_2 can be substantially enhanced by varying its structure in the presence of amorphous SiO_2. In addition, the use of an inexpensive support for TiO2 makes it possible to reduce considerably the cost of the material with retaining its useful properties. The composite material $(TiO_2)_x(SiO_2)_{1-x}$ is also interesting from the viewpoint of investigation of change in the structure of crystalline TiO_2 upon insertion in the amorphous SiO_2 matrix.

For the synthesis of a composite $(TiO_2)_x(SiO_2)_{1-x}$ material, use is largely made of the sol-gel method. The resulting amorphous material is

further subjected to thermal treatment at the temperature above 500 °C to remove the hydroxyl group and the precursor material left.

In [79], amorphous $(TiO_2)_x(SiO_2)_{1-x}$ (x = 0.08, 0.18 and 0.41) was investigated using X-ray phase analysis, neutron diffraction, infra-red spectrometry, thermal gravitometry, and other analytical techniques. As precursor materials use was made of tetraethylorthosilicate (TEOS) and titanium tetraisopropoxide $(C_4H_9O)_4Ti$. It was found out that at a comparatively low concentration (x = 0.08) titanium is embedded into the lattice of titanium dioxide to form the Ti-O-Si bond. This concentration of titanium is below its limit of solubility in silicon dioxide. Given a high concentration (x = 0.41), the phases of titanium dioxide and silicon dioxide are separated already in the initial gel, and the general structure of the resulting material is amorphous. When the composite $(TiO_2)_x(SiO_2)_{1-x}$ (x = 0.41) material is heated to the temperature above 500 ºC, titanium dioxide forms a crystal lattice with the structure of anatase. It was noted in [5] that the presence of amorphous silicon dioxide retards rearrangement of the crystal structure of titanium dioxide of the anatase type into that of the rutile type. No rutile-type lattice was found out when the composite material (x = 0.41) was heated to 800 ºC. Initially, the composite material $(TiO_2)_x(SiO_2)_{1-x}$ with the average concentration of titanium (x = 0.18) was characterized by a Ti-O-Ti bonding. Upon heating the gel to 500 ºC, all the titanium atoms formed a Ti-O-Si structure. When the gel was further heated (750 ºC and higher), this structure was decomposed to form separate phases of silicon dioxide and titanium dioxide (anatase).

In [80] the results of investigation of the composite $(TiO_2)_x(SiO_2)_{1-x}$ (x = 0.1, 0.3 and 0.5) are presented, which was formed by the sol-gel synthesis tetraethylorthosilicate and titanium tetraisopropoxide. The initial gel was a composite of TiO_2 and SiO_2 with a conspicuous number of Si-O-Ti structures. As the temperature was increased, there was an increase in the number of Si-O-Ti bonds that decomposed at higher temperatures. The structure of the composite after thermal treatment was a matrix made up by pure silicon dioxide with particles of crystalline titanium dioxide having either an anatase or rutile lattice, depending on the treatment temperature. A concurrent research in [80] was made into the changes in the structure of titanium dioxide synthesized by the same method from titanium tetraisopropoxide. Initially in the course of heating to 420 ºC, the amorphous gel TiO_2 acquired crystal structure with the anatase-type lattice. When heated to above 800 ºC, it exhibited a rearrangement of its crystal lattice into the rutile form. The composite material rearranged from the amorphous structure into crystalline (anatase) at the temperature above 600 ˚C and maintained the anatase lattice in heating to 1000 ºC.

The results of investigation into the formation of nanosized composite material from a mixture of titanium dioxide (anatase) gel and silicon dioxide gel with different mixture ratios are given in [81]. The mixture of these gels was dried in air at 110 ˚C and was further annealed at 800 ºC for 1 hour. The structure of pure TiO_2 during the high-temperature annealing treatment was partially rearranged into the rutile-type lattice. An addition of silicon dioxide inhibited the rearrangement of the crystal lattice of the former during pyrolysis. The authors conclude that an annealing treatment for 1 hour at 800 ºC did not form any solid solution of Ti-O-Si, and the initial oxides were present in the composite material as separate phases.

A study of the physical characteristics of silicon dioxide aerogel with 5 % titanium dioxide was made in [82]. The composite material was synthesized from nanosized SiO_2 gel in ethanol with an addition of nanosized TiO_2 (anatase). The emulsion was dried in air and subjected to thermal treatment. An IR-spectrometry analysis did not reveal any formation of the Ti-O-Si bonding either in the initial composite material or after annealing up to 1000 ºC, the initial oxides did not form any solid solution. With the use of TEM it was found out that TiO_2 particles are built into the structure of silicon dioxide particles 5 nm in size. As in the previous papers, it was noted that the presence of silicon dioxide inhibits rearrangement of the initial structure of titanium dioxide from anatase to rutile even at 1000 ºC.

In [83], the results of investigation of a composite $(TiO_2)_x(SiO_2)_{1-x}$ material synthesized by a thermal decomposition of the metalloorganic precursor containing silicon and titanium atoms in one molecule. In that work, three compounds were studied $[Si(OBut)_2OTi(acac)_2O]_2$, $[(ButO)_3SiO]_2Ti(OPri)_2$ and $[(ButO)_3SiO]_3Ti(OPri)$, which differed by the number of titanium atoms in the molecule of titansiloxanes. The composite material was formed as a nanostructured film with the grain size from 4 to 200 nm (depending on the pyrolysis temperature). An examination of the adsorption IR-spectra demonstrated that with increase in temperature the intensity of the peak from the Si-O-Ti bond is decreased, while the intensity of the adsorption peaks from the Si-O-Si and Ti-O-Ti bonds is increased. This is indicative of the formation of separate phases of titanium dioxide and silicon dioxide at a high-temperature pyrolysis. At high temperature of decomposition of the initial metalloorganic compound, titanium dioxide formed a crystal anatase-type lattice. It is worth noting that the minimum temperature required for titanium dioxide to crystallize in the composite material under study was 600-800 ˚C for different precursors. With increase in the number of titanium atoms in the precursor mol-

ecule, the minimum pyrolysis temperature at which the formation of crystal structure in TiO_2 is decreased. A crystal phase of titanium dioxide of the rutile type was formed in minor quantities at the pyrolysis temperature 1100 ˚C only.

5.1.3 Non-equilibrium plasmochemical synthesis of nanosized particles of metal oxides

Investigation into the synthesis of oxide nanoparticles was performed with a TEU-500 pulsed electron accelerator [84]. The electron beam parameters were as follows: the kinetic electron energy of 500 keV, the pulse duration (full width at half maximum) of 60 ns, the energy per pulse of 100 J, the pulse repetition frequency of 0.5 Hz, and the beam diameter of 5 cm. The experimental system is presented in Fig. 58.

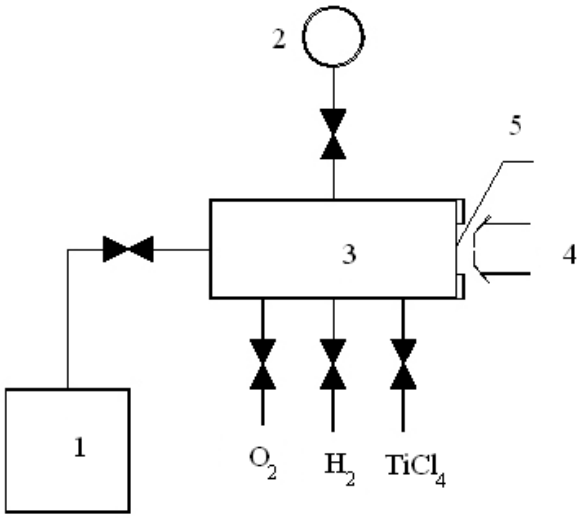

Fig.58. Experimental setup: 1 – vacuum pump; 2 – pressure gauge; 3 – plasmochemical reactor, 4 – electron beam; 5 – anode foil

The reactor was a fused-silica cylinder of 14 cm inner diameter and 6 l volume. Titania nanoparticles were produced by injection of a pulsed electron beam in a gas-phase mixture of $TiCl_4$, oxygen, and hydrogen. The complete conversion of $TiCl_4$ was achieved by passing one electron beam pulse; the energy consumption for conversion was 2.2 kJ/mol. The reactor used was a cylinder made of quartz glass with an internal diameter of 14 cm and a volume of 6 liters. Nanosized titanium dioxide was synthesized by injecting a pulsed electron beam into a gas-phase mixture of titanium tetrachloride, oxygen and hydrogen.

Temperature Regime of Preparation of Oxide Nanoparticles

The use of a closed plasma reactor and the pulsed character of the process make it possible to calculate a change in temperature during the synthesis from pressure changes in the reactor. Fig. 59 shows the time dependence of the reactor temperature. The temperatures were calculated by the ideal gas law from experimentally measured pressures.

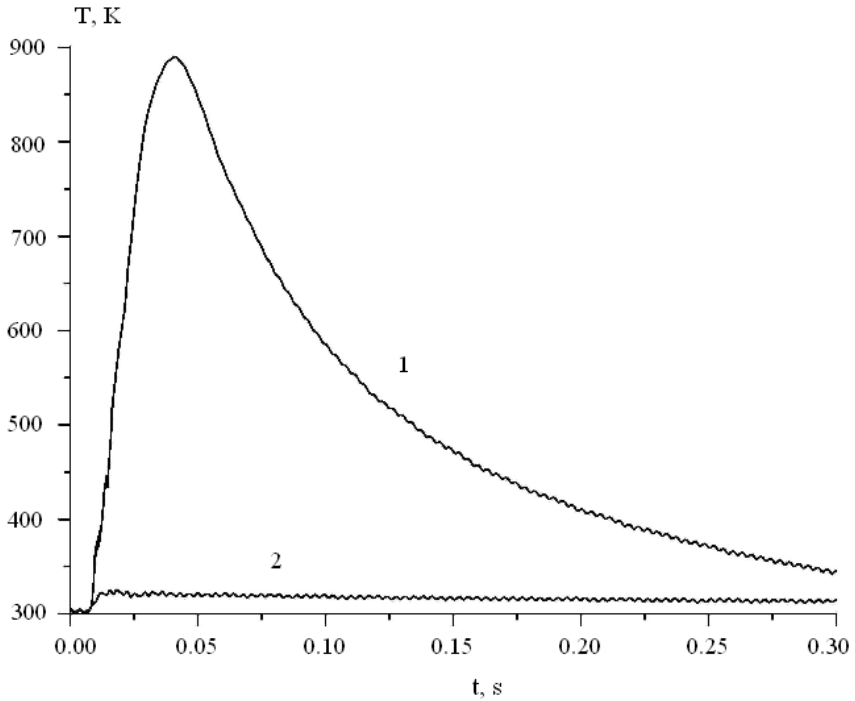

Fig. 59 (1) Change in temperature in the plasma reactor during the manufacture of oxide nanoparticles and (2) the temperature change due to heating a gas mixture by electron beam only (without ignition)

The measurements showed that the temperature of the gas-phase mixture during synthesis did not exceed 600°C and the reaction time was less than 0.1 s. The electron beam-initiated process of $TiCl_4$ degradation in a mixture with hydrogen and oxygen is explosive in nature. Along with the existence of the lower explosion limit (by pressure) and a low energy consumption, this indicates the branched chain character of the process of TiO_2 synthesis by the conversion of $TiCl_4$ in a mixture with oxygen and hydrogen.

Geometric Size of TiO_2 Nanoparticles

The particle size of a TiO_2 powder was determined with a JEM-100CXII electron transmission microscope. Fig. 60 and 61 shows a microphotograph of the particles and grain-size distribution (sample of over 1000 measurements). The grain size varied from 90 to 250 nm.

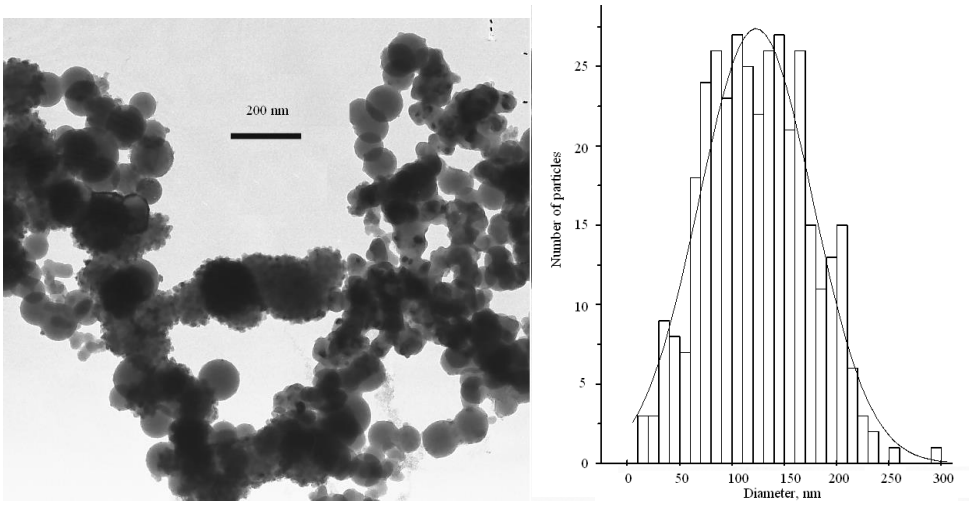

Fig. 60.TEM image and bar chart of grain-size distribution of the nanosized titanium dioxide powder. Initial mixture composition in mmol: H_2 + O_2 + $TiCl_4$ (50 : 25 : 10)

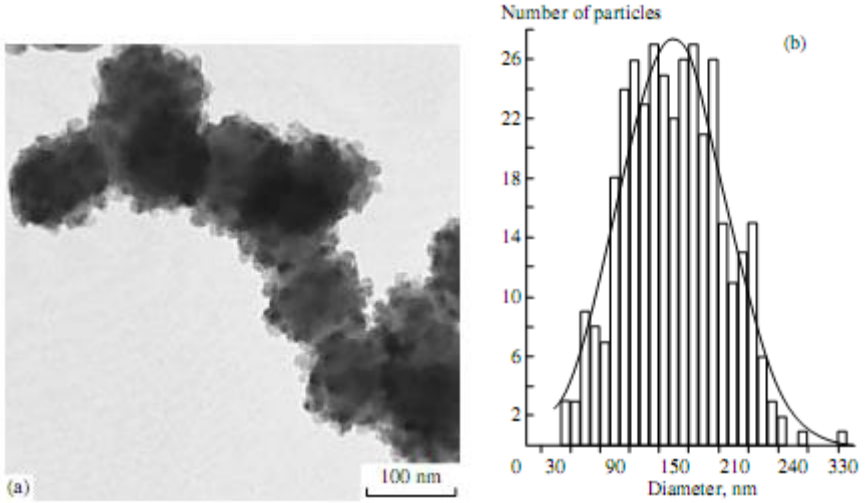

Fig. 61. (a) TEM photograph and (b) the histogram of particle size distribution of a nanosized titanium dioxide powder

The investigations also showed that the geometrical size of the synthesized powder depends on the operating mode of the synthesis. A decrease in the titanium tetrachloride concentration in the initial mixture or an addition of a buffer gas resulted in a grain size decreasing. This is indicative of a bulk character of the process of synthesis. It is noteworthy that the nanosized particles did not have any inner voids.

The shape and structure of nanosized particles of synthesized titanium dioxide were also controlled by the conditions of synthesis. At a low concentration of titanium tetrachloride in the initial reactive mixture, TiO_2 particles had a hexagonal nucleus with a characteristic tubular shell (Fig. 62*a*). With increased concentration of titanium tetrachloride in the initial

mixture, TiO_2 particles mostly round, with the surface covered by smaller-sized round particles (Fig. 62*b*). A further increase in the concentration of $TiCl_4$ in the initial mixture tended to yield particles with hexadral and cubic cut and clear surface (Fig. 62*c*).

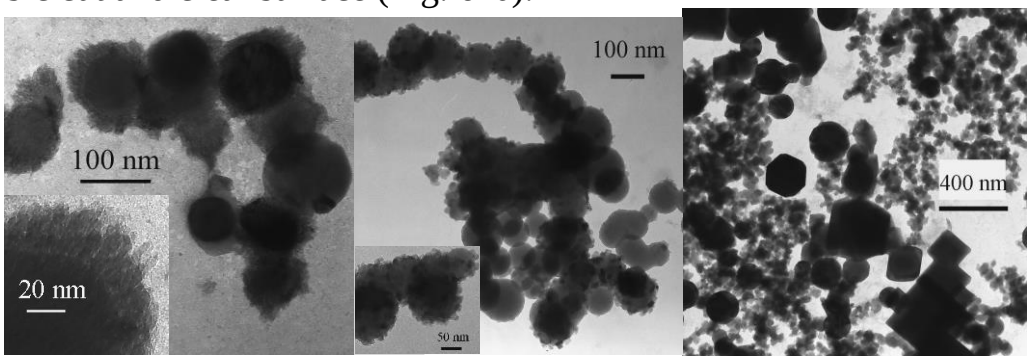

a *b* *c*

Fig. 62. Shape of particles of synthesized titanium dioxide for different concentration of titanium tetrachloride in the initial mixture: 5 mmol (a), 10 mmol (b), and 15 mmol (c) Size of photo 250·250 nm (a), 1000·1000 nm (b) and 2000·2000 nm (c)

The particle size ranged from 90 to 200 nm and depended on synthesis conditions. A decrease in $TiCl_4$ concentration in the initial reactant mixture led to a decrease in the numberaverage particle size to 30–40 nm, thus indicating the occurrence of the process in the bulk. It is also noteworthy that the prepared particles did not have internal voids.

X-ray Diffraction Analysis of TiO_2

A crystalline TiO_2 structure was formed under the given experimental conditions, with the crystal lattice type (anatase or rutile) depending on the synthesis conditions (reactant mixture composition, total pressure, etc.). Fig. 63 depicts X-ray diffraction patterns of a nanosized TiO_2 powder, and Table 1 presents data on the ratio between the rutile and anatase phases for different TiO_2 samples. Table 1 also gives values for the goodness of fit with the relevant tabulated data (21-1275 for anatase and 21-1276 for rutile).

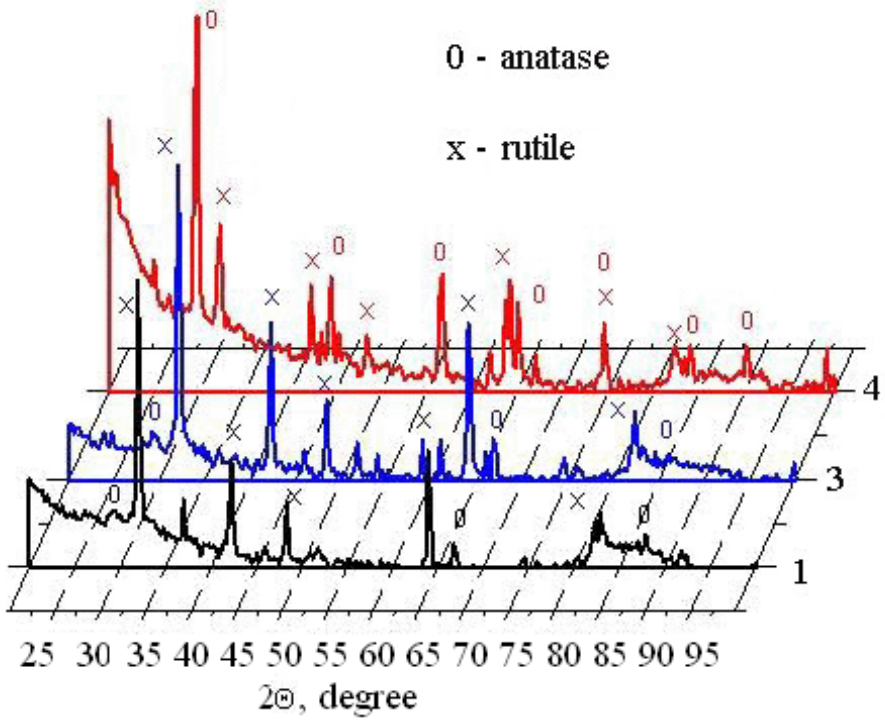

Fig. 63. X-ray diffraction patterns of a nanosized titanium dioxide powder (pattern numbers 1, 3, 4 correspond to sample numbering in Table 1): (0) anatase and (×) rutile

The fifth column in Table 9 gives the values of K, the percentage of coincidence of the X-ray pattern with the tabular data (21-1272 for anatase and 21-1276 for rutile).

Table 9. Results of X-ray diffraction analysis of nanosized titanium dioxide

Specimen	Concentration of $TiCl_4$, mmol	Rutile, %	Anatase, %	K, %	Average size, nm	sd
1	5	93	7	92		
2	5	90	10	84-86	138	44
3	10	86	14	85	148	54
4	15	33	67	80		
5	10 + Ar	39	61	85	77	24

The initial gas-phase mixture had the following molar composition: $H_2 + O_2 + TiCl_4 = 50:25:n$. A high degree of coincidence of X-ray diffraction peaks with data of the standard spectra of crystalline titanium dioxide

indicate a low amount of defects in the crystal structure and the amorphous phase of the prepared TiO_2 samples.

Despite that the temperature of the gas-phase mixture during the synthesis did not reach 800°C, crystalline nanoparticles with the rutile crystal lattice were formed, unlike the case of other TiO_2 preparation methods. This formation is due to the nonequilibrium character of the process. An increase in $TiCl_4$ concentration in the reactant mixture or the addition of an inert gas (argon) primarily led to the formation of an anatase type lattice.

IR Spectrometry of Nanosized TiO_2

The prepared nanosized particles were studied with a Nicolet 5700 IR spectrometer over the range of 400-4000 cm^{-1} (resolution 4 cm^{-1}). Typical IR spectra of nanosized TiO_2 is shown is Fig. 64.

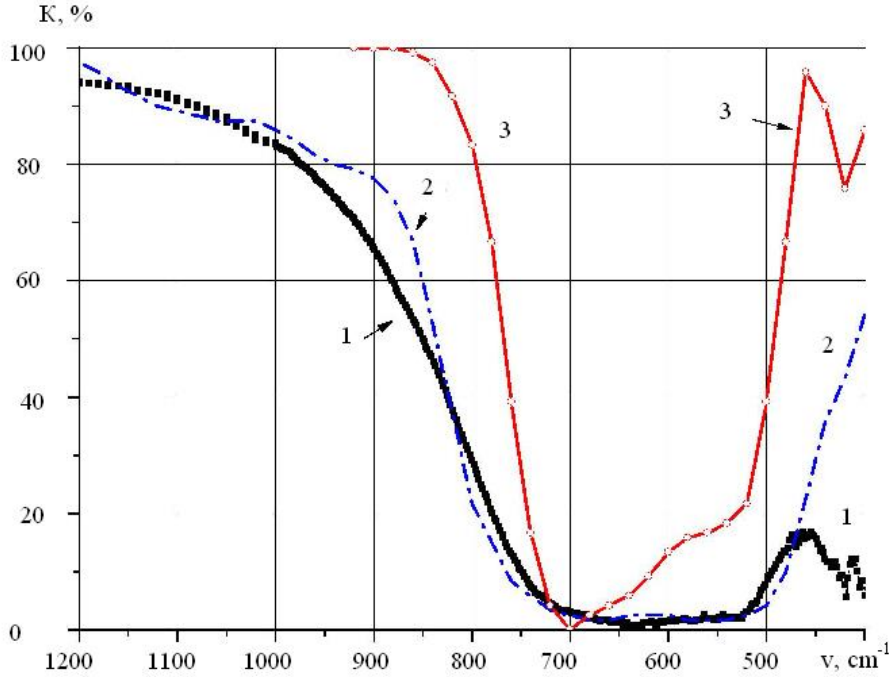

Fig. 64. IR absorption spectra of nanoparticles samples TiO_2 (1), rutile TiO_2 (2), and anatase TiO_2. K is the reflectance

For TiO_2 nanoparticles, the superposition of absorption bands due to vibrations of the Ti-O-Ti bond in the TiO_4 (650 cm^{-1}, anatase lattice) and TiO_6 (500 cm^{-1}, rutile lattice) groups is observed [85, 86].

Chemical composition of synthesized powder

In order to determine the chemical composition of synthesized powders, we performed an X-ray luminescence analysis in an Olympic DC2000. Its results are given in Table 10.

Table 10. The results of X-ray luminescence analysis

Element	Concentration, Wt %	Element	Concentration, Wt %
Ti	99.09 ± 0.08	Fe	0.48 ± 0.04
Si	0.24 ± 0.04	Cu	0.03
Cr	0.10 ± 0.01	Zn	0.03

This spectrometer is capable of registering the elements with the order number more than 10 (Na and higher), so there is no data on oxygen and chlorine. Taking into account the content of oxygen in the synthesized titanium dioxide powder, the impurity density is as low as 0.6 %.

5.1.4 Research of composite nanosized oxides $(TiO_2)_x(SiO_2)_{1-x}$ synthesized using a non-equilibrium plasmochemical process

Nanosized composite $(TiO_2)_x(SiO_2)_{1-x}$ was synthesized by injecting a pulsed electron beam into a gas-phase mixture of titanium tetrachloride, silicon tetrachloride, oxygen and hydrogen. The experimental system is presented in fig. 65.

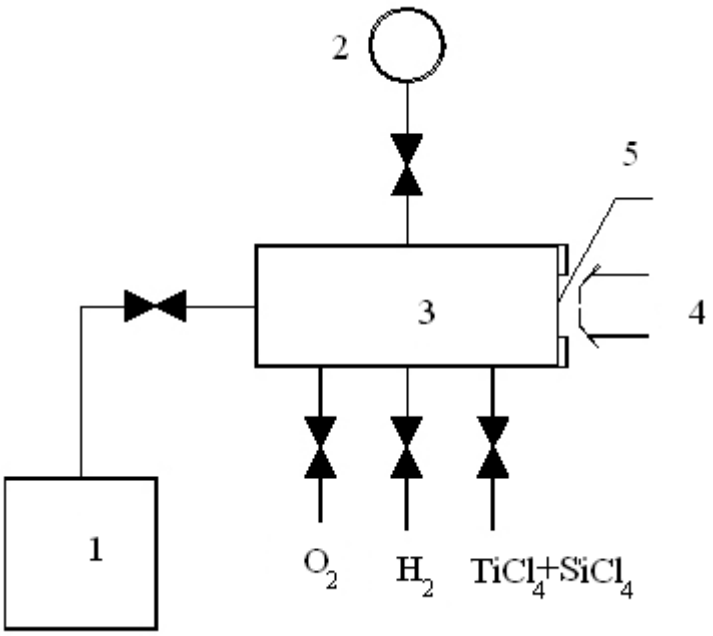

Fig. 65. Experimental setup: 1 – vacuum pump; 2 – pressure gauge; 3 – plasmochemical reactor, 4 – electron beam; 5 – anode foil

Decomposition of mixture of halides ($TiCl_4$+ $SiCl_4$ or $SiCl_4$+CCl_4) was completed within a single electron beam pulse. With the electron beam energy 100 J, the energy consumption for decomposition of mixture of halides was 5 kJ/mol. This is by far smaller than the $TiCl_4$ dissociation energy that is equal to 804 kJ/mol. The process of destruction of $TiCl_4$+ $SiCl_4$ with hydrogen and oxygen with an electron beam injected into this mixture had an explosive character. This circumstance, the presence of a lower limit (on pressure) of the reactive mixture ignition, and the low energy consumption are indicative of a cross-linked chain character of the process of composite $(TiO_2)_x(SiO_2)_{1-x}$ synthesis through decomposition of $TiCl_4$ + $SiCl_4$ in a mixture with oxygen and hydrogen.

In order to understand whether it is possible to simultaneously synthesize nanosized oxides of different materials, a number of experiments have been conducted to excite a mixture of oxygen, hydrogen, titanium tetrachloride and tetrachlorsilane by a pulsed electron beam. For the synthesis of composite oxides use was made of technological tetrachlorsilane. The reactor was heated to 90 ºC and, before filling in the gas mixture, evacuated to ~1 Pa. Upon injecting the electron beam into the following mixture (mmol): H_2 + O_2 + $SiCl_4$ + $TiCl_4$ (50 : 25 : 17 : 10), nanosized powder was formed in the reaction chamber. Fig. 66 shows a SEM image of the resulting powder.

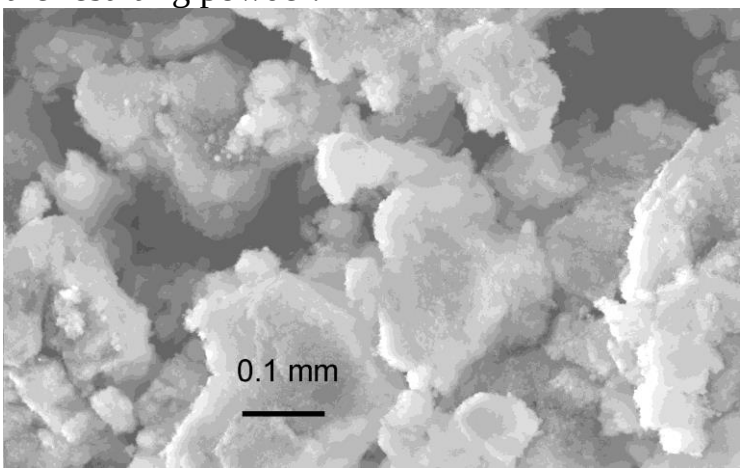

Fig. 66. Scanning electron image of the synthesized composite $(TiO_2)_x(SiO_2)_{1-x}$

Presented in fig. 67 are a TEM image of the powder and a bar chart of grain-size distribution. Note that the mean size of the composite powder particles is smaller compared to that of pure nanosized titanium dioxide synthesized under similar experimental. This might be attributed to a change in the conditions of coagulation of the particles formed upon addition of a new material.

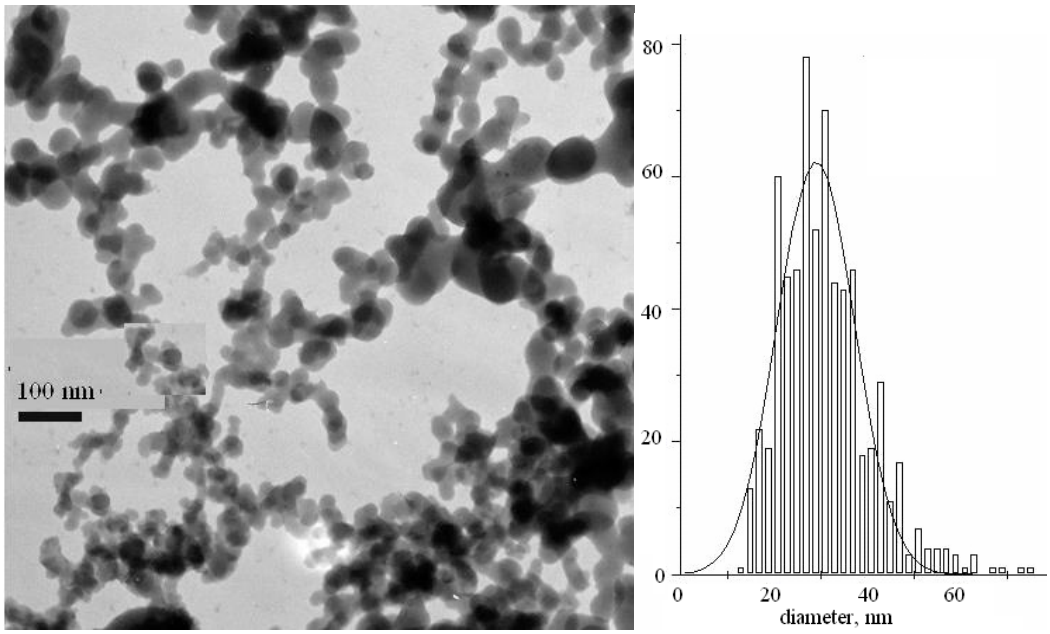

Fig. 67 TEM image and a bar chart of grain-size distribution from $(TiO_2)_x(SiO_2)_{1-x}$ powder. The mean size is 29 nm. The initial mixture in mmol: $H_2 + O_2 + SiCl_4 + TiCl_4$ (50 : 25 : 17 : 10)

The resulting composite nanosized oxides may be present as a mixture of individual particles of silicon dioxide and titanium dioxide proper. In order to determine their lattice structure and mixture ratio, the synthesized powder was analyzed in a high-resolution transmission electron microscope. In addition to TEM images, an analysis was made of the dark-field images of the particles. Brighter images corresponded to the region of coherent scattering. All the particles of the composite oxide under examination exhibited reflections in the diffraction pattern. Smaller particles in the dark-field image were fully bright (fig. 68).

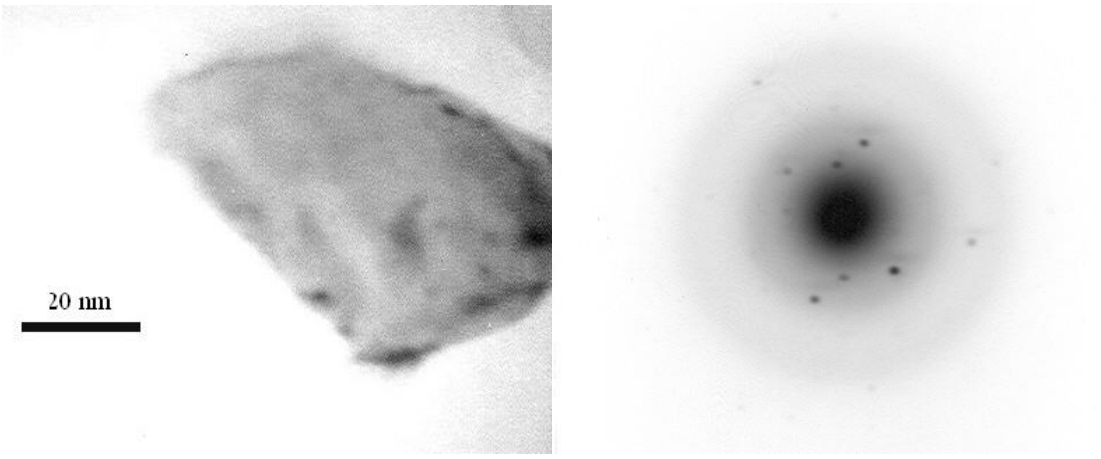

Fig. 68. Dark-field TEM-image of a small composite powder particle and its diffraction pattern

Large particles had individual regions of coherent scattering in their structure (Fig. 50).

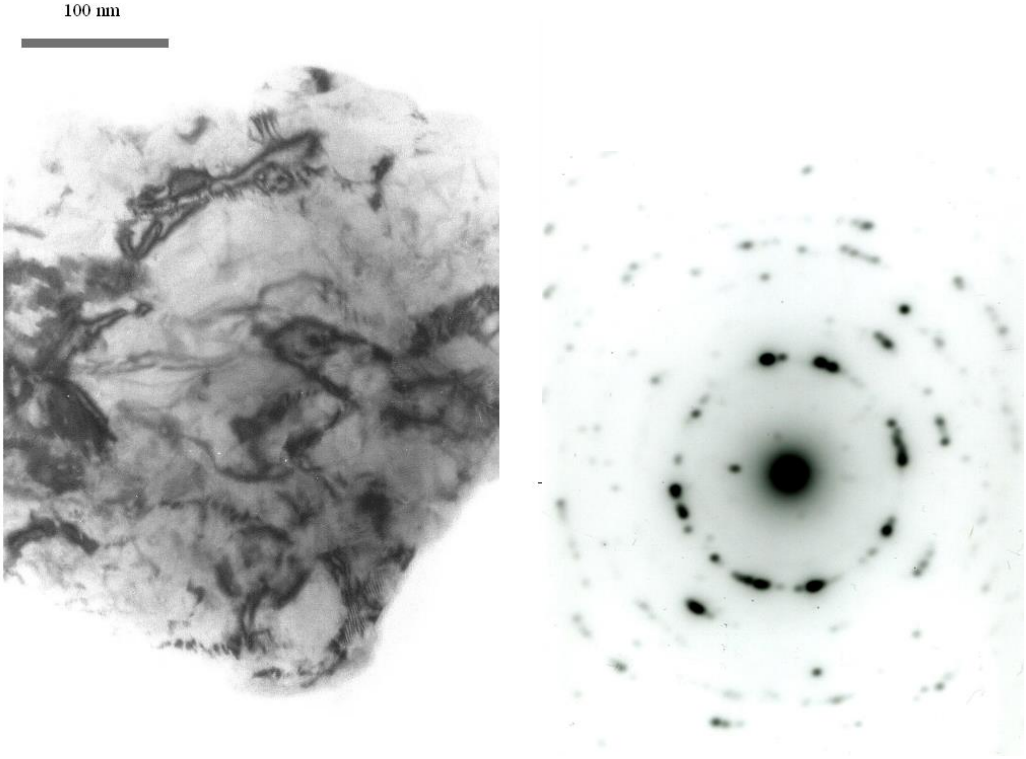

Fig.69. Dark-field TEM-image of a large composite powder particle and its diffraction pattern

The high-resolution electron microscopy examination of the synthesized composite oxide demonstrated that in our case the mixture of SiO_2 and TiO_2 in one particle are formed.

The chemical composition of the synthesized composite powder was determined in an Oxford ED2000 X-ray fluorescence spectrometer, and the results are listed in Table 11. Taking into account the content of oxygen in the synthesized composite powder, the impurity concentration is less than 0.4 %.

Table 11. Chemical composition of the powder $(TiO_2)_x(SiO_2)_{1-x}$

Element	Content, mass %	Element	Content, mass %
Si	55.90±0,08	Mn	0.049±0,01
Ti	43.58±0,01	Cu	0.040±0,01
Fe	0.225±0,01	Zn	0.040±0,01
Cr	0.100±0,01		

The method of plasmochemical synthesis developed here ensures that the chemical composition is maintained for different-size nanoparticles. Presented in Fig. 70 are the images of large (over 100 nm) and small (20…40 nm) particles of $(TiO_2)_x(SiO_2)_{1-x}$ and the total EDX-spectrum. The EDX-spectrum was also measured separately for large and small particles of the synthesized powder. The area of the respective peaks is given in Table 12 (in percent).

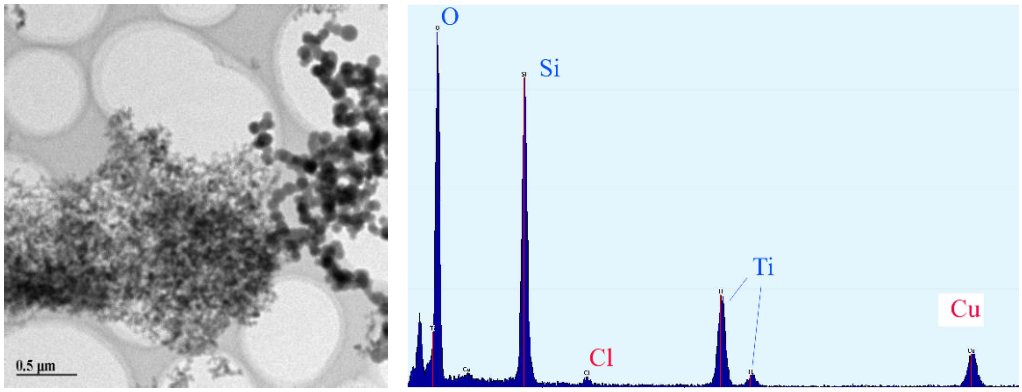

Fig. 70. TEM-image and an EDX-spectrum from the $(TiO_2)_x(SiO_2)_{1-x}$ powder. Large and small nanoparticles together

Table 12. Percentage of oxygen, silicon and titanium in the composite powder $(TiO_2)_x(SiO_2)_{1-x}$ according to the EDX-spectra

Element	Full spectrum, %	Large particles, %	Small particles, %
O	43	41.4	44.7
Si	37.5	39.1	43
Ti	19.4	19.5	12.2

An X-ray diffraction analysis of the synthesized composite nanosized powder demonstrated that both titanium dioxide proper and composite nanopowder $(TiO_2)_x(SiO_2)_{1-x}$ have crystal structure. It is well described by a composition of two types of lattices characteristic of titanium dioxide proper (rutile or anatase). Fig. 71 shows the X-ray diffraction patterns from two specimens of the synthesized oxides (rad. Co, λ =1.7901 A), and table 13 presents the data on the proportion of rutile and anatase phases of $(TiO_2)_x(SiO_2)_{1-x}$ for different specimens.

Table 13. The proportion of rutile and anatase phases of $(TiO_2)_x(SiO_2)_{1-x}$ for different specimens

Specimen	Regime of synthesis	Rutile	Anatase
1	46 mmol H_2+ 23 mmol O_2 +25 mmol $SiCl_4$+ 9 mmol $TiCl_4$	85 %	15%
2	46 mmol H_2+ 23 mmol O_2 +25 mmol $SiCl_4$+ 18 mmol $TiCl_4$	47 %	53%

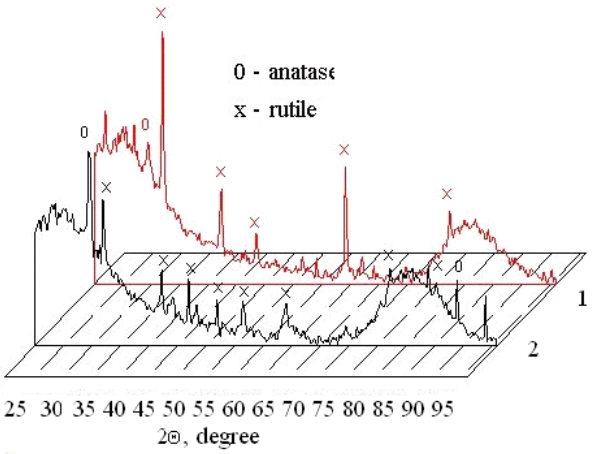

Fig. 71. X-ray diffraction pattern from nanosized $(TiO_2)_x(SiO_2)_{1-x}$ powder (curves 1 and 2 correspond to table 3)

For comparison, Fig. 72 depicts the X-ray diffraction patterns from silicon dioxide, titanium dioxide, and composite dioxide $(TiO_2)_x(SiO_2)_{1-x}$.

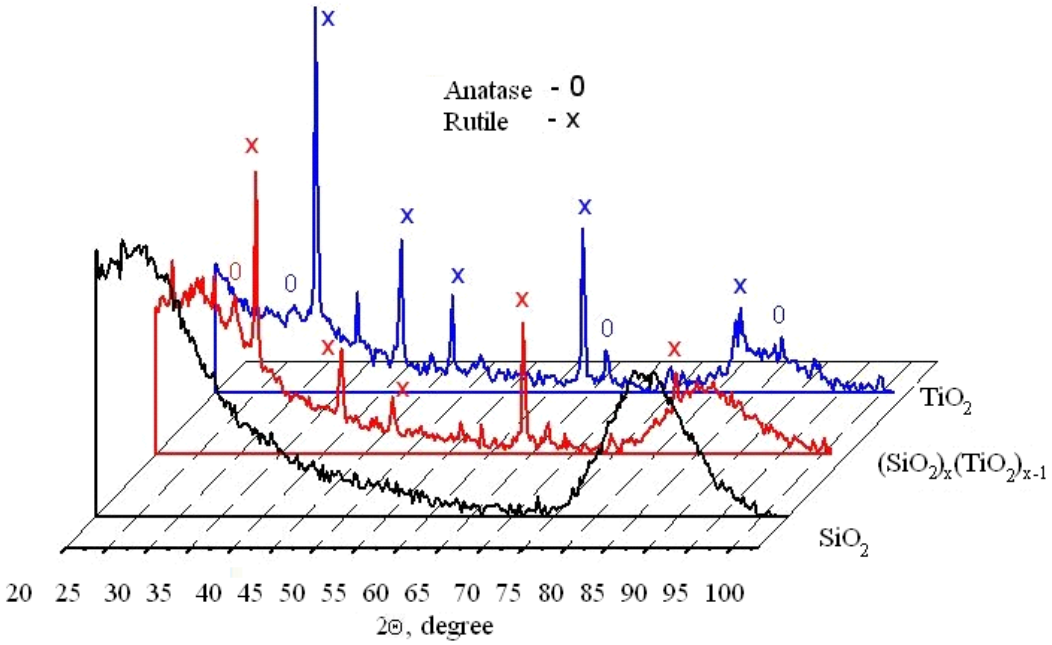

Fig. 72. X-ray diffraction patterns from the TiO_2, SiO_2 and $(TiO_2)_x(SiO_2)_{1-x}$ specimens

All the powders were synthesized by exposing the respective halide with a stoichiometric mixture of oxygen and hydrogen to a pulsed electron beam. A characteristic feature of the composite powder is the presence of a few maximums within the low-angle region (2Θ = 20-45°) and in the region from 75 to 90 degrees, which are due to the presence of an amorphous phase of silicon dioxide.

The synthesized nanoparticles were examined in an IR-spectrometer Nicolet 5700 within the range from 400 to 4000 cm^{-1}, the resolution being 4 cm^{-1}. The powder under study was preliminary mixed with KrB and compacted into a tablet. The reflectance spectrum of KrB proper was deducted from that of the mixture. Fig. 10 presents a characteristic absorption spectrum from composite $(TiO_2)_x(SiO_2)_{1-x}$ nanopowder. For comparison, shown in the figure are also the IR absorption spectra from composite powder and silicon and titanium oxides proper. The absorption peaks with the wave numbers 1190, 1080, and 790 cm^{-1} correspond to tetrahedral structure of silicon dioxide ($\nu_{as}(SiO_4)$ LO, $\nu_{as}(SiO_4)$ TO and $\nu_s(SiO_4)$, respectively) [79]. In [87], absorption at 960 cm^{-1} is attributed to the presence of a Ti-O-Si bond. Absorption in this region, however, is observed not only for the composite oxide $(TiO_2)_x(SiO_2)_{1-x}$ but also for silicon dioxide proper (Fig. 73). It is, therefore, very likely that absorption of IR light at 960 cm^{-1} corresponds to vibrational excitation of a Si-O-H bond, whose absorption peak corresponds to this wave number [87].

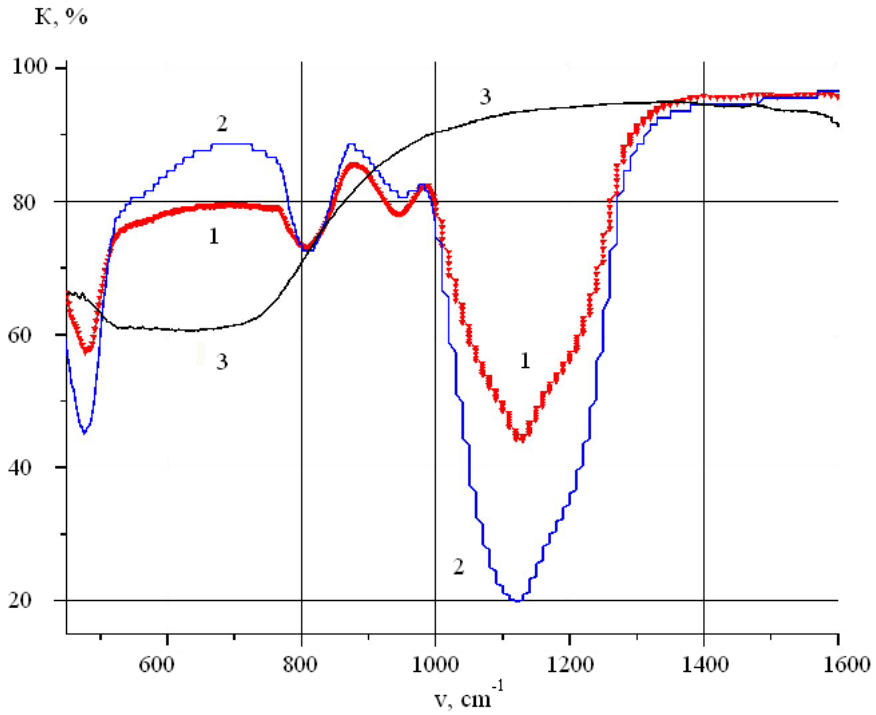

Fig. 73. IR spectra from the specimens made of $(TiO_2)_x(SiO_2)_{1-x}$ (1), SiO_2 (2), and TiO_2 (3)

The proposed method of synthesizing nanosized titanium dioxide and composite nanosized powder $(TiO_2)_x(SiO_2)_{1-x}$ exhibits very high output efficiency (1-1.1 kg/h calculated per final product) and low e-beam energy consumption (0.1-0.15 (kW·h)/kg). The initial bulk density of the nanopowder was (6-10) g/l.

5.1.5 Synthesis of composite oxides Si-C-O_x

One of the large-capacity businesses intensively developing nowadays is the production of technological carbon. The major consumers of carbon – tire manufactures – need high-quality technological carbon that will ensure higher service safety of vehicles. Moreover, an improved quality of technical carbon also reduces fuel consumption and increases tire service life. Composite nanosized materials containing carbon and silicon dioxide have been recently introduced into tire production, which allows the manufacturers to improve a number of service characteristics of the tires. Currently, there is an evident interest to the research into alternative techniques for carbon production, including plasmochemical methods. Our experimental investigations have demonstrated that a non-equilibrium plasmochemical process initiated by a pulsed electron beam is an effective way to synthesize composite nanosized oxides Si-C-O_x.

Shown in Fig. 74 are the TEM-image of the synthesized powder and the bar chart of grain-size distribution.

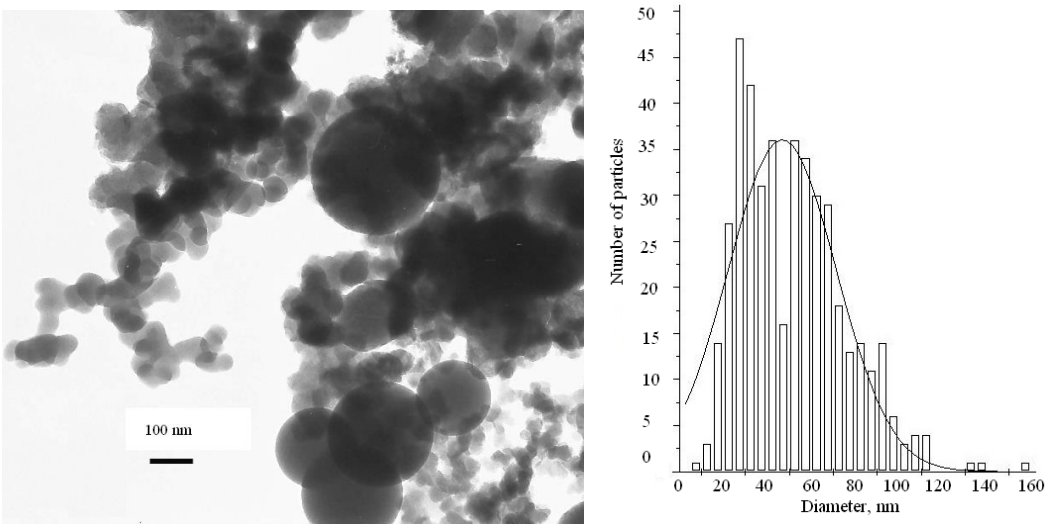

Fig. 74. TEM-image and a bar chart of grain-size distribution in Si-C-O_x. Initial mixture: 23 mmol O_2 +46 mmol H_2 + 25 mmol $SiCl_4$ + 20 mmol CCl_4

The average grain size of the resulting composite Si-C-O_x powder (46.5 nm) is smaller than that of nanosized silicon dioxide proper. An X-ray diffraction analysis of the synthesized powder reveals that it is amourphous. Fig. 75 shows a high-resolution TEM- image of a particle of the synthesized Si-C-O_x powder.

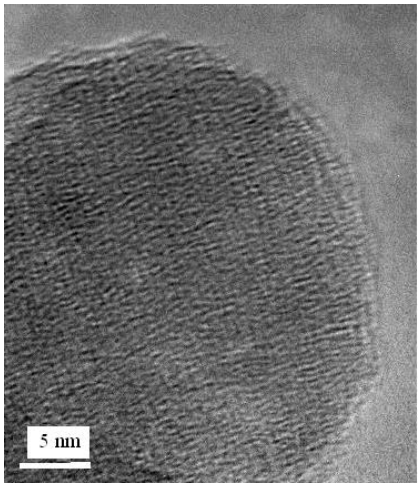

Fig. 75. TEM-image of the synthesized nanosized Si-C-O_x powder

The synthesized nanoparticles were examined in a Nicolet 5700 IR spectrometer within the range from 400 to 4000 cm^{-1}. Fig. 76 presents a characteristic absorption spectrum from the nanosized composite Si-C-O_x powder.

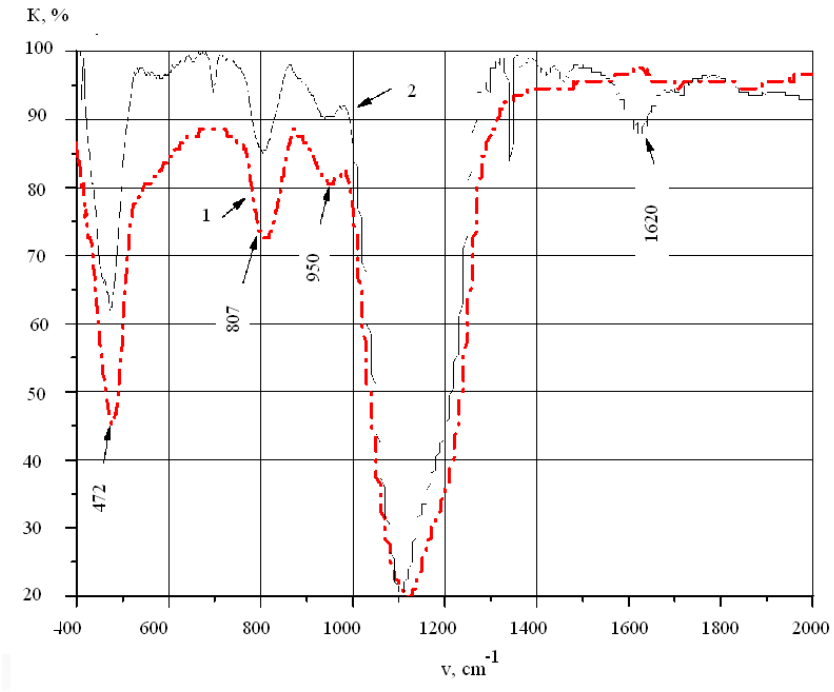

Fig. 76. IR-spectrum from silicon dioxide proper (1) and composite Si-C-O_x oxide (2)

The experimental research carried out in this work has demonstrated that a plasmochemical process initiated by a pulsed electron beam is an effective way to synthesize nanosized composite oxides from a gas-phase mixture of oxygen, hydrogen, and a mixture of halides. The resulting nanooxides exhibit homogeneous composition and their particles are spherical in shape with facetting and without voids. Crystalline TiO_2 nanoparticles were prepared from a gaseous mixture of oxygen, hydrogen, and $TiCl_4$ in a nonequilibrium plasma-chemical process initiated by pulsed electron-beam radiation. The use of a mixture of chlorides $TiCl_4$ and $SiCl_4$ makes it possible to prepare nanoparticles of mixed oxides. The obtained oxides are homogeneous in composition, and their particles have a characteristic faceted shape without inner voids. A change in the composition of the reactant mixture allows the crystal structure, as well as the shape and size, of synthetic TiO_2 to be varied. A distinctive feature of the process developed in this study is a considerable reduction in the synthesis temperature of particles with a crystalline (rutile and anatase) structure, a result which is due to the nonequilibrium nature of the processes involved.

5.2. Plasmochemical conversion of methane

Processing of natural gas and associated hydrocarbon gas is one of the most important tasks of contemporary gas chemistry. Geological studies have shown that not only biogenic methane formation processes, but also the continuing degassing of the Earth play dominating role in the formation of natural gas reserves. As a result, up to 2 trillion cubic meters of gas (its world production level) a year get into the Earth crust. This allows us to treat natural gas as a partially renewable material and energy source.

A wealth of studies on methane conversion in various electric discharges and under continuous and pulsed electron-beam irradiation have been performed to date, thus making it possible to reveal the specifics of methane degradation reactions in a low-temperature plasma. The aim of this review is to analyze the influence of the nonequilibrium conditions in plasma on the energy consumption, selectivity, and the product composition. The studies of the pyrolysis, partial oxidation, and carbon dioxide and steam reforming of methane in a low-temperature plasma are considered.

5.2.1 Plasma pyrolysis of methane

The pyrolysis of methane (conversion without addition of oxygenated compounds) is the most attractive process of natural gas reforming in which compounds with a higher molecular mass of the motor fuel range can be synthesized. The plasma synthesis of acetylene by methane pyrolysis in arc discharge has been studied and worked out on the engineering scale to the greatest extent. The degree of conversion in this process reaches 95-98 % at an acetylene selectivity of 90-95 % and an energy consumption of 2.5-3 eV/molecule [88]. Under equilibrium conditions, an energy consumption of 1.8 eV per methane molecule is required for the reaction $2CH_4 = C_2H_2 + 3H_2$, regardless of the energy source.

Numerous studies of hydrocarbon decomposition upon heating have shown that the process is chain in character (thermal cracking). At low temperatures when thermal initiation of cracking is impossible, an electric discharge generates active centers-free radicals, ions, or excited molecules-which can initiate chain hydrocarbon cracking processes. The chain mechanism of methane pyrolysis in pulsed microwave-discharge plasma (9 GHz, 100 kW) was experimentally studied in [89, 90]. In the case of methane preheating to 700-1100 K, the expenditure of plasma energy for

hydrogen synthesis does not exceed 1 eV/molecule. Similar results were obtained in a study of methane pyrolysis in a gliding alternating-current (50 Hz, 3 kW) arc discharge [91]. At a gas flow rate of 2 m^3/h, a pressure of 6 atm, and a temperature of 1400 K, 34 % of CH_4 was converted into hydrogen and acetylene. The arc-discharge energy consumption for methane pyrolysis was 0.82 eV/molecule.

The pyrolysis of CH_4 in atmospheric-pressure spark, pulsed streamer, and dielectric-barrier (dc and ac) discharges at room temperature requires quite a considerable consumption of energy [92]. For methane degradation, the energy costs (eV/molecule) are 14-25 in spark discharge, 17-21 in streamer discharge, 28-57 in dc dielectric-barrier discharge, and 116-175 in ac barrier discharge. Pulsed spark discharge results in a high yield of acetylene (54%) and hydrogen (51 %) at a CH_4 conversion of 69 %. In the case of barrier discharge, ethane prevails in the conversion products.

A high efficiency and selectivity of thermocatalytic processes of conversion of methane and other hydrocarbons stimulated studies on the plasma pyrolysis of CH_4 in the presence of catalysts. Li et al. [93] reported the results of study of the two-stage pyrolysis process in pulsed spark discharge (first step) and further in a reactor with a catalyst (second step), which was Fe-, Co-, Ni-, Cu-, or Zn-coated grains of the HZSM-5 catalyst (SiO_2/Al_2O_3 = 35). The catalyst temperature was 623 K. In the absence of the catalyst (Fig. 77), the methane conversion was 41 % at an energy consumption of 17 eV/molecule and the product composition was 84 % acetylene and 75 % hydrogen (percent of the maximal theoretical yield).

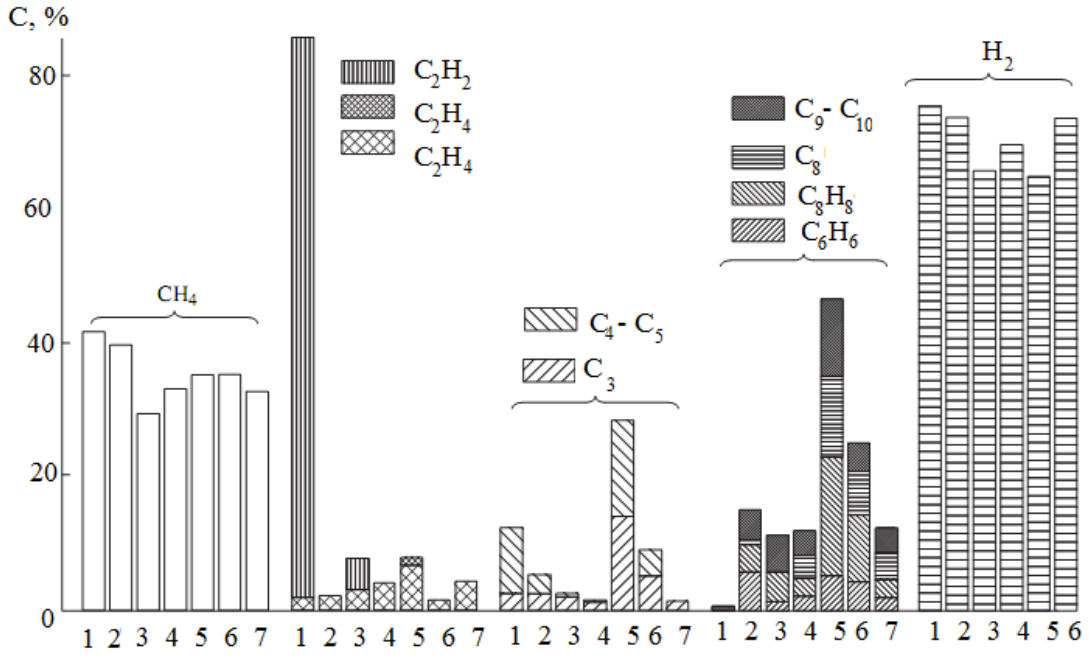

Fig. 77. Methane conversion and product composition (1) in the absence of catalyst and in the presence of the (2) HZSM-5, (3) Fe+HZSM-5, (4) Co+HZSM-5, (5) Ni+HZSM-5, (6) Cu+HZSM-5, and (7) Zn+HZSM-5 catalysts

The addition of the uncoated HZSM-5 catalyst increases the yield of aromatic hydrocarbons (primarily, benzene, toluene, and xylene) to 15 % with rise in the energy costs to 19 eV/molecule. The Ni coating of grains provides for the highest yield of aromatic hydrocarbons (47 %) and a stable catalytic activity for 3 h. Methane pyrolysis in plasma is comprehensively surveyed in [94, 95], and the data are collated in Table 14.

Table 14. Plasma pyrolysis of methane

Discharge type	Reactant mixture	Main products	Conversion %	Energy consumption, eV/molecule
Pulsed microwave, 700 – 1100 K	CH_4	C_2H_2, H_2	90 - 100	1
Gliding arc, 50 Hz, 1400 K	CH_4	C_2H_2, H_2	34	0.82
Gliding, 50 Hz	$CH_4 + H_2 + Ar$	(75 - 84)% C_2	18	1.6 - 4.4
Direct-current arc, 60 kW	$CH_4 + H_2$	C_2H_2	95	4.2
Direct-current arc, 160 V, 75 A	$CH_4 + N_2$	33% H_2	80	8 – 10
Pulsed, 8 kHz	CH_4	-	-	8.5
Pulsed glow, 50 – 200 Hz	CH_4	-	-	9.1 - 10.3
Pulsed double-pointed, 2 – 20 kHz	CH_4	85% C_2H_2	23.5	3.8
Corona, 0.2 – 10 kHz	CH_4	-	25	52
Spark, 50 Hz, 5 kV	CH_4	C_2H_2	70	6.1
Streamer, 4.6 W	CH_4	C_2*	19 - 41	17 - 21
Dielectric-barrier, 75 kHz, 17 W	CH_4	C_2H_6	6 - 13	38 - 57
Pulsed electron beam, 450 kV, 10 kA	CH_4	C_2*	5 - 7	18
Gliding radiofrequency, 13.56 MHz, 60 torr	CH_4 + Ar	C_2H_2, C_2H_4	75	12
Dielectric-barrier with SiO_2 catalyst	CH_4	$C_2H_6 + H_2$	45	52

Spark with Fe, Co, or Ni catalyst on HZSM-5	CH_4	46% (C_6H_6, C_7H_8, C_8H_{10})	40	19
Gliding (50 Hz) with Al_2O_3 catalyst	$CH_4 + H_2$ + Ar	(83 - 100)% C_2*	18	2.4 – 7.3
* C_2 includes ethane, ethylene and acetylene.				

Analysis of studies on the plasma pyrolysis of methane has shown that the minimal energy consumption and the maximal degree of conversion were obtained under equilibrium conditions, in dc arc discharge (3 eV/ molecule, 95 %). The use of different types of pulsed discharge for CH_4 pyrolysis neither reduces the specific energy consumption nor increases the conversion. The best results were obtained in pulsed spark discharge (3.8 eV/molecule, 28.5 %), but they are worse than the results of methane pyrolysis in arc discharge plasma. The main degradation products are C_2 hydrocarbons with the highest proportion of acetylene.

The nonequilbrium character of plasma interaction was revealed only in the case of microwave-discharge or gliding arc discharge treatment of methane preheated to the thermal degradation onset temperature. In this case, the plasma energy consumption for decomposition is lower than that under the equilibrium conditions and does not exceed 1 eV/molecule.

5.2.2 Partial oxidation of methane

At present, the overwhelming bulk of natural gas is processed into synthetic liquid fuel via the Fischer–Tropsch process designed in 1923. For manufacture of liquid fuel, carbon compounds (natural gas, black and brown coals, heavy petroleum fractions, etc.) are converted into synthesis gas (mixture of CO and H_2) and, then, into synthetic crude oil. The liquid fuel manufacture technology requires high capital and operation costs at the syngas production step.

The methane oxidation process is a branched-chain process; it has been thoroughly studied under equilibrium conditions and is described in [96, 97]. The use of low-temperature plasma in the partial oxidation of CH_4 holds promise primarily for initiation of the chain process. Data on the partial oxidation of methane via the chain process in microwave discharges of two types are reported in [98]. The plasma energy consump-

tion was 0.25 eV/molecule at a methane conversion of 70 % and increased to 0.5 eV/molecule when the conversion increased to 100 %.

Data that are interesting from the viewpoint of industrial implementation were obtained in a study of the partial oxidation of methane in arc discharges of different types. In a two-electrode arc plasma reactor, the partial oxidation of CH_4 in a stoichiometric mixture with oxygen is characterized by an energy consumption of at most 1 eV/molecule [99].

Methane conversion in a mixture with oxygen ($CH_4 : O_2 = 1 : 2$) in a rotating-arc plasma reactor also showed a low energy consumption [100]. As the discharge energy input to the gas increased from 2.6 to 4.8 kJ/l at a gas flow rate of 15-30 l/s, the consumption for methane conversion increased from 1.6 to 2.2 eV/molecule. Fig. 78 shows the results of a study of the conversion process.

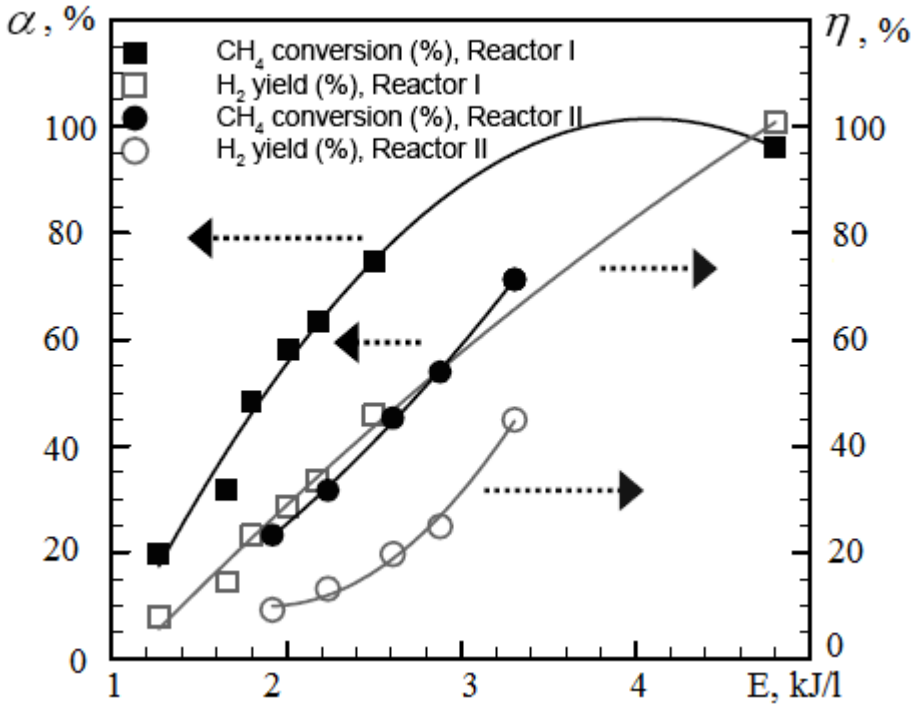

Fig. 78. The degree of conversion of methane α and hydrogen content η in the products conversion versus the input energy of discharge

Similar results were obtained during the partial oxidation of CH_4 in its mixture with air in vortex gliding arc discharge (10 kV, 15–20 kHz) [101]. As the initial methane concentration in the reactant mixture was increased from 20 to 44 %, the energy consumption for conversion increased from 1.4 to 5 eV/molecule. Fig.79 shows the plasma-chemical reactor.

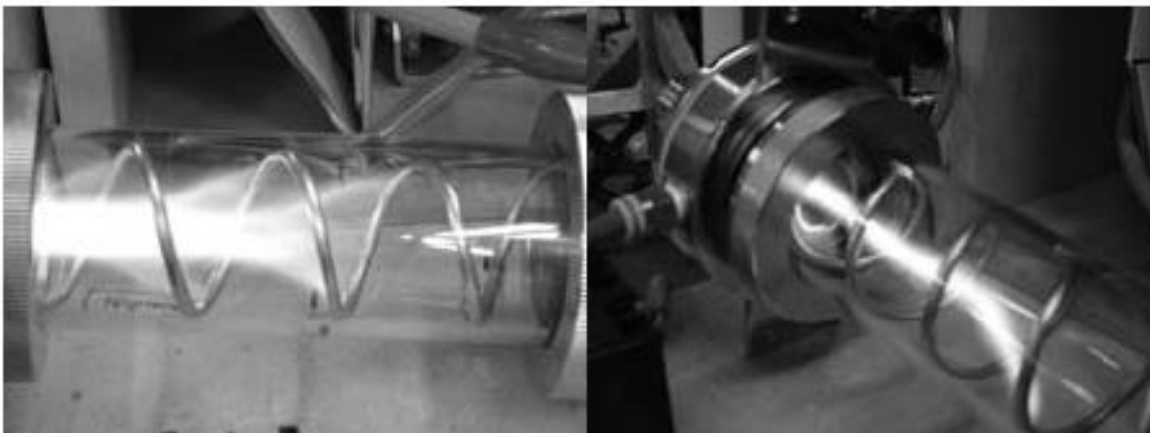

Fig. 79. Plasma-chemical reactor with a surface arc discharge

In the case of pulsed electron-beam irradiation (350–450 keV, 10 kA, 60 ns), partial methane oxidation in a mixture with oxygen and hydrogen occurred in the nonequilibrium mode [102]. The process of incomplete oxidation of CH_4 was effective at a high initial concentration of oxygen (>30 %) in the reactant mixture. As the initial pressure of methane in the $H_2 + O_2 + CH_4$ mixture was increased at a constant oxygen pressure, the proportion of CO and H_2 in the products increased. The energy consumption for CH_4 conversion did not exceed 0.05 eV/molecule.

It was experimentally shown that the joint action of low-temperature plasma and catalyst substantially alters the composition of the products of methane partial oxidation. Indarto et al. [103] studied the conversion of methane in a 4:1 mixture with oxygen into methanol in a dielectric-barrier discharge plasma (10 kV, 50 W). To increase the conversion efficiency, the CZA (copper–zinc–aluminum) catalyst placed at the end of the plasma reactor was used without additional heating. In the absence of the catalyst, the main products of partial methane oxidation in the barrier discharge were CO, CO_2, and H_2, and the methanol content did not exceed 11 %. In the presence of the catalyst, the yield of methanol increased by a factor of 2. The process comprised two steps; the production of synthesis gas in low-tem perature plasma and the subsequent formation of methanol on the catalyst. At CH_4 conversion of 28-33 % and a feed-mixture flow rate of 30 ml/min, the energy consumption for methane conversion was 88-100 eV/molecule. Promoting the catalyst with different metals made it possible to increase the selectivity for methanol (Fig. 80).

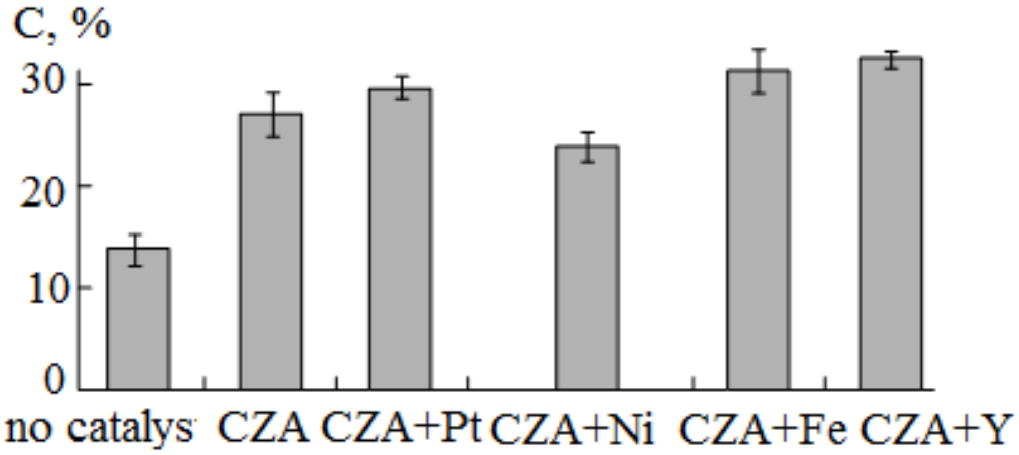

Fig. 80. Concentration of methanol in the products of plasma reforming of the $CH_4 + O_2$ mixture in the presence of different catalysts.

The data on the partial oxidation of CH_4 in different discharges are summarized in Table 15, and a more detailed review is presented in [94, 95].

Table 15. Partial oxidation of methane in plasma

Discharge type	Reactant mixture	Main products	Conversion %	Energy consumption, eV/molecule
Direct-current arc, 10 kW	$CH_4 + O_2$ + Ar	$CO + H_2$	-	1
Rotating arc, 2 kW, 5 - 20 kHz	$CH_4 + O_2$	50-60 % H_2	80	1.6-2.2
Vortex rotating arc	CH_4 + Air	H_2 / CO = 1.1-2.7	30	1.4-5
Microwave, 2.45 GHz, 1-5 kW	$CH_4 + O_2$	$CO + H_2$	100	0.5
Dielectric-barrier, 75 kHz	$CH_4 + O_2$	CO, CH_3OH	14-27	5-13
Dielectric-barrier, 20 kHz	$CH_4 + O_2$	22 % CH_3OH	24	11
Dielectric-barrier with CZA catalyst	$CH_4 + O_2$	30- 35 % CH_3OH	28-33	88-100
Dielectric-barrier with Yt + Zr catalyst	$CH_4 + O_2$	20-23 % CH_3OH	50	88

Thus, the highest yield of the synthesis gas at a low energy consumption was obtained in various arc discharges, which provide a high

methane conversion capacity per unit volume of the reactor and do not require a high-voltage power source. The use of combined (plasma + catalyst) reactors makes it possible to control the composition of conversion products, in particular, to increase the selectivity for CH_3OH from 3 to 35 %.

Carbon dioxide reforming of methane

Methane conversion in the presence of carbon dioxide is considered by many investigators to be an alternative CO_2 utilization process aimed to mitigate the greenhouse effect and to simultaneously synthesize useful products. Under equilibrium conditions, the reaction:

$$CH_4 + CO_2 + 2.5\ eV = 2CO + 2H_2$$

is run over a Ni catalyst at a temperature of 850 ºC and a pressure of 2-3 MPa [97].

Plasma methane conversion in a controlled arc dis charge was studied in [99]. In the case of conversion of the $CH_4 + CO_2$ mixture at atmospheric pressure, the energy consumption for decomposition was 15 eV per methane molecule. The use of an improved reactor design with gliding arc discharge (480 V, 20 A) made it possible to reduce the energy consumption to 1.5-2.3 eV/molecule [99]. At a gas flow rate of 1.8-4.7 m^3/h, atmospheric pressure, and ambient temperature, the main products were H_2, CO, and H_2O.

When the reactant gas mixture was heated to 1200 K, the energy consumption of a pulsed corona discharge for carbon dioxide methane reforming did not exceed 0.7 eV/molecule, thereby indicating the chain mechanism of the conversion [104].

The conversion of methane in a mixture with carbon dioxide ($CH_4/CO_2 = 1$) in dielectric-barrier discharge plasma requires high energy consumption [105, 106]. The study of the degree of conversion depending on the voltage pulse amplitude, pulse repetition frequency, and the form (uni- or bipolar pulses, 4-12 kV, 0.4-2 kHz) shows that the conversion depends only on the specific energy input to the discharge. Variations in the energy input by changing the voltage (pulsed power) and pulse repetition frequency (average power) have the same effect on the conversion. As the energy input was varied from 16 to 70 J/cm^3, the degree of CH_4 conversion in the case of the bipolar pulse form increased from 9.8 to 22.8 %, and the energy consumption increased from 38 to 70 eV/molecule. The data on carbon dioxide reforming of methane in different discharges are collated in Table 16.

Table16. Carbon dioxide reforming of methane in plasma

Discharge type	Reactant mixture	Main products	Conversion, %	Energy Consumption, eV/molecule
Deirect-current gliding arc	CH_4+CO	CO+H_2	_	1.5-3.3
Pulsed corona, 1200K	CH_4+CO_2	CH_2+CO+H_2	16	0.7
Alternating-current glididng arc	CH_4+C_2H_6+CO_2	H_2+C_2	8	20
Dielectric-barrier, 0.4-2 kHz	CH_4+CO_2	CO+H_2	9.8-22.8	38-70
Dielectric-barrier, 2-40 kHz	CH_4+CO_2	CO+H_2	25-65	73-100
Dielectric-barrier, 30 kHz	CH_4+CO_2	CO+H_2+C_2H_6	35-75	52-85
Dielectric-barrier with (Ir,Pd,Re)/γ-Al_2O_3 catalyst	CH_4+CO_2	CO+H_2+C_2	30-50	_
Dielectric-barrier with catalyst	CH_4+CO_2	HCOH,CH_3OH	48	16

The results that hold promise for industrial implementation were obtained only for methane conversion in a gliding discharge. In discharges of other types, the separate conversion of CO_2 into CO and CH_4 into hydrocarbons (C_2H_6, C_2H_4, C_2H_2, etc.) takes place. The electrode material and the catalyst have a great effect on the composition of the conversion products of the CH_4 + CO_2 mixture.

Steam reforming of methane

Steam methane reforming provides the maximal yield of hydrogen and, therefore, holds promise for hydrogen economy and is being inten-

sively studied. Under equilibrium conditions, the steam reforming of methane proceeds in accordance with the reaction:

$$CH_4 + H_2O + 2.1\ eV = CO + 3H_2$$

at a temperature of 1300–1900 K and a pressure above l5 MPa [97].

The conversion of methane in a mixture with steam in gliding discharge plasma is characterized in that the energy consumption for CH_4 decomposition does not exceed 0.92 eV/molecule [107]. A specific feature of the reactor design is the rotation of the plasma string by an external magnetic field (Fig. 81). At a discharge power of 1 kW, a feed mixture flow rate of 30 l/min, a temperature of 150 ºC, a pressure of 0.1 MPa, and a CH_4/H_2O ratio of 0.67, the degree of conversion reaches 50 %. The main products are hydrogen (55 vol %) and CO (10 vol %); the amount of CO_2 and C_2H_2 does not exceed 1 vol %.

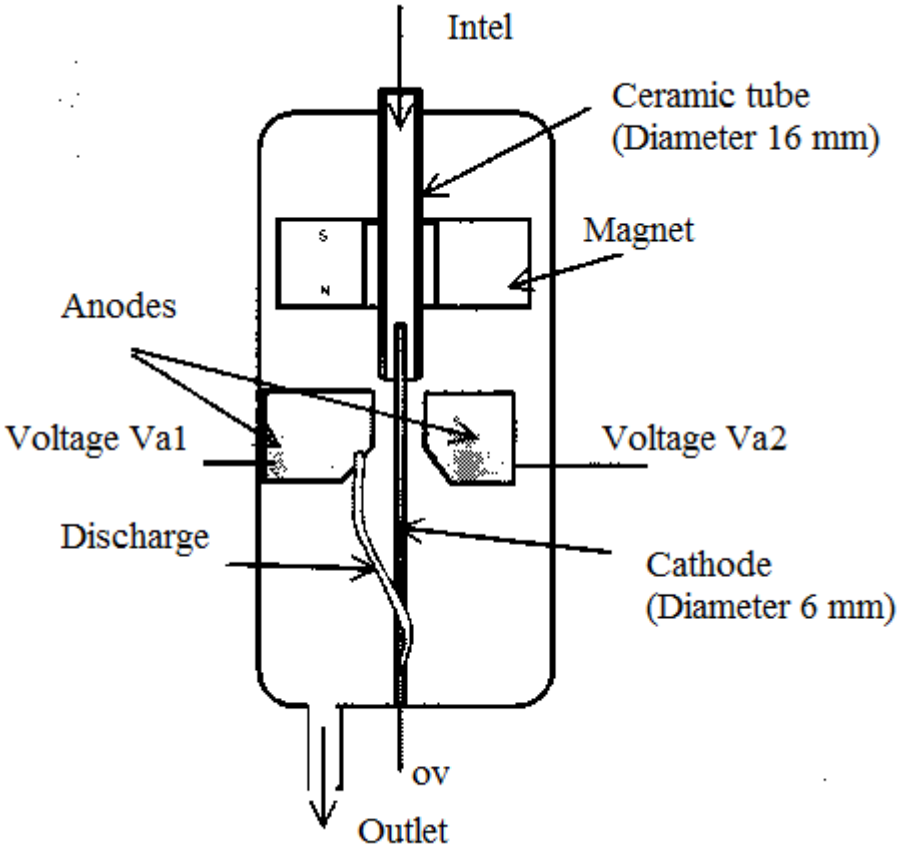

Fig.81: A scematic of a new reactor

Energy consumptions close to the enthalpy of the process were achieved in the case of steam methane reforming in a rotating gliding arc plasma reactor [108]. For the $CH_4/H_2O = 0.2$ mixture, a 44 % conversion was attained at an energy cost of 2.6 eV per methane molecule.

The results of investigation of CH_4 conversion in a mixture with steam via the chain mechanism are reported in [109]. The experiments were conducted in a microwave plasma generator (915 MHz; pulse power, 200 kW) with preheating the reactant mixture to 500-570 ºC; the CH_4/H_2O ratio was varied from 0.5 to 1. The gaseous products of the process were syngas and CO_2. Azizov et al. [109] note that the total energy consumption of the process is reduced by 30-60 % when the discharge is switched on, although the discharge energy does not exceed 5 % of the thermal energy. At a cumulative energy input of 2 J/cm^3, the concentration of the product hydrogen was 11 %, a value that corresponds to the total energy consumption for H_2 synthesis of 4.2 eV/molecule.

Sekine et al. [110] examined the dependence of the conversion and the product composition on the spark-discharge pulse repetition frequency (20-300 Hz) and the proportion of CH_4 in a mixture with water vapor. In all experiments a quartz tube of 4.0 mm inner diameter was used as a flow type reactor as shown in Fig. 82.

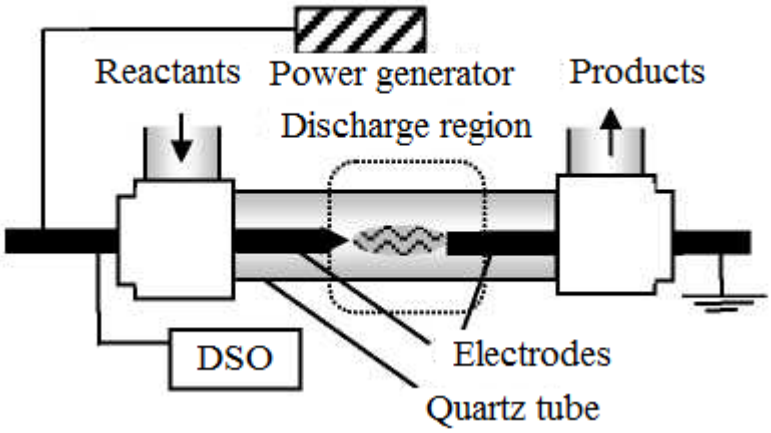

Fig. 82. Experimental setup and configuration

At a methane conversion of 55 %, a discharge power of 2.1 W, and a feed mixture flow rate of 10 cm^3/min, the energy consumption for conversion was 5.2 eV/molecule. A distinguishing feature was a high H_2/CO ratio, 4-4.5. This value is noticeably higher than the ratio characteristic of steam reforming under equilibrium conditions, $H_2/CO = 3$.

In addition to steam reforming of methane, authors [110] investigated about steam reforming of other hydrocarbons and alcohols using non-equilibrium pulsed discharge. Propane served as a model for LPG and n-hexane and cyclohexane served as a model for gasoline. The results are shown in Fig. 83.

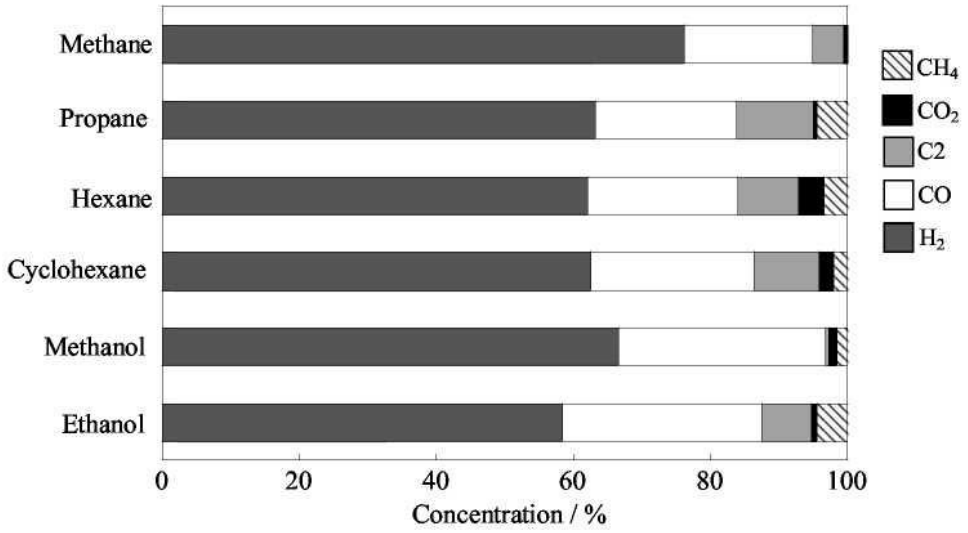

Fig. 83. Steam reforming of various fuels using non-equilibrium pulsed discharge.

The cited authors [110] noted that the energy utilization efficiency of the pulse discharge for the synthesis of hydrogen and CO reached 60 %.

Zhdanok et al. [111] reported the results of study of steam and steam–air methane reforming in a combined reactor employing a high-voltage atmospheric-pressure discharge and catalysts (Ni or Fe_2O_3). Fig. 1 gives a diagram of experimental setup to make studies on partial methane oxidation in APHVD plasma. The major components of the setup are a plasmachemical reactor and a gas chromatograph. A cooler and a hotwell are installed at the reactor output (Fig. 84).

The given experimental study used two types of catalysts: hydro-genation nickel catalyst Synetix PRICAT 400 (RP) 2.5 mm (15.7 % Ni on Al_2O_3) and carbonic oxide conversion catalyst CTK - TZC 3/1 (Fe_2O_3) with chrome additives.

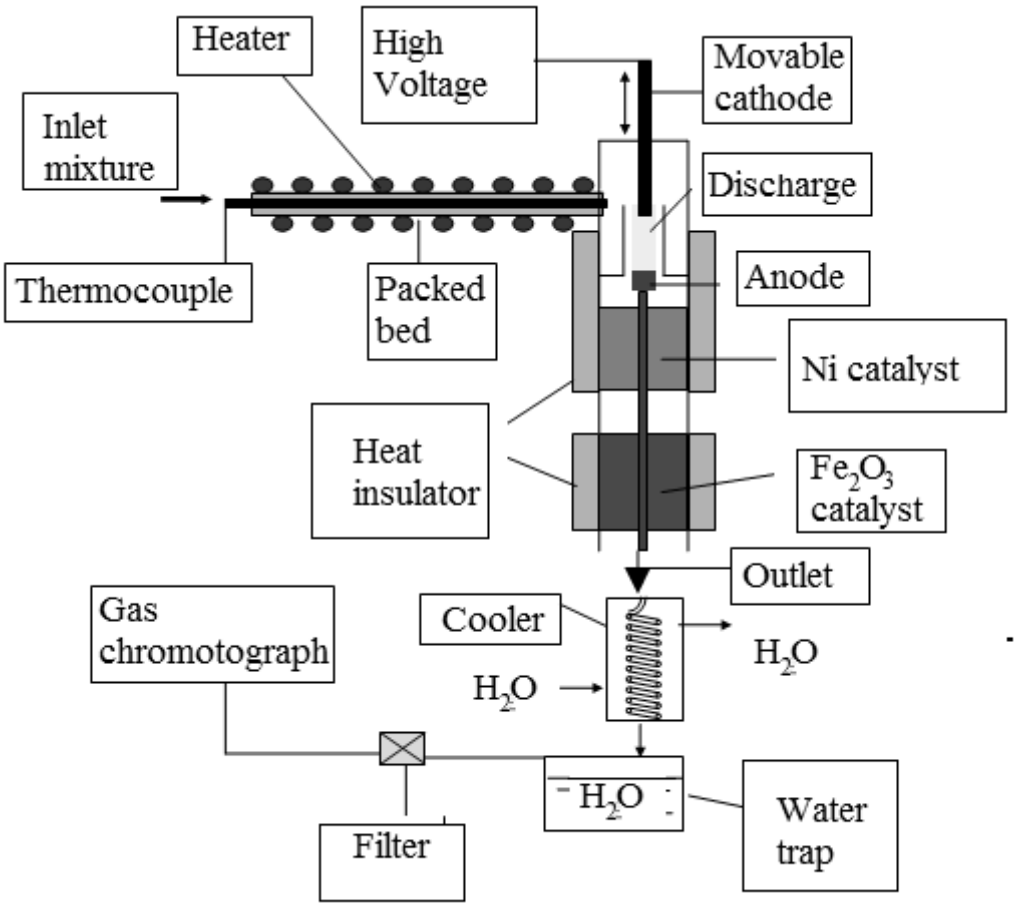

Fig.84. Experimental set-up

The use of nickel made it possible to reduce the discharge energy consumption for H_2 production by a factor of 2.5. Data on steam reforming in discharges of different types are collated in Table 17.

Table 17. Steam methane reforming in plasma

Discharge type	Main products	Conversion, %	Energy consuption eV/molecule
Direct-carrent gliding arc	H_2+CO	50	0.92
	H_2+CO	44	2.6
Direct-current roraiting gliding arc	H_2+CO+CO_2	-	2.1
Microwave discharge, 915 MHz, 500-700 ^{0}C	H_2+CO	55	5.3
Spark discharge, 20-		77	

300 Hz Spark discharge with Ni catalyst	H_2+CO+CO_2		1.6

From the data presented in the table, it is seen that steam methane reforming in most low-temperature discharge plasmas requires a low energy consumption, equal to or lower than the enthalpy of the process. This mode of plasma-assisted conversion of methane is the most promising for industrial implementation; however, it has been little studied.

Combined Processes of methane conversion in plasma

The combination of the endoergonic reactions of carbon dioxide and steam reforming with the exothermic reactions of partial oxidation of methane makes it possible to substantially reduce the energy consumption for CH_4 conversion. The carbon dioxide reforming of natural gas in gliding ac arc discharge was studied by Chavadej et al. [112]. The addition of O_2 to the CH_4 + C_2H_6 + C_3H_8 + CO_2 mixture at a 75 % hydrocarbon content of the initial reactant mixture reduced the energy consumption for the decomposition of reactant molecules from 19.4 to 14.3 eV/molecule, and the energy consumption for H_2 production decreased from 32 to 19.4 eV/molecule.

In a study of the plasma reforming of methane in a mixture of steam and air in a direct-current plasmatron, a 40 % hydrogen yield (on a hydrogen content in methane basis) and an energy consumption of 2.1 eV/molecule were achieved [113]. The use of the Ni/Al_2O_3 catalyst in combined methane reforming in the plasmatron made it possible to increase the yield of H_2 to 100 % and to reduce the energy consumption to 0.9 eV/molecule at a 70 % methane conversion.

To reduce the energy consumption for CH_4 conversion in a mixture with air and steam in an arc plasmatron, the Ni/Al_2O_3 catalyst (United Catalyst C-11) was used [114]. At a 70 % methane conversion, the energy consumption for hydrogen production was reduced from 1 eV/molecule (in the absence of catalyst) to 0.35 eV/molecule.

Steam methane conversion with a an admixture of 5 % oxygen in a continuous microwave discharge (915 MHz, 200 kW) is described in [90]. At a gas flow rate of 200 m^3/h and a pressure of 0.1-1 atm, a 90 % conversion of CH_4 was achieved with an energy consumption for H_2 pro-

duction of 0.9-1.0 eV/molecule. The data on combined methane reforming in plasma are presented in Table 18.

Table 18. Combined reforming of methane in plasma

Discharge type	Reactant mixture	Main products	Conversion, %	Energy consuption eV/molecule
Gliding arc, 17.5 kV,300 Hz	$CH_4+C_2H_6+C_3H_8+CO_2+O_2$	H_2,CH_4,C_2H_2,CO	30-70	14.3
Direct-current arc, 3.5 kW	CH_4+H_2O+air	H_2	80	4.2
Direct-current arc and NiO/Al_2O_3 catalyst	CH_4+_{H2O}+air	H_2, CO, CO_2	70	0.35
Roraiting, 10 kV, 50 Hz	CH_4+H_2O+air	___	2-4	6
Microwave discharge, 915 MHz, 200kW	$CH_4+H_2O+O_2$	___	90	0.9-1

Thus, the most important parameter from the view point of commercialization of the plasma reforming of methane is the energy consumption for its decomposition. All types of discharge can be divided into two groups in accordance with the energy consumption, degree of conversion, and selectivity for products, namely, inhomogeneous (arc, spark, gliding) and space (dielectric-barrier, and corona) discharges.

In inhomogeneous discharges, the methane conversion efficiency is higher, the energy onsumption for decomposition is below
10 eV/molecule; the conversion in arc discharges exceeds 90 % and the selectivity reaches 90 % for certain products (C_2H_2 in plasma pyrolysis, H_2 and CO in steam reforming). In space discharges, a high degree of conversion (>50 %) is reached only at high energy consumptions for methane decomposition (>40-50 eV/molecule) and a broad range of products with a low selectivity are synthesized.

A substantial reduction in the discharge energy consumption for methane decomposition is attained if the conversion is conducted in the chain mode; in this case, the energy consumption does not exceed 1 eV/molecule. A promising line in the plasma reforming of methane is its

conversion in a mixture with steam. In this case, the energy consumption of gliding discharge for CH_4 decomposition is lower than the enthalpy of the steam methane reforming under the equilibrium conditions. The yield of H_2 considerably exceeds the equilibrium values, and the H_2/CO ratio is 5-10.

The review of the experimental works on gas-phase plasmochemical processes has demonstrated that the conditions developed under the action of a pulsed electron beam on gas are favorable for initiation of chain chemical processes. In contrast to other plasma formation techniques, a high-current pulsed electron beam provides a considerable reduction in the energy of electrophysical installation for completing the chemical reaction, which is a critical factor in the case of limited power supply. Under non-equilibrium conditions generated by a pulsed electron beam, no inhibiting effect of high oxygen concentration on partial methane oxidation is manifested. Unlike other techniques, a pulsed electron beam irradiation helps synthesize nanosized titanium dioxide particles with crystal structure at low temperature. A considerable reduction in the temperature threshold of particle crystal structure formation has also been achieved for composite nanosized particles of $(TiO_2)_x(SiO_2)_{1-x}$ oxides.

Conclusion

In conclusion we would like emphysise some other promising areas of practical application of plasma chemistry. The studies of liquid-phase decomposition of hydrocarbons during heating showed that the process is implemented as a chain (thermal cracking). At low temperatures, in the absence of radiation the thermal initiation of the reaction does not occur; as a result of the radiation exposure the active centres are formed, which are free radicals that can start a chain reaction of hydrocarbon cracking. The interaction of radicals containing a small number of carbon atoms with the initial hydrocarbon is a distinct chain process, it is initiated by the radicals formed though the radiation. Such a chain reaction of radiation-thermal cracking will take place at a temperature of 150-200 degrees below the temperature of a normal thermal process, but with the same specific rate, because the radiation facilitates the most energy-intensive stage - the thermal initiation of reaction. In addition, with a sufficient length of chain the total energy consumption for the chemical process can be reduced. The main source of energy in this case is the thermal energy of the original material or the exothermic energy of elementary chemical chain reactions (e.g., oxidation or polymerization). This can significantly reduce the energy consumed by the chemical process. Conducting a chemical process at a low temperature allows one to synthesize compounds which are unstable at higher temperatures or selectivity of synthesis of which at high temperatures is low. The above features from the chain of chemical processes which occur in plasma are particularly relevant for the petrochemical industry.

But at the interaction of ionizing radiation with matter in the liquid phase the major part of the secondary electrons produced though ionization of the medium, have a small path, due to its relatively low energy. Therefore the electrons produce ionization and excitation in a local area, close to the place of their formation. This effect observed in the radiolysis of liquid media is called "Franck-Rabinowitch effect". This effect is to maintain a high concentration of radicals and long-lived excited products formed in the spurs, after the completion of the primary excitation act. The influence of this effect is particularly noticeable in the general output of the radiolysis products, which are less formed in the liquid phase than in the gas phase. This leads to the fact that at temperatures below 600 K, the radiation-chemical yield does not exceed a few molecules per 100 eV.

Pulse radiolysis of liquid-phase hydrocarbons at low temperature under the action of an electron beam with a high current density (200 A/cm^2), is of a great interest. At the same time the conditions favorable to multiple collisions of particles with excess energy stored in the internal

degrees of freedom are formed. These conditions are similar to nonequilibrium excitation of gas-phase environment and contribute to a chain reaction. A requirement for creating of such conditions of radiolysis is a high absorbed dose of the radiation.The tracks are formed during the entire duration of the pulse and during the radiation the relaxation of excited molecules and radicals recombination should be negligible. The lifetime of active radicals formed in the track during the radiolysis does not exceed 10^{-7}-10^{-8} sec. Therefore, the duration of radiation exposure should not exceed 100 ns. Radiolysis of liquid hydrocarbons in these conditions has not been studied and is of scientific and practical interest for studing the mechanism of radiation liquid phase cracking of hydrocarbons at low temperatures.

Another promising area of application of the gas discharge and pulsed electron beams is the initiation of soot formation in non-equilibrium conditions. It is known that the conversion of carbon-hydrogen fuel during the combustion passes through the stage of formation of polycyclic aromatic hydrocarbons. They are the centers of formation of the soot particles (nuclei). For the soot formation the radical-precursors requires; therefore the process under equilibrium conditions does not occur at low temperatures. In addition, the soot precursors are pyrolyzed and oxidized at high temperatures, so that the process of soot formation under equilibrium conditions (1000 - 2000 K) completes the synthesis of pyrolytic carbon. The formation of radicals thought the action of a pulsed electron beam on a mixture of hydrocarbon gases and oxygen can initiate the formation of polycyclic aromatic hydrocarbons at a temperature below the equilibrium sooting. Under these conditions, the process of soot formation can be stopped at the stage of the synthesis of aromatic hydrocarbons, if the duration of external exposure will not exceed the duration of this stage. This may allow the development of a new technology of the synthetic liquid fuels or the complex hydrocarbons with isomeric structure from a natural gas.

Questions

1. Please give the definitions to the following concepts in chemical kinetics: rate of chemical reaction, law of mass action, reaction rate constant.
2. Please explain the following: Arrhenius equation, kinetic equation of the reaction, kinetic scheme of the chemical process
3. Please give the definitions to the following terms: plasma, Debye radius, degree of ionization, electron energy distribution function.
4. Explain the following: elementary processes in plasmas: classification, rate elementary processes, collision cross section.
5. Direct and stepwise ionization in the plasma.
6. The relaxation of excited particles in the plasma. The practical application of the relaxation processes.
7. Treanor mechanism.
8. Mechanisms of electrical discharge. Tawsend discharge
9. Paschen curve. Limitations of the Paschen law.
10. Types of gas discharge
11. The streamer and spark forms of gas discharges.
12. Gas breakdown in an alternating voltage. Microwave discharge.
13. Typical designs of gas-discharge sources of low-temperature plasma.
14. The specific characteristics of plasma-chemical reactions. Quasi-equilibrium plasma-chemical processes.
15. Nonequilibrium plasma-chemical processes. Arrhenius equation for nonequilibrium plasma chemical reactions.
16. Principles of organization of plasma chemical processes.
17. The main types of reactions in plasma chemistry.
18. The methods of nonequilibrium excitation of the molecules.
19. Chain gas-phase processes. The kinetic scheme of chain process.
20. Classification of chain processes. The induction period and limits of ignition.
21. Chain oxidation of hydrogen.
22. Chain-chemical processes under external action. Methods of initiation of chain processes.
23. Conversion of methane in low-temperature plasma. Classification of conversion methods. Conversion products.
24. The kinetic scheme and the main plasma chemical reaction of the methane pyrolysis

25. The steam conversion of methane in low-temperature plasma. The kinetic scheme and conversion products.

26. Combined methods of plasma-chemical conversion of methane

27. Chain plasma-chemical conversion of methane. The kinetic scheme and the energy balance of the chain process.

28. Plasma-chemical synthesis of nanosized particles. Classification, advantages and disadvantages of synthesis methods.

29. Non-equilibrium plasma-chemical synthesis of nanosized metal oxides.

30. Non-equilibrium plasma-chemical synthesis of nanosized composite oxides. The application of titanium nanosized composite oxides.

31. Plasma-chemical methods for the formation of carbon nanostructures. Allotropic forms of carbon.

32. Beam-plasma technology of hardening and surface modification of metal products

33. Applications of low-temperature plasma in chemical production

34. Plasma-chemical processing of medical polymers.

35. Plasma-chemical methods of waste treatment.

References

1. Pushkarev A., Novoselov Yu., Remnev G. Chain processes in low temperature plasma. – Novosibirsk.: Nauka, 2006. – 226 p.

2. Pushkarev A.I., Remnev G.E. Application of Pulsed Electron Beams in Plasma Chemistry // Известия вузов. Физика. – 2006. – Т. 49. – № 11 (Приложение). – С. 462–466.

3. Goldston R.,Rutherford P. Introduction to Plasma Physics. – Philadelphia.: IOP Rublishing Ltd, 1995. – 479 p.

4. Fitzpatrick R. Lectures on Plasma Physics. – Cambridge UK: Cambridge University Press, 1994. – 247 p.

5. Cecchi J. L. Handbook of Plasma Processing Technology Park Ridge, NJ: Noyes Publications, 1990. – 149 p.

6. Thornton J. A, Penfold A. S. Thin Film Processes. – New York: Academic Press, 1978. – 75 p.

7. Chen F. F. Introduction to Plasma Physics and Controlled Fusion, 2nd ed. – New York: Plenum Press, 1984. – 126 p.

8. Venugopalan M. Reactions Under Plasma Conditions. – New York: Wiley-Interscience, 1971. – Vol. 1. – 608 p.

9. Bell A. T. Techniques and Applications of Plasma Chemistry. – New York: John Wiley & Sons, 1974. – 403 p.

10. Cordey J. G., Goldston R. J., Parker R. R. Progress Toward a Tokamak Fusion Reactor // Phys. Today. – 1992 – Vol. 45. – P. 22–28.

11. Raizer Yu.P. Gas discharge physics. – New York: Springer, 1997. – 463 p.

12. Cooray G. V. The Lightning Flash. – London: The Institution of Engineering and Technology ,2003. – 574 p.

13.Weissler G.L. Introduction to Plasma Physics // Encyclopedia of Physics. – 1956 – Vol. 16. – P. 445–454.

14. Richadson O.W. The emission of electricity from hot bodies. – London: LongmansGreen, 1921. – 314 p.

15. Schottky W.Z. Schottky Effect // J. Phys. – 1923. – № 14. – P. 63–74.

16. Fowler R., Nordheim L. Field emission // Proc. R. Soc. – 1928. – Vol. 119. – P. 173–181.

17. Loeb L.B. Basic processes of gaseous electronics. – Los angeles: University of California Press, 1955. – 1029 p.

18.Raether H. Electrical Coronas // J. Angew. Phys. – 1955. – №7. – P.50–57.

19. Loeb L.B., Meek J.M. The mechanism of the electric spark. Stanford: StanfordUniversity Press, 1940. – 211 p.

20. Loeb L.B. Electrical coronas: Their basic physical mechanism. – Los angeles: Universityof California Press, 1965. – 417 p.

21. Raether H. Avalanches and streamers // J. Phys. – 1939. – Vol. 112. – P.464–471.

22. Meek J.M. Formation of a negative streamer // J. Phys. Rev. – 1940. – Vol. 57. – P. 722–762.

23. Dawson G.A., Winn W.P. A spherical space charge // J. Phys. – 1965. – Vol. 183. – P. 159 –163.

24. Gallimberti I.J., Bacchiege G.L., Gazzani A., Bernadi M., and Bondiou A. // Proceedings of the 1994 international aerospace and groundconference on ‘ Lightning and static electricity’. – 1994. – P. 23–29.

25. Gallimberti I. The mechanism of the long spark formation // J. Phys. – 1979. – № 40. – P. 193–250.

26. Towsend J.S. Electricity in gases. – Oxford: Oxford Press, 1914. – 493 p.

27. Nasser E. Fundamentals of gaseous ionization and plasma electronics. – New York:Wiley-Interscience, 1971. – 386 p.

28. Dakin T., Luxa G., Oppermann G., Vigreux J., Wind G. Paschen curve for air // Electra – 1974. – Vol. 32. – P. 61–69.

29. House J. E. Principles of chemical kinetics // James E. House. – 2007. – P. 963–975.

30. Frinman A. Plasma Chemistry. – New York: Cambridge University Press, 2008. – 725 p.

31. Polak L. Elementary chemical processes and kinetics in a nonequilibrium and quasi-equilibrium plasma // J. Applied Chem. – 1970. – P. 307–342.

32. Полак Л.С. Кинетика неравновесной плазмы// Первый всесоюзный симпозиум по плазмохимии. – 1971. С. 1–15.

33. Полак Л.С. Применение вычислтельной математики в физической и химической кинетике. – М.: Наука, 1966. – 421 с.

34. Von Engel A. Ionized Gases. – Clarendon: Oxford, 1955. – 421 p.

35. Spitzer L. Physics of Fully Ionized Gases. – New York.: Interscience: New York, 1962. – 358 p.

36. Shih-J-Pay. Magneto Gas Dynamics and Plasma Dynamics. – Springer: Vienna, 1962. – 412 p.

37. Wall F. T., Hitler L. A., Mazur J. Chemical reactions under low-temperature plasma conditions // J. Chem. Phys. – 1961. – Vol. 35. –

P. 1284–1295.

38. Blais N. C., Bunker D. L. Chemical reactions // J. Che. Phys. – 1963. – Vol. 39. – P. 315–319.

39. Keck J. C. Chemical reactions // J. Chem. Phys. – 1958. – Vol. 29. – P. 410–426.

40. Schmeltekopf A. L., Ferguson E. E. Fesenfeld F. C. Chemical reactions under low-temperature plasma conditions // J. Chem. Phys. – 1968. – Vol. 48. – P. 2966–2974.

41. Месяц Г.А. Импульсная энергетика и электроника. – М.: Наука, 2004. – 704 с.

42. Рыжов В.В., Ястремский А.Г. Распределение энергии электронного пучка в плазме азота // Физика плазмы. – 1978. – Т. 4, вып.6. – С. 1262–1266.

43. Норман Г.Э., Полак Л.С., Сопин П.И., Сорокин Г.А. Сильноточные релятивистские электронные пучки в плазмохимии // Синтез соединений в плазме, содержащей углеводороды. – М.: ИНХС АН СССР, 1985. – 166 с.

44. Налбандян А.Б., Воеводский В.В. Механизм окисления и горения водорода. – М.: Изд-во АН СССР, 1949. – 179 с.

45. Старик А.М., Титова Н.С. О кинетических механизмах инициирования горения водородно-кислородных смесей при возбуждении электронных степеней свободы молекулярного кислорода лазерным излучением // Журнал технической физики. – 2003. – Т. 73. – № 3. – С. 59–68.

46. Пушкарев А.И., Ремнев Г.Е. Инициирование окисления водорода импульсным электронным пучком // Физика горения и взрыва. – 2005. – № 3. – С. 46–51.

47. Пушкарев А.И., Ремнев Г.Е. Колебательный характер процесса окисления водорода при инициировании импульсным электронным пучком // Физика горения и взрыва. – 2005. – № 4. – С. 18–21.

48. Ремнев Г.Е., Фурман Э.Г., Пушкарев А.И. и др. Импульсный сильноточный ускоритель с согласующим трансформатором // Приборы и техника эксперимента. – 2004. – № 3. – С. 130–134.

49. Пушкарев А.И., Пушкарев М.А., Ремнев Г.Е. Исследование звуковых волн, генерируемых при поглощении импульсного электронного пучка в газе // Акустический журнал. – 2002. – Т. 48, №2. – С. 260–265.

50. Pushkarev A., Isakova J., Kholodnaya G., Sazonov R. Sound Waves Generated Due to the Absorption of a Pulsed Electron Beam //Advances in Sound localization. – Vienna: INTECH, 2011. – 672 p.

51. Селезенев А.А., Алейников А.Ю., Ярошенко В.В. Влияние радиолиза на смещение пределов воспламенения водород-кислородной газовой смеси. // Химическая физика. – 1999. – Т. 18. – № 5. – С. 65–71.

52. Комар А.П., Круглов С.П., Лопатин И.В. Измерение полной энергии пучков тормозного излучения от электронных ускорителей. – Л.: Наука. – 1972. –172 с.

53. Радиолиз углеводородов. Некоторые физико-химические проблемы / Под ред. А.В. Топчиева, Л.С. Полака.– М.: Изд-во АН СССР. – 1962. – 208 с.

54. Сараева В.В. Радиолиз углеводородов в жидкой фазе. Современное состояние вопроса. – М.: Изд-во Моск. ун-та. – 1986. – 256 с.

55. Химия высоких энергий / Под ред. Л.Т. Бугаенко, М.Г. Кузьмин, Л.С. Полак. – М.: Химия, 1988. – 368 с.

56. Бабарицкий А.И., Деминский М.А., Демкин С.А., Животов В.К. Эффект плазменного катализа при разложении метана // Химия высоких энергий. – 1999. – Т. 33, №1. – С. 49–56.

57. Бабарицкий А.И., Баранов И.Б., Дёмкин С. А. и др. Плазменный катализ процессов конверсии углеводородов // Химия высоких энергий. – 1999. – Т. 33. – № 6. – С. 458–462.

58. Штерн В.Я. Механизм окисления углеводородов в газовой фазе. – М.: Изд-во АН СССР, 1960. – 496 с.

59. Арутюнов В.С., Крылов О.В. Окислительные превращения метана. – М.: Наука, 1998. – 361 с.

60. Кармилова Л.В., Ениколопян Н.С., Налбандян А.Б. К вопросу о вырожденном разветвлении. Роль формальдегида при окислении метана // Журнал физической химии. – 1957. – Т. 31. – С. 851–864.

61. Михайлов Б.М., Куимова М.Е., Богданов В.С. Действие ионизирующих излучений на неорганические и органические системы. – М.: Изд. АН СССР, 1958. – 223 с.

62. Русанов В.Д., Бабарицкий А.И., Герасимов Е.Н. и др. Стимулирование процесса парциального окисления метана в микроволновом разряде // Доклады Академии наук. – 2003. – Т. 389. – № 3. – С. 324–327.

63. Русанов В.Д., Бабарицкий А.И., Баранов И.Е. и др. Неравновесное воздействие плазмы микроволнового разряда атмосферного давления на процесс конверсии метана и керосина в синтез-газ. // Доклады Академии наук. – 2004. – Т. 395. – № 5. – С. 637–640.

64. Денисов Г.В., Новоселов Ю.Н., Суслов А.И., Устер А.М. Продукты окисления сероуглерода в ионизованном воздухе // Журн. техн. физики. – 2001. – Т. 71. – № 1. – С. 136–138.

65. Новоселов Ю.Н., Суслов А.И., Кузнецов Д.Л. Воздействие импульсных пучков электронов на примесь сероуглерода в воздухе // Журн. техн. физики. – 2003. – Т. 73. – № 6. – С. 123–129.

66. Новоселов Ю.Н., Рыжов В.В., Суслов А.И. Эффект электрического поля при конверсии сероуглерода в ионизованном воздухе. // Письма в ЖТФ. – 2002. – Т. 28. – № 6. – С. 35–41.

67. Remnev G.E. , Pushkarev A.I., Khim. Plasma-chemical synthesis of SiO_2 nanopowders // High Energy Chem. – 2004. – Vol. 38. – №. 5. – P. 348–354.

68. Remnev G.E., Pushkarev A.I. Plasma-chemical synthesis of TiO_2 nanopowders // IEEJ Trans. Fundam. Mater. – 2004. – Vol. 124. – № 6. – P. 483–489.

69. Bin Xia, Li. W., Zhang B. et al. Low temperature vapor-phase preparation of TiO_2 nanopowders // Journal of Materials Science. – 1999. – Vol. 34. – P. 3505 – 3511.

70. Jang H. D., Kim S.-K. and Kim S.-J. Effect of particle size and phase composition of titanium dioxide nanoparticles on the photocatalytic properties // J. of Nanoparticle Res. – 2001. – Vol.3. – № 2 – 3. P. 141–146.

71. Ahonen P.P., Moisala A., et al. Gas-phase crystallization of titanium dioxide nanoparticles // J. of Nanoparticle Res. – 2002. – Vol . 4. – № 1– 2. – P. 43–46.

72. Ayllon J. A., Figueras A., Garelik S., et al. Preparation of TiO2 powder using titanium tetraisopropoxide decomposition in a plasma enhanced chemical vapor deposition (PECVD) reactor // J. of Mater. Sci. Lett. – 1999. – Vol. 16. – № 18. – P. 13– 9.

73. Li W., Ni C., Lin H. et al. Size dependence of thermal stability of TiO2 nanoparticles // J. of Appl. Phys. – 2004. – Vol. 96. – №. 11. – P. 6663–6667.

74. Harano A., Shimada K. et al. Crystal phases of TiO2 ultrafine particles prepared by laser ablation of solid rods // J. of Nanoparticle Res. – 2002. – Vol. 4. – № 3. – P. 215–217.

75. Seto T., Kawakami Y. et al. Evaluation of morphology and size distribution of silicon and titanium oxide nanoparticles generated by laser ablation // J. of Nanoparticle Res. – 2001. – Vol. 3. – № 2–3. – P. 185–189.

76. Oh S.-M., Park D.-W. and Ishigaki T. Plasma Synthesis of Spherical Titanium Dioxide from Titanium Nitride // Proc. of 16th Intern. Symp. on Plasma Chemistry. Taormina. – 2003. – P. 45–52.

77. Kotov Yu A. Electric explosion of wires as a method for preparation of nanopowders // Journal of Nanoparticle Research. – 2003. – № 5. – P. 539–550.

78. Назаренко О.Б. Электровзрывные порошки. Получение, свойства, применение / Под ред. А.П. Ильина. – Томск: Изд-во Томского университета, 2005. – 148 с.

79. Wallidge G. W., Anderson R., Mountjoy G., Pickup D. M., Gunawidjaja P., Newport R. J., Smith M. E. Advanced physical characterization of the structural evolution of amorphous $(TiO_2)x(SiO_2)_{1-x}$ sol-gel materials // Journal of materials science. – 2004. – Vol. 39. – P. 6743–6755.

80. Ingo G. M., Riccucci C., Bultrini G., Dire S. and Chiozzini G. Thermal and microchemical characterization of sol-gel SiO_2, TiO_2 and $xSiO_2$-(1-x)TiO_2 ceramic materials // Journal of Thermal Analysis and Calorimetry. – 2001. – Vol. 66. – P. 37–46.

81. Machida M., Norimoto K., Watanabe T., Hashimoto K., Fujishima A. (1999) The effect of SiO_2 addition in super-hydrophilic property of TiO_2 photocatalyst // Journal of materials science. – 1999. – Vol. 4. – P. 2569–2574.

82. Young-Geun Kwon, Se-Young Choi, Eul-Son Kang, Seung-Su Baek Ambient-dried silica aerogel doped with TiO_2 powder for thermal insulation // Journal of Materials Science. – 2000. – Vol. 35. – № 24. – P. 6075–6079.

83. Takahiro G., Takayuki K., Yoshimoto A. Crystallization Behavior of SiO_2-TiO_2 ceramics derived from titanosiloxanes on pyrolysis // Journal of Sol-Gel Science and Technology. – 1998. – Vol. 13. – №1–3. – P. 975–979.

84. Remnev G.E., Isakov I.F., Pushkarev A.I. A pulsed ion beam accelerator for material modification // Surf. Coat. Technol. – 1999. – Vol. 114. – P. 206–217.

85. Nakamoto K. Infrared and Raman Spectra of Inorganic and Coordination Compounds. – New York: Wiley, 1986. – 326 p.

86. Kuptsov A.Kh., Zhizhin, G.N. Fourier-Transform Raman and Infrared Absorption Spectra of Polymers. – M.: Fizmatlit, 2001 – 126 p.

87. Ahn W.S., Kang K.K., Kim K.Y. Synthesis of TS-1 by microwave heating of template-impregnated SiO2–TiO2 xerogels // Catalysis Letters. – 2001. – Vol. 72. – № 3–4. – P. 229–232.

88. Fincke J. R., Anderson R. P., Hyde T. et al. Plasma thermal conversion of methane to acetylene // Plasma Chemistry and Plasma Processing. – 2002. – Vol. 22. – № 1. – P. 107–138.

89. Babaritskii A.I., Deminskii M.A., Demkin S.A., Zhivotov, V.K., A low temperature thermal initiation of cracking // High Energy Chem. – 1999. – Vol. 33. – № 1. – P. 45–49.

90. Zhivotov V.K., Potapkin B.V., Rusanov V.D. Encyclopedia of Low-Temperature Plasma. – M.: Fizmatlit. – 2005. – 41 p.

91. Czernichowski A., Glid arc assisted production of H_2 from CH_4, CO or H_2S // Proc. Int. Symp. Hydrogen Power, Theoretical and Engineering Solutions. – 1999. – P. 98–104.

92. Li X.S., Zhu A.M., Wang K.J., Xu Y., Song Z.M. Methane conversion to C_2 hydrocarbons and hydrogen in atmospheric non-thermal plasmas generated by different electric discharge techniques // J. Catal. – 2004. – Vol. 98. – P. 617–625.

93. Li X.S., Shi C., Xu Y., Wang K.J., Zhu, A.M. A process for a high yield of aromatics from the oxygen-free conversion of methane: combining plasma with Ni/HZSM-5 catalysts // Green Chem. – 2007. – Vol. 9. – P. 647–689.

94. Pushkarev A.I., Novoselov Yu.N., Remnev G.E., Tsepnye protsessy v nizkotemperaturnoi plazme. – Novosibirsk: Nauka, 2006. – 123 p.

95. Pushkarev A.I, Remnev G.E., and Ponomarev D.V., Fundamental’nye problemy prilozhenii fiziki nizkotemperaturnoi plazmy: Materialy lektsii Vserossiiskogo simpoziuma molodykh uchenykh, studentov i aspirantov // Proc. All-Russia Symp. of Young Scientists, Students, and Aspirants on Fundamental Problems of Application of Low-Temperature Plasma Physics. – 2005. – Vol. 1. – P. 26–29.

96. Shtern V.Ya., Mekhanizm okisleniya uglevodorodov v gazovoi faze. – Moscow: AN SSSR, 1960. – 123 p.

97. Arutyunov V.S. and Krylov O.V. Okislitel’nye prevrashcheniya metana. – M: Nauka, 1998. – 136 p.

98. Rusanov V.D., Babaritskii A.I., Gerasimov E.N., Deminskii M.A., Demkin S.A., Zhivotov V.K, Moskovskii A.S., Potapkin B.V., Smirnov R.V. and Strelkova M.I. Dokl. Akad. Nauk. – 2003. – Vol. 389. – № 3. – P. 324–327.

99. Lesueur H., Czernichowski A., Chapelle A. Electrically assisted partial oxidation of methane //. J. Hydrogen Energy. – 1994. – Vol. 19. – № 2. – P. 139–142.

100. Lee D.H., Kim K.T., Song Y.-H and Cha M.S. Characteristic of Methane Processing by Rotating Arc Reactor Proc. // 18th Int. Symp. on Plasma Chemistry. – 2007. – P. 153–159.

101. Heo J., Choi J.-W., Lee H., Sekiguchi H. and Song H.K. Synthesis Gas Production from Methane and Air Mixture with a Vortex Gliding Arc Reactor Proc. // 18th Int. Symp. on Plasma Chemistry. – 2007. – P. 554–559.

102. Remnev G.E., Pushkarev A.I., Ezhov V.V., Partial methane and nitrogen oxidation initiated by pulsed electron beam Proc // 13th Int. Symp. on High Current Electronics. – 2004. – P. 447–451.

103. Indarto A., Choi J.W., Lee H., Song H.K. Plasma methane oxidation for methanol synthesis with Cu-Zn-Al catalyst Proc. // 18th Int. Symp. on Plasma Chemistry. – 2007. – P. 194–198.

104. Mutaf-Yardimci O., Saveliev A., Fridman A., Kennedy L. Employing plasma as catalyst in hydrogen prodaction Int. // J. Hydrogen Energy. – 1998. – Vol. 23. – № 12. – P. 1109–1114.

105. Lee H., Choi J.-W., Song H.K., Lee C.-H. The effect of the electric pulse polarity on CO_2 reforming of CH_4 using dielectric-barrier discharges Proc. // 4th Int. Symp. on Pulsed Power and Plasma Applications. – 2003. – P. 146–157.

106. Song H., Lee H., Choi J.,Na B. Effect of electrical pulse forms on the CO_2 reforming of methane using atmospheric dielectric barrier discharge // Plasma Chem. Plasma Process. – 2004. – Vol. 24. – №. 1. – P. 57–61.

107. Rusu I. and Cormier J.-M. On a possible mechanism of the methane steam reforming in a gliding arc reactor // Chem. Eng. J. – 2003. – Vol. 91. – № 1. – P. 23–29.

108. Cormier J., Rusu I. Syngas production via methane steam reforming with oxygen: plasma reactors versus chemical reactors // J. Phys. D: Appl. Phys. – 2001. – Vol. 34. – P. 2798–2801.

109. Azizov R.I., Babaritskii A.I., Demkin S.A. In Gazokhimiya v XXI veke. Problemy i perspektivy // Gas Chemistry in XXI Century: Problems and Prospects. – 2003. – P. 45–53.

110. Sekine Y., Urasaki K., Kado S., Asai S., Matsukata M., Kikuchi Steam reforming of hydrocarbons and alcohols using non-equilibrium pulsed discharge E // Proc. 16th Int. Symp. on Plasma Chemistry, Taormina. – 2003. – P. 213–216.

111. Zhdanok S.A., Krauklis A.V., Bouyakov I.F. Studying methane conversion in atmospheric pressure high-voltage discharge with different oxidizers in presence of catalysts // Proc. IV Intern. School-Seminar Modern Problems of Combustion and its Application. – 2001. – P. 66–72.

112. Chavadej S., Rueangjitt N., Sreethawong T. Reforming of CO-containing natural gas with partial oxidation using an AC gliding arc system // Proc. 18th Int. Symp. on Plasma Chemistry. – 2007. – P. 552–561.

113. Bromberg L., Cohn D., Rabinovich A., O'Brien C. and Hochgreb S. Plasma catalytic reforming of methane Energy Fuels // Proc. 18th Int. Symp. on Plasma Chemistry – 1998. – Vol. 1. – №. 1. – P. 11–16.

114. Bromberg L., Cohn D., Rabinovich A., Alexeev N. Partial methane and nitrogen oxidation initiated by pulsed electron beam // Int. J. Hydrogen Energy. – 1999. – Vol. 24. – P. 1131–1136.